

Naturalness and Neutral Naturalness in the LHC Era

THÈSE N° 7739 (2017)

PRÉSENTÉE LE 26 MAI 2017
À LA FACULTÉ SCIENCES DE BASE
LABORATOIRE DE PHYSIQUE THÉORIQUE DES PARTICULES
PROGRAMME DOCTORAL EN PHYSIQUE

ÉCOLE POLYTECHNIQUE FÉDÉRALE DE LAUSANNE

POUR L'OBTENTION DU GRADE DE DOCTEUR ÈS SCIENCES

PAR

Davide GRECO

acceptée sur proposition du jury:

Prof. F. Mila, président du jury
Prof. R. Rattazzi, directeur de thèse
Prof. R. Harnik, rapporteur
Prof. A. Pomarol, rapporteur
Prof. A. Bay, rapporteur



ÉCOLE POLYTECHNIQUE
FÉDÉRALE DE LAUSANNE

Suisse
2017

Ita fac, mi Lucili: vindica te tibi, et tempus quod adhuc aut auferebatur aut subripiiebatur aut excidebat collige et serva. Persuade tibi hoc sic esse ut scribo: quaedam tempora eripiuntur nobis, quaedam subducuntur, quaedam effluunt. Turpissima tamen est iactura quae per negligentiam fit. Et si volueris attendere, magna pars vitae elabatur male agentibus, maxima nihil agentibus, tota vita aliud agentibus. Quem mihi dabis qui aliquod pretium tempori ponat, qui diem aestimet, qui intellegat se cotidie mori? In hoc enim fallimur, quod mortem prospicimus: magna pars eius iam praeterit; quidquid aetatis retro est mors tenet. Fac ergo, mi Lucili, quod facere te scribis, omnes horas complectere; sic fiet ut minus ex crastino pendeas, si hodierno manum inieceris. Dum differtur vita transcurrit. Omnia, Lucili, aliena sunt, tempus tantum nostrum est; in huius rei unius fugacis ac lubricae possessionem natura nos misit, ex qua expellit quicumque vult. Et tanta stultitia mortalium est ut quae minima et vilissima sunt, certe reparabilia, imputari sibi cum impetravere patiantur, nemo se iudicet quicquam debere qui tempus accepit, cum interim hoc unum est quod ne gratus quidem potest reddere.

— L. A. Seneca, *Epistulae morales ad Lucilium*, Liber I.



Acknowledgements

There would be no PhD thesis without a PhD adviser, so I have to thank Riccardo Rattazzi for giving me the opportunity to carry out the research presented in this work under his supervision. Our interaction throughout these four years has been peculiar, at times intensely stormy and always very complicated. Understanding how to work efficiently with Riccardo, and especially how to learn physics from him, has been the most challenging experience of my PhD. After all, he taught me the importance of being scientifically independent, of developing a critical judgment and above all of being honest with myself. Beyond physics, Riccardo really cherishes his students and their advancement as scientists, he always tries to help them when difficulties arise and he always feels responsible even when the student is clearly at fault. For all this, for your support, for your effort to conclude our endless paper, for standing by my side when I did not deserve it, Riccardo, thank you!

During my PhD, I had the opportunity of meeting and working with people who taught me a lot and to which I am indebted. In particular, I want to thank Riccardo Barbieri, Andrea Wulzer and Roberto Contino, who very patiently waited for me to grasp the most abstract concepts, even when I was almost completely lost. I thank them for having collaborated with me in two projects and for having given me the chance of co-authoring a paper with them.

Before arriving to Lausanne, I met extraordinary people who taught me the passion for theoretical physics and inspired me to continue the quest for answers with a PhD. I heartily thank Alessandro Tomasiello, the first person I had the chance to work with, for introducing me many years ago to the world of mathematical physics and for the many passionate discussions we had about physics. More than a supervisor, he has been a friend for me. I also thank Alberto Zaffaroni, my Master adviser, who further pushed me to investigate, formulate and answer the right theoretical questions and who supported me when I applied for a PhD and even after. I am indebted for your help.

This PhD thesis is the result of a very long process that dates back when I started my elementary school and I discovered how exciting it was to study, to learn and to improve my understanding in many different fields. I want to thank all the passionate teachers that I met throughout the

Acknowledgements

years, who did their job not with the prospect of a competitive salary but because of their vocation to cherish the growth of their students. I take then the occasion to name some of them; even if many years have passed, I still cannot forget some of their lectures and how they inspired me and impacted my life with the decision to keep studying and learning at higher and higher levels. So I want to thank my elementary school teachers Rosanna, Antonella, Liliana, my middle school teachers Roberta Tozzi, Claudia Poltronieri, Chiara Fumarola, my secondary school teachers Silvia Caralli, Claudia Malberti, Maria Teresa Parolini, Carmen de Toffol and especially Aurora Tarsia and Franca Sormani whose passion for physics and mathematics inspired me to study these subjects at university. During my bachelor and master years in Milano, I had the chance to learn physics from passionate researchers who always thrilled my curiosity and instilled in me the pleasure of science; I want to name here Antonino Pullia, Roberto Paoletti, Tommaso Tabarelli de Fatis, Silvia Penati, Federico Rapuano, Claudio Destri, Carlo Oleari, Luciano Girardello. Thank you for teaching me everything I know about physics!

I would not have survived four years of PhD without the help and support of all the postdocs and students I was lucky to meet and to share this experience with. They made my work enjoyable, discussed with me about physics and life and provided a helping hand whenever I was feeling I was breaking down. I have no space to recall them all, but they all made the Cubotron, the seventh floor and especially the open space a familiar place where to spend my time. Thank you to you all! Among them, I want to thank especially Sasha, for playing tennis table with me and for chatting with me whenever I was feeling lonely, Tommaso, Benjamin, Andrea T., for her support and help during my first year in Lausanne, Francesco, who passed me his passion for biking, Javier, Alberto, who turned me into a cinematic expert after all the movies we watched together, Andrea M., for the many exciting games in Risiko, Lorenzo, who shared with me the most adventurous journeys of my life in America and in Norway, David, for the many pizzas we ate together, Riccardo T., for his patience and his friendship, Davide F., who after an initial contrast toured with me the Lac Léman by bike and became a good friend. Outside Cubotron, Lausanne offers a fantastic mountain scenery and the possibility to meet new people from all over the world. I want to thank Gigi, for all the times we met at CERN and for the many parties he invited me to, Giulia and Lea, for their genuine spontaneity.

Finally, I thank my family for always being supportive and for always encouraging me to pursue my interests and my passions, no matter how risky it was, without any restriction.

Lausanne, 22 March 2017

Davide Greco

Abstract

We present two different approaches to solve the hierarchy problem of the Standard Model and to provide a consistent dynamical mechanism for electroweak symmetry breaking. As a first scenario, we follow the naturalness paradigm as realized in Composite Higgs theories, which conceive the Higgs particle as a bound state of a new strongly interacting sector confining at the TeV scale. We present a minimal implementation of the model and study in detail the phenomenology of vector resonances, which are predicted as states excited from the vacuum by the conserved currents of the new strong dynamics. This analysis allows us to derive constraints on the parameter space of Composite Higgs models from the presently available LHC data and to confront naturalness with experimental results. Motivated by the rising tension between theoretical expectations and the absence of new physics signals at the LHC, we consider as a second possibility the neutral naturalness paradigm and address the hierarchy problem by posing the existence of a mirror copy of the Standard Model, as realized in Twin Higgs theories. This new color-blind sector is the main actor in protecting the Higgs mass from large radiative corrections and is un-discoverable at the LHC, allowing us to push far in the ultraviolet the scale where the Standard Model effective theory breaks down and colored resonances appear. We present an implementation of the Twin Higgs program into a composite model and discuss the requirements for uplifting the symmetry protection mechanism also to the ultraviolet theory. After introducing a consistent Composite Twin Higgs model, we consider the constraints imposed on the scale where colored resonances are expected by the determination of the Higgs mass at three loops order, electroweak precision tests and perturbativity of the ultraviolet-complete model. We show that, although allowing in principle the new physics scale to lie far out of the LHC reach, these constructions need the existence of light colored top partners, with a mass of around 2-4 TeV, to comply with indirect observations. Neutral naturalness models may then evade detection at the LHC, but they can be probed and falsified at future colliders.

Key words: electroweak symmetry breaking, LHC phenomenology, Physics beyond the Standard Model, Composite Higgs, Twin Higgs, effective field theories.

Résumé

Nous présentons deux différentes approches pour résoudre le problème de la hiérarchie du Modèle Standard et pour fournir un mécanisme consistant de brisure spontanée de symétrie électrofaible. Comme premier scénario, nous considérons le paradigme de naturalité dans le cadre des théories de Higgs composite, qui conçoivent la particule de Higgs comme un état lié d'un nouveau secteur fortement couplé et confinant à l'échelle de quelques TeV. Nous présentons une implémentation minimale du modèle et nous étudions en détail la phénoménologie des résonances vectorielles qui sont prédites comme états excités du vide par les courants conservés du nouveau secteur interagissant fortement. Cette analyse permet de dériver des limites sur l'espace des paramètres du modèle de Higgs composite à partir des dernières mesures du LHC et de tester le paradigme de naturalité avec les résultats expérimentaux. Motivés par la tension croissante entre les attentes théoriques et l'absence de signaux de nouvelle physique au LHC, nous considérons comme deuxième scénario le paradigme de naturalité neutre et nous adressons le problème de la hiérarchie en supposant l'existence d'une copie spéculaire du Modèle Standard, comme réalisée en théories de Twin Higgs. Ce nouveau secteur incolore protège la masse du boson de Higgs contre les grandes corrections radiatives et il est impossible à découvrir au LHC, en permettant de pousser loin dans l'ultraviolet l'échelle où la théorie effective du Modèle Standard n'est plus valide et les résonances colorées apparaissent. Nous fournissons une implémentation du paradigme du Twin Higgs dans un modèle composite et nous discutons des conditions nécessaires pour que le mécanisme de protection soit respecté par la théorie ultraviolette aussi. Après avoir introduit un modèle consistant de Twin Higgs composite, nous considérons les limites imposées sur l'échelle où les résonances colorées sont expectées par la détermination de la masse du Higgs à l'ordre de trois boucles, les tests de précision électrofaibles et la condition de calculabilité du modèle complet ultraviolet. Nous montrons que, bien qu'elles permettent en principe que l'échelle de nouvelle physique soit au dehors de la portée du LHC, ces constructions exigent l'existence de résonances colorées légères, avec une masse d'environ 2-4 TeV, pour satisfaire les observations indirectes. Les modèles de naturalité neutre peuvent donc échapper à la détection au LHC, mais ils pourront définitivement être explorés et falsifiés avec un futur accélérateur.

Mots-clés : brisure spontanée de symétrie, phénoménologie du LHC, physique au-delà du Modèle Standard, Composite Higgs, Twin Higgs, théories effectives des champs.

Contents

| | |
|--|------------|
| Acknowledgements | i |
| Abstract/Résumé | iii |
| List of figures | xi |
| List of tables | xv |
| 1 Introduction | 1 |
| 2 Hunting composite vector resonances at the LHC: naturalness facing data | 17 |
| 2.1 Behind the models | 19 |
| 2.1.1 The symmetry structure and the degrees of freedom | 19 |
| 2.1.2 Dynamical assumptions | 22 |
| 2.2 The models | 24 |
| 2.2.1 A Lagrangian for ρ_μ^L | 24 |
| 2.2.2 A Lagrangian for ρ_μ^R | 32 |
| 2.2.3 Two Lagrangians for ρ_μ^X | 35 |
| 2.3 Production and decay of vector resonances at the LHC | 39 |
| 2.3.1 Production cross section | 39 |
| 2.3.2 Branching ratios | 43 |
| 2.4 Bounds from LHC direct searches | 47 |
| 2.4.1 Bounds on ρ_μ^L | 48 |
| 2.4.2 Bounds on ρ_μ^R | 51 |
| 2.4.3 Bounds on ρ_μ^X | 53 |
| 2.5 Discussion | 55 |
| 3 A Composite UV completion of the Twin Higgs scenario | 59 |
| 3.1 A model example | 59 |
| 3.1.1 The gauge sector | 60 |
| 3.1.2 The fermionic sector | 67 |
| 3.2 Electroweak symmetry breaking | 73 |
| | vii |

Contents

| | | |
|----------|---|------------|
| 3.3 | Discussion | 77 |
| 4 | The RG-improved Twin Higgs effective potential at NNLL | 79 |
| 4.1 | The Twin Higgs low-energy Lagrangian | 81 |
| 4.1.1 | The Higgs mass and the LL result | 85 |
| 4.2 | The NLL effective potential | 86 |
| 4.2.1 | The background field | 87 |
| 4.2.2 | β -functions in the Higgs background | 90 |
| 4.2.3 | RG-improved Coleman-Weinberg formula and Higgs mass | 93 |
| 4.3 | The NNLL effective potential | 94 |
| 4.3.1 | Running of the strong couplings and scalar contribution to the Coleman-Weinberg potential | 95 |
| 4.3.2 | Renormalization of the twin top mass in the Higgs background | 96 |
| 4.3.3 | Higgs mass at the NNLL | 101 |
| 4.4 | Results | 101 |
| 4.5 | Discussion | 105 |
| 5 | Precision Tests and Fine Tuning in Twin Higgs models | 107 |
| 5.1 | A classification of Twin Higgs scenarios | 110 |
| 5.1.1 | Structure and Parametrics | 110 |
| 5.2 | The Composite Twin Higgs: a comprehensive construction | 116 |
| 5.2.1 | A simplified model | 118 |
| 5.2.2 | Perturbativity of the simplified model | 122 |
| 5.3 | Higgs Effective Potential: a brief reminder | 123 |
| 5.4 | Electroweak Precision Observables | 127 |
| 5.4.1 | \hat{S} parameter | 129 |
| 5.4.2 | \hat{T} parameter | 131 |
| 5.4.3 | δg_{Lb} | 132 |
| 5.5 | Results | 134 |
| 5.6 | Discussion | 138 |
| 6 | Conclusion | 141 |
| A | CCWZ variables | 145 |
| A.1 | CCWZ construction for the $SO(5)/SO(4)$ coset | 145 |
| A.2 | CCWZ construction for the $SO(8)/SO(7)$ coset | 147 |
| B | Heavy vector contribution to the Electroweak Precision Observables | 151 |
| C | Heavy vector couplings | 153 |

| | | |
|----------|--|------------|
| D | Effects of a degenerate vector spectrum | 157 |
| E | A MadGraph5 model for heavy vector phenomenology | 161 |
| F | Fermionic spectrum of the SO(8)/SO(7) Twin Higgs model | 163 |
| G | Diagrammatic renormalization of the Twin Higgs effective potential | 169 |
| H | Correlation between the IR contributions to $\Delta\hat{T}_\Psi$ and to δg_{Lb} | 173 |
| I | Operator analysis of the heavy-vector contribution to δg_{Lb} | 177 |
| J | Explicit formulae for the EWPO | 181 |
| J.1 | Computation of the \hat{S} and \hat{T} parameters | 181 |
| J.2 | Computation of δg_{Lb} | 184 |
| J.3 | Results | 186 |
| K | The EW fit | 191 |
| L | Estimates of the perturbativity bound | 193 |
| | Bibliography | 197 |

List of Figures

- 2.1 Fundamental cross sections as functions of the physical mass of the resonance at $\sqrt{s} = 8$ TeV. Left panel: fundamental cross sections for the DY process. Right panel: fundamental cross sections for the VBF process. 41
- 2.2 Contours of constant cross section (blue lines for the DY process, red dashed lines for the VBF process) in the plane (M_ρ, g_ρ) for the production of the charged (left panel) and neutral (right panel) left-handed (top) and right-handed (bottom) vector triplets. The yellow region corresponds to $\xi > 0.4$, the light blue one to $\xi > 1$ 42
- 2.3 Contours of constant cross section (blue lines for the DY process, red dashed lines for the VBF process) in the plane (M_{ρ_X}, g_{ρ_X}) for the production of the vector singlet. The yellow region corresponds to $\xi > 0.4$, the light blue one to $\xi > 1$ 43
- 2.4 Decay branching ratios of the neutral left-handed vector as a function of the resonance mass for $g_{\rho_L} = 3$, $M_\Psi = 800$ GeV and two different sets of the free parameters. The various curves correspond to the following decay channels: $WW + Zh$ (blue), $t\bar{t} + b\bar{b}$ (red), $l^+ l^-$ (brown), $u\bar{u} + d\bar{d}$ (cyan), $X_{\frac{5}{3}} \bar{X}_{\frac{5}{3}} + X_{\frac{2}{3}} \bar{X}_{\frac{2}{3}}$ (purple), $T\bar{T} + B\bar{B}$ (orange), $X_{\frac{2}{3}} \bar{T}$ (yellow), $X_{\frac{2}{3}} \bar{t}$ (magenta), $T\bar{t} + B\bar{b}$ (green). 44
- 2.5 Decay branching ratios of the charged left-handed (top) and right-handed (bottom) vectors as a function of the resonance mass for $g_{\rho_{LR}} = 3$, $M_\Psi = 800$ GeV and two different sets of the free parameters. The various curves correspond to the following decay channels: $WZ + Wh$ (blue), $t\bar{b}$ (red), lv (cyan), $u\bar{d}$ (brown), $X_{\frac{5}{3}} \bar{X}_{\frac{2}{3}}$ (purple), $T\bar{B}$ (orange), $X_{\frac{5}{3}} \bar{T} + X_{\frac{2}{3}} \bar{B}$ (yellow), $X_{\frac{5}{3}} \bar{t} + X_{\frac{2}{3}} \bar{b}$ (magenta), $T\bar{b} + B\bar{t}$ (green). 45
- 2.6 Decay branching ratios of the vector singlet as a function of the resonance mass for $g_{\rho_X} = 3$ and $M_\Psi = 800$ GeV in models \mathbf{M}_X^1 (left panel) and \mathbf{M}_X^2 (right panel). The various curves correspond to the following decay channels: $WW + Zh$ (blue), $t\bar{t}$ (red), $l^+ l^-$ (cyan), $u\bar{u} + d\bar{d}$ (brown), $b\bar{b}$ (purple), $\tilde{T}\tilde{t}$ (orange), $\tilde{T}\tilde{T}$ (green). 46

List of Figures

- 2.7 Excluded regions in the (M_{ρ_L}, g_{ρ_L}) plane for the charged left-handed vector resonance for two different sets of the free parameters and for $M_\Psi = 800$ GeV. The exclusions are derived from the $\rho^+ \rightarrow t\bar{b}$ searches in [88] (blue), the $\rho^+ \rightarrow l\bar{\nu}$ searches in [90] (red), the $\rho^+ \rightarrow WZ \rightarrow jj$ searches in [85] (purple) and the $\rho^+ \rightarrow WZ \rightarrow 3l\nu$ searches in [96] (green). The plot also shows the contours of constant Γ/M_{ρ_L} (dashed black lines), of constant ξ (dashed blue lines) and of constant g_Ψ (dashed red lines). The region on the left of the thick black line is excluded by experimental constraints on the \hat{S} parameter. The yellow region corresponds to $\xi > 0.4$, the light blue one to $\xi > 1$ 49
- 2.8 Excluded regions in the (M_{ρ_R}, g_{ρ_R}) plane for the neutral right-handed vector resonance for two different sets of the free parameters and for $M_\Psi = 800$ GeV. The exclusions are derived from the $\rho^0 \rightarrow l\bar{l}$ searches in [82] (in red for $c_4 = 1$, in blue for $c_4 = 0$) and the $\rho^0 \rightarrow WW \rightarrow l\nu jj$ searches in [83] (in green for $c_4 = 1$, in orange for $c_4 = 0$). The plot also shows the contours of constant Γ/M_{ρ_R} (dashed black lines), of constant ξ (dashed blue lines) and of constant g_Ψ (dashed red lines). The region on the left of the thick black line is excluded by experimental constraints on the \hat{S} parameter. The yellow region corresponds to $\xi > 0.4$ 52
- 2.9 Excluded regions in the (M_{ρ_X}, g_{ρ_X}) plane for the vector singlet in models \mathbf{M}_X^1 (left) and \mathbf{M}_X^2 (right), fixing $M_\Psi = 800$ GeV. The exclusions are derived from the $\rho^0 \rightarrow l\bar{l}$ searches in [82]. Left panel: in red the excluded region for $c_5 = 1$, in green for $c_5 = 0.5$, in blue for $c_5 = 0$. Right panel: in red the excluded region for $c_6 = 1$, in green for $c_6 = 0.5$, in blue for $c_6 = 0$. The plot also shows the contours of constant Γ/M_{ρ_X} (dashed black lines), of constant ξ (dashed blue lines) and of constant g_Ψ (dashed red lines). The yellow region corresponds to $\xi > 0.4$ 54
- 3.1 A pictorial view of the Composite Higgs framework. 61
- 3.2 The mass spectrum in the gauge (left) and fermionic (right) sectors. 63
- 4.1 One loop diagrams contributing to the wave function renormalization (on the left) and to the running of c'_H (on the right). The external dotted lines denote the background field H_c 90
- 4.2 One-loop diagrams displaying the renormalization of the top quark propagator due to the interaction with the Higgs quantum fluctuations (on the left) and with gluons (on the right). The solid black lines denote the fermion field, either the SM tops or their $\widetilde{\text{SM}}$ mirrors, whereas the curly line stands both for the $SU(3)$ and the $\widetilde{SU}(3)$ gluons. The dashed line stands for the quantum fluctuation. 92

| | | |
|-----|--|-----|
| 4.3 | One-loop diagrams displaying the renormalization of the twin top quark mass. On the left, the diagram correcting the twin top propagator with loops of scalars; in the middle the one generating the four-fermion operator of Eq. (4.38); on the right, the renormalization of the twin top propagator due to the four-fermion interaction. Solid lines indicate the twin quarks, dashed lines the scalar fluctuation. 97 | 97 |
| 4.4 | The one loop-diagrams displaying the generation of the operator \mathcal{O}_\square (on the left) and the renormalization of the twin top mass (one the right). The blob in the last diagram denotes insertions of \mathcal{O}_\square . The external dotted lines indicate the background field, the internal dashed ones the dynamical fluctuation; the solid lines indicate again the twin tops. 99 | 99 |
| 4.5 | IR contributions to the Higgs mass in logarithmic scale, both in the full Twin Higgs theory and in the pure SM: LL contribution (dashed black curve), NLL contribution (dashed dotted black curve), NNLL contribution (thick black curve), LL SM contribution (dashed red curve), NLL SM contribution (dashed dotted red curve), NNLL SM contribution (thick red curve), re-summed total SM contribution (dotted red curve). 103 | 103 |
| 4.6 | Contour plots of the renormalized Higgs mass (in GeV) at NNLL in the plane (m_*, ξ) . . . 103 | 103 |
| 5.1 | Diagrams with loops of twin tops contributing to the β -function of λ_h . Crosses denote mass insertions. The first diagram features two insertions of a dimension-5 operator, while the interaction vertex in the second diagram arises from a dimension-7 operator. 125 | 125 |
| 5.2 | IR contribution to the Higgs mass as a function of the scale m_* for $\xi = 0.1$. The dashed and dot-dashed curves denote respectively the LO and NLO result in a combined perturbative expansion in $(\alpha \log)$ and ξ . The continuous curve corresponds to the NNLO calculation of ref. [122]. 126 | 126 |
| 5.3 | Allowed regions in the (M_Ψ, ξ) plane for $F_1 = 0.3$ (left panel) and $F_1 = 1$ (right panel). See the text for an explanation of the different regions and of the choice of parameters. 136 | 136 |
| 5.4 | Allowed regions in the (c, α) plane, with $c = c_L = c_R$, for $F_1 = 0.3$ (left panel) and $F_1 = 1$ (right panel). The yellow, orange and red regions correspond to $\xi = 0.05$, 0.1 and 0.15 respectively. See the text for an explanation of the choice of the other parameters. 137 | 137 |
| D.1 | Cascade decay branching ratios as a function of the heavier resonance mass, for the benchmark value $g_\rho = 3$, for case (I) (left plot) and case (III) (right plot) of Eq. (D.4). The blue line corresponds to $\text{BR}(\rho_1^+ \rightarrow W^+ \rho_2^0)$ and the red curve corresponds to $\text{BR}(\rho_1^+ \rightarrow \rho_2^+ Z)$ 160 | 160 |

List of Figures

| | | |
|-----|---|-----|
| G.1 | Topology of the diagrams inducing the running of the Wilson coefficients in the Twin sector. The last diagram on the right contains an insertion of c_H in the four-scalars vertex. | 172 |
| J.1 | The one-loop diagram displaying the fermion contribution to the gauge boson vacuum polarization amplitude. Two virtual fermions with generically different masses, m_i and m_j , circulate in the loop. | 182 |
| J.2 | The four one-loop diagrams displaying the fermion contribution to the $Z \rightarrow b_L \bar{b}_L$ vertex. | 185 |
| J.3 | The one-loop diagram displaying the divergent contribution to the $Z \rightarrow b_L \bar{b}_L$ vertex originating from the renormalization of the Z boson propagator. | 186 |

List of Tables

- 2.1 List of the couplings arising before EWSB and their scaling with the strong coupling constant g_{ρ_L} in the mass eigenstate basis, for the ρ_L^μ resonance coupled to top partners. 32
- 2.2 List of the couplings arising before EWSB and their scaling with the strong coupling constant g_{ρ_R} in the mass eigenstate basis, for the ρ_R^μ resonance coupled to top partners. 35
- 2.3 List of the couplings arising before EWSB and their scaling with the strong coupling constant g_{ρ_X} in the mass eigenstate basis, for the ρ_X^μ resonance in models \mathbf{M}_X^1 and \mathbf{M}_X^2 . 39

1 Introduction

The Standard Model (SM) is an elegant and compact theory to describe all the known fundamental interactions between elementary particles. More than a century of experiments have shaped our understanding of nature at its deepest level and the SM emerged as an extremely successful theory in predicting a vast amount of results; its agreement with empirical data is impressive. From the theoretical point of view, decades of developments have made it possible to unify seemingly unrelated phenomena in a comprehensive perspective. In fact, even though the weak, electromagnetic and strong forces appear very different at low-energy scales, they are intimately related and described within the same mathematical language of gauge theories. Specifically, all phenomenological observations indicate that nature can be interpreted at its most fundamental level as a quantum field theory invariant under the gauge group $SU(3)_c \times SU(2)_L \times U(1)_Y$, $SU(3)_c$ accounting for the strong force and $SU(2)_L \times U(1)_Y$ jointly unifying the weak and electromagnetic interactions at short distances. This latter electroweak gauge symmetry, however, is hidden at low-energies, namely it is *spontaneously broken* by the ground state, the vacuum of the theory. The spontaneous breakdown of this symmetry is the origin of the generation of vector boson and fermion masses and it is also the most debated phenomenon of the SM. Despite the abundance of data collected by the Large Hadron Collider (LHC) at CERN, in fact, the dynamics responsible for spontaneously breaking the electroweak symmetry is still unclear, or, at least, the way the SM introduces the mass generation cries out for additional explanations.

The SM accounts for electroweak symmetry breaking (EWSB) in the simplest and most economical way, just by adding one fundamental elementary scalar, the Higgs boson. Together with the would-be Goldstone bosons associated with the third polarization of the massive vectors, the Higgs forms a single multiplet of scalars whose potential is responsible for the generation of a vacuum expectation value (vev) for the Higgs field and ultimately for the origin of fermion and boson masses. The discovery of a Higgs-like scalar resonance at the LHC, with properties stunningly in agreement with the SM expectations, suggests that this theoretical

description is indeed realized in nature and that the dynamics responsible for EWSB is weakly coupled. However, a theoretical problem arises when considering the existence of an elementary scalar, like the Higgs particle. According to our current understanding of quantum field theory, in fact, elementary scalars are unstable under radiative corrections unless there exists a symmetry that is restored when their mass goes to zero [1]¹. In the case of the Higgs boson, no symmetry enhancement appears when its mass, M_H , vanishes, so that this latter should be sensitive to the scale where the SM breaks down and new physics comes into play. Interpreting the SM as an effective field theory valid up to a cut-off scale m_* , the quantum corrections to the Higgs boson mass should therefore make it as heavy as m_* , barring additional fine-tuning of the mass parameter in the theory. This argument can be easily understood on general grounds considering the presence of a relevant operator, the Higgs boson mass term $\mathcal{O}_m = H^\dagger H$, in the SM Lagrangian. Using a Wilsonian approach, the infrared (IR) Lagrangian describing the Higgs boson mass is generated from the ultraviolet (UV) theory as the result of integrating out high-energy degrees of freedom. Using only dimensional analysis, we then expect the IR mass term to be proportional to

$$\mathcal{L}_{Mass} = c m_*^2 H^\dagger H, \quad (1.1)$$

where c is an $\mathcal{O}(1)$ parameter that is originated along the renormalization flow while integrating out the UV modes. The IR scalar mass is consequently related to the UV cut-off by the relation:

$$M_H = c^{\frac{1}{2}} m_*, \quad (1.2)$$

so that we naturally expect to have a small hierarchy between the two scales for c in its $\mathcal{O}(1)$ range.

There would be no theoretical challenge in having an elementary Higgs in the spectrum if we had experimental indications of a small cut-off scale, around a few TeV, for the SM. On the contrary, many of the successes of the SM suggests that m_* be very far in the UV: low energy constraints from flavor changing neutral currents (FCNC), the smallness of neutrino masses and the stability of the proton are just a few examples of phenomena hinting that the SM should be valid up to very small distances. The need of incorporating gravity in a complete description of fundamental interactions at the quantum level would suggest that the SM cut-off be identified with the Planck scale, $M_{Pl} \sim 10^{18}$ GeV, where new physics must necessarily appear. All experimental indications would be consistent with $m_* \sim M_{Pl}$, but according to our

¹This is why elementary fermions can be naturally light, for instance: when the fermion mass goes to zero, *chiral symmetry* is restored. Therefore, all radiative corrections must be proportional to the fermion mass itself, in order to preserve the chiral symmetry restoration at all orders. As a result, the quantum contributions are small and controllable, thus making the fermion mass term naturally light.

previous discussion this would in turn imply the Higgs mass to be very heavy. What the LHC has experimentally discovered is instead a very light Higgs with mass $M_H \sim 125$ GeV, implying the existence of a huge hierarchy between the Higgs mass and the most obvious SM cut-off, the Planck scale. In order to justify this hierarchy, we need to adjust very cleverly the initial conditions for the running of the Higgs mass operator so that the parameter c in the IR turns out to be very small. This is what is usually defined as the *fine-tuning* problem, namely to understand why a parameter that we usually expect to be of $\mathcal{O}(1)$ must be unnaturally small to explain the mass hierarchy between the electroweak scale and the SM cut-off.

An obvious solution to the *hierarchy problem* is to lower the SM cut-off assuming the existence of new physics just above the electroweak scale that justifies the lightness of the Higgs scalar. However, lowering the cut-off immediately spoils the success of the SM in accounting for many experimental facts that need a very high value for m_* . Moreover, there is no experimental evidence yet of the existence of new particles or forces at the TeV scale; the LHC has provided no convincing proof that the SM breaks down any scale near the electroweak one. As a consequence, the most important problem of high energy physics is this intrinsic and unavoidable contradiction between on one side the agreement of the SM with experiments that apparently suggest m_* to be way far in the UV and on the other side the consistency of the SM as an effective field theory that would require a much lower cut-off. Any attempt to solve naturally the hierarchy problem by introducing new physics at the TeV scale forces to model building gymnastics in order to satisfy all the other constraints, especially from flavor physics, that require a much higher cut-off. At the same time, the absence of new signals at the LHC puts all the known natural extensions of the SM under severe pressure and is pushing them into more and more fine-tuned regions. Using naturalness as a guiding principle for new physics searches calls therefore for more clever constructions that could explain the lightness of the Higgs while having a cut-off scale higher than a few TeV. It is the object of this thesis to critically assess such constructions in some detail and provide examples of natural theories beyond the SM that could be in agreement with the absence of new physics signals at the LHC.

Naturalness

The known solutions to the hierarchy problem imply the existence of a New Physics (NP) sector not far above the electroweak (EW) scale that is endowed with a protection mechanism, either a symmetry or the absence of relevant operators, responsible for screening the Higgs boson mass from large radiative corrections and for keeping it light. Following this *naturalness paradigm*, we would expect to find striking new signals and evidence of NP at the LHC, at around the TeV scale. There are different ways to realize this idea, but we can broadly classify them under two categories: *weakly coupled* or *strongly coupled* extensions of the SM. Theories falling in the first category can be analyzed perturbatively and allow a better understanding of

their implications for direct or indirect searches of NP effects, which are calculable. In the case of a new strongly interacting sector, instead, we must give up full calculability and resort to simplified effective models to compute relevant physical quantities, the results being reliable only under certain conditions and in a window of parameter space where the effective models are perturbative. The concrete examples of this two scenarios are *Supersymmetry*, for weakly coupled natural extensions of the SM, and *Composite Higgs* theories, for the strongly coupled solution to the hierarchy problem.

According to the Coleman-Mandula theorem [2, 3], Supersymmetry is the largest possible space-time symmetry of the S-matrix and consists in adding a supersymmetric partner to all the SM particles; the partner has the same quantum numbers except for spin. In particular, in the most economical incarnation like the minimal supersymmetric SM (MSSM), each SM fermion must be related to a new bosonic superpartner, whereas SM bosons are coupled with fermionic superpartners. The known SM particles and their supersymmetric companions form thus supermultiplets, through which the chiral symmetry protecting the light SM fermions is extended to the Higgs sector, solving the hierarchy problem and making the Higgs naturally light. However, no superpartners have been observed yet, so that this scenario must be complemented with an additional supersymmetry breaking mechanism to render the superpartners consistently heavier than the SM particles. In general, this requires the introduction of *soft* supersymmetry breaking operators, so that radiative corrections to the Higgs mass can be kept under control without spoiling the chiral protection offered by unbroken supersymmetry. The scale m_* where NP appears can then be identified with the mass of the soft terms, m_{soft} , in the supersymmetric Lagrangian. In order to reproduce the observed Higgs mass with a fine-tuning which is no worse than 10%, light stops (scalar superpartners of the top quark) must be present in the spectrum; the actual value of the stop masses is model-dependent, but in general they shouldn't be heavier than ~ 1 TeV [5, 6]. Current constraints from LHC direct searches exclude the existence of these new particles up to around the same scale, 1 TeV, pushing the minimal realizations of supersymmetry in more fine-tuned regions [4]. Although the tension between predictions and observations is making the MSSM and other more elaborate realizations of supersymmetry more unnatural, this scenario offers calculability and several other advantages, like gauge coupling unification or candidates for dark matter, thus making it still interesting to explore. We will not focus on supersymmetric extensions of the SM in this thesis, devoting most of our effective models to Composite Higgs (CH) scenarios.

The second possibility for solving the hierarchy problem is offered by the putative existence of a new strongly coupled sector just above the EW scale. This idea exploits the analogy with the known example of QCD to make the Higgs boson a composite scalar, like the QCD pions; these latter are naturally light due to the asymptotic freedom of the SM strong interaction. In QCD,

in fact, the separation between the confinement scale $\Lambda_{QCD} \sim 200$ MeV and the Planck scale is not affected by the hierarchy problem because Λ_{QCD} is generated dynamically by dimensional transmutation due to the running of the strong fine-structure constant, α_s . The scale of QCD, in fact, originates as the scale where α_s becomes strong in the IR:

$$\Lambda_{QCD} = M_{Pl} e^{-\frac{2\pi}{b\alpha_s(M_{Pl})}}. \quad (1.3)$$

The small logarithmic running of the strong coupling, which is related to a marginal operator, ensures that the radiative corrections be always small, so that a huge hierarchy between M_{Pl} and Λ_{QCD} can be generated with only moderately small initial conditions for the strong coupling. No unnaturally small parameters are required in the theory. As a result, the QCD pions are naturally light and are not quadratically sensitive to the scale of NP. To be more specific, the pions can be interpreted as the Goldstone bosons associated with the spontaneous breakdown of chiral symmetry. When the quark masses vanish and before turning on the weak interactions, the QCD Lagrangian enjoys in fact an exact chiral symmetry which is spontaneously broken to its diagonal subgroup when confinement takes place and Λ_{QCD} is generated by dimensional transmutation. As a consequence, several Goldstone bosons (GB) are delivered in the spectrum; restricting to the simplest case of having only two quark flavors, there are three GBs in the IR associated with the $SU(2)_L \times SU(2)_R \rightarrow SU(2)_V$ spontaneous symmetry breaking pattern. The GBs are exactly massless, but, when turning on the electroweak interactions, the chiral symmetry is explicitly broken and a potential for the three pions is generated. Together with the explicit breaking due to the quark masses, this phenomenon generates a mass term for the GBs turning the pions into pseudo Nambu-Goldstone bosons (pNGB). Therefore the pions are not exactly massless, but they must be naturally light because in the limit of vanishing gauge couplings and quark masses they would be the exact GBs of the spontaneous chiral symmetry breaking.

The interesting aspect of the identification of the QCD pions with pNGBs is the fact the phenomenon by which the pions acquire a small mass term is also intimately related with EWSB. Since the QCD vacuum breaks explicitly the EW invariance, in a world without the Higgs particle the gauging of $SU(2)_L \times U(1)_Y$ would result in the Goldstone bosons being eaten by the W and Z particles, while the surviving unbroken electromagnetic group would leave the photon massless. We can write the pion effective action using a standard non-linear sigma model realization of the spontaneous symmetry breaking pattern; the three GBs are incorporated into the Σ matrix,

$$\Sigma(x) = e^{i \frac{\sigma^a \pi^a}{f_\pi}}, \quad (1.4)$$

Chapter 1. Introduction

and the Lagrangian takes the form

$$\mathcal{L}_\pi = \frac{f_\pi^2}{4} \text{Tr} \left[(D_\mu \Sigma)^\dagger D^\mu \Sigma \right], \quad (1.5)$$

where f_π is the pion decay constant, $f_\pi \sim 90$ MeV, and D_μ is the covariant derivative containing the gauge fields. By deriving from Eq. (1.5) the interactions between the GBs and the gauge fields, one finds that the W and Z propagators acquire a pole at the tree-level due to the exchange of pions. The resulting mass term for the gauge bosons is of order $\sim \frac{g f_\pi}{2} \sim 30$ MeV. This is not enough to account for the observed EWSB and the gauge bosons masses, so the SM needs the Higgs sector for a realistic description. Therefore, in the SM only a small fraction of EWSB is due to QCD effects [20]: a combination of the QCD pions and of the GBs from the Higgs sector is eaten to give mass to the gauge bosons, whereas the orthogonal combination remains in the spectrum and it is what we identify as the charged π^\pm and the neutral π^0 .

From our previous discussion, we can imagine to render the SM Higgs sector natural by postulating the existence of a new strongly coupled dynamics just above the EW scale. Exactly like in QCD, this dynamics preserves a global symmetry when the gauge interactions are turned off and when the quark masses are neglected. After confinement, the global symmetry is broken down to an unbroken subgroup, delivering a set of GBs. We can identify the SM GBs with the ones resulting from the spontaneous breaking of the global symmetry in the strong sector; these pions are eaten by the gauge bosons which in turn acquire a mass term. This is in complete analogy with QCD, except that no light pNGB survives in the IR. The simplest realization of this idea is *Technicolor*, a $SU(N_{TC})$ gauge theory with a $SU(2)_L \times SU(2)_R$ flavor group broken down to $SU(2)_V$; the GB decay constant of the new strongly interacting pions is identified with the EW scale. In this simple scenario, however, no light Higgs is present in the spectrum, contradicting the LHC evidence of a new light scalar resonance. Technicolor theories also suffer for other problems, in particular they predict a too big contribution to the \hat{S} parameter and they are strongly constrained by FCNC and other flavor observables at low energies [20]. A more clever construction is required that can accommodate a light Higgs particle, predict its mass in the experimental range and possibly ameliorate the tension with indirect and direct measurements. We will explore now an example of such constructions and try to summarize both its strengths and limitations; this is the CH scenario.

The Composite Higgs

Composite Higgs theories provide a good alternative to simple technicolor models, postulating the existence of a new strongly interacting sector which delivers a light Higgs particle together with the GBs eaten by the gauge fields. Differently from the SM, the Higgs is not elementary and it is naturally light because of the protection offered by the asymptotic freedom of the new

strong fine structure constant, exactly like the pions in QCD. The Higgs emerges as a pNGB of an approximate global symmetry of the strongly interacting dynamics. In general, the global symmetry group G is spontaneously broken down to an unbroken subgroup H ; the scale where the symmetry breakdown takes place is the GB decay constant, f . The process delivers $\dim(G) - \dim(H)$ GBs, part of which are eaten to give mass to the W and Z gauge fields, the remaining being pNGBs. All the SM particles, gauge bosons and fermions, are assumed to be external to the composite sector and are thus elementary. They interact with the strong dynamics either via gauging of the EW group or via linear coupling to the new composite resonances (this is especially valid for fermions). In order to identify the Higgs as one of the pNGBs present in the spectrum, the SM gauge group must be embeddable in the unbroken subgroup H and the coset G/H must contain a $SU(2)_L$ doublet, which is identified with the Higgs doublet. A possible example is the *minimal Composite Higgs model* [19], which we will work out in detail in Chapter 2 of the thesis; the symmetry breaking coset is $SO(5)/SO(4)$ which delivers exactly four GBs to be identified with the Higgs doublet. Other more exotic constructions are also possible, but they involve in general the presence of extra light degrees of freedom.

In all possible realizations, the Higgs potential vanishes at tree-level due to the non-linearly realized Goldstone symmetry. However, the gauging of the SM group and the linear coupling between fermions and operators in the strong sector both explicitly break the global symmetry. A potential for the Higgs doublet is therefore generated at one loop, eventually triggering EWSB. In this way, the EW scale $v \sim 246$ GeV is dynamically generated and it can be smaller than the GB decay constant f . This is different from Technicolor theories, where only one scale is present and v must necessarily coincide with f . The degree of vacuum misalignment between the true vacuum of the theory at the scale f and the preferred orientation generated by the external gauging of the SM group determines the size of the ratio

$$\xi = \left(\frac{v}{f} \right)^2, \quad (1.6)$$

which is a general measure of the degree of fine-tuning in CH theories. For instance, the $SO(5)/SO(4)$ coset is a four-dimensional sphere; the true vacuum of the theory is determined after the first spontaneous symmetry breaking at the scale f . A second spontaneous breaking takes place when the Higgs field acquires a potential due to the radiative corrections originated at one-loop by the interactions with the elementary fields. This phenomenon selects a preferred orientation in the sphere and the angle between this latter and the original vacuum of the theory determines how the EW symmetry is broken and how much fine-tuning the construction suffers. In the most natural case, $v \sim f$ and there is no separation of scales; in the most phenomenologically viable constructions, instead, the vacuum misalignment is such that $v \ll f$ and $\xi \sim 10\%$. For smaller values of ξ , the theory becomes more fine-tuned and less

natural, despite the existence of the symmetry protection provided by the new strong dynamics. Notice that the fine-tuning parameter ξ controls the deviations from the SM theoretical prediction of many observables, including the Higgs couplings and the electroweak precision tests (EWPT). The actual corrections with respect to the SM depend on the specific model realization; in the minimal scenario, for instance, the coupling of the composite Higgs to the gauge bosons is $g_{VVH} = g_{VVH}^{SM} \sqrt{1 - \xi}$, where g_{VVH}^{SM} is the SM prediction. Current measurements of the Higgs couplings at the LHC put an important constraint on the value of the fine-tuning, which must be of the order of $\xi \lesssim 10 - 20\%$ [99] in the most promising scenario. As regards the EWPT, strong limits on the value of ξ are derived when considering the corrections to the \hat{S} and \hat{T} parameters originated by a composite Higgs particle with respect to the SM. In the SM, in fact, all the corrections to the EW parameters must be finite due to the renormalizable nature of the theory. One can show that the divergences that arise from vector polarization diagrams with the Higgs circulating in the loop exactly cancel against those generated by loops of GBs [20, 102]. Since the CH effective theory is non-renormalizable, instead, this cancellation does not hold any more and, in particular, the modified Higgs couplings to the SM gauge fields generate a logarithmically divergent contribution to the gauge boson self-energies [102, 108]. Therefore, the Higgs compositeness introduces a logarithmic sensitivity to the scale where the heavy resonances of the new strong sector reside; this is exactly the SM cut-off scale m_* . One finds

$$\Delta \hat{S} = \frac{g^2}{192\pi^2} \xi \log \left(\frac{m_*^2}{M_H^2} \right), \quad \Delta \hat{T} = -\frac{3(g')^2}{64\pi^2} \xi \log \left(\frac{m_*^2}{M_H^2} \right). \quad (1.7)$$

Measurements at LEP put a strong bound on the value ξ must have in order to satisfy the experimental constraints; in general, $\xi \lesssim 10\%$, similarly to the limit from the Higgs coupling deviation. We shall return on the problem of EWPT in CH theories also in Chapter 5, where we shall analyze in detail under which conditions the EWPT can be satisfied and how they constrain the parameter space of this class of theories.

The Composite Higgs Potential and Light Top Partners

As we saw in the previous discussion, CH models offer the possibility to naturally solve the hierarchy problem exploiting the symmetry protection of strongly coupled Technicolor theories while at the same time allowing the existence of a light scalar resonance identifiable with the Higgs particle. The most important question is now to understand how light a Higgs these scenarios can accommodate and if they are capable of predicting the Higgs mass in the correct experimental range. In general, a light pNGB Higgs comes at the price of having light fermionic resonances connected to the top sector of the theory; they are called *top partners*. The top Yukawa coupling, y_t , breaks in fact the global symmetry G generating a contribution

to the Higgs potential; since y_t is the biggest coupling among the Yukawas and the gauge interactions, its contribution is also the most sizable and relevant. It is then natural to expect that a good prediction for the Higgs mass can be obtained just by computing the top quark effects and how they enter the Higgs effective potential. The result shows that there exists an intimate and structural correlation between the light Higgs mass and the top partners mass, so that a light Higgs with mass $M_H \sim 125$ GeV and a fine-tuning not worse than $\sim 10 - 20\%$ requires the existence of fermionic resonances not heavier than ~ 800 GeV – 1.5 TeV [29–34]. The discovery of such new particles would be a striking evidence of the composite nature of the Higgs and this is why they have been the subject of avid research both experimentally and theoretically. We shall now briefly analyze this connection between a light Higgs and the top partner mass, using only symmetries and selection rules; this will show that, regardless of the model, natural CH theories need resonances at the TeV scale, where the SM effective theory is expected to break down.

We consider for concreteness the minimal composite Higgs model, although the analysis can be easily generalized to other non-minimal scenarios and the conclusions hold for a broader class of theories. The Higgs arises as a pNGB of the $SO(5)/SO(4)$ spontaneous symmetry breaking pattern. In particular, as already seen before, the GBs are parametrized by the matrix

$$\Sigma = e^{i \frac{\sqrt{2}}{f} \Pi^a T^a}, \quad (1.8)$$

where Π^a are the Goldstone fields and T^a are the broken generators. Since we are interested in the top contribution to the Higgs potential, we should focus on the part of the Lagrangian involving the linear coupling between the elementary fermions and the operators in the strong sector. The top-bottom doublet can be then uplifted to a linear representation of the global symmetry through the introduction of *spurions* that allow us to write the elementary-composite mixing Lagrangian in the UV as:

$$\mathcal{L} = y_L \bar{q}_L^\alpha \Delta_{\alpha I}^L \mathcal{O}_R^I + y_R \bar{t}_R \Delta_I^R \mathcal{O}_L^I, \quad (1.9)$$

where the fermionic operators \mathcal{O}_L and \mathcal{O}_R also transform under a linear representation of $SO(5)$. The tensors $\Delta^{L,R}$ are the spurions and they are uniquely determined once the representation for the composite operators is defined. The index α runs over the $SU(2)_L$ gauge representation, whereas I is an $SO(5)$ index depending on the chosen representation for the operators. The parameters $y_{L/R}$ are small couplings in the UV and they are assumed to stay small while flowing to the IR, allowing a perturbative treatment. In the IR, the Lagrangian in Eq. (1.9) translates into a linear coupling between the elementary fermions and the composite fermions excited from the vacuum by the strong sector operators, thus introducing a direct mixing with the top partners. The spurions parametrize the breaking of the global symmetry and they can be associated fictitious transformation properties under $SO(5)$ so that the mixing Lagrangian

Chapter 1. Introduction

is formally invariant under global transformations. This invariance survives in the IR if we write the effective operators as functions of all the possible invariants that can be constructed using the spurions $\Delta^{L,R}$ and their transformation properties. As regards the Higgs potential, it must be a function of all the non-derivative invariant operators containing the Higgs and the spurions. Taking into account that the global symmetry is non-linearly realized, the Σ matrix transforms as

$$\Sigma \rightarrow g \Sigma h^\dagger, \quad (1.10)$$

where $g \in SO(5)$ and $h \in SO(4)$. Using this transformation rule, we can easily construct all the possible invariants arising at the quadratic order in the expansion parameters $y_{L/R}$. We have:

$$\mathcal{J}_L = \text{Tr} \left[\Sigma^\dagger (\Delta^L)^\dagger \Delta^L \Sigma \right], \quad \mathcal{J}_R = \text{Tr} \left[\Sigma^\dagger (\Delta^R)^\dagger \Delta^R \Sigma \right]. \quad (1.11)$$

The actual expression of the invariants depends on the choice of representation for the operators in the strong sector; in general, they are trigonometric functions of the Higgs field. For example, when considering the fundamental representation, one has

$$\mathcal{J}_L \propto \sin^2 \left(\frac{h}{f} \right), \quad \mathcal{J}_R \propto \cos^2 \left(\frac{h}{f} \right) = 1 - \sin^2 \left(\frac{h}{f} \right), \quad (1.12)$$

where h is the Higgs field and the formulae are valid in the unitary gauge. In order to construct a realistic potential which can allow for EWSB, higher order terms must be constructed, since the two invariants have the same functional forms. Analogously to what we did for the quadratic order, we can easily find the operators entering at quartic order, which will bring a functional dependence of the form $\sin^4(h/f)$. The general structure of the potential can be inferred now using dimensional analysis, see for instance [24]. The Higgs effective potential takes therefore the generic form:

$$V(h) = \frac{N_c m_*^2 f^2}{16\pi^2} (c_L y_L^2 + c_R y_R^2) \sin^2 \left(\frac{h}{f} \right) + \frac{N_c f^4}{16\pi^2} c_4 y^4 \sin^4 \left(\frac{h}{f} \right), \quad (1.13)$$

where y collectively indicates terms going like $y_L^4, y_R^4, y_L^2 y_R^2$, N_c is the number of QCD colors and c_L, c_R, c_4 are $\mathcal{O}(1)$ parameters. m_* is generically the scale of the fermionic top partners mass. Notice that the quadratic term in the effective potential is directly sensitive to this scale, whereas quartic contributions only depend on the GB decay constant f by dimensional analysis. A realistic EWSB pattern can now be obtained by tuning the coefficients of the different trigonometric structures against each other, in such a way to derive $\xi \ll 1$ with a light Higgs in the spectrum. The Higgs mass can be estimated from the quartic coupling to be

$$M_H^2 \sim \frac{N_c y_t^2}{16\pi^2} \xi m_*^2. \quad (1.14)$$

For $\xi \sim 0.1$, as required for satisfying EWPT constraints, a Higgs mass of 125 GeV can be predicted only for values of the top partners mass scale of order $m_* \lesssim 1$ TeV. For smaller values of ξ , heavier top partners are needed, but the theory becomes more fine-tuned and less natural. This connection between a light Higgs and light top partners intrinsically depend on the symmetry structure of the theory and, as we have shown, can be easily understood using selection rules for the potential and dimensional analysis. The presence of new fermionic resonances at the TeV remains a general requirement for all the other natural realizations of CH theories, with different coset structures or considering other representations for the composite operators linearly coupled to the elementary fermions.

The prediction of the Higgs mass in the correct experimental range requires finally light top partners in CH theories. Searches for these particles at the LHC have produced negative results so far, putting strong limits on their mass and therefore severely constraining this class of models. Direct measurements exclude the existence of new heavy fermions up to ~ 1 TeV [36, 37, 67–80], implying a growing level of fine-tuning for any CH construction. The contradiction between the need of light resonances and the absence of new signals at the LHC requires a further understanding of our interpretation of naturalness as a guiding principle for new physics. On one side, considering that both supersymmetric and composite natural extensions of the SM are under pressure, we could think to give up naturalness and introduce some new principle or accept the possibility of a huge hierarchy between the EW scale and the Planck scale. On the other, naturalness could be implemented in a more clever way so that the Higgs can be protected by a symmetry without necessarily requiring the existence of new particles close to the TeV scale. We will focus now on this second possibility, showing that natural models exist which are not accompanied by new colored resonances discoverable at the LHC.

Neutral Naturalness

As we saw in the previous discussion, any natural theory beyond the SM requires the existence of new light resonances not heavier than ~ 1 TeV. This is true both for supersymmetric and Composite Higgs theories, the new resonances being the stops in the former case and the top partners in the latter. These new particles have been implicitly assumed to be charged under the SM gauge interactions and, in particular, under color. As a result, they should be copiously produced at the LHC, a proton-proton collider, so that the current limits from direct searches put any of the extensions of the SM under severe pressure. An interesting alternative to these scenarios is to confine the NP responsible for protecting the Higgs from large radiative corrections to a color-blind sector. In this way, the resonances needed to compensate the quantum contributions to the Higgs mass generated by loops of SM particles can be as light as naturally required without being in any way discoverable at the LHC. This

general idea would open up the possibility of saving naturalness as a guiding principle for particle physics while at the same time avoiding any tension with the LHC direct searches. Invoking a *neutral naturalness paradigm*, we can parametrize the NP beyond the SM with two scales. The first one is the scale where a SM-neutral sector reside; this latter is responsible for keeping the Higgs boson light and we can set its scale at $\sim 700 - 800$ GeV for a maximally natural light Higgs. No particle accelerator can detect the light resonances associated with this sector since they are uncolored; only indirect observations, like the Higgs invisible decay width, could give a confirmation of its existence. The second scale is the true SM cut-off m_* where the SM-charged resonances are expected to be found. Differently to the original supersymmetric and composite models, these latter particles do not intervene in the protection of the Higgs mass from large radiative corrections. As a result, they can be as heavy as required to avoid present constraints from direct searches and to be out of the LHC reach. Despite being colored, they are therefore un-discoverable with the existing collider and effectively push the SM cut-off scale up in the TeV range. We could expect to construct a neutral natural theory with $m_* \sim 5 - 10$ TeV. At this scale, a UV completion must be specified and the neutral natural model must be embedded into a composite or supersymmetric picture. Several concrete examples of neutral natural theories have been proposed; the simplest one goes under the name of *Twin Higgs* (TH) [125] and this is the scenario we will mainly be studying throughout this thesis.

The Twin Higgs

Twin Higgs theories represent the most economical realization of neutral naturalness and they offer a simple mechanism to protect the Higgs mass from quadratically divergent corrections while concealing the lightest resonances into a hidden, uncolored mirror world. From the low-energy perspective, these models are characterized by the existence of a mirror copy of the SM, charged under an identical gauge group. More specifically, we introduce a $\widetilde{\text{SM}}$, made up of twin gauge bosons and fermions, and described as a $\widetilde{SU}(3)_C \times \widetilde{SU}(2)_L \times \widetilde{U}(1)_Y$ gauge theory. The two copies of the SM are related by a discrete Z_2 symmetry that interchanges every SM particle with its mirror; if this symmetry were to be exact, it would imply that all the SM gauge and Yukawa couplings be identical with their twins. As we shall see, this symmetry is the crucial ingredient for a naturally light Higgs, although it must be explicitly broken for a phenomenologically viable model [125]. The Higgs sector of TH models enjoys an approximate global $SU(4)$ symmetry which is spontaneously broken down to its $SU(3)$ subgroup. As a result, seven GBs are delivered, six of which are eaten to give mass to the SM gauge bosons and their twins, the last one being identified as the physical Higgs boson. As in CH models, the Yukawa and gauge interactions in the SM and $\widetilde{\text{SM}}$ sectors explicitly break the $SU(4)$ symmetry generating a potential for the Higgs which in turn becomes a pNGB. The

presence of the Z_2 symmetry introduces additional constraints to the form of the quadratically divergent corrections to the Higgs mass, allowing natural EWSB.

To illustrate the model and how the mechanism protects the Higgs mass, let us consider a simple linear realization. The Higgs field is now part of a complex scalar \mathcal{H} forming a fundamental representation of $SU(4)$. Under the $SM \times \widetilde{SM}$ gauge groups, this complex field can be decomposed as $\mathcal{H} = (H, \tilde{H})$, the first doublet being a fundamental of $SU(2)_L$, the second transforming only under $\widetilde{SU}(2)_L$. We can write down a potential of the form

$$V_{TH}(\mathcal{H}) = -\mu^2 \mathcal{H}^\dagger \mathcal{H} + \lambda (\mathcal{H}^\dagger \mathcal{H})^2; \quad (1.15)$$

analogously to what happens in the SM, \mathcal{H} develops a vev, $\langle \mathcal{H} \rangle = \mu/\sqrt{2\lambda} \equiv f$, so that the $SU(4)$ symmetry is spontaneously broken to $SU(3)$. When gauging the $SM \times \widetilde{SM}$ groups, six GBs are eaten and disappear from the spectrum, whereas the Higgs picks up a mass and becomes a pNGB; this mass term must be proportional to the gauge couplings which explicitly break the global symmetry. Focusing for simplicity on the $SU(2)_L$ groups, the one loop corrections generate a quadratically divergent mass term,

$$\Delta V_{TH} = \frac{9g^2 m_*^2}{64\pi^2} H^\dagger H + \frac{9\tilde{g}^2 m_*^2}{64\pi^2} \tilde{H}^\dagger \tilde{H}, \quad (1.16)$$

where \tilde{g} is the twin gauge coupling. Imposing now the Z_2 symmetry, the two gauge couplings must be equal so that $g = \tilde{g}$ and the one-loop corrections can be recombined to form a $SU(4)$ invariant:

$$\Delta V_{TH} = \frac{9g^2 m_*^2}{64\pi^2} \mathcal{H}^\dagger \mathcal{H}. \quad (1.17)$$

Since this latter term does not break the global symmetry, it cannot contribute a potential for the Higgs and no mass term is generated. The Higgs is therefore insensitive to quadratic divergences from gauge loops. This reasoning can be easily extended to the fermionic corrections, in particular in the top sector, and it can be shown that this quadratic divergence cancellation mechanism still holds [125]. The Higgs sector does not feel the scale m_* and it is therefore natural. The particles responsible for this cancellation are SM-blind and cannot be detected at the LHC.

Gauge and top loops will however generate a potential for the Higgs and eventually a mass through the $SU(4)$ breaking term $k (H^4 + \tilde{H}^4)$, which is indeed produced by radiative corrections. Since this is a marginal operator, it cannot be quadratically sensitive to m_* , but it will only be logarithmically dependent on the cut-off scale. k must be of the order

$$k \sim \frac{g^4}{16\pi^2} \log\left(\frac{m_*^2}{gf}\right), \quad (1.18)$$

where g indicates collectively the gauge or Yukawa couplings in the SM sector or in its copy. This term is perfectly natural and under control, the weak scale being dynamically generated and protected from large radiative corrections by the TH mechanism. As we mentioned before, however, this potential is not phenomenologically viable because it contains only a quartic term, whereas a quadratic piece is needed for a minimum to exist. This quadratic term can be generated by breaking the Z_2 parity explicitly. If this breaking is small, it will reintroduce a mass term in the effective potential without worsening the fine-tuning, since the Higgs will be only mildly sensitive to m_* . One way to achieve this goal is to introduce a μ -term that softly breaks the twin parity; for example a contribution of the form $\mu H^\dagger H$ will contribute to the mass allowing a natural pattern of EWSB. Another conceivable possibility is not to gauge the twin hypercharge, introducing an explicit breaking in the far UV that will generate a small difference between the SM couplings and their twins in the IR. In both cases, the known SM Higgs potential can be reproduced once integrating out the twin Higgs doublet \tilde{H} . The mass term will be proportional to the small Z_2 breaking effects, therefore relieving the quadratic dependence on the cut-off scale, whereas the quartic coupling comes naturally as a radiative effect due to loops of SM and $\tilde{\text{SM}}$ particles. The bulk of the contribution to the physical Higgs mass is due to this quantum contributions which should be capable of reproducing its experimental value.

Several questions arise when considering the TH mechanism as a realistic paradigm for EWSB. A first important problem is the embedding of this scenario in a broader picture valid up to the Planck scale. The general features we discussed so far, in fact, are related to the low-energy implementation of the TH scenario, but at the scale m_* , where the SM-charged resonances are expected, we must specify whether the TH is UV-completed into a supersymmetric or a composite picture. We then have to understand how this UV-completion can be constructed and if the TH symmetry protection mechanism is still a valid proposal also when considering the quantum corrections due to new heavy particles. In the IR, the TH allows the cancellation of the quadratically divergent corrections due to the high-energy loop propagation of the light degrees of freedom; in the UV, similar contributions arise when considering loops of supersymmetric or composite resonances. As a consequence, when constructing a realistic UV completion, we must understand under which conditions the TH symmetry protection can be uplifted to a full mechanism that shields the Higgs also from the corrections due to the new high energy sector. A second question is how well any TH scenario, however UV completed, can reproduce the experimental value of the Higgs mass. This problem requires a precise assessment of the radiative corrections to the Higgs effective potential and a derivation of the physical mass beyond the simple one-loop approximation. Finally, as we mentioned above, we might believe that a UV completed TH model could push the SM cut-off scale higher in the TeV range, out of the LHC reach. We may naively estimate this scale as $m_*^{TH} \sim 10$ TeV, but we need actually to be more careful and study for each specific UV completed model if

this is an overestimate of the cut-off and if we need to be more accurate. For example, in composite Higgs models the requirement that the effective constructions be perturbative puts an important constraint on the overall maximum allowed value of the cut-off scale, which may result to be closer to the TeV scale than in the most promising expectations. We shall deal with these problems in the main part of the thesis.

Plan of the Thesis

This thesis is organized as follows.

In Chapter 2, we give a closer look to natural extensions of the SM, in particular to CH theories. We introduce a simplified low-energy effective Lagrangian description of the phenomenology of heavy vector resonances in the minimal composite Higgs model, based on the coset $SO(5)/SO(4)$, analysing in detail their interaction with lighter top partners. Our construction is based on robust assumptions on the symmetry structure of the theory and on plausible natural assumptions on its dynamics. We apply our simplified approach to triplets in the representations $(\mathbf{3}, \mathbf{1})$ and $(\mathbf{1}, \mathbf{3})$ and to singlets in the representation $(\mathbf{1}, \mathbf{1})$ of $SO(4)$. Our model captures the basic features of their phenomenology in terms of a minimal set of free parameters and can be efficiently used as a benchmark in the search for heavy spin-1 states at the LHC and at future colliders. We devise an efficient semi-analytic method to convert experimental limits on $\sigma \times BR$ into bounds on the free parameters of the theory and we recast the presently available 8 TeV LHC data on experimental searches of spin-1 resonances as exclusion regions in the parameter space of the models. These latter are conveniently interpreted as a test of the notion of naturalness.

In Chapter 3, based on an explicit model, we propose and discuss the generic features of a possible implementation of the Twin Higgs program in the context of composite Higgs models. We find that the Twin Higgs quadratic divergence cancellation argument can be uplifted to a genuine protection of the Higgs potential, based on symmetries and selection rules, but only under certain conditions which are not fulfilled in some of the existing models. We also find that a viable scenario, not plagued by a massless Twin Photon, can be obtained by not gauging the Twin Hypercharge and taking this as the only source of Twin Symmetry breaking at a very high scale.

In Chapter 4, we present the Renormalization Group (RG) improvement of the Twin Higgs effective potential at cubic order in logarithmic accuracy. We first introduce a model-independent low-energy effective Lagrangian that captures both the pseudo-Nambu-Goldstone boson nature of the Higgs field and the twin light degrees of freedom charged under a copy of the Standard Model. We then apply the background field method to systematically re-sum all

the one loop diagrams contributing to the potential. We show how this technique can be efficient to implicitly renormalize the higher-dimensional operators in the twin sector without classifying all of them. A prediction for the Higgs mass in the Twin Higgs model is derived and found to be of the order of $M_H \sim 120$ GeV with an ultraviolet cut-off $m_* \sim 10 - 20$ TeV. Irrespective of any possible ultraviolet completion of the low-energy Lagrangian, the infrared degrees of freedom alone are therefore enough to account for the observed value of the Higgs mass through running effects.

In Chapter 5, we analyze the parametric structure of TH theories and assess the gain in fine tuning which they enable compared to extensions of the Standard Model with colored top partners. Estimates show that, at least in the simplest realizations of the TH idea, the separation between the mass of new colored particles and the electroweak scale is controlled by the coupling strength of the underlying UV theory, and that a parametric gain is achieved only for strongly-coupled dynamics. Motivated by this consideration we focus on one of these simple realizations, namely composite TH theories, and study how well such constructions can reproduce electroweak precision data. The most important effect of the Twin states is found to be the infrared contribution to the Higgs quartic coupling, while direct corrections to electroweak observables are sub-leading and negligible. We perform a careful fit to the electroweak data including the leading-logarithmic corrections to the Higgs quartic up to three loops computed in Chapter 4. Our analysis shows that agreement with electroweak precision tests can be achieved with only a moderate amount of tuning, in the range 5-10%, in theories where colored states have mass of order 3-5 TeV and are thus out of reach of the LHC. For these levels of tuning, larger masses are excluded by a perturbativity bound, which makes these theories possibly discoverable, hence falsifiable, at a future 100 TeV collider.

We finally summarize our results and discuss open problems and new directions in the Conclusion, Chapter 6.

2 Hunting composite vector resonances at the LHC: naturalness facing data

The discovery of a new scalar resonance at the LHC marked an important step towards our comprehension of the dynamics hiding behind electroweak symmetry breaking (EWSB). The remarkable compatibility of its properties with those of the Standard Model (SM) Higgs boson and the absence of any new physics predicted by many beyond-the-Standard-Model (BSM) scenarios are forcing us to deeply reconsider the role of naturalness in the dynamics of this particle. A concrete realization of naturalness is offered by the composite Higgs scenario: a new strongly coupled sector confining at the TeV scale and inducing the spontaneous breaking of a global symmetry can produce a light pseudo Nambu-Goldstone boson (pNGB) Higgs at 125 GeV, [14]. Probing the compositeness of the newly discovered scalar is therefore a crucial task for understanding how natural its features are. This is indeed the main question we would like to address in this Chapter: assuming naturalness as a good guiding principle for the existence of a new strongly coupled physics at the TeV scale, how can the presently available LHC data be used to test the validity of our notion of naturalness?

A possible way to answer this question is to study the phenomenological properties and the possibility of a direct discovery of other composite resonances generated by the strong sector. In particular, one of the robust predictions of this class of theories is the existence of spin-1 resonances excited from the vacuum by the conserved currents of the strong dynamics. They form multiplets of the unbroken global symmetry and can behave rather differently from the heavy Z' states in weakly coupled extensions of the SM. These vectors, in fact, interact strongly with the longitudinally polarized W and Z bosons and the Higgs and thus tend to be broader than the weakly coupled ones. The strength of their interactions with the SM fermions depends on whether these latter participate to the strong dynamics or are purely elementary states. A simple possibility is that SM fermions couple to the EWSB dynamics according to their masses, so that the lightest ones are the most weakly coupled. This idea has an elegant implementation in the framework of partial compositeness [15] and can give a qualitative understanding of the hierarchies in the Yukawa matrices of the SM fermions in terms of RG

flows [18, 19]. A second robust characteristic of composite Higgs models is the existence of spin-1/2 resonances, the top partners. In the most natural realizations, these fermionic states are lighter than the heavy vector particles, [29–34]. In a natural scenario we therefore expect the phenomenology of spin-1 states to be significantly affected by the presence of lighter composite fermions.

In this Chapter, we study the phenomenology of spin-1 resonances in composite Higgs theories by means of a simplified description based on an effective Lagrangian, focussing on their interaction with lighter top partners. This is aimed at capturing the main features relevant for the production and decay of the heavy vectors at high-energy colliders and their effects in low-energy experiments, avoiding the complications of a full model. Although simplified, our procedure will be sophisticated enough to properly include those aspects which are distinctive predictions of the class of theories under consideration, such as for example the pNGB nature of the Higgs boson. We will focus on the minimal $SO(5) \times U(1)_X / SO(4) \times U(1)_X$ composite Higgs model and consider vector triplets transforming as a $(\mathbf{3}, \mathbf{1})$ and $(\mathbf{1}, \mathbf{3})$ of $SO(4) \sim SU(2)_L \times SU(2)_R$ and vector singlets transforming only under the unbroken $U(1)_X$. We will study in detail the interactions of these bosonic states with top partners and include the effects implied by the partial compositeness of SM fermions. The importance of lighter composite fermions on the phenomenology of vector resonances has been pointed out also in [47] and in [51]; this latter considered the case of a $SU(2)_L$ charged heavy spin-1 state. Our approach, however, differs for the method used in deriving the effective Lagrangian and for taking into account all the spin-1 resonances in the simplest representations of H .

Our construction provides a benchmark model to be used in searches for heavy spin-1 states at the LHC and at future colliders. A simple kinematic model based on the width and the production cross section times decay branching ratio ($\sigma \times BR$) is sufficient to guide searches for narrow resonances in individual channels and to set limits, see the discussion in [40]. However, combining the results obtained in different final states as well as interpreting the limits on $\sigma \times BR$ in explicit models of BSM physics and developing a detailed analysis of the interaction with lighter fermionic states requires an underlying dynamical description, such as the one given by a simplified Lagrangian. Here we provide such a dynamical description for spin-1 resonances coupled to lighter top partners appearing in a natural and sufficiently large class of composite Higgs theories. Our simplified Lagrangian fully takes into account the non-linear effects due to multiple Higgs vev insertions and does not rely on an expansion in v/f , where v is the electroweak scale and f is the decay constant of the pNGB Higgs. In the limit $v/f \ll 1$, it can be matched onto the more general one of [40], which covers a more ample spectrum of possibilities in terms of a larger number of free parameters. In this sense, the main virtue of our model is that of describing the phenomenology of spin-1 resonances in composite Higgs theories in terms of a minimal set of physical quantities: one mass and

one coupling strength for each heavy vector. Expressing the experimental results in such a restricted parameter space is thus extremely simple and gives an immediate understanding of the reach of current searches in the framework of strongly interacting models for EWSB. It also provides an immediate way to test how natural the Higgs sector is expected to be.

This Chapter is organized as follows. In Section 2.1, we review the most important characteristics of the minimal composite Higgs model that are relevant for our construction and we analyse the dynamical assumptions that justify our effective Lagrangian approach. In Section 2.2, we introduce the models for the three vector resonances under consideration and we discuss their mass spectrum and physical interactions.¹ The main production mechanisms and decay modes are discussed in Section 2.3, where we describe the most important channels that can be relevant for a future discovery at the LHC. The presently available 8 TeV LHC data are used to derive exclusion limits on the parameter space of our models in Section 2.4. Our conclusions are finally summarized in Section 2.5.

2.1 Behind the models

Our main purpose is to introduce an effective Lagrangian description of the interactions between heavy vectors and top partners in the minimal composite Higgs scenario. We aim at deriving a simplified model, based on a minimal set of free parameters, which is suitable for studying the production and decay of these new heavy states at colliders, but still capable of capturing the most important features of the underlying strong dynamics. We will indeed make some robust assumptions on the symmetry structure of the theory, dictated by the pNGB nature of the Higgs, and some plausible dynamical assumptions on its spectrum, dictated by naturalness arguments, that can provide enough information to determine the most prominent phenomenological aspects of these constructions.

2.1.1 The symmetry structure and the degrees of freedom

We start analysing the basic features of the minimal composite Higgs model that will have relevant consequences for the phenomenology of the heavy resonances. We assume the existence of a new strongly interacting sector with an approximate global symmetry in the UV, $G = SO(5) \times U(1)_X$, spontaneously broken to $H = SO(4) \times U(1)_X \sim SU(2)_L \times SU(2)_R \times U(1)_X$ at an energy scale f .² The four Goldstone bosons, $\Pi^{\hat{a}}$, resulting from the spontaneous breaking of the global symmetry transform as a $(\mathbf{2}, \mathbf{2})_0$ under the linearly-realized unbroken subgroup, H ; in the absence of an explicit breaking of $SO(5)$ they are exactly massless. The SM electroweak

¹Part of the results appearing in this section has already been presented in [52].

²The abelian group $U(1)_X$ must be included in order to reproduce the correct hypercharge of the fermion fields, which is given by $Y = T_R^3 + X$, T_R^3 being the third generator of $SU(2)_R$

bosons gauge the $SU(2)_L \times U(1)_Y$ subgroup of the global group, thus introducing a preferred orientation in the coset space $SO(5)/SO(4)$ with respect to the global $SO(4)$. The misalignment between the direction fixed by the local group and the vacuum where the theory is realized can be conveniently parametrized by an angle θ , which serves as an order parameter for EWSB, [8]. The interaction between the Goldstone bosons and the SM fields explicitly breaks the global symmetry and generates a potential for the Higgs at loop level resulting in a non-vanishing vev for its modulus. As a consequence, three Goldstone bosons are eaten to give mass to the SM gauge bosons and a massive Higgs field, $h(x)$, remains in the spectrum. The misalignment angle can be identified as $\theta = \langle h \rangle / f$ and the electroweak scale is dynamically generated at $v = f \sin \theta$. It is convenient to introduce the parameter

$$\xi = \sin^2 \theta = \left(\frac{v}{f} \right)^2 \quad (2.1)$$

characterising the separation between the electroweak and the strong scale; in a natural theory, we expect $\xi \sim 1$, but it is conceivable that a small amount of tuning can give rise to $\xi \ll 1$. In particular, compatibility with the constraints coming from electroweak precision tests and Higgs coupling measurements generically implies $\xi \lesssim 0.2$, [40, 53, 56].

In this framework, we will construct effective Lagrangians respecting the non-linearly realized $SO(5)$ global group using the standard CCWZ formalism, as developed in [9] and [10]. According to this procedure, a Lagrangian invariant under the global $SO(5)$ can be written following the rules of a local $SO(4)$ symmetry; the basic building blocks are given by the Goldstone boson matrix, $U(\Pi)$, and the d_μ and E_μ symbols, resulting from the Maurer-Cartan form $U^\dagger D_\mu U$, which are reviewed in Appendix A.

Considering now the degrees of freedom, they comprise elementary states, which include the gauge bosons W_μ and B_μ and the SM fermions, and composite states, which, besides the pNGB Higgs and the longitudinally polarized W and Z bosons, include particles with specific transformation properties under the unbroken $SO(4)$. As regards the interactions between these two sectors, the gauge bosons couple through the gauging of the SM subgroup of G , whereas the elementary fermions couple linearly to the composite dynamics, according to the paradigm of partial compositeness, [13]. Since this linear interaction is responsible for generating the masses of leptons and quarks, we expect the heaviest SM fermions to be more strongly coupled to the new sector and to have the strongest interactions with the composite resonances. At the energy scale that can be probed at the LHC, it is therefore a well justified approximation to consider all leptons and quarks, except for the heaviest doublet $q_L = (t_L, b_L)$ and the right-handed top quark t_R , to be fully elementary and massless, so that we can neglect their linear coupling to the strong dynamics. On the other hand, the top-bottom doublet is taken to have a direct linear interaction with an operator $\mathcal{O}_{\mathcal{R}}$, transforming in a representation

$r_{\mathcal{O}}$ of $SO(5) \times U(1)_X$, so that in the UV the Lagrangian is:

$$\mathcal{L} = y_L \bar{q}_L^\alpha \Delta_{\alpha, I_{\mathcal{O}}} \mathcal{O}_{\mathcal{R}}^{I_{\mathcal{O}}} + \text{h.c.} = y_L (\bar{Q}_L)_{I_{\mathcal{O}}} \mathcal{O}_{\mathcal{R}}^{I_{\mathcal{O}}} + \text{h.c.}, \quad (2.2)$$

where $I_{\mathcal{O}}$ denotes the indices of the operator $\mathcal{O}_{\mathcal{R}}$ and $(\bar{Q}_L)_{I_{\mathcal{O}}} = \bar{q}_L^\alpha \Delta_{\alpha, I_{\mathcal{O}}}$ indicates the embedding of q_L into a full representation of $SO(5)$, as discussed in [20]. This kind of mixing explicitly breaks the global symmetry of the strong dynamics, $y_L \Delta$ being a spurion under G , generating a contribution to the Higgs potential via loop effects. In order to obtain a sufficiently light Higgs, we therefore expect y_L to be a relatively small parameter. The choice of the representation $r_{\mathcal{O}}$ does not depend on the details of the low-energy physics and it is to some extent free. Many possibilities have been studied in the literature, [7, 42]; for simplicity, we will only consider the minimal case where $r_{\mathcal{O}} = \mathbf{5}_{2/3}$, so that the form of the embedding will be unambiguously fixed:

$$(Q_L^5)_I = \frac{1}{\sqrt{2}} (i b_L \quad b_L \quad i t_L \quad -t_L \quad 0)^T, \quad (2.3)$$

which formally transforms under $g \in SO(5)$ as $(Q_L^5)_I \rightarrow g_I^J (Q_L^5)_J$ and has X -charge equal to $2/3$. As regards the t_R , we will consider two different scenarios. First, we will assume that this particle arises as a composite resonance of the strong sector, transforming like a singlet under $SO(4)$ and with hypercharge $2/3$. Then, similarly to what happens to the heaviest doublet, we will be interested in studying the phenomenological implications of a partially composite t_R , for reasons that will become clear in the following. In this particular case, the t_R is assumed to be linearly coupled to an operator \mathcal{O}_L of the strong sector transforming as a $\mathbf{5}_{2/3}$, with the UV lagrangian

$$\mathcal{L} = y_R \bar{t}_R \Delta_I \mathcal{O}_L^I + \text{h.c.} = y_R (\bar{Q}_R^5)_I \mathcal{O}_L^I + \text{h.c.}, \quad (2.4)$$

where the embedding is in this case fixed by the standard model quantum numbers to be:

$$(Q_R^5)_I = (0 \quad 0 \quad 0 \quad 0 \quad t_R)^T. \quad (2.5)$$

$(Q_R^5)_I$ formally transforms under $SO(5)$ like $(Q_L^5)_I$ and has X -charge $2/3$. The parameter y_R is expected to be of the order of the corresponding y_L in order to accommodate a reasonably tuned light Higgs in the spectrum.

We have discussed all the basic ingredients of the model, concerning both the new symmetries and the particles we have to deal with. In this work, as highlighted in the Introduction, we will be mainly interested in studying the phenomenology of composite spin-1 states, ρ_μ , focusing on triplets transforming as a $(\mathbf{3}, \mathbf{1})_0$ and $(\mathbf{1}, \mathbf{3})_0$ under the unbroken $SO(4) \times U(1)_X$ and on vector singlets, which are left invariant by $SO(4)$ and transform only under the abelian group $U(1)_X$,

analysing in detail their interplay with lighter spin-1/2 heavy states.

2.1.2 Dynamical assumptions

Since we aim at building a simplified description of the interactions between vectors and top partners, we need to make some generic assumptions on the dynamics of the strong sector that can guide us in the construction of an effective Lagrangian and can give a basic understanding of its regime of validity. Following the SILH approach, [24], we can broadly parametrize the new confining dynamics with a mass scale m_* and a coupling g_* , which are related by the NDA estimate

$$m_* \sim g_* f, \quad (2.6)$$

reproducing the usual relation between the Goldstone boson decay constant and the mass of the composite states. We will however generalize this simple approximation, taking into account both the theoretical implications of naturalness and the constraints coming from electroweak precision tests. On the theoretical level, in fact, we naturally expect the fermionic resonances to be light, since they are directly responsible for cutting off the quadratically divergent contributions to the Higgs mass coming from the SM top quark loops, as explained in [29–34]. In particular, a reasonably tuned pNGB Higgs generically requires top partners to have a mass around 1 TeV. On the other hand, as described also in Appendix B, vector resonances contribute at tree level to the \hat{S} parameter, thus implying their mass to be generically bigger than 2 TeV.

These considerations are the main reason for parametrizing the confining dynamics with two different scales, a lighter one for the spin-1/2 and a heavier one for the spin-1 resonances, pointing towards a natural scenario where the phenomenology of vector particles can be considerably affected by the presence of a lower-lying layer of fermionic states. We therefore introduce a mass scale, m_ψ , and a coupling, g_ψ , for the top partners, such that

$$m_\psi = a_\psi g_\psi f, \quad (2.7)$$

and a mass scale, m_ρ , and a coupling, g_ρ , for the vector resonances, with the analogous relation

$$m_\rho = a_\rho g_\rho f, \quad (2.8)$$

where a_ψ and a_ρ are $O(1)$ parameters, as implied by NDA. Supposing the fermionic scale to be smaller than the vector scale therefore implies the obvious relation between the two couplings

of the new dynamics:

$$g_\psi < \frac{a_\rho}{a_\psi} g_\rho. \quad (2.9)$$

In particular, a naturally light composite Higgs generically requires the fermionic coupling constant to be favoured in the range $1 \lesssim g_\psi \lesssim 3$. We will be mainly interested in studying how these assumptions on the strong sector can be tested in the context of a phenomenological model for the production of heavy spin-1 states and their decay to top partners and SM particles.

We have some other considerations to make on the two scales in order to justify our effective Lagrangian approach. Following the criterion of *partial UV completion*, firstly introduced in [8], we assume that the bosonic resonances we want to study have a mass M_ρ much lower than the vector scale and bigger than the fermionic scale, $m_\psi < M_\rho \ll m_\rho$, so that we can integrate out all the heavier states and write a Lagrangian in an expansion of M_ρ/m_ρ . This approximation obviously starts loosing its validity as soon as the mass separation becomes smaller, $m_\psi \ll M_\rho \sim m_\rho$, in which case the interference effects with other resonances become non-negligible and our analysis is only a qualitative description of the underlying dynamics. We apply this point of view to the triplets in the representation $(\mathbf{3}, \mathbf{1})_0$, ρ_μ^L , and $(\mathbf{1}, \mathbf{3})_0$, ρ_μ^R , and to the singlet, ρ_μ^X , building one model for each of them. In every case we will suppose that the other two vectors have a mass $M_\rho \sim m_\rho$, so that they belong to the tower of heavier resonances that are being integrated out, resulting in a great simplification of the phenomenology. This assumption is dictated mainly by the need of building the simplest description of the interplay between heavy vectors and top partners and we have no deep reasons for excluding the opposite case, namely that the spin-1 resonances are almost degenerate in mass. We will however make some comments about this possibility in Appendix D, showing under which conditions the mutual interaction between the vectors can be safely neglected even when their spectrum is degenerate.

Finally, we must discuss the role of the fermionic scale in our effective expansion. In fact, since we are about to derive a phenomenological Lagrangian which is valid up to the first vector resonance, we should in principle include its interactions with all the fermions at the scale m_ψ and falling into various representations of the unbroken $SO(4)$. In order to avoid the complications arising from such a full model, we will only take into account the lightest heavy fermions, assuming that their mass satisfies the condition $M_\Psi < m_\psi$, so that the decay channel of the vectors to these fermionic states is the most favoured one among the decays to other resonances. Under this conditions, we can more safely neglect the remaining tower of spin-1/2 states. For our construction to be fully meaningful, we need a criterion to understand under which representation of $SO(4)$ the lightest heavy fermions should transform. This is easily found by noticing that in explicit models the lightest fermionic resonances that must be

present in the spectrum are the top partners falling into the representations of H that can be excited from the vacuum by the operators \mathcal{O}_R and \mathcal{O}_L linearly coupled to the q_L doublet and the t_R , when this latter is partially composite, [30]. Since we chose $r_{\mathcal{O}} = 5_{2/3}$ for both cases, we can decompose \mathcal{O}_R and \mathcal{O}_L under $SO(4)$, obtaining $5_{2/3} = 4_{2/3} + 1_{2/3}$, therefore justifying the introduction of top partners in the fourplet and in the singlet of the unbroken group. Moreover, we must notice that limiting our analysis to the lightest fermionic resonances becomes a very crude approximation when $M_\Psi \sim m_\psi$, requiring a more complete construction; we leave this study to future work, with the aim to provide in the present analysis a simplified model with a few degrees of freedom and parameters that can be more thoroughly used to guide searches of new physics at the LHC.

We now have all the elements to derive a phenomenological Lagrangian describing the interplay between vector and fermion resonances, based on symmetry principles and general reasonable assumptions on the nature of the strong dynamics. In conclusion, we will write three models, one for a ρ_μ^L and top partners in the fourplet, one for a ρ_μ^R and again top partners in the fourplet, and a last one for a ρ_X^μ and top partners in the singlet.

2.2 The models

After the clarification of the symmetries and the dynamical assumptions behind our approach, we are now in a good position for explicitly introducing the Lagrangians for the three vector resonances. We will devote this section to describe the three models and some of their basic phenomenological characteristics.

2.2.1 A Lagrangian for ρ_μ^L

We start considering a theory for the $(\mathbf{3}, \mathbf{1})_0$ triplet and top partners in the fourplet, introducing therefore the fermionic field

$$\Psi = \frac{1}{\sqrt{2}} \begin{pmatrix} iB - iX_{5/3} \\ B + X_{5/3} \\ iT + iX_{2/3} \\ -T + X_{2/3} \end{pmatrix}, \quad (2.10)$$

which has X-charge 2/3. The vector resonance transforms non-homogeneously under the unbroken $SO(4)$,

$$\rho_\mu^L \rightarrow h(\Pi, g) \rho_\mu^L h^\dagger(\Pi, g) - i h(\Pi, g) \partial_\mu h^\dagger(\Pi, g), \quad (2.11)$$

where $h(\Pi, g) \in SO(4)$, as described in Appendix A. The partner field transforms instead linearly, so that

$$\Psi \rightarrow h(\Pi, g)\Psi, \quad (2.12)$$

and it decomposes into two doublets under $SU(2)_L \times U(1)_Y$, the (T, B) doublet with the same quantum numbers of top and bottom quarks and the $(X_{5/3}, X_{2/3})$ doublet with an exotic particle of charge 5/3 and a second top-like resonance, $X_{2/3}$.

Following now the CCWZ prescription and considering the t_R a full composite condensate of the strong sector, at leading order in the derivative expansion the Lagrangian is:

$$\mathcal{L}_L = \mathcal{L}_{light} + \mathcal{L}_\Psi + \mathcal{L}_{\rho_L}, \quad (2.13)$$

where the three different contributions stand for:

$$\begin{aligned} \mathcal{L}_{light} &= \frac{f^2}{4} (d_\mu^a)^2 - \frac{1}{4} W_{\mu\nu}^a W^{a\mu\nu} - \frac{1}{4} B_{\mu\nu} B^{\mu\nu} + \bar{\psi} \gamma^\mu (i\partial_\mu + g_{el} \frac{\sigma^a}{2} W_\mu^a P_L + g'_{el} Y B_\mu) \psi \\ &\quad + i \bar{q}_L \mathcal{D} q_L + i \bar{t}_R \mathcal{D} t_R, \\ \mathcal{L}_\Psi &= \bar{\Psi} \gamma^\mu (i\nabla_\mu + X g'_{el} B_\mu - M_\Psi) \Psi + [i c_1 \bar{\Psi}_R^i \mathcal{D}_i t_R + y_L f (\bar{Q}_L^5)^I U_{Ii} \Psi_R^i \\ &\quad + y_L c_2 f (\bar{Q}_L^5)^I U_{I5} t_R + \text{h.c.}], \\ \mathcal{L}_{\rho_L} &= -\frac{1}{4} \rho_{\mu\nu}^{a_L} \rho^{a_L\mu\nu} + \frac{m_{\rho_L}^2}{2g_{\rho_L}^2} (g_{\rho_L} \rho_\mu^{a_L} - E_\mu^{a_L})^2 + c_3 \bar{\Psi}^i \gamma^\mu (g_{\rho_L} \rho_\mu^{a_L} - E_\mu^{a_L}) T_{ij}^{a_L} \Psi^j. \end{aligned} \quad (2.14)$$

In the first Lagrangian, containing the kinetic terms of the elementary sector, the composite Goldstone bosons and third family quarks, we have collectively indicated with ψ all the massless fermions, namely the leptons and the first two quark families, so that the ψ field has to be understood as a sum over these different species. The second Lagrangian, \mathcal{L}_Ψ , on the other hand, describes the kinetic term of the top partners and their interactions with third family quarks, which are generated in the IR by the UV Lagrangian (2.2). We have used the notation of Appendix A to indicate the CCWZ covariant derivative, ∇_μ , which is necessary to respect the non-linearly realised $SO(5)$, and we have added the contribution of the B_μ field in order to preserve the SM gauge invariance. Finally, the last Lagrangian, \mathcal{L}_{ρ_L} , introduces the kinetic and mass terms of the vector resonance and its interaction with the top partners. In particular, since ρ_L transforms non-homogeneously under the unbroken $SO(4)$, the field strength must be

$$\rho_{\mu\nu}^{a_L} = \partial_\mu \rho_\nu^{a_L} - \partial_\nu \rho_\mu^{a_L} + g_{\rho_L} \epsilon^{a_L b_L c_L} \rho_\mu^{b_L} \rho_\nu^{c_L}. \quad (2.15)$$

We note that additional higher derivative operators can in general be included in the previous Lagrangian and they can play a relevant role at energies of order of the resonances mass, as

discussed for example in [8]. We will omit them for simplicity, referring to [40] for a more complete discussion of the effects of these additional terms on the phenomenology of vector resonances.

From Eq. (2.14), we immediately see that the only source of interactions among the composite ρ_L and the elementary gauge fields is the $\rho_L - W$ and the $\rho_L - B$ mass mixings that follow from the mass term in \mathcal{L}_{ρ_L} . Given the expression of the CCWZ connections, the global mass matrix of spin-1 fields (W, B, ρ_L) is non-diagonal and must be diagonalised by a proper field rotation, in order to obtain the couplings and the Lorentz structure of the vertices in the mass eigenstate basis. Similarly, the mass matrix of these spin-1/2 fields arising from the Lagrangian \mathcal{L}_Ψ is in general non-diagonal and we need another rotation, on the fermionic sector, in order to describe the particle spectrum.

Before discussing the two rotations, let us first count how many parameters appear in our Lagrangian. There are eight couplings, $(g_{el}, g'_{el}, g_{\rho_L}, c_1, c_2, c_3, y_L, f)$, two mass scales, (m_{ρ_L}, M_Ψ) , and the misalignment angle, that can be conveniently traded for the variable ξ , for a total of eleven free parameters. Notice that we have listed the NG decay constant f as a coupling, since it controls the strength of the NG boson interactions. The couplings g_{el} and g'_{el} arise as a result of the weak gauging of the SM subgroup of H , g_{ρ_L} instead sets the strength of the interactions between the vectors and other composite states, including the Higgs and the longitudinally polarized W and Z bosons, whereas c_1, c_2 and c_3 are $O(1)$ parameters, as suggested by power counting. All the Lagrangian input parameters can be re-expressed in terms of physical quantities in the mass eigenstate basis. Three of them must be fixed in order to reproduce the basic electroweak observables, which we conveniently choose to be G_F , α_{em} and m_Z . Of the remaining eight input parameters, ξ controls the modifications of the Higgs couplings from the SM values and is thus an observable, c_2 will be fixed in order to reproduce the physical top mass and the other six can be traded for the following physical quantities: the masses of two top partners, for instance $m_{X_{5/3}}$ and m_B , the mass of the charged heavy vector and its couplings to elementary fermions and to the top-bottom pair, and finally the coupling of one heavy fermion to a gauge boson and top quark.

In order to fix three of the input parameters in terms of G_F , α_{em} and m_Z , we need the expression of the latter in terms of the former. It turns out that G_F and α_{em} are very simple to compute and read:

$$G_F = \frac{1}{\sqrt{2}f^2\xi}, \quad \frac{1}{4\pi\alpha_{em}} = \frac{1}{g_{el}^2} + \frac{1}{g_{\rho_L}^2} + \frac{1}{g_{el}'^2} = \frac{1}{g^2} + \frac{1}{g'^2}, \quad (2.16)$$

where we have conveniently defined the SM coupling g and g' as

$$\frac{1}{g^2} \equiv \frac{1}{g_{el}^2} + \frac{1}{g_{\rho_L}^2}, \quad g' \equiv g'_{el}. \quad (2.17)$$

It is important to notice that α_{em} does not get corrections after EWSB at any order in ξ , due to the surviving electromagnetic gauge invariance. The formula for G_F can be most easily derived by integrating out first the composite ρ using the equations of motion at leading order in the derivative expansion, $\rho_\mu^{a_L} = E_\mu^{a_L} + O(p^3)$. From equation (2.14), one can then see that the low-energy Lagrangian for the elementary fields contains one extra operator, $(E_{\mu\nu}^L)^2$, which however does not contribute to G_F . This means that the expression of G_F in terms of the elementary parameters does not receive any tree-level contribution from the composite ρ , hence the simple formula in (2.16). Finally, the expression for m_Z is in general quite complicated and can be obtained only after the rotation to the mass eigenstate basis; we will not report it here, but we will discuss its approximation while describing the physical spectrum of our theory. By making use of such a formula and of equation (2.16), for given values of the other input parameters, we can fix g_{el} , g'_{el} and f so as to reproduce the experimental values of G_F , α_{em} and m_Z .

We now discuss the rotation to the mass eigenstate basis and the physical spectrum of the model. As regards the fermionic mass matrix, it has already been extensively analysed in [7] and we will not examine here the details, limiting ourselves to report the basic results. After the diagonalization, it is straightforward to derive the masses of the top quark and of the four top partners; they are found to be:

$$\begin{aligned} m_{top} &= \frac{c_2 y_L f}{\sqrt{2}} \frac{M_\Psi}{\sqrt{M_\Psi^2 + y_L^2 f^2}} \sqrt{\xi} [1 + O(\xi)], & m_{X_{5/3}} = m_{X_{2/3}} = M_\Psi, \\ m_T &= \sqrt{M_\Psi^2 + y_L^2 f^2} - \frac{y_L^2 f^2 (M_\Psi^2 - (c_2^2 - 1) y_L^2 f^2)}{4 (M_\Psi^2 + y_L^2 f^2)^{3/2}} \xi + O(\xi^2), & m_B = \sqrt{M_\Psi^2 + y_L^2 f^2}, \end{aligned} \quad (2.18)$$

where we have listed the expressions at leading order in ξ . The lightest top partners are $X_{5/3}$ and $X_{2/3}$, whose mass is exactly equal to the Lagrangian parameter M_Ψ and does not receive any correction after EWSB; in particular the $X_{5/3}$ particle cannot mix because of its exotic charge and it is left invariant by the rotation. The B fermion is the heaviest particle and also in this case its mass is not altered after EWSB. The T partner, on the other hand, is relatively lighter than B , due to $O(\xi)$ corrections, whereas the bottom quark remains massless, since we are not including the linear coupling of b_R to the strong sector. This latter interactions will in general induce small corrections to the above relations of order $O(m_b/m_{top})$. In order to obtain the correct order of magnitude for the top mass, we expect $y_L \sim y_t$, where y_t is the top Yukawa coupling. We will use the above expression for m_{top} in the following in order to fix the parameter c_2 to reproduce the top quark mass. Finally, neglecting EWSB effects, we can find

very simple expressions for the rotation angles; the mass matrix is in fact diagonalised by the following field rotation:

$$t_L \rightarrow \frac{M_\Psi}{\sqrt{y_L^2 f^2 + M_\Psi^2}} t_L - \frac{y_L f}{\sqrt{y_L^2 f^2 + M_\Psi^2}} T_L, \quad b_L \rightarrow \frac{M_\Psi}{\sqrt{y_L^2 f^2 + M_\Psi^2}} b_L - \frac{y_L f}{\sqrt{y_L^2 f^2 + M_\Psi^2}} B_L, \quad (2.19)$$

with the T_L and B_L particles transforming orthogonally. The right-handed t_R , T_R and B_R and the top partner $X_{\frac{2}{3}}$ are instead left unchanged.

Let us now focus on the spin-1 sector of the theory. The mass term of the Lagrangian can be written as

$$\mathcal{L}_{mass} = X^+ M_\pm^2 X^- + \frac{1}{2} X^0 M_0^2 X^0, \quad (2.20)$$

where $X^\pm = (X^1 \pm iX^2)/\sqrt{2}$, with $X^{1,2} = \{W^{1,2}, \rho_L^{1,2}\}$, and $X^0 = \{W^3, \rho_L, B\}$. The mass matrix therefore decomposes in a 2×2 charged block, M_\pm^2 , and a 3×3 neutral block, M_0^2 . The expression for the charged sector is

$$M_\pm^2 = \begin{pmatrix} \frac{g_{\text{el}}^2}{4g_{\rho_L}^2} (g_{\rho_L}^2 f^2 \xi + A(\xi) m_{\rho_L}^2) & -\frac{g_{\text{el}}}{2g_{\rho_L}} B(\xi) m_{\rho_L}^2 \\ -\frac{g_{\text{el}}}{2g_{\rho_L}} B(\xi) m_{\rho_L}^2 & m_{\rho_L}^2 \end{pmatrix}, \quad (2.21)$$

while the neutral block can be easily found to be

$$M_0^2 = \begin{pmatrix} \frac{g_{\text{el}}^2}{4g_{\rho_L}^2} (g_{\rho_L}^2 f^2 \xi + A(\xi) m_{\rho_L}^2) & -\frac{g_{\text{el}}}{2g_{\rho_L}} B(\xi) m_{\rho_L}^2 & \frac{g_{\text{el}} g'_{\text{el}}}{4g_{\rho_L}^2} (m_{\rho_L}^2 - f^2 g_{\rho_L}^2) \xi \\ -\frac{g_{\text{el}}}{2g_{\rho_L}} B(\xi) m_{\rho_L}^2 & m_{\rho_L}^2 & -\frac{g'_{\text{el}}}{2g_{\rho_L}} C(\xi) m_{\rho_L}^2 \\ \frac{g_{\text{el}} g'_{\text{el}}}{4g_{\rho_L}^2} (m_{\rho_L}^2 - f^2 g_{\rho_L}^2) \xi & -\frac{g'_{\text{el}}}{2g_{\rho_L}} C(\xi) m_{\rho_L}^2 & \frac{(g'_{\text{el}})^2}{4g_{\rho_L}^2} (g_{\rho_L}^2 f^2 \xi - D(\xi) m_{\rho_L}^2) \end{pmatrix}, \quad (2.22)$$

where we have expressed the misalignment angle θ as a function of ξ , according to equation (A.28), and we have defined the functions

$$\begin{aligned} A(\xi) &= \left(2\sqrt{1-\xi} + 2 - \xi \right), & B(\xi) &= \left(1 + \sqrt{1-\xi} \right), \\ C(\xi) &= \left(1 - \sqrt{1-\xi} \right), & D(\xi) &= \left(2\sqrt{1-\xi} - 2 + \xi \right). \end{aligned} \quad (2.23)$$

It is now straightforward to analytically diagonalise the two matrices, but in general the expressions for the eigenvalues and the eigenvectors are quite complicated. It is thus more convenient to perform a numerical diagonalization, unless specific limits are considered in which expressions simplify. We will provide in Appendix E a *Mathematica* code which makes such a numerical diagonalization for given values of the input parameters and generates all

the relevant couplings and masses. In the rest of our study, however, we will work in the limit $\xi \ll 1$, which, besides being experimentally favoured, can also lead to simple analytical formulae for the physical couplings between the heavy triplet and the other particles in our theory. We will therefore expand the mass matrix and its eigenvectors and eigenvalues at leading order in ξ so that our approximation will break down when $\xi \gtrsim 0.4$, in which case the corrections coming from subsequent powers in the expansion become non-negligible.

The spectrum of the spin-1 sector is easily found once the mass matrix is diagonalised at linear order in ξ ; after EWSB, the only massless state is the photon, since it is the gauge field associated with the unbroken $U(1)_{em}$, whereas for the remaining massive bosons we get:³

$$\begin{aligned} m_W^2 &= \frac{g^2}{4} f^2 \xi, & m_Z^2 &= \frac{g^2 + g'^2}{4} f^2 \xi, \\ M_{\rho_L^\pm}^2 &= M_{\rho_L^0}^2 = \frac{g_{\rho_L}^2}{g_{\rho_L}^2 - g^2} m_{\rho_L}^2 - \frac{g^2 \xi}{4} \left(\frac{f^2 g^2 - 2m_{\rho_L}^2}{g^2 - g_{\rho_L}^2} \right), \end{aligned} \quad (2.24)$$

where we have used the SM couplings g and g' introduced in equation (2.17). As it is clear from the previous expression, the masses of the W and Z bosons originate only after EWSB; if we now define the electroweak scale as $v = \sqrt{\xi} f$, through equation (2.16), then m_W and m_Z have formally the same expression as in the SM.⁴ The masses of the heavy triplet arise instead at zeroth order in ξ and get corrections after EWSB; at leading order in ξ , these corrections are equal for the two charged and the neutral resonances, since they do not depend on g' , which is the only parameter in the bosonic sector to break the custodial symmetry. This degeneracy will be in general removed by $O(\xi^2)$ contributions.

Once the form of the rotation to the mass eigenstate basis is derived, it is straightforward to obtain the physical interactions between the vector resonances, the SM fields and the top partners. We will focus in the following on trilinear vertices, which are the most relevant ones for studying the production and decay of heavy spin-1 states at the LHC, and we will refer to Appendix C for the expression of the Lagrangian and the couplings in the mass eigenstate basis.

We start analysing some qualitative features of the interactions among the vector resonances, the gauge bosons and the Higgs field. We notice first of all that the Lorentz structure of the vertices involving the heavy spin-1 states and two gauge bosons is the same as the one for triple gauge vertices in the SM. This is because the kinetic terms for both composite and elementary

³Here and in the following we will generically indicate with m_ρ the lagrangian parameters corresponding to the mass of one of the vector resonances and with M_ρ the corresponding physical masses obtained by inverting the expressions of the latter in terms of the former.

⁴With this choice, the $O(\xi^2)$ corrections appear in m_W and m_Z , but not in v . One could equivalently define v through the formula $m_W = \frac{g v}{2}$, so that G_F in equation (2.16) deviates from its SM expression at $O(\xi^2)$, once rewritten in terms of v .

fields in Eq. (2.14) imply interactions of the SM type, since \mathcal{L}_L has been truncated to two derivatives interactions, and rotating to the mass eigenbasis does not obviously change their Lorentz structure. Moreover, the values of the $g_{\rho_L^+ WZ}$, $g_{\rho_L^+ WH}$, $g_{\rho_L^0 WW}$ and $g_{\rho_L^0 ZH}$ couplings can be easily extracted by using the Equivalence Theorem for $M_{\rho_L} \gg m_{Z/W}$; in this limit, the leading contribution to the interaction comes from the longitudinal polarizations of the SM vector fields and the overall strength equals that of the coupling of one ρ_μ^L to two NG bosons, $\rho_\mu^L \pi\pi$, up to small corrections of order $O(m_{Z/W}^2/M_{\rho_L}^2)$. As it can be directly seen from equation (2.14), the $\rho_\mu^L \pi\pi$ coupling is proportional to $g_{\rho_L} a_{\rho_L}^2$, where the $O(1)$ parameter $a_{\rho_L} = m_{\rho_L}/(g_{\rho_L} f)$ is introduced analogously to Eq. (2.6) in order to enforce the NDA relation between the mass and coupling of the resonance. The free parameter g_{ρ_L} plays therefore a dominant role in setting the strength of the interaction between the vectors and the SM gauge fields and Higgs.

The interactions of the heavy vectors with the SM leptons and first two quark families, on the other hand, follow entirely from the universal composite-elementary mixing, that is from the elementary component of the heavy spin-1 mass eigenstate. As a consequence, the three couplings $g_{\rho_L^+ ffL}$, $g_{\rho_L^0 ffL}$ and $g_{\rho_L^0 ffY}$ do not depend on the fermion species and are therefore universal. After rotation to the mass eigenstate basis, the first two couplings scale like $\sim g^2/g_{\rho_L}$, whereas the last one is of order $\sim g'^2/g_{\rho_L}$. Moreover, since the ρ_μ^L triplet mixes with the elementary W_μ before EWSB and with the gauge field B_μ only after EWSB, the functions $g_{\rho_L^+ ffL}$ and $g_{\rho_L^0 ffL}$ arise at zeroth order in ξ and they are equal up to $O(\xi)$ terms, since the breaking of the custodial symmetry due to the hypercharge g' enters only through EWSB effects. The coupling $g_{\rho_L^0 ffY}$ is instead generated only by the $\rho_\mu^L - B_\mu$ mixing and is therefore proportional to ξ , so that its contribution to the interaction between the neutral vector and massless fermions is sub-leading. From the above discussions it obviously follows that, in the limit $g_{\rho_L} \gg g$, the heavy resonances are most strongly coupled to composite states, namely the longitudinal W and Z bosons and the Higgs, whereas their coupling strength to lighter fermions is extremely weak.

Let us now consider the interactions among the heavy triplet and the partially composite top-bottom pair and the t_R . Besides the universal terms in the functions $g_{\rho_L^+ tb}$, $g_{\rho_L^0 t_L t_L}$ and $g_{\rho_L^0 b_L b_L}$ coming from the vector elementary-composite mixing, these couplings also receive an additional contribution before EWSB, due to the fermionic mixing, from the direct interaction of the vector resonances with top partners proportional to the $O(1)$ parameter c_3 . The heaviest SM quarks are thus effectively more strongly coupled to the resonances than the lighter ones. After rotation to the mass eigenstate basis, all the previous functions scale in the same way and are of order

$$g_{\rho_L^+ tb} \sim \frac{g^2}{g_{\rho_L}} + c_3 g_{\rho_L} \frac{y_L^2 f^2}{y_L^2 f^2 + M_\Psi^2}. \quad (2.25)$$

As regards the t_R , the additional contributions to the function $g_{\rho_L^0 t_R t_R}$ must arise only after EWSB, because this particle is a singlet under the unbroken group H , whereas the ρ_μ^L resonance has isospin 1 under the $SU(2)_L$ subgroup of $SO(4)$. Isospin conservation therefore forbids any new interaction coming both from the term proportional to the parameter c_1 in \mathcal{L}_Ψ and from the term proportional to c_3 in \mathcal{L}_{ρ_L} before EWSB, so that this coupling does not receive a relevant enhancement for small values of the misalignment angle.

The last set of interactions that has a prominent role in the phenomenology of composite vectors is that involving the top partners; we start considering how the spin-1 resonances couple with a heavy fermion and one third family quark. Before EWSB, the only couplings allowed by isospin conservation are $g_{\rho_L^+ T_L b_L}$, $g_{\rho_L^+ B_L t_L}$, $g_{\rho_L^0 T_L t_L}$, $g_{\rho_L^0 B_L b_L}$; they are generated by the last term in \mathcal{L}_{ρ_L} , since the kinetic terms are invariant under the rotation in the fermionic sector and the interaction $i c_1 \bar{\Psi}_i \not{D}^i t_R$ in \mathcal{L}_Ψ can only contribute after EWSB. Once the rotation to the mass eigenstate basis is performed, all the previous couplings scale obviously like

$$g_{\rho_L^+ T_L b_L} \sim c_3 g_{\rho_L} \frac{y_L f M_\Psi}{y_L^2 f^2 + M_\Psi^2}, \quad (2.26)$$

and will receive further $O(\xi)$ corrections for non-zero values of the misalignment angle. We thus expect the decay channels to $T\bar{b}$, $B\bar{t}$, $T\bar{t}$ and $B\bar{b}$ to play an important role in the decay of the heavy vectors, especially for large values of the strong coupling constant g_{ρ_L} and for high degrees of quark compositeness. All the remaining couplings between a spin-1 resonance, a top partner and a third family quark must originate after EWSB, since at least an insertion of the Higgs vev is needed to conserve the isospin, so that they will in general give a sub-dominant contribution to the phenomenology of vector resonances.

We now consider the couplings between two heavy fermions and one heavy boson. The same analysis made for the previous situation is valid also in this case and we still expect the dominant interaction to be given by the term proportional to c_3 in \mathcal{L}_{ρ_L} . The universal contribution due to the elementary-composite mixing in the top partners kinetic term scales indeed like g^2/g_{ρ_L} and the direct interaction between spin-1 and spin-1/2 resonances induces an additional contribution proportional to g_{ρ_L} . For large values of the strong coupling constant, the universal piece will therefore be suppressed whereas the second will be enhanced, analogously to what happens for the partially composite quarks. The functions generated before EWSB are those allowed by isospin conservation, namely $g_{\rho_L^+ T_L B_L}$, $g_{\rho_L^0 T_L T_L}$, $g_{\rho_L^0 B_L B_L}$, which all scale like

$$g_{\rho_L^+ T_L B_L} \sim \frac{g^2}{g_{\rho_L}} + c_3 g_{\rho_L} \frac{M_\Psi^2}{y_L^2 f^2 + M_\Psi^2}, \quad (2.27)$$

and $g_{\rho_L^+ X_{\frac{2}{3}} X_{\frac{5}{3}}}$, $g_{\rho_L^+ T_R B_R}$, $g_{\rho_L^0 X_{\frac{5}{3}} X_{\frac{5}{3}}}$, $g_{\rho_L^0 X_{\frac{2}{3}} X_{\frac{5}{3}}}$, $g_{\rho_L^0 T_R T_R}$ and $g_{\rho_L^0 B_R B_R}$, which instead are all of order

$$g_{\rho_L^+ X_{\frac{2}{3}} X_{\frac{5}{3}}} \sim \frac{g^2}{g_{\rho_L}} + c_3 g_{\rho_L}. \quad (2.28)$$

These second set of couplings does not receive any contribution from the rotation angles in Eq. (2.19) because the $X_{2/3}$, T_R and B_R fields are left invariant by the rotation in the fermionic sector before EWSB. We therefore expect the decay channel of vectors to $T\bar{B}$, $T\bar{T}$, $B\bar{B}$, $X_{\frac{2}{3}}\bar{X}_{\frac{5}{3}}$, $X_{\frac{5}{3}}\bar{X}_{\frac{5}{3}}$ and $X_{\frac{2}{3}}\bar{X}_{\frac{2}{3}}$ to be the most important one, when kinematically allowed, among the decays to two top partners. The other possible decay channels will instead be suppressed by the small value of ξ since they must originate only after EWSB.

We have finally summarized these results in Table 1, where we have listed all the relevant couplings arising before EWSB, neglecting the $O(\xi)$ corrections.

| Couplings | Scaling |
|---|--|
| $g_{\rho_L^+ W_L Z_L}$, $g_{\rho_L^+ W_L H}$, $g_{\rho_L^0 W_L W_L}$, $g_{\rho_L^0 Z_L H}$ | $a_{\rho_L}^2 g_{\rho_L}$ |
| $g_{\rho_L^+ f f L}$, $g_{\rho_L^0 f f L}$ | $\frac{g^2}{g_{\rho_L}}$ |
| $g_{\rho_L^+ t b}$, $g_{\rho_L^0 t_L t_L}$, $g_{\rho_L^0 b_L b_L}$ | $\frac{g^2}{g_{\rho_L}} + c_3 g_{\rho_L} \frac{y_L^2 f^2}{y_L^2 f^2 + M_\Psi^2}$ |
| $g_{\rho_L^+ T_L b_L}$, $g_{\rho_L^+ B_L t_L}$, $g_{\rho_L^0 T_L t_L}$, $g_{\rho_L^0 B_L b_L}$ | $c_3 g_{\rho_L} \frac{y_L f M_\Psi}{y_L^2 f^2 + M_\Psi^2}$ |
| $g_{\rho_L^+ T_L B_L}$, $g_{\rho_L^0 T_L T_L}$, $g_{\rho_L^0 B_L B_L}$ | $\frac{g^2}{g_{\rho_L}} + c_3 g_{\rho_L} \frac{M_\Psi^2}{y_L^2 f^2 + M_\Psi^2}$ |
| $g_{\rho_L^+ X_{\frac{2}{3}} X_{\frac{5}{3}}}$, $g_{\rho_L^+ T_R B_R}$, $g_{\rho_L^0 X_{\frac{5}{3}} X_{\frac{5}{3}}}$, $g_{\rho_L^0 X_{\frac{2}{3}} X_{\frac{5}{3}}}$, $g_{\rho_L^0 T_R T_R}$, $g_{\rho_L^0 B_R B_R}$ | $\frac{g^2}{g_{\rho_L}} + c_3 g_{\rho_L}$ |

Table 2.1 – List of the couplings arising before EWSB and their scaling with the strong coupling constant g_{ρ_L} in the mass eigenstate basis, for the ρ_L^μ resonance coupled to top partners.

2.2.2 A Lagrangian for ρ_μ^R

We now introduce the Lagrangian for the $(\mathbf{1}, \mathbf{3})_0$ vector resonance coupled to top partners in the fourplet, with fully composite t_R ; it is given by:

$$\mathcal{L}_R = \mathcal{L}_{light} + \mathcal{L}_\Psi + \mathcal{L}_{\rho_R}, \quad (2.29)$$

where \mathcal{L}_{light} and \mathcal{L}_Ψ have the same expression as in Eq. (2.14), whereas \mathcal{L}_{ρ_R} is

$$\mathcal{L}_{\rho_R} = -\frac{1}{4}\rho_{\mu\nu}^{a_R}\rho^{a_R\mu\nu} + \frac{m_{\rho_R}^2}{2g_{\rho_R}^2}(g_{\rho_R}\rho_\mu^{a_R} - E_\mu^{a_R})^2 + c_4\bar{\Psi}^i\gamma^\mu(g_{\rho_R}\rho_\mu^{a_R} - E_\mu^{a_R})T_{ij}^{a_R}\Psi^j. \quad (2.30)$$

The theory possesses again eleven parameters with m_{ρ_R} , g_{ρ_R} and c_4 indicating respectively the mass and strong coupling constant of the ρ_R^μ resonance and the $O(1)$ parameter which plays the analogous role of c_3 . As in the previous case, we can re-express all the Lagrangian input parameters in terms of physical quantities and fix g_{el} , g'_{el} and f in order to reproduce the experimental values of α , G_F and m_Z , as described in Eq. (2.16). We can define the SM g and g' weak couplings as

$$g \equiv g_{el} \quad \frac{1}{g'^2} \equiv \frac{1}{g_{el}^2} + \frac{1}{g_{\rho_R}^2}, \quad (2.31)$$

so that, differently to the ρ_μ^L case, we can now identify g as the elementary gauge coupling constant.

Due to the interaction between the composite ρ_R and the elementary gauge fields induced by the $\rho_R - W$ and $\rho_R - B$ mixings, the mass matrix of the bosonic sector of the theory is again non-diagonal. Analogously to Eq. (4.32), we can introduce the 2×2 charged block

$$M_\pm^2 = \begin{pmatrix} \frac{g_{el}^2}{4g_{\rho_R}^2}(g_{\rho_R}^2 f^2 \xi - D(\xi)m_{\rho_R}^2) & -\frac{g_{el}}{2g_{\rho_R}}C(\xi)m_{\rho_R}^2 \\ -\frac{g_{el}}{2g_{\rho_R}}C(\xi)m_{\rho_R}^2 & m_{\rho_R}^2 \end{pmatrix} \quad (2.32)$$

and the 3×3 neutral block

$$M_0^2 = \begin{pmatrix} \frac{(g'_{el})^2}{4g_{\rho_R}^2}(g_{\rho_R}^2 f^2 \xi - D(\xi)m_{\rho_R}^2) & -\frac{g'_{el}}{2g_{\rho_R}}C(\xi)m_{\rho_R}^2 & \frac{g_{el}g'_{el}}{4g_{\rho_R}^2}(m_{\rho_R}^2 - f^2 g_{\rho_R}^2)\xi \\ -\frac{g'_{el}}{2g_{\rho_R}}C(\xi)m_{\rho_R}^2 & m_{\rho_R}^2 & -\frac{g_{el}}{2g_{\rho_R}}B(\xi)m_{\rho_R}^2 \\ \frac{g_{el}g'_{el}}{4g_{\rho_R}^2}(m_{\rho_R}^2 - f^2 g_{\rho_R}^2)\xi & -\frac{g_{el}}{2g_{\rho_R}}B(\xi)m_{\rho_R}^2 & \frac{g_{el}^2}{4g_{\rho_R}^2}(g_{\rho_R}^2 f^2 \xi + A(\xi)m_{\rho_R}^2) \end{pmatrix}, \quad (2.33)$$

that can be diagonalized numerically with the code provided in Appendix E. The spectrum contains the massless photon, the W and Z boson, whose masses, at linear order in ξ , get the same expression as in Eq. (2.24), and the right-handed triplet with masses

$$M_{\rho_R^\pm}^2 = m_{\rho_R}^2 + O(\xi^2), \quad M_{\rho_R^0}^2 = \frac{g_{\rho_R}^2}{g_{\rho_R}^2 - g'^2}m_{\rho_R}^2 - \frac{g'^2 \xi}{4} \left(\frac{f^2 g'^2 - 2m_{\rho_R}^2}{g'^2 - g_{\rho_R}^2} \right) + O(\xi^2). \quad (2.34)$$

We see that the mass of the charged heavy vector coincides with the Lagrangian parameter

m_{ρ_R} , up to $O(\xi^2)$ corrections, and that the spectrum is degenerate even at zeroth order in ξ due to the dependence on g' which explicitly breaks the custodial symmetry.

We can easily derive the couplings of the spin-1 resonance to SM particles and top partners in the mass eigenstate basis once the rotation is performed; we will briefly describe their most important features, stressing the main differences from the left-handed vector.

Following the same reasoning of the previous analysis, we can verify that the functions $g_{\rho_R^+ ZW}$, $g_{\rho_R^+ WH}$, $g_{\rho_R^0 WW}$, $g_{\rho_R^0 ZH}$ scale all like $a_{\rho_R}^2 g_{\rho_R}$, in the limit when the Equivalence Theorem is a very good approximation, namely $M_{\rho_R^{\pm/0}} \gg m_{W/Z}$. As regards the fully elementary fermions, the universal composite-elementary mixing is such that also the couplings $g_{\rho_R^+ ffL}$, $g_{\rho_R^0 ffL}$ and $g_{\rho_R^0 ffY}$ scale in the same way as in left-handed case. However, since the ρ_μ^R triplet mixes with the elementary W_μ field after EWSB and with the gauge boson B_μ before EWSB, the couplings $g_{\rho_R^+ ffL}$ and $g_{\rho_R^0 ffL}$ arise at linear order in ξ and are no longer equal due to the effects of the hypercharge g' , whereas the $g_{\rho_R^0 ffY}$ function, induced only by the $\rho_\mu^R - B_\mu$ mixing, is generated at zeroth order in ξ and gives the most relevant contribution. As a consequence, the charged heavy vectors couple very weakly to the lightest SM fermions, contrary to the ρ_μ^L resonance. Finally, the couplings to the partially composite t_L and b_L are enhanced by the interaction proportional to c_4 . However, being ρ_R an $SU(2)_L$ singlet, before EWSB it can couple only to the $SU(2)_L$ singlet current $(t\bar{t} + b\bar{b})$, so that the enhancement in $g_{\rho_R^+ tb}$ is proportional to ξ and therefore suppressed by the small value of the misalignment angle. On the other hand, the couplings $g_{\rho_R^0 t_L t_L}$ and $g_{\rho_R^0 b_L b_L}$ are allowed by isospin conservation even at zeroth order in ξ and they scale like their left-handed counterparts.

Considering now the couplings to one top partner and one third family quark, the functions arising before EWSB are $g_{\rho_R^+ X_{\frac{2}{3}L} b_L}$, $g_{\rho_R^+ X_{\frac{5}{3}L} t_L}$, $g_{\rho_R^0 T_L t_L}$ and $g_{\rho_R^0 B_L b_L}$ and again they are generated by the interaction proportional to c_4 . Differently to the previous case, the charged resonance will therefore be more strongly coupled to $X_{\frac{2}{3}} \bar{b}$ and $X_{\frac{5}{3}} \bar{t}$, since it can interact only to the $SU(2)_L$ singlet current $(X_{\frac{2}{3}} \bar{b} + X_{\frac{5}{3}} \bar{t})$ at zeroth order in ξ . For the neutral vector, on the other hand, the decays to $T\bar{t}$ and $B\bar{b}$ will still be the most important one among the heavy-light channels, analogously to the ρ_μ^L heavy vector. Finally, as regards the couplings to two top partners, the situation is similar to the previous one: the relevant interactions of the neutral resonance are the same as the ones listed for the left-handed case, whereas the charged ρ_R^+ will couple preferably to $X_{\frac{2}{3}} \bar{B}$ and $X_{\frac{5}{3}} \bar{T}$, again because of the different quantum numbers of the left-handed and right-handed vectors.

We have summarized all the relevant couplings for this second model in Table 2, where their scaling with g_{ρ_R} is given neglecting corrections arising after EWSB.

| Couplings | Scaling |
|---|---|
| $\mathcal{G}_{\rho_R^+ W_L Z_L}, \mathcal{G}_{\rho_R^+ W_L H}, \mathcal{G}_{\rho_R^0 W_L W_L}, \mathcal{G}_{\rho_R^0 Z_L H}$ | $a_{\rho_R}^2 \mathcal{G}_{\rho_R}$ |
| $\mathcal{G}_{\rho_R^0 f f^Y}$ | $\frac{g'^2}{\mathcal{G}_{\rho_R}}$ |
| $\mathcal{G}_{\rho_R^0 t_L t_L}, \mathcal{G}_{\rho_R^0 b_L b_L}$ | $\frac{g'^2}{\mathcal{G}_{\rho_R}} + c_4 \mathcal{G}_{\rho_R} \frac{y_L^2 f^2}{y_L^2 f^2 + M_\Psi^2}$ |
| $\mathcal{G}_{\rho_R^+ X_{\frac{2}{3}L} b_L}, \mathcal{G}_{\rho_R^+ X_{\frac{5}{3}L} t_L}$ | $c_4 \mathcal{G}_{\rho_R} \frac{y_L f}{\sqrt{y_L^2 f^2 + M_\Psi^2}}$ |
| $\mathcal{G}_{\rho_R^0 T_L t_L}, \mathcal{G}_{\rho_R^0 B_L b_L}$ | $c_4 \mathcal{G}_{\rho_R} \frac{y_L f M_\Psi}{y_L^2 f^2 + M_\Psi^2}$ |
| $\mathcal{G}_{\rho_R^+ X_{\frac{2}{3}L} B_L}$ | $c_4 \mathcal{G}_{\rho_R} \frac{M_\Psi}{\sqrt{y_L^2 f^2 + M_\Psi^2}}$ |
| $\mathcal{G}_{\rho_R^0 T_L T_L}, \mathcal{G}_{\rho_R^0 B_L B_L}$ | $\frac{g'^2}{\mathcal{G}_{\rho_R}} + c_4 \mathcal{G}_{\rho_R} \frac{M_\Psi^2}{y_L^2 f^2 + M_\Psi^2}$ |
| $\mathcal{G}_{\rho_R^+ X_{\frac{5}{3}L} T_L}, \mathcal{G}_{\rho_R^+ X_{\frac{5}{3}R} T_R}, \mathcal{G}_{\rho_R^+ X_{\frac{2}{3}R} B_R}, \mathcal{G}_{\rho_R^0 X_{\frac{5}{3}} X_{\frac{5}{3}}}, \mathcal{G}_{\rho_R^0 X_{\frac{2}{3}} X_{\frac{2}{3}}}, \mathcal{G}_{\rho_R^0 T_R T_R}, \mathcal{G}_{\rho_R^0 B_R B_R}$ | $\frac{g'^2}{\mathcal{G}_{\rho_R}} + c_4 \mathcal{G}_{\rho_R}$ |

Table 2.2 – List of the couplings arising before EWSB and their scaling with the strong coupling constant \mathcal{G}_{ρ_R} in the mass eigenstate basis, for the ρ_R^μ resonance coupled to top partners.

2.2.3 Two Lagrangians for ρ_μ^X

We consider now the phenomenology of a spin-1 resonance transforming only under the abelian $U(1)_X$ as a gauge field,

$$\rho_\mu^X \rightarrow \rho_\mu + \partial_\mu \alpha^X, \quad (2.35)$$

with $\alpha^X \in U(1)_X$, and interacting with top partners in the singlet of $SO(4)$, \tilde{T} . This vector has very different properties with respect to the left-handed and right-handed cases; we expect it to be more strongly coupled to particles which do not transform under $SO(4)$, t_R and \tilde{T} , so that its phenomenology can be significantly different if the t_R belongs to the composite sector or if it is an elementary state linearly coupled to the new dynamics. We explore both these possibilities building two models, \mathbf{M}_X^1 for the first situation and \mathbf{M}_X^2 for the second. The Lagrangians for the two models read, respectively,

$$\mathcal{L}_{\mathbf{M}_X^1} = \mathcal{L}_{light} + \mathcal{L}_{\tilde{T}^1} + \mathcal{L}_{\rho_X^1}, \quad \mathcal{L}_{\mathbf{M}_X^2} = \mathcal{L}_{light} + \mathcal{L}_{\tilde{T}^2} + \mathcal{L}_{\rho_X^2}, \quad (2.36)$$

with

$$\begin{aligned}
 \mathcal{L}_{\tilde{T}1} &= \tilde{T} i \not{D} \tilde{T} - M_\Psi \tilde{T} \tilde{T} + [y_L f(\tilde{Q}_L^5)^I U_{I5} \tilde{T}_R + y_L c_2 f(\tilde{Q}_L^5)^I U_{I5} t_R + \text{h.c.}], \\
 \mathcal{L}_{\rho_X^1} &= -\frac{1}{4} \rho_{\mu\nu}^X \rho^{X\mu\nu} + \frac{m_{\rho_X}^2}{2g_{\rho_X}^2} (g_{\rho_X} \rho_\mu^X - g'_{el} B_\mu)^2 + c_5 \tilde{t}_R \gamma^\mu (g_{\rho_X} \rho_\mu^X - g'_{el} B_\mu) t_R \\
 &\quad + c_6 \tilde{T} \gamma^\mu (g_{\rho_X} \rho_\mu^X - g'_{el} B_\mu) \tilde{T},
 \end{aligned} \tag{2.37}$$

and

$$\begin{aligned}
 \mathcal{L}_{\tilde{T}2} &= \tilde{T} i \not{D} \tilde{T} - M_\Psi \tilde{T} \tilde{T} + [y_L f(\tilde{Q}_L^5)^I U_{I5} \tilde{T}_R + y_R f(\tilde{Q}_R^5)^I U_{I5} \tilde{T}_L + \text{h.c.}], \\
 \mathcal{L}_{\rho_X^2} &= -\frac{1}{4} \rho_{\mu\nu}^X \rho^{X\mu\nu} + \frac{m_{\rho_X}^2}{2g_{\rho_X}^2} (g_{\rho_X} \rho_\mu^X - g'_{el} B_\mu)^2 + c_6 \tilde{T} \gamma^\mu (g_{\rho_X} \rho_\mu^X - g'_{el} B_\mu) \tilde{T}.
 \end{aligned} \tag{2.38}$$

The Lagrangians $\mathcal{L}_{\tilde{T}1}$ and $\mathcal{L}_{\tilde{T}2}$ contain the kinetic term of the top partner and its interaction with the t_R allowed by the symmetries; the fermion mass matrix is in general non-diagonal and must be diagonalised in both cases. The Lagrangians $\mathcal{L}_{\rho_X^1}$ and $\mathcal{L}_{\rho_X^2}$ describe the kinetic term of the vector singlet, with the field strength $\rho_{\mu\nu}^X$ obviously defined as

$$\rho_{\mu\nu}^X = \partial_\mu \rho_\nu^X - \partial_\nu \rho_\mu^X,$$

and its direct coupling with \tilde{T} . In model \mathbf{M}_X^1 also a direct coupling with t_R is present whereas the same interaction is forbidden for a partially composite t_R . The ρ_μ^X mixes in every case with the abelian gauge field B_μ , which is needed to preserve invariance under $U(1)_X$, so that the mass matrix of the neutral spin-1 sector must be diagonalised by a field rotation. The two models have nine parameters in common, g , g'_{el} and f , that will be fixed to reproduce the experimental values of α , G_F and m_Z according to Eq. (2.16), ξ , y_L , the mass scales M_Ψ and m_{ρ_X} , the strong coupling g_{ρ_X} and the $O(1)$ parameter c_6 . Model \mathbf{M}_X^1 has two additional parameters, c_2 , which must be fixed in order to reproduce the top mass, and c_5 ; apart from ξ which is an observable, the six unfixed parameters could be traded for the mass of the heavy fermion, $m_{\tilde{T}}$, and its coupling to a gauge boson and top quark, the mass of the heavy vector, its coupling to leptons, to the top quark and to the \tilde{T} particle. Model \mathbf{M}_X^2 , on the other hand, has one additional parameter, y_R ; in this case we will fix y_L to reproduce the top mass and the remaining free parameters can be expressed in terms of physical quantities similarly to the \mathbf{M}_X^1 case.

We discuss now the rotation to the mass eigenstate basis and the spectrum of the models. As regards model \mathbf{M}_X^1 , the mass matrix of the fermionic sector has already been analysed in [7], which we refer for the details. We just report here the expressions for the masses of the top

quark and \tilde{T} at leading order in ξ ,

$$m_{top} = \frac{c_2 y_L f}{\sqrt{2}} \sqrt{\xi}, \quad m_{\tilde{T}} = M_\Psi + \frac{y_L^2 f^2}{4M_\Psi} \xi, \quad (2.39)$$

and we notice that the two fields do not mix before EWSB, because the mass matrix is diagonal when $\xi = 0$. On the other hand, the mass matrix in model \mathbf{M}_X^2 is

$$\begin{pmatrix} \tilde{t}_L \\ \tilde{\tilde{t}}_L \end{pmatrix} \begin{pmatrix} 0 & -\frac{y_L f}{\sqrt{2}} \sqrt{\xi} \\ f \sqrt{1-\xi} y_R & -M_\Psi \end{pmatrix} \begin{pmatrix} t_R \\ \tilde{T}_R \end{pmatrix}, \quad (2.40)$$

with eigenvalues

$$m_{top} = \frac{y_L y_R f^2 \sqrt{\xi}}{\sqrt{2} \sqrt{y_R^2 f^2 + M_\Psi^2}}, \quad m_{\tilde{T}} = \sqrt{f^2 y_R^2 + M_\Psi^2} - \frac{f^2 (2f^2 y_R^4 - M_\Psi^2 (y_L^2 - 2y_R^2))}{4(f^2 y_R^2 + M_\Psi^2)^{3/2}} \xi, \quad (2.41)$$

which receive further corrections from higher orders in an expansion in ξ . In this case, the field rotation needed to diagonalise the mass matrix before EWSB is

$$t_R \rightarrow \frac{M_\Psi}{\sqrt{y_R^2 f^2 + M_\Psi^2}} t_R - \frac{y_R f}{\sqrt{y_R^2 f^2 + M_\Psi^2}} \tilde{T}_R, \quad (2.42)$$

with the orthogonal transformation for the \tilde{T}_R field. Considering, on the other hand, the spin-1 sector, the mass matrix is the same for both models and, in the basis of Eq. (4.32), it is given by:

$$M_0^2 = \begin{pmatrix} \frac{1}{4} g_{\text{el}}^2 f^2 \xi & 0 & -\frac{1}{4} g_{\text{el}} g'_{\text{el}} f^2 \xi \\ 0 & m_{\rho_X}^2 & -\frac{g'_{\text{el}}}{g_{\rho_X}} m_{\rho_X}^2 \\ -\frac{1}{4} g_{\text{el}} g'_{\text{el}} f^2 \xi & -\frac{g'_{\text{el}}}{g_{\rho_X}} m_{\rho_X}^2 & \frac{(g'_{\text{el}})^2}{4} \left(\frac{4m_{\rho_X}^2}{g_{\rho_X}^2} + f^2 \xi \right) \end{pmatrix}, \quad (2.43)$$

where we notice that the zero entries are due to the absence of mixing of the ρ_μ^X singlet with W_μ^3 . The spectrum of the neutral sector contains the massless photon, the W and Z boson, whose masses have the same expressions as in Eq. (2.24) at linear order in ξ , and the vector singlet, with mass

$$M_{\rho_X}^2 = \frac{g_{\rho_X}^2}{g_{\rho_X}^2 - (g')^2} m_{\rho_X}^2 + \frac{(g')^4}{g_{\rho_X}^2 - (g')^2} \frac{f^2 \xi}{4} + O(\xi^2), \quad (2.44)$$

where we have defined the SM coupling g' as in Eq. (2.31), with g_{ρ_R} replaced by g_{ρ_X} .

Once the rotation is performed, it is straightforward to derive the couplings of the vector singlet to the heavy fermions and SM particles in the mass eigenstate basis; we discuss here their basic phenomenological features, stressing the differences with respect to the left-handed and right-handed cases. First of all, the couplings to gauge bosons and fully elementary fermions are the same in both models. Since ρ_μ^X is not charged under $SO(4)$, it cannot couple directly with the longitudinally polarized W and Z bosons, so that the functions $g_{\rho_X WW}$ and $g_{\rho_X ZH}$ arise only because of the mixing with the B_μ gauge field and must be generated after EWSB. They scale like $g'^2/g_{\rho_X}\xi$ and are therefore strongly suppressed, contrary to what happens for ρ_μ^L and ρ_μ^R . The couplings to elementary fermions, on the other hand, behave similarly to the previous cases: they are generated only because of the universal composite-elementary mixing and scale like g'^2/g_{ρ_X} . In particular, the function $g_{\rho_X ffY}$ is produced before EWSB, because the mixing with B_μ arises at zeroth order in ξ , whereas $g_{\rho_X ffL}$ must be proportional to ξ , since the singlet does not mix with W_μ^3 .

The two models differ in the couplings of the vector singlet to the top quark and \tilde{T} , as it can be seen from Table 3, where we have summarized the scaling of the relevant couplings arising before EWSB. In both models, the function $g_{\rho_X t_R t_R}$, besides the universal contribution from the elementary-composite mixing, receives an additional enhancement which in model \mathbf{M}_X^1 is due to the direct interaction proportional to c_5 and in model \mathbf{M}_X^2 results from the interaction proportional to c_6 as a consequence of the fermionic rotation. The coupling $g_{\rho_X \tilde{T}_L t_L}$ must be generated in both cases at linear order in ξ , since t_L and \tilde{T}_L do not mix before EWSB, whereas the function $g_{\rho_X \tilde{T}_R t_R}$ arises after EWSB in model \mathbf{M}_X^1 , because in this case t_R and \tilde{T}_R mix when $\xi \neq 0$, and before EWSB in model \mathbf{M}_X^2 , since now the two fields mix even before EWSB and the coupling is proportional to the rotation angle. Finally, as regards the interaction between the vector singlet and two top partners, following the same reasoning, it is clear that the function $g_{\rho_X \tilde{T}_L \tilde{T}_L}$ must be the same for both models, whereas the coupling $g_{\rho_X \tilde{T}_R \tilde{T}_R}$ receives the contribution of the rotation angle before EWSB in model \mathbf{M}_X^2 , which is instead absent if the t_R is a full singlet of the strong dynamics.

As a result of the previous analysis, we expect a relevant decay channel of the vector singlet to be $t\bar{t}$ in both models; among the channels involving the top partners, $\tilde{T}\tilde{T}$ has great importance in both cases, whereas $\tilde{T}\bar{t}$ is suppressed by the small value of ξ in model \mathbf{M}_X^1 and is instead enhanced in model \mathbf{M}_X^2 . This features will lead to a different phenomenology for the two models, so that the vector singlet is particularly sensitive to the degree of compositeness of the t_R quark.

2.3. Production and decay of vector resonances at the LHC

| Couplings | Scaling \mathbf{M}_X^1 | Scaling \mathbf{M}_X^2 |
|--------------------------------------|--|---|
| $g_{\rho_X f f Y}$ | $\frac{g'^2}{g_{\rho_X}}$ | $\frac{g'^2}{g_{\rho_X}}$ |
| $g_{\rho_X t_R t_R}$ | $\frac{g'^2}{g_{\rho_X}} + c_5 g_{\rho_X}$ | $\frac{g'^2}{g_{\rho_X}} + c_6 g_{\rho_X} \frac{y_R^2 f^2}{y_R^2 f^2 + M_\Psi^2}$ |
| $g_{\rho_X \tilde{t}_R t_R}$ | | $c_6 g_{\rho_X} \frac{y_R f M_\Psi}{y_R^2 f^2 + M_\Psi^2}$ |
| $g_{\rho_X \tilde{t}_L \tilde{t}_L}$ | $\frac{g'^2}{g_{\rho_X}} + c_6 g_{\rho_X}$ | $\frac{g'^2}{g_{\rho_X}} + c_6 g_{\rho_X}$ |
| $g_{\rho_X \tilde{t}_R \tilde{t}_R}$ | $\frac{g'^2}{g_{\rho_X}} + c_6 g_{\rho_X}$ | $\frac{g'^2}{g_{\rho_X}} + c_6 g_{\rho_X} \frac{M_\Psi^2}{y_R^2 f^2 + M_\Psi^2}$ |

Table 2.3 – List of the couplings arising before EWSB and their scaling with the strong coupling constant g_{ρ_X} in the mass eigenstate basis, for the ρ_X^μ resonance in models \mathbf{M}_X^1 and \mathbf{M}_X^2 .

2.3 Production and decay of vector resonances at the LHC

We discuss in this section the main LHC production mechanisms and the decay channels of the vector resonances under consideration. We will parametrize the production cross section in terms of some fundamental functions that can be computed with a Monte Carlo code, like MadGraph5 [65], and some universal couplings, whose expressions can be derived either analytically or numerically once the rotation to the mass eigenstate basis has been performed. This procedure is very useful to scan the parameter space of the theories, as we shall see when discussing the bounds from LHC direct searches. We will then study the most relevant decay channels and introduce an efficient analytical computation of the branching ratios with the FeynRules package, [64], as functions of the couplings in Appendix C.

2.3.1 Production cross section

The main production mechanisms of the vector resonances at the LHC, at a center of mass energy of $\sqrt{s} = 8$ TeV, are Drell-Yan processes and VBF. Under the validity of the Narrow Width Approximation (NWA), each production rate can be factorized into an on-shell cross section times a decay branching fraction. For the Drell-Yan case, the on-shell cross sections are controlled by the universal couplings $g_{\rho^+ f f L}$, $g_{\rho^0 f f L}$, $g_{\rho^0 f f Y}$ and can be written as

$$\begin{aligned}
 \sigma(pp \rightarrow \rho^+ + X) &= g_{\rho^+ f f L}^2 \cdot \sigma_{u\bar{d}}, \\
 \sigma(pp \rightarrow \rho^- + X) &= g_{\rho^- f f L}^2 \cdot \sigma_{d\bar{u}}, \\
 \sigma(pp \rightarrow \rho^0 + X) &= g_{\rho^0 uu}^2 \cdot \sigma_{u\bar{u}} + g_{\rho^0 dd}^2 \cdot \sigma_{d\bar{d}},
 \end{aligned} \tag{2.45}$$

where ρ stands for ρ_L , ρ_R or ρ_X and $g_{\rho^0 uu}$ and $g_{\rho^0 dd}$ are the coupling strength of respectively up- and down-type fermions to the resonance,

$$\begin{aligned} g_{\rho^0 uu} &= \left[\left(\frac{1}{2} (g_{\rho^0 ffL} - g_{\rho^0 ffY}) + \frac{2}{3} g_{\rho^0 ffY} \right)^2 + \left(\frac{2}{3} g_{\rho^0 ffY} \right)^2 \right]^{1/2}, \\ g_{\rho^0 dd} &= \left[\left(-\frac{1}{2} (g_{\rho^0 ffL} - g_{\rho^0 ffY}) - \frac{1}{3} g_{\rho^0 ffY} \right)^2 + \left(\frac{-1}{3} g_{\rho^0 ffY} \right)^2 \right]^{1/2}. \end{aligned} \quad (2.46)$$

We have furthermore defined the partonic cross sections as

$$\begin{aligned} \sigma_{u\bar{d}} &= \sum_{\psi_u, \psi_d} \sigma(pp \rightarrow \psi_u \bar{\psi}_d \rightarrow \rho^+ + X) |_{g_{\rho^+ ffL}=1}, \\ \sigma_{d\bar{u}} &= \sum_{\psi_u, \psi_d} \sigma(pp \rightarrow \psi_d \bar{\psi}_u \rightarrow \rho^0 + X) |_{g_{\rho^+ ffL}=1}, \\ \sigma_{u\bar{u}} &= \sum_{\psi_u} \sigma(pp \rightarrow \psi_u \bar{\psi}_u \rightarrow \rho^0 + X) |_{g_{\rho^0 uu}=1}, \\ \sigma_{d\bar{d}} &= \sum_{\psi_d} \sigma(pp \rightarrow \psi_d \bar{\psi}_d \rightarrow \rho^0 + X) |_{g_{\rho^0 dd}=1}, \end{aligned} \quad (2.47)$$

where we have schematically indicated $\psi_u = u, c$ and $\psi_d = d, s$. The total production rates (2.45) are thus simply given in terms of the fundamental cross sections, which include the contributions of all the initial partons and can be computed with a Monte Carlo code, appropriately rescaled by the couplings $g_{\rho^+ ffL}$, $g_{\rho^0 uu}$ and $g_{\rho^0 dd}$.

Analogously, the VBF production cross sections are controlled by the couplings $g_{\rho^+ WZ}$, $g_{\rho^0 WW}$ and can be parametrized as

$$\begin{aligned} \sigma(pp \rightarrow \rho^+ + X) &= g_{\rho^+ WZ}^2 \cdot \sigma_{W^+ Z}, \\ \sigma(pp \rightarrow \rho^- + X) &= g_{\rho^+ WZ}^2 \cdot \sigma_{W^- Z}, \\ \sigma(pp \rightarrow \rho^0 + X) &= g_{\rho^0 WW}^2 \cdot \sigma_{WW}, \end{aligned} \quad (2.48)$$

with the fundamental cross sections now given by:

$$\begin{aligned} \sigma_{W^+ Z} &= \sigma(pp \rightarrow W^+ Z \rightarrow \rho^+ + X) |_{g_{\rho^+ WZ}=1}, \\ \sigma_{W^- Z} &= \sigma(pp \rightarrow W^- Z \rightarrow \rho^- + X) |_{g_{\rho^+ WZ}=1}, \\ \sigma_{W^+ W^-} &= \sigma(pp \rightarrow W^+ W^- \rightarrow \rho^0 + X) |_{g_{\rho^0 WW}=1}. \end{aligned} \quad (2.49)$$

Again, once these cross sections are computed numerically at the partonic level, we can get the total production rates by simply rescaling with the couplings of the vectors to gauge bosons which are easily computed in the mass eigenstate basis. Finally, since both the couplings of the resonance to lighter quarks and to gauge bosons depend on ξ , g_ρ and M_ρ , the production cross section for Drell-Yan and VBF processes is a function of only these three parameters.

We now discuss the relevance of these two production mechanisms for the three vectors in our models. In general, we expect the fundamental cross sections for the VBF process to

2.3. Production and decay of vector resonances at the LHC

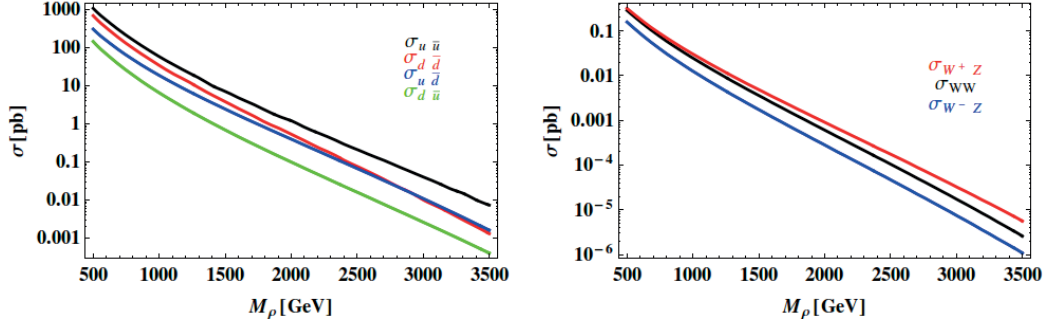


Figure 2.1 – Fundamental cross sections as functions of the physical mass of the resonance at $\sqrt{s} = 8$ TeV. Left panel: fundamental cross sections for the DY process. Right panel: fundamental cross sections for the VBF process.

be much smaller than the corresponding ones for the DY process. In fact, DY is a one-body process and the corresponding cross section goes like $\sim g^4/g_\rho^2$, whereas VBF is a three-body process, so that the cross section is further suppressed by a phase space factor and scales like $\sim g^4/((16\pi^2)^2 g_\rho^2)$. This is confirmed by a quantitative estimation of the two mechanisms, as it can be seen in Fig. (2.1), where the various fundamental cross sections are plotted as a function of the resonance mass. The relative importance of the two complete production rates depends however on the coupling strengths that rescale the partonic cross sections. Since the couplings of the resonances to elementary fermions decrease with increasing g_ρ , the Drell-Yan process is smaller for larger values of the strong coupling constant. On the other hand, the couplings to longitudinally polarized gauge bosons increase with g_ρ , so that the VBF mechanism can have a chance to compete with the DY one for more strongly coupled scenarios. The total production cross sections for the two processes are illustrated in Figs. (2.2) and (2.3), where we plot the contours of constant cross sections, both for DY and VBF processes, for the three heavy vectors in the (M_ρ, g_ρ) plane. In every case, in order to enforce the NDA relation (2.8) between the coupling and the mass, we have rescaled ξ as

$$\xi = a_\rho^2 \frac{1}{\sqrt{2}G_F} \left(\frac{g_\rho}{M_\rho} \right)^2, \quad (2.50)$$

and we have fixed $a_\rho = 1$, for illustration. We have also indicated the region of the parameter space where the value of ξ exceeds 1, and is therefore not allowed, and the region where ξ exceeds 0.4, which corresponds to the experimentally disfavoured limit where our analytical expressions for the couplings at leading order in ξ start losing their validity. From Fig. (2.2), we see that, despite the suppressed couplings of the resonances to elementary fermions, the DY cross section for both the charged and neutral ρ_μ^L vector dominates over the VBF one even for large g_ρ and increases for smaller values of the strong coupling, since in that limit the

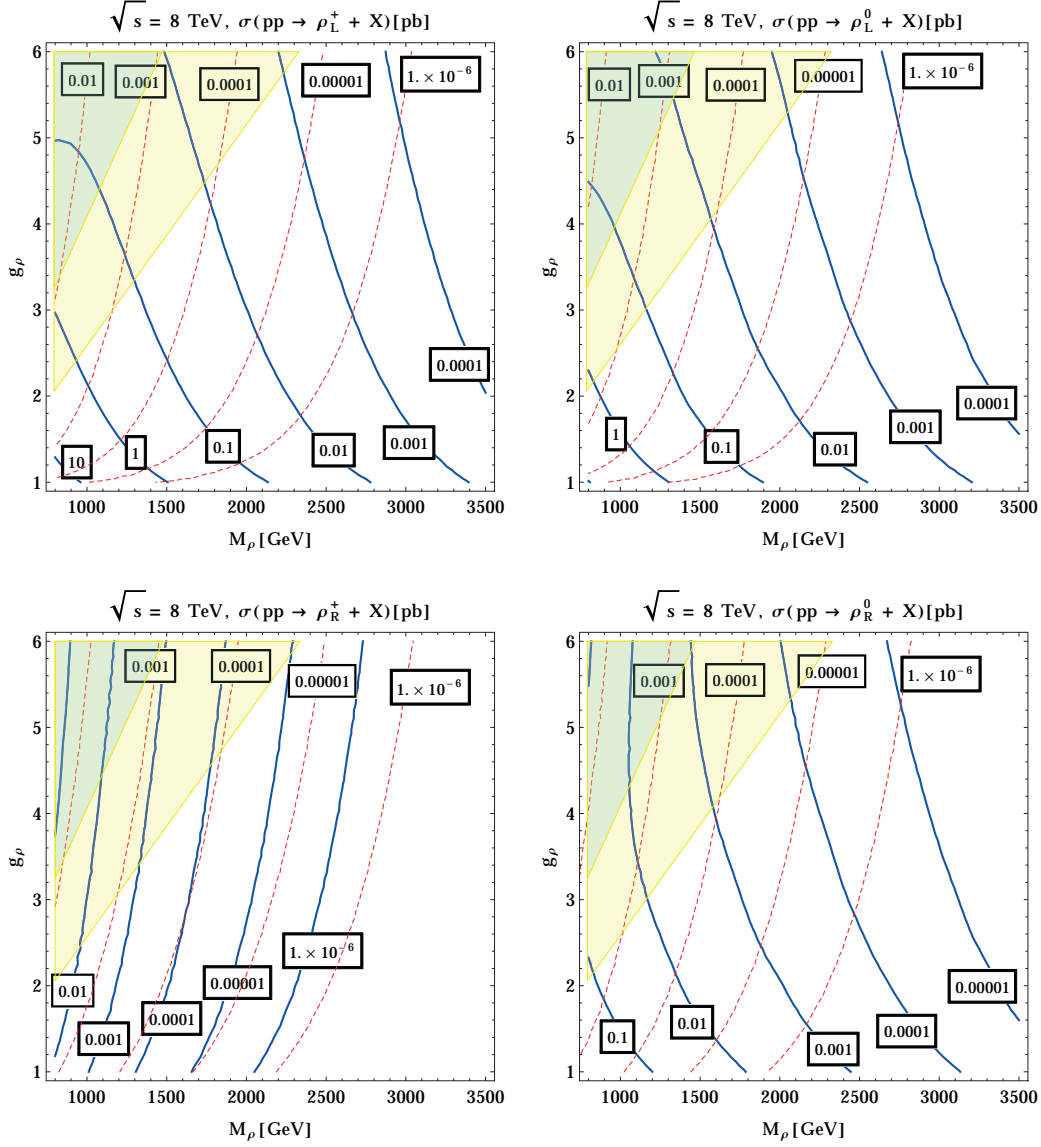


Figure 2.2 – Contours of constant cross section (blue lines for the DY process, red dashed lines for the VBF process) in the plane (M_ρ, g_ρ) for the production of the charged (left panel) and neutral (right panel) left-handed (top) and right-handed (bottom) vector triplets. The yellow region corresponds to $\xi > 0.4$, the light blue one to $\xi > 1$.

couplings to SM fermions get larger as a result of the larger elementary-composite mixing. The VBF cross section increases for higher values of g_ρ , but remains nevertheless sub-dominant in all regions of the parameter space where $\xi < 0.4$. Analogous considerations are valid also for the production cross section of the neutral ρ_μ^R ; the shapes of the contours are similar, but the overall size of the cross section is smaller by a factor $\sim (g'/g_\rho)^2$. As regards the charged ρ_μ^R vector, the couplings to the SM fermions are weaker than the previous cases, since they

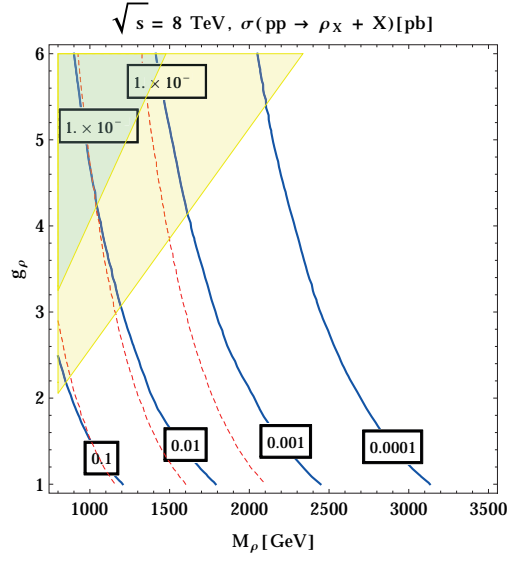


Figure 2.3 – Contours of constant cross section (blue lines for the DY process, red dashed lines for the VBF process) in the plane (M_{ρ_X}, g_{ρ_X}) for the production of the vector singlet. The yellow region corresponds to $\xi > 0.4$, the light blue one to $\xi > 1$.

arise after EWSB; as a result, the two production rates are both very small and comparable, so that in this case the VBF mechanism competes with the DY in every region of the parameter space. Since for both mechanisms the production cross section is extremely small, however, this resonance is produced at low rate at the LHC and is much more difficult to discover. Finally, the vector singlet will be mostly produced by DY process, as shown in Fig. (2.3), since it does not interact with longitudinally polarized gauge bosons before EWSB and the VBF cross section is therefore further suppressed. These results on the behaviour of the production cross sections for the various kinds of vector resonances are in agreement with those obtained in a similar context in [43–48].

2.3.2 Branching ratios

We now turn to the study of the vector resonances decays. Following our natural assumptions on the dynamics of the strong sector, we consider the top partners to be the lightest heavy states and we fix for illustration $M_\Psi = 800$ GeV. This value for the masses of the $X_{\frac{5}{3}}$ and $X_{\frac{2}{3}}$ fields is in agreement with the bounds coming from the LHC direct searches of new exotic quarks of charge 5/3, [81], and automatically satisfies the bounds from searches of other top-like fermions, which are generally weaker. Under these conditions, we will study the most relevant decay channels of the heavy bosons and how the presence of the lighter top partners affects their branching ratios. All the partial decay widths described in this section can be

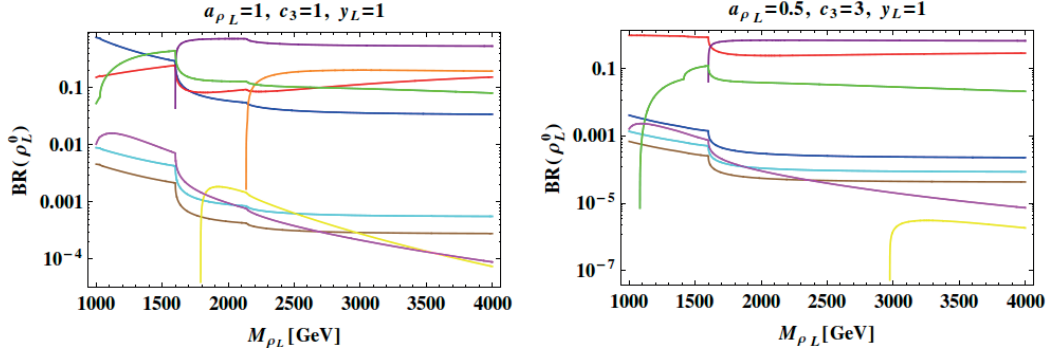


Figure 2.4 – Decay branching ratios of the neutral left-handed vector as a function of the resonance mass for $g_{\rho_L} = 3$, $M_\Psi = 800$ GeV and two different sets of the free parameters. The various curves correspond to the following decay channels: $WW + Zh$ (blue), $t\bar{t} + b\bar{b}$ (red), $l^+ l^-$ (brown), $u\bar{u} + d\bar{d}$ (cyan), $X_{\frac{5}{3}} \bar{X}_{\frac{5}{3}} + X_{\frac{2}{3}} \bar{X}_{\frac{2}{3}}$ (purple), $T\bar{T} + B\bar{B}$ (orange), $X_{\frac{2}{3}} \bar{T}$ (yellow), $X_{\frac{2}{3}} \bar{t}$ (magenta), $T\bar{t} + B\bar{b}$ (green).

computed analytically by using the Feynrules package once the couplings in Appendix C are derived at leading order in ξ .

We start considering the case of the neutral right-handed and left-handed vector resonances; their decay widths are very similar, since they couple to the same top partners fields before EWSB and their couplings to gauge bosons and SM fermions are comparable. We have therefore shown in Fig. (2.4) the different branching ratios as a function of the resonance mass only for ρ_L^0 , omitting the analogous case of ρ_R^0 , for the benchmark value of the strong coupling constant $g_{\rho_L} = 3$ and varying ξ as in Eq. (2.50). The importance of the different decay channels depends obviously on the choice of the various free parameters of the theory; in particular, a_{ρ_L} , c_3 and y_L play a dominant role in setting the strength of the interaction with gauge bosons, third family quarks and heavy fermions, whereas we do not expect c_1 to give a relevant contribution to the different decays. We have thus set $c_1 = 1$ and shown the branching ratios for two different choices of the remaining parameters that change the behaviours of the branching ratios as a function of M_{ρ_L} . In the first case, the three relevant parameters are all set to one, according to the most natural expectations dictated by NDA. We see that in the lower mass region, $M_{\rho_L} < 2M_\Psi$, the dominant decays are WW/Zh , $t\bar{t}/b\bar{b}$ and $T\bar{t}/B\bar{b}$,⁵ whereas above threshold, $M_{\rho_L} > 2M_\Psi$, the vector resonance will mainly decay to pairs of heavy fermions, in particular $X_{\frac{2}{3}}$ and $X_{\frac{5}{3}}$. The relevance of the light decay channels below threshold, when the free parameters are chosen so as to perfectly match their NDA estimate, has also been pointed out in [15]. The situation can be considerably changed with a slight violation of NDA, as shown for the second choice of free parameters, $a_\rho = 0.5$ and $c_3 = 3$. In this case, the decay width to gauge bosons and Higgs is extremely reduced in the lower mass region, since their couplings now get smaller, and the heavy vector mainly decays to two tops or two

⁵For the importance of heavy-light decay channels in a similar context, see for example [49].

2.3. Production and decay of vector resonances at the LHC

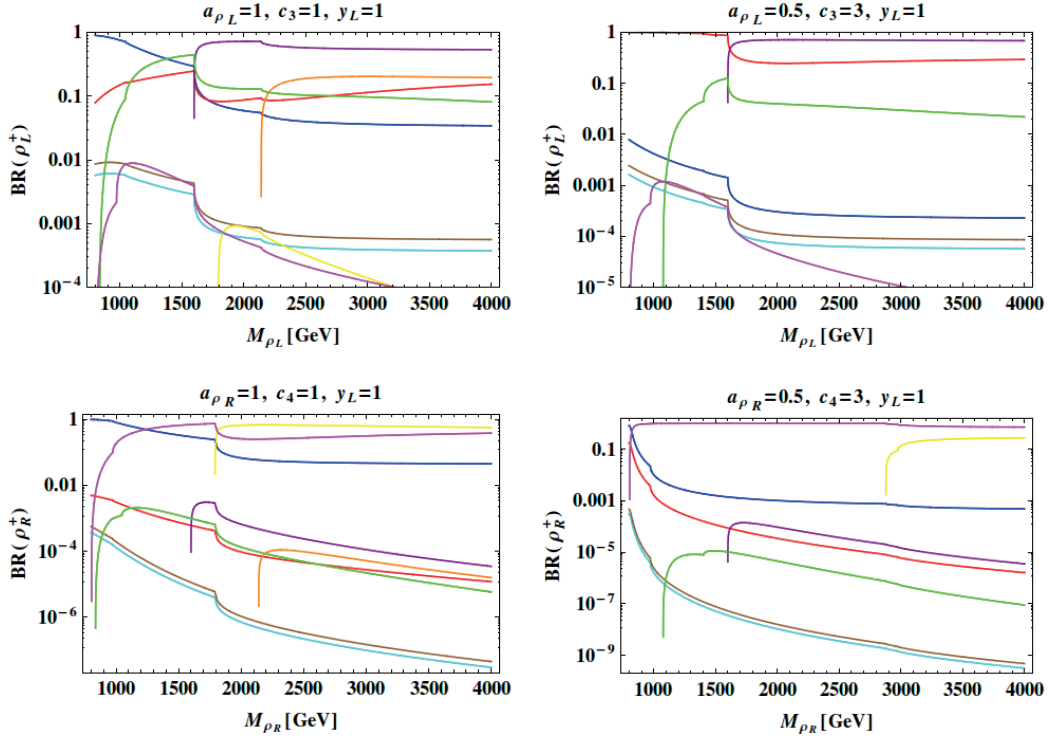


Figure 2.5 – Decay branching ratios of the charged left-handed (top) and right-handed (bottom) vectors as a function of the resonance mass for $g_{\rho_{L/R}} = 3$, $M_\Psi = 800$ GeV and two different sets of the free parameters. The various curves correspond to the following decay channels: $WZ + Wh$ (blue), $t\bar{t}$ (red), $l\nu$ (cyan), $u\bar{d}$ (brown), $X_{\frac{5}{3}}\bar{X}_{\frac{2}{3}}$ (purple), $T\bar{B}$ (orange), $X_{\frac{5}{3}}\bar{T} + X_{\frac{2}{3}}\bar{B}$ (yellow), $X_{\frac{5}{3}}\bar{t} + X_{\frac{2}{3}}\bar{b}$ (magenta), $T\bar{b} + B\bar{t}$ (green).

bottoms, whereas above threshold the decays to two 5/3 charged exotic states and to two top-like $X_{\frac{2}{3}}$ particles remain still the dominant ones. We notice that for this particular choice of parameters the fermionic elementary-composite mixing is stronger, so that the couplings of the vector resonance to a heavy fermion and a third family quark are weaker than the corresponding couplings to two tops or bottoms. The branching ratio for the heavy-light decay channels is therefore reduced, whereas the $t\bar{t}$ and $b\bar{b}$ decays are considerably enhanced. In both cases, the branching ratios for decays to leptons and first two quark families are instead strongly suppressed, as expected, as well as the decays to the top partners whose couplings to the heavy vectors are not allowed by isospin conservation before EWSB. We note finally that the branching fractions to WW and Zh are equal to a very good approximation, as implied by the Equivalence Theorem, which works well since $M_{\rho_L} \gg m_{W/Z}$ for the chosen values of parameters. The approximate custodial symmetry also implies that $BR(t\bar{t}) \sim BR(b\bar{b})$ and $BR(u\bar{u}) \sim BR(d\bar{d}) \sim 3BR(l^+l^-)$.

As concerns the decay channels of the charged left-handed and right-handed vector reso-

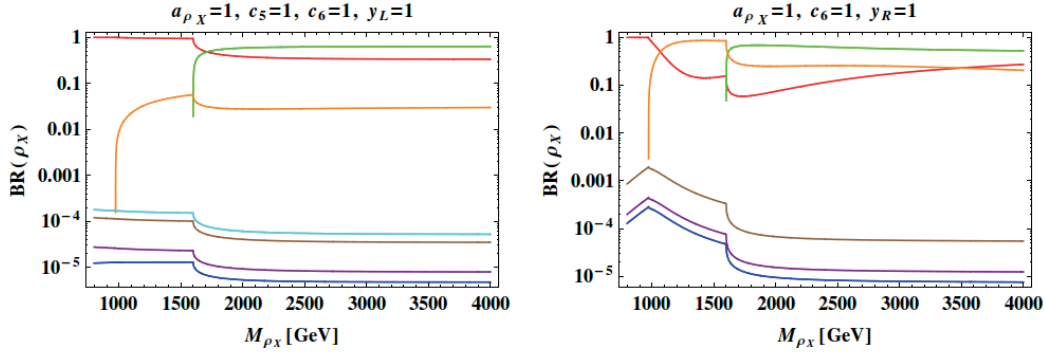


Figure 2.6 – Decay branching ratios of the vector singlet as a function of the resonance mass for $g_{\rho_X} = 3$ and $M_\Psi = 800$ GeV in models M_X^1 (left panel) and M_X^2 (right panel). The various curves correspond to the following decay channels: $WW + Zh$ (blue), $t\bar{t}$ (red), l^+l^- (cyan), $u\bar{u} + d\bar{d}$ (brown), $b\bar{b}$ (purple), $\tilde{T}\tilde{T}$ (orange), $\tilde{T}\tilde{T}$ (green).

nances, their behaviour is now completely different, as implied by their different quantum numbers. The branching ratios for both cases are shown in Fig. (2.5), for the same value of the strong coupling as before and the same two sets of free parameters, the first one fully matching the NDA estimate, the second one slightly departing from the natural expectations. The decay to two gauge bosons, WZ , and to Wh is dominant in the low mass region for both resonances when $a_\rho = 1$, but as soon as a_ρ gets smaller and $c_{3/4}$ is increased this channel is strongly suppressed. The $t\bar{b}$ decay becomes the most important one in the low mass region when $a_\rho = 0.5$ and $c_3 = 3$, for the ρ_L^+ particle, as implied by partial compositeness, whereas it is always sub-dominant for the ρ_R^+ case, because of its suppressed couplings to third family quarks. The heavy-light decay channel for the charged left-handed vector is again reduced for the second choice of parameters because, analogously to its neutral counterpart, for smaller values of a_{ρ_L} the couplings to one heavy fermion and a third family quark are weaker. Above threshold, the most relevant decay channel of the left-handed vector is that involving two top partners, for every choice of the free parameters. This latter charged vector will in fact mainly decay to $X_{\frac{5}{3}}\bar{X}_{\frac{2}{3}}$, with almost unit branching ratio. Among the ρ_R^+ decays involving top partners, on the other hand, the dominant ones are the channels $X_{\frac{5}{3}}\bar{t}/X_{\frac{2}{3}}\bar{b}$, which is kinematically favoured since it opens up as soon as $M_{\rho_R} > M_\Psi$, and $X_{\frac{5}{3}}\bar{T}/X_{\frac{2}{3}}\bar{B}$. They are both dominant above the threshold for the first choice of parameters, whereas in the second case the decay to $X_{\frac{5}{3}}\bar{t}/X_{\frac{2}{3}}\bar{b}$ is the most relevant one among all the others for every value of the resonance mass. Finally, the decay to leptons and first two quark families are again suppressed, but the branching ratios for the ρ_R^+ are much smaller, since its couplings to fully elementary fermions are further suppressed by a factor of ξ .

We finally discuss the most important decay channels of the singlet in the two models M_X^1 and M_X^2 ; the branching ratios are shown in Fig. (2.6), for $g_{\rho_X} = 3$. In both models, the decays to

lighter SM fermions, gauge bosons and Higgs are always suppressed, due to their extremely weak couplings to the vector resonance; the parameter a_{ρ_x} therefore does not play any major role in improving the relevance of the WW and Zh channels. The most important decays are thus $t\bar{t}$, $\tilde{T}\tilde{t}$ and $\tilde{T}\tilde{\bar{T}}$, as expected. In the \mathbf{M}_X^1 case, the two important parameters are c_5 and c_6 ; setting them to one, as illustration, shows that, below the threshold for the production of two heavy fermions, the singlet mainly decays to two tops, whereas above the threshold the channel to two top partners becomes the dominant one. The decay width to one top partner and the top quark, on the other hand, is smaller since it is generated only after EWSB. The situation is different in model \mathbf{M}_X^2 ; after setting the relevant parameter c_6 to one, we see that the channel $\tilde{T}\tilde{t}$ is the most important one below the threshold, because it now arises before EWSB. When $M_{\rho_x} > 2M_\Psi$, on the other hand, the decay to two top partners is still the most relevant, even if now the channel involving the top and \tilde{T} is stronger than in the previous model.

2.4 Bounds from LHC direct searches

Many searches of spin-1 resonances have been performed by the ATLAS and CMS collaborations, with the data collected at the 8 TeV LHC, both for neutral and charged heavy vector particles. The main decay channels that have been considered for the charged resonance can be summarized as follows:

- the decay to third family quarks, $\rho^+ \rightarrow t\bar{b}$, both by ATLAS in [95] and CMS in [88],
- the leptonic decay $\rho^+ \rightarrow l\bar{\nu}$, by ATLAS in [94] and by CMS in [90],
- the fully hadronic decay to gauge bosons, $\rho^+ \rightarrow WZ \rightarrow jj$, by CMS in [85] and in [86],
- the fully leptonic decay to gauge bosons, $\rho^+ \rightarrow WZ \rightarrow 3l\nu$, by ATLAS in [96] and by CMS in [89].

As regards the searches of new neutral resonant states, the decay channels which have been extensively analysed by the two experiments are:

- the leptonic decay, $\rho^0 \rightarrow l^+ \bar{l}^-$, by ATLAS in [92] and by CMS in [82],
- the decay to two tops, $\rho^0 \rightarrow t\bar{t}$, by ATLAS in [91] and by CMS in [84],
- the decay channels to two τ leptons, $\rho^0 \rightarrow \tau\bar{\tau}$, by ATLAS in [93],
- the semi-leptonic decay to two gauge bosons, $\rho^0 \rightarrow WW \rightarrow l\bar{\nu}jj$, by CMS in [83],
- the fully hadronic decay to two gauge bosons, $\rho^0 \rightarrow WW \rightarrow jj$, by CMS in [85].

The results of these searches are all presented as limits on the production cross section times branching ratio, $\sigma \times BR$, as a function of the resonant mass. This allows us to recast very easily these analyses as exclusion regions in the parameter space of our models: once the cross section is computed semi-analytically with the method described in the previous section and the branching ratios are derived as a function of the couplings, we can immediately compare the theoretical predictions with the experimental data. Similar exclusion contours on the parameters of a vector resonance, charged under $SU(2)_L$, have already been presented in [40], without considering the effects of partial compositeness or lighter heavy fermions. We will show how these bounds are altered by the stronger coupling of third family quarks to the resonance and by the presence of lighter top partners, for which we will conveniently choose again $M_\Psi = 800$ GeV, and compare them with the indirect information coming from the resonances contribution to Electroweak Precision Observables, derived in Appendix B. In deriving the exclusion bounds on the parameters of our models, we will finally take into account only the DY production mechanism and compute the total production cross section without considering the contribution of the VBF process, this latter being much smaller than the DY one.

We finally stress that the results presented in this section are based on the validity of the Narrow Width Approximation. This latter assumes that the production rate can be factorized into an on-shell cross section times a decay branching ratio and neglects the interference with the SM background. Experimental analyses performed by following this approach must be carried out consistently with its underlying assumptions, namely that the limits on the production rate of the new particles should be set by focussing on the on-shell signal region; for a detailed discussion of these aspects see Ref. [40]. We will take into account the limitations of the NWA approach by showing in the exclusion plots the contours of constant Γ/M_ρ in the parameter space of our models. In the region where this ratio is less than 10%, the resonance is narrow enough for the Narrow Width Approximation to be a reliable estimate of the production rate, otherwise a more refined description must be considered in order to analyse the results of the experimental searches.

2.4.1 Bounds on ρ_μ^L

We start the study of the experimental constraints on the parameters of our models by considering the case of the left-handed heavy vector. The tree-level exchange of this particle contributes to the \hat{S} and W parameters [55–57], among which the most stringent bounds come from the first one, since W is smaller by a factor of $g^2/g_{\rho_L}^2$. In Fig. (2.7) we show the excluded regions in the (M_{ρ_L}, g_{ρ_L}) plane from four different direct searches, one for each of the main decay channels considered by the experimental groups, and we compare them with the limits coming from the \hat{S} variable. We also show how the bounds change for two different

choices of the free parameters: in one case, we fix $a_{\rho_L} = c_3 = y_L = 1$; in the second case we have analysed the set $a_{\rho_L} = c_3 = 0.5$, $y_L = 3$. The variable ξ always scales as in Eq. (2.50). Only the bounds for the charged heavy vector case are presented, for illustration; the exclusion limits for the neutral resonance are similar and are not reported here.

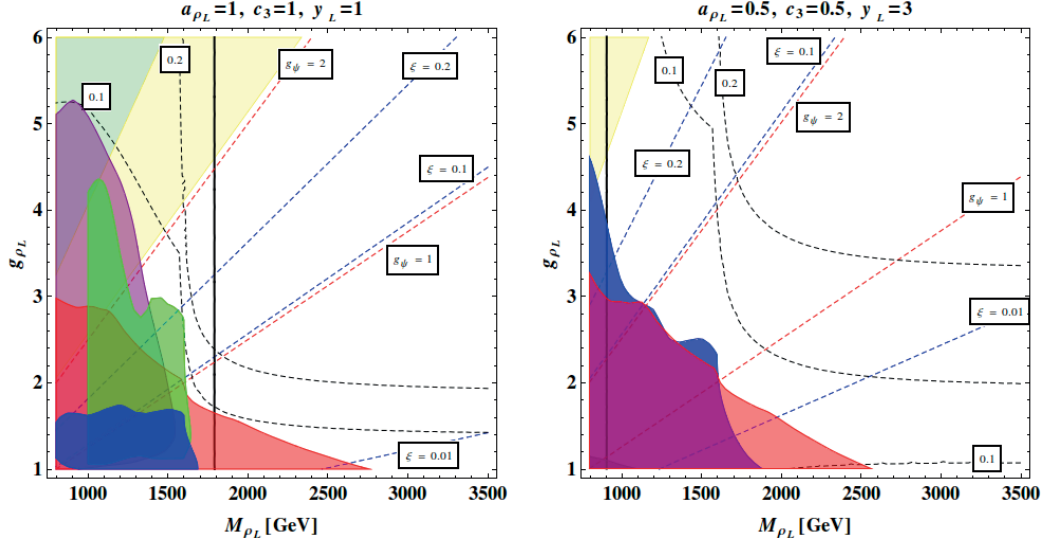


Figure 2.7 – Excluded regions in the (M_{ρ_L}, g_{ρ_L}) plane for the charged left-handed vector resonance for two different sets of the free parameters and for $M_\Psi = 800$ GeV. The exclusions are derived from the $\rho^+ \rightarrow t\bar{b}$ searches in [88] (blue), the $\rho^+ \rightarrow l\bar{\nu}$ searches in [90] (red), the $\rho^+ \rightarrow WZ \rightarrow jj$ searches in [85] (purple) and the $\rho^+ \rightarrow WZ \rightarrow 3l\nu$ searches in [96] (green). The plot also shows the contours of constant Γ/M_{ρ_L} (dashed black lines), of constant ξ (dashed blue lines) and of constant g_ψ (dashed red lines). The region on the left of the thick black line is excluded by experimental constraints on the \hat{S} parameter. The yellow region corresponds to $\xi > 0.4$, the light blue one to $\xi > 1$.

Let us discuss the results for the first choice of parameters. The searches of a heavy vector decaying to gauge bosons, which subsequently decay fully leptonically or fully hadronically, give the most important constraints in the low mass region, $M_{\rho_L} < 2M_\Psi$, since for the chosen value of a_{ρ_L} the branching ratio of the WZ channel is still dominant below the threshold. These searches do not give any information in the high mass region, $m_{\rho_L} > 2M_\Psi$, however, due to the opening of the $X_{\frac{2}{3}} \bar{X}_{\frac{2}{3}}$ channel, which significantly reduce the branching ratio to gauge bosons. On the other hand, despite the suppressed couplings to the vector resonance of SM leptons, the searches in the $l\bar{\nu}$ channel are competitive with the previous ones and can also provide exclusion limits above the threshold for small values of the strong coupling constant. From Fig. (2.7), we also see how the direct results compete with the indirect bounds from the \hat{S} parameter; this latter excludes the mass of the heavy resonance up to ~ 1.8 TeV and still gives the most powerful information on the parameter space of the model.

These bounds derived for the charged left-handed heavy vector, for $a_{\rho_L} = 1$, agree with the

results obtained in analogous contexts; the relevance of the experimental searches in the gauge bosons and leptonic channels was for instance already discussed in [40]. However, taking into account the enhanced coupling of third family quarks to the resonance, we see that exclusion limits can be obtained below threshold and for small values of g_{ρ_L} also from the $t\bar{b}$ search, which does not give any constraint when treating the top-bottom doublet as fully elementary.

Fig (2.7) also shows different contours in the plane (M_{ρ_L}, g_{ρ_L}) which provides information on the validity of the NWA approach and of our theoretical assumptions based on naturalness requirements. The curves corresponding to the contours of constant Γ/M_{ρ_L} show that the experimental constraints are always confined in the region when this ratio is smaller than 10%, so that the NWA works well for all the four main searches. The dashed blue lines, on the other hand, correspond to contours of constant ξ and give thus information on the amount of tuning required for different combination of the mass and coupling of the heavy resonance. The most natural region compatible with the experimental constraints on ξ is the window between $\xi \sim 0.1$ and $\xi \sim 0.2$, a portion of which is already excluded by the direct searches below the threshold; below the $\xi \sim 0.1$ line, more tuning is required to accommodate a reasonably light Higgs in the spectrum, so that these regions correspond to the more unnatural ones where our hypothesis of lighter top partners is no longer justified. Contours of constant g_Ψ are also shown; the fermionic coupling constant can be in fact derived, using both Eq. (2.7) and Eq. (2.8), as

$$g_\Psi = \frac{a_{\rho_L}}{a_\Psi} \frac{M_\Psi}{M_{\rho_L}} g_{\rho_L}; \quad (2.51)$$

we have shown the lines corresponding to the naturally favoured values $g_\Psi = 1$ and $g_\Psi = 2$ fixing $a_\Psi = a_{\rho_L}$ for illustration. We see that the preferred natural window corresponds also to the portion of parameter space where the fermionic coupling is in its theoretically expected range; the region where $g_\Psi \lesssim 1$, on the other hand, coincides with the unnatural one, where ξ assumes very small values and the lightness of top partner can no longer be justified by naturalness arguments.

We focus now on the exclusion limits for the second set of parameters. In this case, the values of a_{ρ_L} and c_3 are reduced and y_L is instead incremented in order to show the effects on the bounds of the reduced interaction strength between gauge bosons and heavy vectors, on one side, and of a higher top quark degree of compositeness, on the other side. Since now the branching ratio to gauge bosons is suppressed even in the low mass region, no excluded region can be extracted from any of the searches involving the WZ decay channel. On the other hand, the experimental analyses in $t\bar{b}$ channel provide a bigger exclusion limit with respect to the previous case, due to the bigger value of y_L which now increases the strength of the

interaction between the charged resonance and the q_L doublet despite the reduced value of c_3 . The constraints coming from the $l\bar{\nu}$ searches are still competitive and important above the threshold, so that this decay channel is extremely powerful in providing information on the physics of new heavy states or for a potential discovery. Another main difference with respect to the previous study is that, choosing $a_{\rho_L} = 0.5$, the limit coming from the \hat{S} parameter is reduced by a factor of two, excluding the mass of the heavy vector up to ~ 1 TeV. When the a_{ρ_L} parameter is lower than one, we therefore find that the direct searches are much more competitive and can exclude portions of the parameter space beyond the reach of indirect information.

As regards the NWA approach, also in this case the bounds are well constrained in the region where this approximation is reliable and valid. The natural window $0.1 \lesssim \xi \lesssim 0.2$ is now achieved in more strongly coupled scenarios, due to the reduced value of a_{ρ_L} , and still part of it is excluded by the two shown searches. The contours of constant g_Ψ are derived again for $a_\Psi = a_{\rho_L}$ and, as before, the less fine-tuned region coincides with higher values of the fermionic coupling.

2.4.2 Bounds on ρ_μ^R

We consider now the bounds on the parameter space of the right-handed resonance. This heavy particle contributes at tree level to the \hat{S} and Y parameters; this latter being suppressed by a factor of $g'^2/g_{\rho_R}^2$, we again expect the most stringent limit on the mass of the new state to come from the \hat{S} variable. Since the total production cross section of the charged right-handed vector is very small, for both VBF and DY mechanisms at the LHC, we can only extract bounds on the model parameters for the neutral ρ_R^0 ; these are shown in Fig. (2.8), as excluded regions in the (M_{ρ_R}, g_{ρ_R}) plane for two different sets of the free parameters and recasting the results of the searches in the lepton channel and in the semi-leptonic WW channel. We have presented the different exclusion contours for two values of c_4 , when it is vanishing and when it is 1, in order to clearly analyse the effects of the lighter top partners on the bounds from direct searches.

Let us start briefly considering the case in which $a_{\rho_R} = 1$ and $y_L = 1$. For these values of the free parameters, the WW channel provides constraints in the low mass region, analogously to the left-handed resonance, and it is not sensitive to the portion of parameter space above the threshold $2M_\Psi$. In the extreme situation where $c_4 = 0$ and the direct coupling to top partners is completely eliminated, the constraints are obviously much stronger and they gradually reduce as c_4 is increased and the branching ratios for the top partners channels become important. As regards the experimental search in the leptonic channel, the bounds can give exclusions above the threshold and again they are stronger for small c_4 , as expected. We note also the

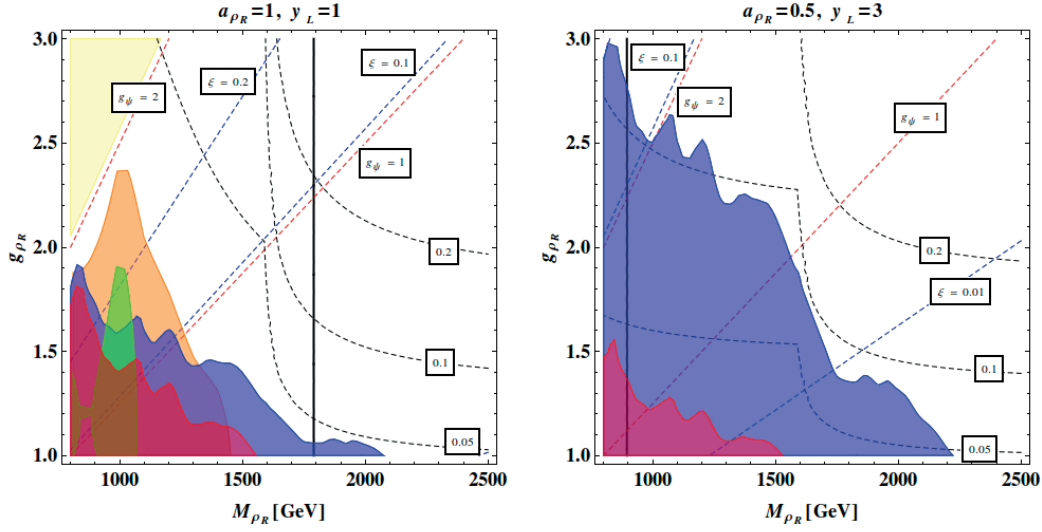


Figure 2.8 – Excluded regions in the (M_{ρ_R}, g_{ρ_R}) plane for the neutral right-handed vector resonance for two different sets of the free parameters and for $M_\Psi = 800$ GeV. The exclusions are derived from the $\rho^0 \rightarrow l\bar{l}$ searches in [82] (in red for $c_4 = 1$, in blue for $c_4 = 0$) and the $\rho^0 \rightarrow WW \rightarrow lvjj$ searches in [83] (in green for $c_4 = 1$, in orange for $c_4 = 0$). The plot also shows the contours of constant Γ/M_{ρ_R} (dashed black lines), of constant ξ (dashed blue lines) and of constant g_Ψ (dashed red lines). The region on the left of the thick black line is excluded by experimental constraints on the \hat{S} parameter. The yellow region corresponds to $\xi > 0.4$.

main difference between the right-handed and the left-handed case: the production cross section for the ρ_R resonance being smaller by a factor $(g'/g_\rho)^2$, the bounds in the parameter space of the right-handed vector are in general much weaker than those of the left-handed counterpart. Finally, the NWA approach works well also in this situation, the excluded regions being confined in the portion of the (M_{ρ_R}, g_{ρ_R}) plane where $\Gamma/M_{\rho_R} < 0.1$. The discussion on the natural window and the comparison with the limits from the \hat{S} variable are similar to the ρ_L case.

We discuss now how the bounds change for $a_{\rho_R} = 0.5$ and $y_L = 3$. As expected, no exclusion contours can be derived from the WW search channel, since the branching ratios to gauge bosons are now suppressed. The only bounds come from the analysis performed with the ll decay channel; for $c_4 = 0$, they are much stronger, whereas, when the decay to top partners and third family quarks are enhanced with $c_4 = 1$, a very tiny region of parameter space is excluded. This is again due to the smaller production cross section that makes this resonance in general much harder to constrain and to discover with respect to the previous one. The NWA is again well satisfied and the region where our natural assumptions are well justified has the same behaviour as the analogous left-handed case.

We finally notice that no exclusion regions can be derived from the experimental search

of neutral resonances in the $t\bar{t}$ channel. The experiments performed using this particular decay are indeed much less sensitive than the others, so that, despite the enhanced coupling strength of the top quark to the neutral vector, we find no bounds even for high degrees of top compositeness and for larger values of c_4 . For this reasons, we do not expect this final state to be enough powerful for the discovery of a neutral spin-1 particle.

2.4.3 Bounds on ρ_μ^X

The experimental searches for a neutral heavy resonance can also be recast as a bound on the parameter space of the vector singlet. This heavy particle contributes only to the Y parameter, which however always gives very weak constraints; in this case, the exclusion limits from direct searches are therefore the most relevant ones and electroweak precision measurements have very little exclusion power.⁶ The excluded regions in the (M_{ρ_X}, g_{ρ_X}) plane are presented in Fig. (2.9), both for model \mathbf{M}_X^1 and \mathbf{M}_X^2 and for different values of the free parameters. In both cases, the most relevant experimental search is always the decay channel to the ll final state, since the searches involving the decay to WW do not obviously give any constraint, due to the extremely weak coupling strength of the singlet to the W boson. We will therefore fix $a_{\rho_X} = 1$ in all the cases considered, since different values of this parameter will only alter the shape of the contours of constant ξ and g_Ψ , but will not significantly change the exclusion contours. Despite the enhanced coupling strength to top quarks, finally, the searches with the $t\bar{t}$ final state produce no limits on the parameter space of the two models, similarly to the right-handed neutral resonance.

Considering now the specific results for model \mathbf{M}_X^1 , we have fixed $y_L = 1$ and shown the bounds for three different values of c_5 . The most stringent constraints on the parameter space of the singlet are obviously obtained when $c_5 = 0$; in this extreme case, the direct coupling to the t_R quark is suppressed and the branching ratio to leptons increases, so that the experimental search under consideration gives stronger bounds. Increasing c_5 , on the other hand, makes the bounds much weaker and for $c_5 = 1$ only a very tiny portion of parameter space is excluded. This is due again to the g' suppression in the coupling of the vector singlet to lighter quarks, which makes the total production cross section smaller than the left-handed case. All the exclusion regions are concentrated in the low mass region, $M_{\rho_X} < M_\Psi$, and abruptly end when $M_{\rho_X} = 2M_\Psi$, due to the opening of the decay channel to two top partners.

The situation is similar for model \mathbf{M}_X^2 ; we have shown the exclusion regions for $a_{\rho_X} = y_R = 1$

⁶Since the vector singlet does not contribute to the \hat{S} parameter, our theoretical picture of heavier spin-1 resonances and lighter top partners could be not so well justified for this particle, allowing the possible existence of a vector which is as light as or lighter than the spin-1/2 resonances. Consistency with the idea that the new strong sector should be characterised by only two mass scales and that all spin-1 heavy states should behave similarly, however, leads us to consider also the singlet to belong to the tower of heavier resonances at the m_ρ scale.

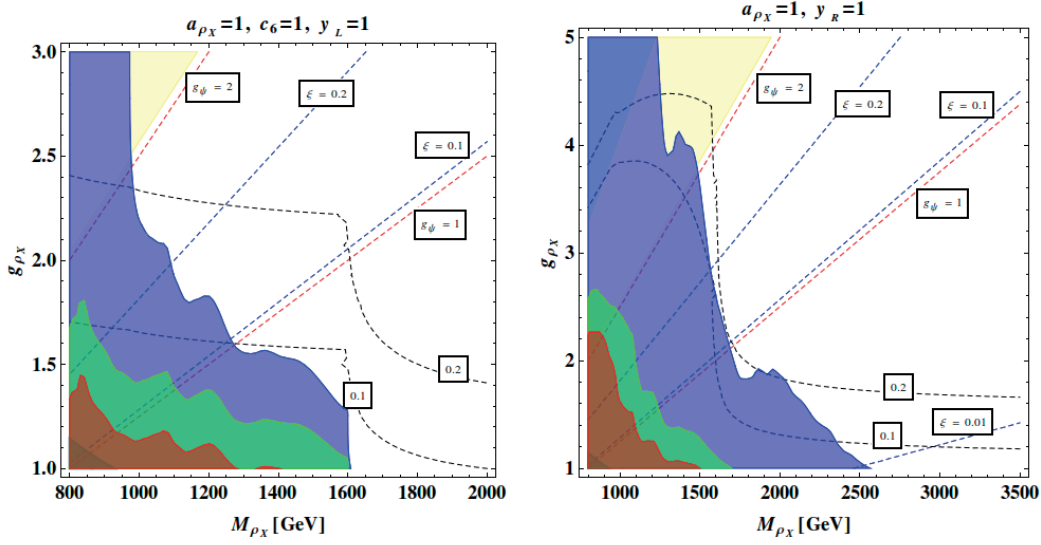


Figure 2.9 – Excluded regions in the (M_{ρ_X}, g_{ρ_X}) plane for the vector singlet in models \mathbf{M}_X^1 (left) and \mathbf{M}_X^2 (right), fixing $M_\Psi = 800$ GeV. The exclusions are derived from the $\rho^0 \rightarrow l\bar{l}$ searches in [82]. Left panel: in red the excluded region for $c_5 = 1$, in green for $c_5 = 0.5$, in blue for $c_5 = 0$. Right panel: in red the excluded region for $c_6 = 1$, in green for $c_6 = 0.5$, in blue for $c_6 = 0$. The plot also shows the contours of constant Γ/M_{ρ_X} (dashed black lines), of constant ξ (dashed blue lines) and of constant g_Ψ (dashed red lines). The yellow region corresponds to $\xi > 0.4$.

and for three values of the free parameter c_6 , ranging from 0 to 1. When c_6 is vanishing, the bounds are much stronger and they can extend above the threshold due to the absence of a direct interaction with the \tilde{T} heavy fermion. Increasing c_6 makes the exclusion limits weaker; the bounds are now confined in the low mass region and are less stringent than the neutral left-handed case due to the hypercharge suppression.

Finally, the NWA approach is reliable for both models. In Fig. (2.9), we have in fact shown the contours of constant Γ/M_{ρ_X} only for $c_5 = 1$ and $c_6 = 1$, corresponding to the excluded region in red. The contours for the other two smaller values of these parameters, corresponding to the excluded regions in blue and green, lie outside the portion of the (M_{ρ_X}, g_{ρ_X}) plane which is presented. Therefore, the bounds corresponding to $c_5 = 0, 0.5$ and to $c_6 = 0, 0.5$ automatically satisfy the requirements of a narrow resonance, whereas the bound for $c_5 = 1$ and $c_6 = 1$ lie completely in the portion of parameter space where the total decay width in units of M_{ρ_X} is less than 10%. Also in this final case the NWA is therefore a valid prescription for analysing the experimental results. For both models, the natural window where our theoretical assumptions are well justified is excluded in the low mass region, but still allowed for larger values of the resonant mass and for more strongly coupled scenarios.

2.5 Discussion

In this Chapter we have introduced a simplified description based on an effective low-energy Lagrangian of the phenomenology of heavy vector resonances in the minimal composite Higgs model, studying their interaction with lighter top partners. Our approach is based on two classes of assumptions, one regarding the symmetry structure of the theory and one regarding its dynamical features. As concerns the symmetries, we considered the minimal case of a new confining dynamics with an approximate global $G = SO(5) \times U(1)_X$ symmetry spontaneously broken to $H = SO(4) \times U(1)_X$. The Higgs boson emerges as pNGB and the electroweak scale is dynamically generated via loop effects. In this framework, we focussed on heavy vector triplets, transforming as a $(\mathbf{3}, \mathbf{1})$ and $(\mathbf{1}, \mathbf{3})$, and on heavy vector singlets, transforming as a $(\mathbf{1}, \mathbf{1})$ of $SO(4)$. Following the paradigm of partial compositeness, we introduced a linear coupling to the strong sector for the top-bottom doublet and we considered the t_R to be a bound state of the strong dynamics, except in one case in which we studied the implications of a partially composite t_R quark. In this scenario, we characterised the couplings of heavy vectors to top partners in the singlet and in the fourplet of $SO(4)$. In the most natural realizations of the composite Higgs idea these are indeed the lightest fermionic resonances that must be present in the spectrum. We constructed four simplified models which are suitable for studying the phenomenology of heavy vectors, capturing the most important features of the underlying symmetry structure.

As concerns the dynamics, we parametrised the new strong sector with two mass scales, a heavier one for vector resonances, m_ρ , and a lighter one for fermionic resonances, m_ψ . We have clarified under which conditions our effective Lagrangian description is a good approximation of the full underlying dynamics and what its regime of validity is. Our simplified approach is in fact reliable whenever the mass of the heavy vector satisfies the relation $m_\psi < M_\rho \ll m_\rho$, in which case, using the criterion of partial UV completion [8], the tower of the remaining and unknown resonances can be integrated out of the spectrum. Our approximate models provide therefore a systematic simplified description of the phenomenology of spin-1 heavy states in an expansion of M_ρ/m_ρ . These constructions lose their validity as soon as $M_\rho \sim m_\rho$, in which case using an effective Lagrangian is formally inappropriate. However, we expect our approach to provide a good interpretation of the experimental results, at least qualitatively, also in this second case. We have assessed this issue considering the particular situation in which two vector resonances of the composite tower are present in the spectrum. We show in Appendix D that neglecting the spectrum degeneracy is a reliable approximation for a basic quantitative description of their phenomenology.

One of the most important simplification of our procedure is to describe the phenomenology of heavy vectors in terms of a manageable set of free parameters. Once the basic electroweak

observables and the top mass are fixed, we are left with one mass and one coupling for each resonance, the misalignment angle and some additional $O(1)$ parameters controlling the interaction with top partners and SM fermions. Of these, c_1 has no role in the production and decay of the vector resonances, so that their phenomenology can be significantly affected only by the remaining (c_3, y_L) for ρ_μ^L , (c_4, y_L) for ρ_μ^R , (c_5, c_6, y_L) in model \mathbf{M}_X^1 and (c_6, y_R) in model \mathbf{M}_X^2 . In this sense, the effective Lagrangian approach based on specific underlying assumptions on the symmetry structure of the theory has the virtue of expressing all the couplings of the vectors to top partners and SM particles in terms of only these quantities. This reduces considerably the degrees of freedom that one would have in a complete model-independent procedure, like in [40, 41], and allows us to formulate a consistent description of the interaction with lighter fermions, which necessarily requires some knowledge of the underlying symmetries, [7]. Our model-dependent approach is therefore essential in order to capture the most important features of the interplay between heavy vectors and top partners, that would be impossible to analyse without any robust assumption on the symmetry structure of the theory.

For each resonance, we studied the main phenomenological features, analysing the mixing angles, the spectrum and the most important couplings arising before EWSB. We have shown that the left-handed and right-handed vectors couple strongly to the longitudinally polarized W and Z bosons and Higgs, thanks to the Equivalence Theorem, and that they both couple very weakly to fully elementary SM fermions. Concerning their interaction with top partners and third family quarks, conservation of isospin gives the most important rationale to extract the relevant couplings: only those conserving isospin without any Higgs vev insertion can arise before EWSB and the corresponding decay channels give a dominant contribution to the decay width. We have also considered the very different case of the singlet, which has peculiar properties with respect to the other resonances. It couples very weakly both to SM fermions and to gauge bosons, whereas it interacts strongly with the t_R and the top partner \tilde{T} , with interaction strength depending on whether the t_R is partially composite or not. This vector is also special since it does not give any contribution to the \hat{S} parameter, so that direct searches are the most important mean to constrain its parameter space. We have finally studied the decay branching ratios of all the three vectors, noticing the dominance of the top partner decay channel above the threshold $M_\rho = 2M_\psi$ and studying the relevance of the decays to SM particles below the threshold for different values of the free parameters.

Using our effective Lagrangian description, we have devised an efficient semi-analytical method to compare the theoretical predictions of our models with the LHC data on direct searches of vector resonances. These latter are given as exclusion limits of $\sigma \times BR$ as a function of the resonance mass, under the validity of the Narrow Width Approximation. In order to compute the total production cross section, we have numerically calculated the parton level

contribution once for all, setting the relevant trilinear couplings to unity, and we have then rescaled with the analytical expression of the couplings at linear order in ξ . We have also studied the main production mechanisms, DY and VBF, noticing that the former is the most relevant one in all cases of interest. Following this method, it is very fast to analytically recast the experimental searches as bounds on the parameter space of the resonances, once the LHC data are rescaled with the BRs that can be computed analytically in our models. The calculation of the cross sections as well as the numerical diagonalization of the vector mass matrices, at every order in ξ , have been implemented in a Mathematica notebook that is available on a dedicated website, [66].

We have applied this methodology to extract exclusion limits on the parameter space of our models using the presently available 8 TeV LHC data. The results can be found in Figs. (2.7), (2.8) and (2.9), where exclusion regions are shown for some relevant direct searches of heavy vectors. We have analysed what information can be obtained from the decay channels considered by the experimental groups for different values of the free parameters of the theories. For the left-handed vector, we concluded that the most constraining decay channels at the LHC are WZ and $l\bar{\nu}$, when the free parameters are chosen so as to respect the NDA estimate. A slight violation of NDA, obtained by reducing a_{ρ_L} , shows, however, that the decay channels to gauge bosons can give no bound at all and that a very important decay channel that can be extensively studied in the future is the $t\bar{t}$, since partially composite quarks are more strongly coupled to the heavy vectors than to the other SM fermions. The situation is similar for the neutral right-handed resonance; again, for values of the free parameters respecting the NDA expectations, the WW and the $l\bar{l}$ channels give the most stringent bounds, whereas reducing the value of a_{ρ_R} shows that exclusion regions can be drawn only from the leptonic decay channel. As regards the searches with a $t\bar{t}$ final state, in this case they do not provide any constraint, since the production cross section for ρ_μ^R is smaller than the corresponding one for the left-handed vector by a factor $(g'/g)^2$. This suppression is the reason why the enhanced coupling to top quarks does not improve the sensitivity of this channel. Finally, considering the ρ_μ^X case, the most constraining decay channel is the $l\bar{l}$, since the couplings of the singlet to W bosons are very weak. Also in this case, the $t\bar{t}$ channel does not give any significant bound, the production cross section being again reduced by a factor $(g'/g)^2$. The suppression in the production cross sections of the right-handed vector and of the singlet is in general the reason why the bounds for the ρ_μ^R and ρ_μ^X resonances are much weaker than the bounds on ρ_μ^L , making them more difficult to constrain or discover at the LHC. Finally, all these results can be readily interpreted as a test of our notion of naturalness and of our dynamical assumptions on the nature of the strong dynamics. We have shown the most natural expected window of parameter space and considered how the data already exclude part of it in the low-mass and small coupling region. But for bigger values of the mass and for more strongly coupled scenarios, there is still room for a natural realization of the composite Higgs idea with heavier

vectors decaying to lighter top partners.

3 A Composite UV completion of the Twin Higgs scenario

The possibility that there exist models of electroweak symmetry breaking with a minimal amount of fine tuning (less than 10% or so) and the simultaneous absence below a few TeV of any new particle charged under the Standard Model (SM) gauge group deserves attention. Generically the idea behind this possibility goes under the name of Twin Higgs. In this Chapter we discuss an explicit example where this idea is implemented in the context of a composite Higgs picture. We do that with the purpose of proposing and analyzing a few generic features of such an implementation, which will be illustrated in the course of the exposition.

3.1 A model example

The situation which we have in mind, depicted in Figure 3.1, is that there exist a new “Composite Sector” (CS), endowed with a global symmetry group G , which confines at a scale m_* in the TeV or multi-TeV range. In the process, G gets spontaneously broken to a subgroup H and the order parameter for this breaking, f , is related to the confinement scale by $m_* = g_* f$. The scale m_* sets the typical mass of the Composite Sector resonances and g_* sets their typical interaction strength [24]. The Composite Sector itself originates from some unspecified dynamics at a very high scale $\Lambda_{UV} \gg m_*$ and the large separation among these two scales is ensured by the hypothesis that the Composite Sector flows toward a conformal fixed point below Λ_{UV} and it remains close to it until m_* . Also one “Elementary Sector” (ES) is generated at the high scale Λ_{UV} . The latter is composed of weakly-interacting fields, among which the SM ones with the possible exception of the right-handed Top quark, which could also be a fully composite degree of freedom originating from the CS. In the ordinary, or Minimal [19], Composite Higgs construction, the ES comprises just the SM fields. Instead, as described below, in the Twin Composite Higgs, the ES also comprises Extra “Twin” degrees of freedom. The CS does exactly respect G invariance, but the ES breaks it badly because its degrees of freedom do not come in G multiplets. Explicit G symmetry-breaking effects are communicated to

the CS through the Elementary/Composite interactions, denoted as \mathcal{L}_{INT} in Figure 3.1. They come as weak interactions at Λ_{UV} and they are assumed not to be strongly relevant operators such as to remain weak when evolved down at the IR scale m_* . Therefore it makes sense to treat perturbatively their effects on the IR dynamics as tiny G -breaking perturbations.

Let us now come to our specific construction. The relevant global symmetry group of the CS is $SO(8)$, which gets spontaneously broken to an $SO(7)$ subgroup delivering 7 Goldstone Bosons in the **7** of the unbroken $SO(7)$, out of which only the Higgs boson will survive as a physical particle. A total of 7 Elementary gauge fields are introduced, and coupled to the CS by weakly gauging 7 of the 28 $SO(8)$ generators, whose explicit form is reported in Appendix A for the Fundamental representation. In particular, we gauge some of the generators which live in the block-diagonal $SO(4) \times \widetilde{SO}(4)$ subgroup, namely those of the $SU(2)_L \times U(1)_{3,R}$ and $\widetilde{SU}(2)_L$ subgroups of the two $SO(4) \simeq SU(2)_L \times SU(2)_R$. The group $SO(4)$ is taken to be part of the unbroken $SO(7)$, while $\widetilde{SO}(4)$ is partially broken by the CS, namely $\widetilde{SO}(4) \rightarrow \widetilde{SO}(3)$ at the scale f . The SM group being embedded in the unbroken $SO(4)$ ensures Custodial protection and avoids unacceptably large tree-level corrections to the T parameter of ElectroWeak Precision Tests (EWPT). This Custodial protection is one reason for having an $SO(8)/SO(7)$ spontaneous symmetry breaking pattern in the CS, as already noted in [120].

The $SU(2)_L \times U(1)_{3,R}$ group is identified with the electroweak SM gauge group and the corresponding gauge fields thus deliver the EW bosons and the photon. The remaining 3 elementary vector fields gauging $\widetilde{SU}(2)_L$ correspond instead to new particles, which we call the “Twin partners” of the SM W fields. They are associated with generators that commute with the SM group and are thus EW-neutral objects. Given that $\widetilde{SU}(2)_L$ is broken by the CS, the Twin W ’s are massive and acquire their longitudinal components from 3 of the 7 Goldstones, which thus disappear from the spectrum. The remaining 4, associated with the generators $T_{1,\dots,4}^7$ in Appendix A, are in the **4** of $SO(4)$ and they have precisely the SM quantum numbers of the ordinary Higgs doublet. The latter will eventually acquire a vacuum expectation value (VEV), which we take along T_4^7 , give a mass to the EW bosons and deliver just one physical scalar, the SM Higgs boson. Unlike in the original Twin Higgs proposal [125] and in the subsequent literature, [120, 126–129, 132–136], no mirror partner is introduced for the SM Hypercharge field in order to avoid the appearance of an exactly massless Twin photon in the spectrum.

3.1.1 The gauge sector

Aside from the Higgs, the EW bosons and the Twin W ’s, extra massive resonances are present, originating as bound states of the CS. They could come in a variety of spin and $SO(7)$ quantum numbers but in particular we do expect some of them to be spin-one vectors and to have the quantum numbers of the global currents associated to the unbroken group $SO(7)$, *i.e.*

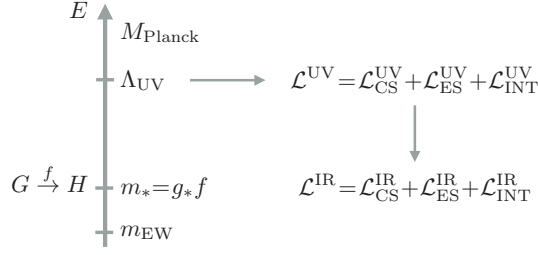


Figure 3.1 – A pictorial view of the Composite Higgs framework.

to live in the Adjoint. The QCD analog of these particles are the ρ mesons, which are the lightest spin-one hadrons. Vectors in the Adjoint would also appear in a 5d holographic implementation of our setup. It is thus reasonable to take them as representatives of the CS particle content. Therefore, we introduce an Adjoint (the **21** of $SO(7)$) of vectors ρ_a and we define a 2-site model, constructed by the standard rules of Ref. [117], to describe their dynamics. We regard this model as a simple illustrative implementation of the Composite Twin Higgs idea. Its Lagrangian reads

$$\mathcal{L}^{\text{gauge}} = -\frac{1}{4g_\rho^2} \sum_{a=1}^{21} \rho_{\mu\nu}^a \rho_a^{\mu\nu} + \frac{f^2}{4} \text{Tr}[(D_\mu \Sigma)^t D^\mu \Sigma] - \frac{1}{4g_2^2} W_{\mu\nu}^\alpha W_a^{\mu\nu} - \frac{1}{4g_1^2} B_{\mu\nu} B^{\mu\nu} - \frac{1}{4\tilde{g}_2^2} \widetilde{W}_{\mu\nu}^\alpha \widetilde{W}_a^{\mu\nu}, \quad (3.1)$$

where $\rho_{\mu\nu}^a$ are the field-strength tensors of the resonance fields –which are treated in the 2-site model as gauge fields of a local $SO(7)$ group–, $W_{\mu\nu}^\alpha$ and $B_{\mu\nu}$ are the usual SM field-strengths and $\widetilde{W}_{\mu\nu}^\alpha$ those of the 3 Twin W partners. The field Σ is a generic $SO(8)$ matrix containing 28 real scalar fields. However, 21 of these can be eliminated by gauge-fixing the local $SO(7)$ associated with the ρ 's, making Σ become the exponential of the 7 broken generators only. In this gauge, Σ can be interpreted as the Goldstone Matrix of the $SO(8)/SO(7)$ coset, namely

$$\Sigma = U = e^{-\frac{2i}{f} \Pi^\alpha T_\alpha^7}. \quad (3.2)$$

All the 7 remaining scalars, but one, can be eliminated by gauge-fixing the local $\widetilde{SU}(2)_L$ associated with the Twin W 's and the broken SM generators. This defines the Unitary Gauge, in which Σ reads

$$\Sigma = U = e^{-\frac{2i}{f} H T_4^7} = \begin{pmatrix} \mathbb{I}_3 & 0 & 0 & 0 \\ 0 & \cos \frac{H}{f} & 0 & \sin \frac{H}{f} \\ 0 & 0 & \mathbb{I}_3 & 0 \\ 0 & -\sin \frac{H}{f} & 0 & \cos \frac{H}{f} \end{pmatrix}, \quad (3.3)$$

Chapter 3. A Composite UV completion of the Twin Higgs scenario

where H is the real neutral component of the Higgs doublet (times $\sqrt{2}$) which, after EWSB, decomposes in VEV plus physical Higgs fluctuation as $H(x) = V + h(x)$.

It is important to interpret properly the various terms that appear in Eq. (3.1). The first one comes purely from the CS and describes the kinetic term of the resonances and their self-interactions. The corresponding coupling g_ρ is therefore of the order of the typical CS coupling g_* . The last three terms are purely Elementary. In accordance with the hypothesis that the ES is weakly-coupled and gives a subdominant correction to the CS dynamics, the associated couplings are assumed to satisfy

$$g_{1,2} \sim \tilde{g}_2 \ll g_\rho \sim g_*, \quad (3.4)$$

The second term is instead a mixed one. It contains both purely CS operators, among which the Goldstone bosons kinetic term and a mass for the ρ 's, and Elementary/Composite interactions. Indeed, the covariant derivative of Σ reads

$$D_\mu \Sigma = \partial_\mu \Sigma - i A_\mu^A T^A \Sigma + i \Sigma \rho_\mu^a T_{21}^a, \quad (3.5)$$

where we collected in A_μ^A , $A = 1, \dots, 7$, all the Elementary gauge fields appropriately embedded in the Adjoint of $SO(8)$, namely

$$A_\mu^A T^A = W_\mu^\alpha (T_L)^\alpha + B_\mu (T_R)^3 + \tilde{W}_\mu^\alpha (\tilde{T}_L)^\alpha, \quad (3.6)$$

in terms of the generators defined in Appendix A.

The mass-spectrum of the theory is immediately worked out in the weak Elementary coupling expansion of Eq. (3.4). First, we do find the massless photon and the W and Z bosons with masses

$$M_W^2 \simeq \frac{1}{4} g_2^2 f^2 \sin^2 \frac{V}{f} = \frac{1}{4} g_2^2 v^2, \quad M_Z^2 \simeq \frac{1}{4} (g_2^2 + g_1^2) f^2 \sin^2 \frac{V}{f} = M_W^2 / \cos^2 \theta_W, \quad (3.7)$$

where we identified $g_{1,2}$ with the SM $g_{1,2}$ couplings –which holds up to $g_{1,2}^2/g_\rho^2$ corrections– and we defined the EWSB scale as

$$v = f \sin \frac{V}{f} \simeq 246 \text{ GeV}, \text{ thus } \xi \equiv \frac{v^2}{f^2} = \sin^2 \frac{V}{f}. \quad (3.8)$$

Like in the ordinary Composite Higgs setup, we do have plenty of phenomenological reasons to take ξ small. Indeed ξ controls the departures of the Higgs couplings from the SM expectations, which are constrained both from the direct LHC measurements and from their indirect effects on EWPT [102]. The maximal defensible value of ξ is around 0.2, given that making it small requires fine-tuning in the potential we will take it close to the maximum, which corresponds

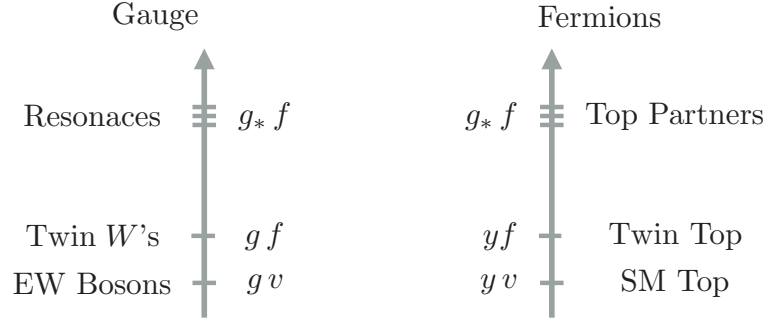


Figure 3.2 – The mass spectrum in the gauge (left) and fermionic (right) sectors.

to a Goldstone scale $f \sim 500$ GeV.¹ The second set of particles are the Twin W 's, which are 3 EW-neutral particles with a common mass

$$M_W^2 \simeq \frac{1}{4} \tilde{g}_2^2 f^2 \cos^2 \frac{V}{f} = \frac{1}{4} \tilde{g}_2^2 f^2 (1 - \xi). \quad (3.9)$$

For $\tilde{g}_2 \sim g_2$ the Twin W 's are light, only a factor of $\frac{1}{\sqrt{\xi}}$ heavier than the W . Finally, we do have the 21 strong sector resonances which are all degenerate at the leading order in the $g_{1(2)}/g_\rho$ expansion because of the unbroken $SO(7)$, with a common mass $g_\rho f/2 \sim m_*$. The ES couplings break the degeneracy and the 21 resonances organize themselves into one real $\mathbf{3}_0$, one complex $\mathbf{1}_1$ and three $\mathbf{2}_{1/2}$'s of the SM group, plus four real $\mathbf{1}_0$ singlets with masses

$$M_{\mathbf{3}_0}^2 \simeq \frac{1}{4} f^2 (g_\rho^2 + g_2^2), \quad M_{\mathbf{1}_1}^2 \simeq \frac{1}{4} f^2 g_\rho^2, \quad M_{\mathbf{2}_{1/2}}^2 \simeq \frac{1}{4} f^2 g_\rho^2, \\ M_{\mathbf{1}_{0,1}}^2 \simeq \frac{1}{4} f^2 (g_\rho^2 + g_1^2), \quad M_{\mathbf{1}_{0,2}}^2 \simeq \frac{1}{4} f^2 (g_\rho^2 + \tilde{g}_2^2). \quad (3.10)$$

Notice that many of the composite resonances are charged under the EW group, unlike the elementary Twin W 's which are EW-singlets, and thus they could be directly produced at the LHC at a significant rate. However their coupling to SM fermions rapidly decrease for increasing g_ρ making current limits on their mass safely below 2 TeV already for $g_\rho \gtrsim 2$ [40]. The leading constraint comes from their contribution to the \hat{S} parameter of EWPT, which places them above 2 or 3 TeV [56]. This threshold corresponds, for $f = 500$ GeV, to a large but still reasonable coupling $g_\rho \simeq g_* \sim 6$. The spin-one particle spectrum of our construction, summarized in the left panel of Figure 3.2, displays the typical pattern of Twin Higgs models.

The advantage of a 2-site model is that it makes the Composite Higgs potential calculable at

¹A quantitative compatibility with EWPT is actually possible in ordinary Composite Higgs models only relying on the radiative effects of somewhat light colored Top Partners [102], [108], whose presence is precisely what we want to avoid with our construction. A careful assessment of EWPT would be needed to establish if $\xi \simeq 0.2$ is still viable in the Twin case or if instead a stronger limit applies.

one loop up to logarithmic divergences. The potential arises from loops of the ES, which, as explained above, breaks of the Goldstone symmetry. Focusing momentarily on the loops of the SM W 's and of their Twin partners, and working at the leading order in the g_2/g_ρ expansion we obtain

$$V_{g_2}[H] = \frac{9g_\rho^2 f^4}{512\pi^2} \left(g_2^2 \sin^2 \frac{H}{f} + \tilde{g}_2^2 \cos^2 \frac{H}{f} \right) \left(1 + \log \frac{4\mu^2}{g_\rho^2 f^2} \right). \quad (3.11)$$

The logarithmic term in the equation stems for the previously-mentioned divergent contribution to the potential, which will be cut-off at the scale μ where other CS resonances, not included in our description, appear. Given that we expect those not to be far, we will not take this logarithm seriously and treat it as order one in our estimates.²

What is remarkable and non-generic in Eq. (3.11) is that for g_2 exactly equal to \tilde{g}_2 the \sin^2 and \cos^2 terms sum up to 1 and the potential becomes an irrelevant shift of the vacuum energy. This result is compatible with the original Twin Higgs argument [125], according to which the quadratically divergent contributions to the Higgs potential, of order $g^2 f^2 \Lambda^2 / 16\pi^2$, cancel in the Twin-symmetric limit $g = \tilde{g}$. Given that from the low-energy perspective of Ref. [125] the cutoff Λ is the resonance scale $m_* \simeq g_\rho f$, this is precisely what we are finding here. However the true reason that underlies the cancellation is slightly different and we believe it is important to clarify this conceptual point. This also has a practical implication we will describe below.

The functional form of the potential in Eq. (3.11) can be obtained by spurion analysis, with the method developed in [38], by assigning G quantum numbers to the Elementary/Composite couplings which break the Goldstone symmetry. The ES couples via gauging to the Composite one, *i.e.* by mixing with the corresponding global current operators. By focusing on the W and \tilde{W} interactions, which are the ones responsible for the potential (3.11), these can be written as

$$\mathcal{L}_{\text{INT}} = g_2 W_\mu^\alpha (J_L)_\alpha^\mu + \tilde{g}_2 \tilde{W}_\mu^\alpha (\tilde{J}_L)_\alpha^\mu, \quad (3.12)$$

where J_L and \tilde{J}_L are the currents associated with the generators T_L and \tilde{T}_L . With respect to our previous notation here we performed a field redefinition $W \rightarrow g_2 W$ and $\tilde{W} \rightarrow \tilde{g}_2 \tilde{W}$ to move the couplings from the kinetic term to the interaction terms. We can then uplift the couplings to two spurions G_α^A and \tilde{G}_α^A with an index A in the **28** of $SO(8)$ and an index $\alpha = 1, 2, 3$, so as to rewrite \mathcal{L}_{INT} in a formally invariant fashion

$$\mathcal{L}_{\text{INT}} = W_\mu^\alpha G_\alpha^A (J_L)_A^\mu + \tilde{W}_\mu^\alpha \tilde{G}_\alpha^A (\tilde{J}_L)_A^\mu. \quad (3.13)$$

²The potential could be made fully calculable with a 3-site model [117] and no large logarithm would appear in this case barring an unnatural separation among the two layers of resonances.

The two spurions are identical from the viewpoint of the CS and thus they enter the potential in exactly the same way. What makes them different is the physical values to which we will eventually set them. By switching to a matrix notation we have

$$G_\alpha \equiv G_\alpha^A T^A = g_2 T_L^\alpha, \quad \tilde{G}_\alpha \equiv \tilde{G}_\alpha^A T^A = \tilde{g}_2 \tilde{T}_L^\alpha. \quad (3.14)$$

Finding the structures that can appear in the potential at order g_2^2 and \tilde{g}_2^2 amounts to classifying the G -invariants that can be constructed with two of those spurions and the Goldstone Matrix in Eq. (3.3). It has been shown in Ref. [38] that the number of independent invariants is equal to the number of singlets of the unbroken group H that can be obtained out of the various spurion components, minus the number of singlets of the full group G . In the present case the spurions are in the Adjoint of $G = SO(8)$, which decomposes as $\mathbf{28} = \mathbf{21} \oplus \mathbf{7}$ under $H = SO(7)$. Since one $SO(7)$ singlet is present in the product of two $\mathbf{21}$'s and one in the product of two $\mathbf{7}$'s, but one full $SO(8)$ singlet arises from two $\mathbf{28}$'s, only one invariant exists, given by

$$I = \sum_{\alpha, \hat{a}} \left\{ \text{Tr}[T_7^{\hat{a}} U^t G_\alpha U] \right\}^2. \quad (3.15)$$

Depending on which of the physical spurions is inserted, we obtain a different dependence on the Higgs field

$$I = \frac{3}{4} g_2^2 \sin^2 \frac{H}{f}, \quad \tilde{I} = \frac{3}{4} \tilde{g}_2^2 \cos^2 \frac{H}{f}. \quad (3.16)$$

The two spurions are treated by the CS in exactly the same way, therefore the two terms above must appear in the potential with the same coefficient. That explains the form of Eq. (3.11) and originates the cancellation at $g_2 = \tilde{g}_2$.

The above argument is based on the symmetries and the selection rules of the underlying UV theory and is thus completely conclusive. That is instead not the case of the original Twin Higgs reasoning, which only establishes the cancellation of quadratic divergences. The reason why this could not be enough is that the quadratic divergence corresponds, from the UV viewpoint, only to some of the contributions to the potential, namely the ones coming from the high-scale propagation of the light degrees of freedom. The effects of heavy resonances are equally sizable and they cannot be controlled by a purely low-energy “calculation” of the quadratic divergence. One might thus expect that in some situations the quadratic divergence might cancel in the low-energy theory, but still equally large finite contributions arise in the complete models making the Twin Higgs cancellation ineffective. One example of that is provided by the non-custodial Twin Higgs model, based on the $SU(4)/SU(3)$ coset where the W and their Twins gauge the $SU(2) \times \widetilde{SU}(2)$ subgroup. As we explicitly verified the cancellation does not occur in a 2-site implementation of this scenario, meaning that order $g^2 f^2 m_\rho^2 / 16\pi^2$ term are

present also in the Twin-symmetric limit and should be taken into account in the study of the potential. A straightforward spurion analysis offers a simple criterion to understand under what condition the quadratic divergence argument will either fail, as in the $SU(4)/SU(3)$ case, or be uplifted to a proper selection rule, as in the case of $SO(8)/SO(7)$. The point is that the quadratic divergence contribution to the potential itself does respect the symmetries and the selection rules of the theory, and therefore it must have a functional form which is allowed by the spurion analysis. In $SO(8)/SO(7)$ there is only one invariant, and thus the g^2 and \tilde{g}^2 terms in the quadratic divergence must have the same functional dependence on the Higgs VEV as the corresponding terms in the full potential. If from the low-energy calculation we find that they have the appropriate form to cancel, for instance a \sin^2 plus \cos^2 structure, the same must occur for the complete potential. The $SU(4)/SU(3)$ Twin Higgs fails because two independent invariants exist. The naive quadratic divergence is proportional to one invariant, for which the cancellation occurs, but also the other invariant arises in general in the complete potential.³

The reader might wonder at this point what is the role of the Twin Parity symmetry in our discussion. It actually played no role up to now, but it becomes essential when trying to really realize the cancellation via the condition $g_2 = \tilde{g}_2$. This can be enforced by Twin Parity, which is defined as the operation

$$W_\mu \leftrightarrow \widetilde{W}_\mu, \quad (3.17)$$

which flips the W 's with their Twin partners, supplemented by a transformation on the CS which interchanges the $SO(4)_L$ and $\widetilde{SO}(4)_L$. The latter is an element of $SO(8)$,

$$\mathcal{P}_{\text{Twin}} = \begin{bmatrix} 0 & \mathbb{1}_4 \\ \mathbb{1}_4 & 0 \end{bmatrix}, \quad (3.18)$$

and thus it is automatically a symmetry of our construction.

³An argument showing that $SO(8)$ is sufficient in order to fully protect the Higgs mass at $O(g^2)$ can also be found in Appendix B of Ref. [128]. Freed of inessential details, the argument can be synthesized as follows. Under the $SU(4) \times U(1)$ subgroup of $SO(8)$, the adjoint and fundamental irreps of $SO(8)$ decompose respectively as $\mathbf{28} = \mathbf{1}_0 + \mathbf{6}_2 + \mathbf{6}_{-2} + \mathbf{15}_0$ and $\mathbf{8} = \mathbf{4}_1 + \mathbf{\bar{4}}_{-1}$. Each different generator of $SU(2)_L \times \widetilde{SU}(2)_L$ with definite twin parity ($T_L^a \pm \widetilde{T}_L^a$) transforms as the singlet $\mathbf{1}_0$ of a different $SU(4) \times U(1)$ subgroup. In the twin symmetric limit, $g = \tilde{g}$, the vector bosons associated with the above twin parity eigenstates are also propagation eigenstates and the $O(g^2)$ correction to the effective action can be written as the sum over single exchanges of such eigenstates. Therefore each such contribution respects a different $SU(4) \times U(1)$. Now, $SU(4) \times U(1)$ invariants built from the submultiplets of the $\mathbf{8}$ of $SO(8)$ accidentally respect the full $SO(8)$. As the Goldstone bosons of $SO(8) \rightarrow SO(7)$ can be made to live inside the $\mathbf{8}$ of $SO(8)$, we conclude that at $O(g^2)$ the potential respects $SO(8)$ and thus the Goldstone bosons remain massless. While the above argument is not unrelated to our derivation, we find it specific to that particular case. We think our methodology, based on the analysis of the invariants constructed with “Goldstone-dressed” external couplings, is both more systematic, encompassing in particular fermionic couplings, and more direct. For instance, it immediately outlines the structural difference between $SU(4)$ and $SO(8)$, which was in fact not appreciated in Ref. [128].

An exact Twin symmetry requires $g_2 = \tilde{g}_2$, but it would also require the existence of a Twin partner of the Hypercharge gauge boson, which however we have not introduced. Twin Parity is thus broken by the Hypercharge and thus in the Higgs potential we find an unsuppressed g_1^2 contribution of the form

$$V_{g_1^2} = \frac{3g_\rho^2 f^4}{512\pi^2} g_1^2 \sin^2 \frac{H}{f} \left(1 + \log \frac{4\mu^2}{g_\rho^2 f^2} \right). \quad (3.19)$$

3.1.2 The fermionic sector

To understand the symmetry breaking potential it is crucial to describe properly the source of the top mass. It originates, as in the canonical Composite Higgs, from a linear interaction among the elementary top fields and some Composite Sector fermionic operators. This realizes the so-called “Partial Compositeness” paradigm [13]. The low-energy description of the setup depends on the choice of the quantum numbers of the latter fermionic operators under the CS global group. Here we take the elementary q_L doublet to interact with an **8** of $SO(8)$ and the elementary t_R to interact with a singlet operator. This choice is not only simple and minimal, it is also suited to discuss the case of a composite t_R field, as we will see below.

Adding fermions requires, again as in the ordinary Composite Higgs, the presence of additional unbroken global symmetries of the CS. In the first place, a q_L doublet with 1/6 Hypercharge does not fit in an **8** if the Hypercharge is completely internal to the $SO(8)$ group. We will thus consider a global $U(1)_X$, define Hypercharge as $Y = T_R^3 + X$ and assign appropriate $U(1)_X$ quantum numbers to our fields. Second, and more importantly, the $SU(3)_c$ color group of QCD must be assumed to be an unbroken symmetry of the CS. This is because the quarks are color triplets and thus the CS must carry QCD color to interact linearly with them. Clearly there is additional structure in the Twin Composite Higgs. First of all, a second set of ES doublet and singlet fields \tilde{q}_L and \tilde{t}_R are introduced and coupled to an **8** and to a singlet of $SO(8)$, respectively. We call these particles the “Twin Partners” of the Top (and b_L) quarks. Second, since we do not want them to be colored or charged under any of the SM groups but still we want them to be related by a symmetry to q_L and t_R , also Twin $\tilde{U}(1)_X$ and Twin $\tilde{SU}(3)_c$ color global groups have to be introduced.

Let us now turn to our model, which incorporates fermions by a standard 2-site construction [117]. The spirit is again to describe a minimal set of CS resonances, compatible with the structure of the underlying CS theory. Given that we assumed the elementary q_L to be coupled to one fermionic operator in the **8** of $SO(8)$, which decomposes under the unbroken $SO(7)$ as $\mathbf{8} = \mathbf{7} \oplus \mathbf{1}$, it is reasonable to expect a **7** and a singlet of fermionic resonances in the spectrum,

namely

$$\Psi = \begin{pmatrix} \Psi_7 \\ \Psi_1 \end{pmatrix}, \quad (3.20)$$

The operators, and consequently the associated resonances, must be in a color triplet and must carry $U(1)_X$ charge $2/3$ in order to couple to q_L . Similar considerations hold for the t_R , which mixes with a singlet operator with $X = 2/3$. This suggests the existence of a singlet, which however we have already incorporated by the field Ψ_1 . The Ψ resonances are the so-called ‘‘Top Partners’’, they carry QCD color as in the ordinary Composite Higgs scenario. However in the Twin Higgs case naturalness will place a weaker bound on their mass. Identical considerations hold for the Twin Tops and their couplings to the CS, which suggest the existence of a second set of fermionic resonances

$$\tilde{\Psi} = \begin{pmatrix} \tilde{\Psi}_7 \\ \tilde{\Psi}_1 \end{pmatrix}. \quad (3.21)$$

Those are once again a **7** and a singlet of $SO(7)$, but they are not identical to the untilded Ψ because they are neutral under the ordinary color and $U(1)_X$ while they are charged under the Twin $\widetilde{SU}(3)$ and $\widetilde{U}(1)_X$.

The decomposition of the Top Partners Ψ and their Twins $\tilde{\Psi}$ into SM representations is described in Appendix F. As far as Ψ is concerned, its 8 components decompose under the standard electroweak gauge group into one $\mathbf{2}_{1/6}$ and one $\mathbf{2}_{7/6}$ plus four states in the $\mathbf{1}_{2/3}$. The phenomenology of these particles is expected to be similar to that of the Top Partners in the ordinary Composite Higgs model [7]. The eight components of the Twin $\tilde{\Psi}$ ’s decompose into a $\mathbf{2}_{1/2}$, a $\mathbf{2}_{-1/2}$ and four neutral singlets $\mathbf{1}_0$. Unlike the Ψ ’s, they carry no QCD color but some of them still communicate directly with the SM by EW interactions.

Now that the field content has been specified, we can write down our Lagrangian. Leaving aside the kinetic terms, the gauge interactions and the couplings of the fermions with the vector resonances which will not play any role in what follows, we have

$$\begin{aligned} \mathcal{L}_{top} = & \left[y_L f (\bar{Q}_L)^I \Sigma_{Li} (\Psi_R)^i + \tilde{y}_L f (\bar{\tilde{Q}}_L)^I \Sigma_{Li} (\tilde{\Psi}_R)^i + \right. \\ & \left. y_R f \bar{t}_R \Psi_{L1} + \tilde{y}_R f \bar{\tilde{t}}_R \tilde{\Psi}_{L1} + \text{h.c.} \right] \\ & - M_\Psi \bar{\Psi}_7 \Psi_7 - \widetilde{M}_\Psi \bar{\tilde{\Psi}}_7 \tilde{\Psi}_7 - M_S \bar{\Psi}_1 \Psi_1 - \widetilde{M}_S \bar{\tilde{\Psi}}_1 \tilde{\Psi}_1, \end{aligned} \quad (3.22)$$

where the Elementary q_L and its mirror are embedded into incomplete octets

$$Q_L = \frac{1}{\sqrt{2}} \begin{pmatrix} i b_L \\ b_L \\ i t_L \\ -t_L \\ 0 \\ 0 \\ 0 \\ 0 \end{pmatrix}, \quad (\tilde{Q}_L)^I = \frac{1}{\sqrt{2}} \begin{pmatrix} 0 \\ 0 \\ 0 \\ 0 \\ i \tilde{b}_L \\ \tilde{b}_L \\ i \tilde{t}_L \\ -\tilde{t}_L \end{pmatrix}. \quad (3.23)$$

Notice that the ES fields, compatibly with the Partial Compositeness hypothesis, are taken to interact linearly with the CS through mass-mixings with the resonance fields. The non-vanishing entries of the embeddings Q_L and \tilde{Q}_L are of course precisely designed to make q_L and \tilde{q}_L couple to components of Ψ and $\tilde{\Psi}$ with the appropriate gauge quantum numbers. The couplings y_L and \tilde{y}_L control the strength of the interaction between Elementary and Composite fermions and are assumed to be weak, namely $y_L, \tilde{y}_L \ll g_*$. The mass parameters $M_\Psi(\tilde{M}_\Psi)$ and $M_S(\tilde{M}_S)$ come instead purely from the CS. We thus expect them to be of order m_* , around the scale of the vector resonances described in the previous section. As far as the t_R and \tilde{t}_R mixing are concerned, two interpretations are possible which lead to different estimates for the size of the associated couplings y_R and \tilde{y}_R . If we regard t_R and \tilde{t}_R as ES fields, the couplings have to be weak, much below g_* and possibly close to their left-handed counterparts. However we can also interpret t_R and \tilde{t}_R as completely composite chiral bound states originating from the CS, perhaps kept exactly massless by some anomaly matching condition. If it is so, their mixing is a purely CS effect and thus $y_R, \tilde{y}_R \sim g_*$. We will consider both options in what follows taking also into account the possibility of smoothly interpolating between the two.

As a part of the Composite Twin Higgs construction we do have to impose Twin Parity, at least to some extent as described in the previous section. Twin Parity acts as

$$Q_L \leftrightarrow \tilde{Q}_L, \quad t_R \leftrightarrow \tilde{t}_R, \quad \Psi \leftrightarrow \tilde{\Psi}, \quad (3.24)$$

times the $SO(8)$ transformation in Eq. (3.18) acting on the resonance fields Ψ and $\tilde{\Psi}$.⁴ If it were an exact symmetry it would imply all masses and couplings in the Lagrangian (3.22) to be equal to their Twin, un-tilded, counterparts. We notice that the implementation of Twin Parity is slightly different in the fermionic and gauge sectors. In the gauge sector of the CS, Twin Parity was acting just like an $SO(8)$ transformation and thus it was automatically a symmetry.

⁴We have not mentioned the mirror gluons which gauge $\widetilde{SU}(3)_C$, needless to say they also get exchanged with the SM gluons.

Chapter 3. A Composite UV completion of the Twin Higgs scenario

Now instead Twin Parity entails the exchange of different fermionic CS resonances, charged under different global groups. Imposing Twin Parity thus becomes a non-trivial constraint on the CS.

We can now turn to the determination of the mass spectrum. By working in the limit $y_L, \tilde{y}_L \ll g_*$, we will focus on the leading relevant order in an expansion in powers of y_L and \tilde{y}_L . We will instead not treat y_R and \tilde{y}_R as small parameters, so that our formulae will hold for both completely composite and partially elementary right-handed fields. Aside from the exactly massless b_L and \tilde{b}_L —which will get a mass by mixing with other resonances or by some other unspecified mechanism—, the lightest particles are the Top quark and its Twin partner, with masses

$$m_t^2 \simeq \frac{f^4}{2} \frac{y_L^2 y_R^2}{M_S^2 + y_R^2 f^2} \xi, \quad m_{\tilde{t}}^2 \simeq \frac{f^4}{2} \frac{\tilde{y}_L^2 \tilde{y}_R^2}{\tilde{M}_S^2 + \tilde{y}_R^2 f^2} (1 - \xi). \quad (3.25)$$

If we remember that $M_S \sim m_* = g_* f$ and $y_R f$ is either $\sim m_*$ or smaller for a partially elementary t_R , we see that the Top mass respects the usual Partial compositeness estimate

$$m_t = \frac{y_t}{\sqrt{2}} \cdot v \sim \frac{y_L y_R}{g_*} \cdot v, \quad (3.26)$$

out of which we can determine the size of y_L in terms of the other parameters. If t_R is completely Composite, we expect $y_R \sim g_*$ and thus y_L must be around the physical Top Yukawa coupling $y_t \sim 1$. Larger values are obtained in the case of a partially Elementary t_R . The same parametric estimate can be performed for the Twin Top, whose mass scales like

$$m_{\tilde{t}} \sim \frac{\tilde{y}_L \tilde{y}_R}{g_*} \cdot f. \quad (3.27)$$

Differently from the Top one, the Twin Top mass is not proportional to v but to f because the Twin $\widetilde{SU}(2)_L$ is broken by the CS directly at the scale f .

The rest of the spectrum comprises the 16 components of Ψ and $\tilde{\Psi}$. They all have masses of order m_* , though not degenerate because of the freedom to choose the CS mass parameters $M_\Psi \neq M_S$, $\tilde{M}_\Psi \neq \tilde{M}_S$. We expect two almost degenerate 7-plets, with mass M_Ψ and \tilde{M}_Ψ respectively, plus 2 singlets whose masses are controlled by M_S and \tilde{M}_S and by the $y_R f$ and $\tilde{y}_R f$ mixings. The interaction with q_L and \tilde{q}_L remove part of the degeneracy and the spectrum organizes in degenerate SM multiplets as described above, with splitting of order $y_L^2 f^2$ and $\tilde{y}_L^2 f^2$ in the mass squared. Further tiny splitting emerge after EWSB. The qualitative structure of the spectrum respects the Twin Higgs expectation depicted in the right panel of Figure 3.2.

Let us finally turn to the calculation of the Higgs potential, working once again in the weak

coupling expansion $y_L, \tilde{y}_L \ll g_*$. Notice that y_L and \tilde{y}_L are the only sources of $SO(8)$ breaking in our fermionic Lagrangian, therefore the Higgs potential must be proportional to powers of those couplings. It receives its formally leading contribution at second order in the coupling expansion, through a term

$$V_{y^2}(H) = \frac{N_c f^2}{32\pi^2} \left\{ y_L^2 \left[M_\Psi^2 \log \frac{\mu^2}{M_\Psi^2} - M_S^2 \log \frac{\mu^2}{M_S^2 + f^2 y_R^2} \right] \cdot \sin^2 \frac{h}{f} + \tilde{y}_L^2 \left[\tilde{M}_\Psi^2 \log \frac{\mu^2}{\tilde{M}_\Psi^2} - \tilde{M}_S^2 \log \frac{\mu^2}{\tilde{M}_S^2 + f^2 \tilde{y}_R^2} \right] \cdot \cos^2 \frac{h}{f} \right\}. \quad (3.28)$$

Again, as in the order g_2^2 potential in the previous section, we see the Twin Higgs cancellation mechanism at work. If Twin Parity is exact so that tilded and un-tilded quantities are equal, the \sin^2 and \cos^2 sum up to one and no contribution is left to the Higgs potential. As in the gauge sector this cancellation can be explained in terms of symmetries and selection rules. The relevant spurions in this case are the Elementary q_L and \tilde{q}_L couplings, which transform in the **8** of $SO(8)$. Only one non-trivial invariant can be formed out of two **8**'s, and that precisely takes the \sin^2 and \cos^2 forms of the equation above.

The second relevant term in the potential is due to an IR effect. By looking at the spectrum of the theory in Figure 3.2 we see that there is a considerable gap among the Top Partner scale $m_* = g_* f$ and the Top plus its Twin, with masses of order $y_L v$ and $\tilde{y}_L f$. The low-energy Higgs potential thus receives a considerable log-enhanced contribution that corresponds to the RG evolution of the Higgs quartic coupling down from the scale m_* . In our model, the well known effect of the Top is complemented by the effect of its Twin, so that the potential reads

$$V_{IR}(H) = \frac{N_c}{16\pi^2} \left[m_t(H)^4 \log \frac{m_*^2}{m_t(H)^2} + m_{\tilde{t}}(H)^4 \log \frac{m_*^2}{m_{\tilde{t}}(H)^2} \right], \quad (3.29)$$

where $m_t(H)$ and $m_{\tilde{t}}(H)$ are the Higgs-dependent Top and Twin Top masses which we can extract from Eq. (3.25). They can be expressed as

$$m_t(H)^2 = \frac{y_t^2}{2} f^2 \sin^2 \frac{H}{f}, \quad m_{\tilde{t}}(H)^2 = \frac{y_{\tilde{t}}^2}{2} f^2 \cos^2 \frac{H}{f}, \quad (3.30)$$

in terms of the physical Top Yukawa and its Twin

$$y_t^2 = \frac{y_L^2 y_R^2 f^2}{M_S^2 + y_R^2 f^2}, \quad y_{\tilde{t}}^2 = \frac{\tilde{y}_L^2 \tilde{y}_R^2 f^2}{\tilde{M}_S^2 + \tilde{y}_R^2 f^2}. \quad (3.31)$$

Chapter 3. A Composite UV completion of the Twin Higgs scenario

This allows to rewrite the IR potential in an explicit form

$$V_{IR}(H) = \frac{N_c f^4}{64\pi^2} \left[y_t^4 \sin^4 \frac{H}{f} \log \frac{2m_*^2}{y_t^2 f^2 \sin^2 \frac{H}{f}} + y_{\tilde{t}}^4 \cos^4 \frac{H}{f} \log \frac{2m_*^2}{y_{\tilde{t}}^2 f^2 \cos^2 \frac{H}{f}} \right]. \quad (3.32)$$

Notice that an analogous IR term plays an important role in the Higgs dynamics of the MSSM with heavy stops, and so it will in our case.

The last term which we have to discuss is the contribution purely of order y^4 , not enhanced by any IR log. The resulting expression is complicated and it will not be reported here, what matters is that it has the parametric form

$$V_{y^4}(H) = \frac{N_c f^4}{128\pi^2} \left[(y_L^4 F_1 + \tilde{y}_L^4 \tilde{F}_1) \left(\sin^4 \frac{H}{f} + \cos^4 \frac{H}{f} \right) + (y_L^4 F_2 - \tilde{y}_L^4 \tilde{F}_2) \left(\sin^2 \frac{H}{f} - \cos^2 \frac{H}{f} \right) \right], \quad (3.33)$$

Here F_1, F_2 are $O(1)$ functions of the mass ratios M_S/M_Ψ and y_R/M_Ψ . The same comment applies to the corresponding tilded quantities. The coefficient in the first parenthesis is even under the exchange of tilded with un-tilded objects, while the second one is odd and thus vanishes for exact Twin Parity.

Notice finally that, in analogy with the gauge sector, also the fermion contribution to the effective potential has a structure that is dictated solely by symmetries and selection rules. One can indeed find all the possible invariants that can appear in the top sector contributions to the Higgs potential by means of the spurion technique. We can generically write the coupling of the elementary top-bottom doublets, q_L^α and \tilde{q}_L^α , to the composite sector as:

$$\mathcal{L}_{mix} = f(\tilde{q}_L)^\alpha (y_L)_\alpha^I \Sigma_{Ii} (\Psi_R)^i + f(\tilde{\tilde{q}}_L)^\alpha (\tilde{y}_L)_\alpha^I \Sigma_{Ii} (\tilde{\Psi}_R)^i + \text{h.c.}, \quad (3.34)$$

where $(y_L)_\alpha^I$ and $(\tilde{y}_L)_\alpha^I$ are 2×8 matrices that act as spurions under the global symmetry group. We have explicitly:

$$(y_L)_\alpha^I = \frac{1}{\sqrt{2}} \begin{pmatrix} i y_L & y_L & 0 & 0 & 0 \times \mathbb{I}_4 \\ 0 & 0 & i y_L & -y_L & 0 \times \mathbb{I}_4 \end{pmatrix}, \quad (\tilde{y}_L)_\alpha^I = \frac{1}{\sqrt{2}} \begin{pmatrix} 0 \times \mathbb{I}_4 & i \tilde{y}_L & \tilde{y}_L & 0 & 0 \\ 0 \times \mathbb{I}_4 & 0 & 0 & i \tilde{y}_L & -\tilde{y}_L \end{pmatrix}. \quad (3.35)$$

Introducing the vector

$$U^I = \Sigma^{Ii} v_i \quad (3.36)$$

with

$$\nu_i = (1, 0, 0, 0, 0, 0, 0)^t, \quad (3.37)$$

we can easily form one invariant at order y^2 and two invariants at order y^4 . We have:

$$I_{y^2} = (y_L)_I^\alpha (y_L^*)_{\alpha J} U^I U^J + (\tilde{y}_L)_I^\alpha (\tilde{y}_L^*)_{\alpha J} U^I U^J = \frac{1}{2} y_L^2 \sin^2 \frac{h}{f} + \frac{1}{2} \tilde{y}_L^2 \cos^2 \frac{h}{f}, \quad (3.38)$$

$$\begin{aligned} I_{y^4}^1 = & (y_L)_I^\alpha (y_L)_K^\beta (y_L^*)_{\alpha J} (y_L^*)_{\beta L} U^I U^J U^K U^L + (\tilde{y}_L)_I^\alpha (\tilde{y}_L)_K^\beta (\tilde{y}_L^*)_{\alpha J} (\tilde{y}_L^*)_{\beta L} U^I U^J U^K U^L = \\ & \frac{1}{4} y_L^4 \sin^4 \frac{h}{f} + \frac{1}{4} \tilde{y}_L^4 \cos^4 \frac{h}{f} \end{aligned} \quad (3.39)$$

$$\begin{aligned} I_{y^4}^2 = & (y_L)_I^\alpha (y_L)_K^\beta (y_L^*)_{\alpha J} (y_L^*)_{\beta K} U^I U^J + (\tilde{y}_L)_I^\alpha (\tilde{y}_L)_K^\beta (\tilde{y}_L^*)_{\alpha J} (\tilde{y}_L^*)_{\beta K} U^I U^J = \\ & \frac{1}{2} y_L^4 \sin^2 \frac{h}{f} - \frac{1}{2} \tilde{y}_L^4 \cos^2 \frac{h}{f} \end{aligned} \quad (3.40)$$

As expected, the spurion technique gives the exact trigonometric dependence on the Higgs field that one finds by a direct computation as in Eq. (3.33).

3.2 Electroweak symmetry breaking

Let us now discuss if and under what conditions we can achieve a realistic vacuum dynamics in our model. That amounts to producing electroweak symmetry breaking, the correct Higgs mass and a sufficiently small (tunable) value of the ratio $\xi = v^2/f^2$, which controls Higgs couplings and precision electroweak observables. In the spirit of Twin Higgs, and differently from ordinary Composite Higgs models, we would like to obtain that without the need of relatively light Top Partner(s) close to the Goldstone scale f . Namely, we would like to keep $M_\Psi/f \equiv g_\Psi \sim g_*$ large and possibly close to the perturbativity bound $g_* \sim 4\pi$.

Let us consider first the exact Twin Parity limit, in which the untilded and tilded parameters are taken to coincide and moreover the SM hypercharge coupling g_1 is set to vanish. Remember indeed that in our proposal the Twin Hypercharge is not gauged and thus the SM Hypercharge gauging breaks Twin Parity. The potential, as computed in the previous section, can be written as

$$V^{sym.}(H) = f^4 \beta \left(s^4 \log \frac{a}{s^2} + c^4 \log \frac{a}{c^2} \right), \quad (3.41)$$

where

$$s^2 \equiv \sin^2 \frac{H}{f}, \quad c^2 \equiv \cos^2 \frac{H}{f}, \quad (3.42)$$

$$\beta = \frac{3y_t^4}{64\pi^2}, \quad (3.43)$$

and

$$\log a = \log \frac{2\mu^2}{y_t^2 f^2} + \frac{y_L^4}{y_t^4} F_1, \quad (3.44)$$

where F_1 , which coincides with \tilde{F}_1 in the Twin symmetric case, was introduced in Eq. (3.33). This potential is not realistic. For $\log a > 3/2 - \log 2$ it is minimized at the Twin symmetric point $s = c = 1/\sqrt{2}$, while for $\log a < 1/2$ it has Twin breaking minima at respectively $s = 0$, $c = 1$ and $s = 1$, $c = 0$. In the intermediate range $1/2 < \log a < 3/2 - \log 2$ it does have a tunable minimum with $c \neq s \neq 0$: when $\log a$ approaches $1/2$ from the above, ξ approaches 0. However the effective Higgs quartic in this case is purely generated by RG evolution in the SM, and it results too small unless $f \geq 10^{10}$ GeV, which we find unacceptable from the standpoint of fine tuning. In conclusion none of the above cases corresponds to a realistic phenomenology.

A realistic potential can only be obtained by turning on the Twin Parity breaking sources. We think a consistent picture can be obtained by treating Hypercharge as the main source of that breaking. Its effects can be classified by the loop order at which they arise. At one loop there is the gauge contribution in Eq. (3.19). That equation features a logarithmic divergence, but in a realistic model, that logarithm would be saturated at the scale of the strong resonances: $\mu \rightarrow m_*$. However, known theorems fix the sign of that contribution to the potential to always be positive. That is indeed compatible with the leading log behaviour at $\mu \gg m_\rho$ in Eq. (3.19). Another source of breaking is the Hypercharge contribution to the RG evolution of the top sector parameters, down to m_* from the UV scale $\Lambda_{UV} \gg m_*$, where our model is microscopically defined. In general this RG contribution may turn on several effects in the composite sector. In particular each and every Yukawa and mass parameter in the top sector can be affected. However under the assumption that the composite sector does not possess any twin-parity-odd relevant or marginal operator, the only couplings that will be affected are the elementary-composite mixings y_L and potentially, if t_R is Elementary, y_R . Focusing on y_L , which affects the potential, we expect RG evolution to generate a twin breaking splitting (for the couplings renormalized at the scale m_*) of the form

$$y_L^2 - \tilde{y}_L^2 = \frac{bg_1^2}{16\pi^2} y_L^2 \log \frac{\Lambda_{UV}}{m_*} \equiv \Delta y_L^2 \quad (3.45)$$

where b is an unpredictable numerical coefficient of order unity. In principle if the strong sector between Λ_{UV} and m_* is approximately conformal, b could be related to the OPE coefficients performing conformal perturbation theory. In the case of perturbative theories, where the mixing is simply provided by mass terms, we know that $b > 0$. That is the well known sign of the running of masses induced by gauge interactions: it makes y_L grow when running towards the IR, and does not affect \tilde{y}_L as it involves hypercharge neutral states. Although we have not studied the problem, we suspect $b > 0$ is a robust feature also at strong coupling, though we shall not strongly rely on that. The insertion of Eq. (3.45) in the fermion induced 1-loop potential will give rise to a two-loop contribution enhanced by the UV log. We should also notice that analogous effects are induced on the $SU(3)$ and $SU(2)$ gauge couplings but they are numerically irrelevant.

The net effect of all the above considerations is the addition to the potential in Eq. (3.41) of a Twin breaking term

$$\Delta V(H) = \alpha f^4 s^2 \quad (3.46)$$

$$\alpha = \frac{3g_1^2 g_\rho^2}{512\pi^2} A + \frac{3\Delta y^2 g_\Psi^2}{32\pi^2} B, \quad (3.47)$$

where $g_\Psi = M_\Psi / f$ is the effective coupling associated with the overall size of the fermion masses introduced above –which we expect to be of order g_* – and g_ρ is the vector coupling, which is also expected to be around g_* . Finally A and B are numerical coefficients that depend on the details of the model. A , as we mentioned, is robustly predicted to be positive, while B can take either sign.

The overall potential

$$\frac{V(H)}{f^4} = \alpha s^2 + \beta \left(s^4 \log \frac{a}{s^2} + c^4 \log \frac{a}{c^2} \right) \quad (3.48)$$

is now capable to give rise to the desirable pattern of electroweak symmetry breaking. In order to achieve that, α must be positive. One is immediately convinced of that, by working with the non canonical field $\phi = f \sin h / f$. In this parametrization α only affects the quadratic part of the potential, and the quartic term ϕ^4 purely comes from the twin symmetric contribution: a positive effective quartic of the right size can only be achieved for $a \gg 1$. But for $a \gg 1$ the twin symmetric potential contributes a negative ϕ^2 term when expanded around $H = 0$ and this must be compensated by tuning against a positive α , thus obtaining a vacuum expectation value $\langle \sin^2 H / f \rangle = \xi \ll 1$. A value $\xi \sim 0.2$ could be sufficient to account for present bounds on the Higgs couplings (see however Footnote 1).

Chapter 3. A Composite UV completion of the Twin Higgs scenario

From equation (3.48) we can readily study the condition for having a tunable minimum with $\xi \ll 1$. The minimization of Eq. (3.48) yields

$$\frac{\alpha}{\beta} = -1 + 2 \log \frac{a}{1-\xi} + 2\xi \left[1 - 2 \log \frac{a}{\sqrt{\xi(1-\xi)}} \right]. \quad (3.49)$$

On the extremum defined by the above equation the Higgs mass is

$$\frac{m_H^2}{v^2} = 8\beta(1-\xi) \left[\log \frac{a^2}{\xi(1-\xi)} - 3 \right]. \quad (3.50)$$

For a given ξ , the observed masses of the Higgs and of the Top, which controls β through Eq. (3.43), fix then the value of a . Using the $\overline{\text{MS}}$ Top Yukawa coupling at the scale v , we have $y_t^4 \sim 0.8$ in β , so that we find

$$\log a \simeq 6 + \log \sqrt{\xi} \quad (3.51)$$

which for a realistic $\xi \sim 0.1$ corresponds to $\log a \sim 5$. Now notice that the definition of a in Eq. (5.5) depends on μ . In a reasonable model we expect this contribution to be saturated at the mass $m_* \sim g_* f$ of the composite sector. With this interpretation, the first term in Eq. (5.5) is $\sim \log(g_*/y_t)^2$. For a maximally strongly coupled theory $g_* \sim 4\pi$, this is in the right ballpark to match Eq. (3.51). For smaller g_* , that is for lighter resonances, the remaining term in Eq. (5.5) can bridge the gap and produce the needed value of $\log a$. The situation in our model is reminiscent of the MSSM with moderately large $\tan \beta$ and heavy stops. In that case the correct quartic is produced in equal measure by the tree level electroweak D-terms and by the top/stop renormalization of the quartic. In our case the electroweak D-term is basically replaced by the Twin Top contribution. One also has to pay attention not to make $\log a$ too large, producing a too heavy Higgs. This would tend to be the case for a considerably Elementary t_R . Indeed if for instance left- and right-handed couplings were comparable, *i.e.* $y_L \sim y_R$, from Eq. (3.26) we would obtain $y_L^2 \sim g_\Psi y_t$ and thus too a large contribution to $\log a$ from the second term in Eq. (5.5) unless $g_\Psi < \sqrt{6} \simeq 2.4$, which means relatively Light Top Partners as in the ordinary Composite Higgs scenario. Total t_R compositeness, or at least a larger compositeness for the t_R than for the q_L , is thus preferred in our scenario.

Consider now the value of α/β needed to be able to tune $\xi \ll 1$. Eq. (3.49) requires a sizeable value $\alpha/\beta \sim 9$. One can check what that relation requires given our estimate of α . Assuming α is dominated by the 1-loop IR dominated effect implies

$$A \frac{g_\rho^2 g_1^2}{80 y_t^4} \sim 1 \quad (3.52)$$

which seems to require even for $g_\rho \sim 4\pi$ a sizeable $A \sim 4$, borderline but perhaps acceptable.

On the other hand assuming α is dominated by the RG contribution we find

$$\frac{Bb}{80\pi^2} \frac{y_L^2}{y_t^2} \frac{g_\Psi^2}{g_1^2} \log \frac{\Lambda_{UV}}{m_*} \sim 1. \quad (3.53)$$

This is satisfied for completely composite t_R , $y_L = y_t$, when

$$\log \frac{\Lambda_{UV}}{m_*} \sim \frac{80\pi^2}{bB} \frac{y_t^2}{g_1^2 g_\Psi^2} \gtrsim \frac{50}{bB}, \quad (3.54)$$

i.e. for a large separation among the IR CS confinement scale and the UV one where it originates. Overall this seems like a plausible picture.

3.3 Discussion

A (partial) mirroring of the particles and interactions of the SM and of the new CS may give rise to non-minimal Composite Higgs models where a minimal amount of fine tuning is needed to be consistent with current bounds and, most importantly, where there is no new particle carrying SM charge below a few TeV. This eliminates one possible signature of Composite Higgs models, namely the production of colored Partners of the Top quark [35], which need to be light in the ordinary constructions [29–34]. The limits from the non-observation of the latter particles are currently comparable with other constraints. However they could become the strongest limit after the second run of the LHC. In that case the Composite Twin Higgs scenario might come to rescue.

A consistent picture emerges with the following salient features. First, mirroring the top Yukawa and gauge couplings is enough to render innocuous the usual quadratic divergence of the Higgs mass but does not guarantee, per se, the absence of finite but large corrections proportional to the squared mass of the resonances carrying SM charges. Extra hypotheses, which hold automatically in our construction, are needed to uplift the divergence cancellation to a structural protection of the potential. Second, the breaking of the mirror symmetry needed to get a realistic minimum of the Higgs potential may be realized by not mirroring the weak hypercharge. This is how the potential acquires a positive squared mass term, necessary to counteract the negative term from the mirror symmetric term, quartic in the top Yukawa coupling. The cancellation between these two terms is the unavoidable tuning needed to explain the smallness of the ratio $(v/f)^2$, currently below about 0.2, as in any Twin model. On the other hand the size of the individual terms, both quadratic and quartic, is right, without any further tuning, provided the RG evolution of the top sector parameters due to hypercharge is active already at a high UV scale which might not be far from the GUT scale⁵.

⁵Needless to say, without a mirror hypercharge no extra massless vector occurs in the spectrum, thus avoiding

Chapter 3. A Composite UV completion of the Twin Higgs scenario

We think that the phenomenology of composite twin Higgs models deserves attention. The infrared effects on the EWPT is well known since long time [126]. The search for relatively light mirror states, without SM charges, may also be possible in the next LHC run. Needless to say, to see the entire spectrum of these models in its full glory requires a Future Circular Collider in the hadronic mode.

possible unpleasant cosmological consequences.

4 The RG-improved Twin Higgs effective potential at NNLL

The Twin Higgs paradigm [125] offers a clever alternative to more common natural extensions of the SM: as we saw in the Introduction and in the previous Chapter, the new sector responsible for protecting the Higgs mass from large radiative corrections is given by a copy of the SM particles. This latter is color-blind, namely it is not charged under the SM strong interactions. The new mirror partners which are required for the Higgs mass to be light are then invisible and cannot be detected at a hadronic collider. They are related to the SM fermions and bosons by a discrete Z_2 symmetry which, together with the spontaneous breaking of a global symmetry that turns the Higgs into a pseudo Nambu-Goldstone boson (pNGB), guarantees that the Higgs mass be insensitive to the UV contributions. The resulting possibility of having a natural EWSB with the absence of detectable new physics at the LHC has sparked interest in this class of models in the last years, [118, 119], [120, 127], [128, 129, 132–137], but many questions still remain open. In particular, an important problem is to analyze the capability of this scenario to reproduce the observed value of M_H , irrespective of any possible UV completion, supersymmetric or composite, of the low-energy Lagrangian. Since the Higgs mass is insensitive to the UV physics, in fact, the sole infrared (IR) degrees of freedom, namely the elementary SM particles and their mirrors, should be enough to account for the experimental indications. The Higgs mass receives then its most important contributions from the Renormalization Group (RG) evolution of the scalar potential from the UV down to the IR scale where M_H is measured. Computing these running effects is crucial for an understanding of the feasibility of the Twin Higgs program as a new paradigm for physics at the electroweak (EW) scale.

In this Chapter, we study the Renormalization Group (RG) improvement of the Twin Higgs effective potential taking systematically into account the most important effects, due to QCD interactions and to loops of SM quarks and their twin copies. Our starting point will be a low-energy effective Lagrangian that we write in full generality following the basic prescriptions of the Twin Higgs paradigm. These are the spontaneous breaking of a UV global symmetry and the existence of an extra elementary sector charged under a mirror of the SM gauge groups.

The effective action is then simply given by the renormalizable SM interactions supplemented by two sets of higher-dimensional operators. The first set accounts for the non-linear Higgs interactions due to the pNGB nature of the Higgs scalar and it comprises the six-dimensional operators classified for instance in [25–28]. The leading contribution to the potential generated by these latter is suppressed by the fine-tuning parameter $\xi = (\nu/f)^2$, where f denotes the scale where the global symmetry is spontaneously broken. In presence of solely marginal and irrelevant interactions, in fact, the six-dimensional operators cannot renormalize the SM quartic coupling and mass parameter, but they can only affect the running of other non-renormalizable operators with dimension $D \geq 6$. The effective potential must contain one operator of this type, $\mathcal{O}_6 = (H^\dagger H)^3$, where H is the Higgs doublet. Its RG-evolution induced both by the linear and the non-linear interactions accounts for the contributions to the Higgs mass proportional to ξ . These effects are also common to any other natural extension of the SM with a pNGB Higgs in the spectrum.

The second set of operators, specific to the Twin Higgs construction, describes the interactions between the Higgs boson and the twin fermions. Its most distinctive feature is the existence of a relevant term with dimension $D = 3$, namely the twin quark mass parameter, that is generated before EWSB, [118]. Together with this latter, a series of non-renormalizable operators must be taken into account, whose leading contribution to the potential is not necessarily proportional to ξ , unlike the case of the six-dimensional operators made up of SM fields only. Due to the super-renormalizable mass term, in fact, the higher-dimensional interactions in the Twin sector can not only affect the running of other irrelevant operators with $D > 4$, but they can also renormalize the SM quartic coupling and mass term. If we consider, for instance, the dimension-five operator $\mathcal{O}_5 = (H^\dagger H) \tilde{q} \tilde{q}$, with \tilde{q} a twin quark, we can easily construct a one-loop diagram contributing to the running of the quartic coupling. If two vertices are given by \mathcal{O}_5 , two insertions of the twin quark mass are enough to generate a marginal operator. Similar considerations are valid for the other higher-dimensional operators, which can always renormalize the lower-dimensional ones through the insertion of an increasing number of the relevant three-dimensional interaction. In particular, we would need to classify all the non-renormalizable operators in the twin sector up to dimension $D = 9$ in order to fully capture the correction to the Higgs mass up to the order ξ . As a consequence, a diagrammatic computation of the RG-evolution of the effective potential results to be quite complicated, since no existing classification of the Twin non-renormalizable operators exists. Moreover, the number of diagrams one has to compute to renormalize the quartic coupling and \mathcal{O}_6 is big enough to discourage the usage of this diagrammatic approach.

It is possible to avoid the full classification of the operators in the Twin sector by making use of a more clever technique to compute the Higgs effective potential, the background field method. As it is well known, this procedure allows to derive the RG-improved action

automatically re-summing a whole series of diagrams and without needing to calculate all the single operators that are renormalized along the RG flow. If this method may be just an alternative in the SM, for the Twin Higgs model it provides instead the fastest way to calculate the contribution of the extra light degrees of freedom. We will therefore derive our expression for the Higgs mass using the background field method. The result will be organized as an expansion in logarithms, as usual, and we will show how to systematically include all the contributions to the effective potential that are generated along the flow as higher powers in the logarithmic series are included. We will renormalize the effective action up to the third order in the expansion parameter, classifying and discussing separately the leading contribution, the quadratic correction and finally the cubic expression for the Higgs mass.

This Chapter is organized as follows. In Section 4.1, we will review the Twin Higgs paradigm and write down its effective low-energy Lagrangian. After briefly recalling the leading result for the effective potential, in Section 4.2 we will apply the background field method to the Twin Higgs model and show how to derive the RG-improved effective potential at quadratic order. In Section 4.3, we shall extend the computation to include the cubic terms. Section 4.4 contains a discussion of the final results, the validity of our approximation and the prediction for the Higgs mass that we get in the Twin Higgs model. In particular, Figs. (4.5) and (4.6) represent the most important result of this work and contain the numerical estimation of M_H both in the SM and in its Twin extension. We conclude summarizing our findings in Section 4.5.

4.1 The Twin Higgs low-energy Lagrangian

The Twin Higgs paradigm is an interesting alternative to theories which conceive the Higgs scalar as a pNGB, like for instance the Composite or the Little Higgs [19, 23]. Two are the basic assumptions of any realization of this scenario [125]. First of all, at a generic UV scale m_* there must exist some extension of the SM whose Higgs sector enjoys an approximate global symmetry, G . This latter is spontaneously broken at an IR scale f to some unbroken subgroup H so that seven Goldstone bosons (GB) are delivered in the spectrum; four of them are identified as the Higgs doublet. The second element is an approximate discrete Z_2 symmetry that interchanges in the UV every SM particle with a corresponding mirror particle charged under a twin copy of the SM gauge groups, $\widetilde{\text{SM}}$.

The mechanism that allows a natural EWSB employs the explicit breaking of both these symmetries. The weak and electromagnetic interactions together with the Yukawa couplings violate, in fact, the global symmetry G . As a result, three of the seven GB's are eaten to give mass to the twin gauge bosons, a potential for the Higgs doublet is generated and the Higgs scalar is turned into a pNGB. An exact discrete symmetry, on the other hand, guarantees that the

mass term in the Higgs potential be trivially invariant under G , so that it does not contribute a physical mass to the GB's. These latter are then completely insensitive to any quadratic contribution proportional to m_*^2 and originated by loops of heavy particles or by the high-energy propagation of the light degrees of freedom. The G -breaking terms in the potential, like the Higgs quartic coupling, are at most only logarithmically sensitive to the scale m_* and must be proportional to g^4 and y^4 , where g collectively indicate the weak gauge couplings and y the Yukawas. An explicit soft breaking of the Z_2 symmetry is however necessary to generate a small quadratic mass term that in turn allows a tunable minimum of the potential to exist. Therefore the discrete symmetry, while being potentially respected by all the SM and $\widetilde{\text{SM}}$ interactions, must be softly broken by some UV effects. A natural hierarchy between the EW scale ν and the GB decay constant f is generated without requiring the existence of new light particles charged under the SM. The UV scale m_* , where the heavy fields with SM quantum numbers reside, can thus be pushed up to $m_* \sim 10$ TeV, out of the LHC reach, without in any way worsening the tuning between ν and f .

The Higgs effective potential being largely insensitive to the UV scale, it is crucial to study how it is affected by the IR physics. In particular, it is important to derive an expression for the Higgs boson mass and understand how light it can be, also in comparison with its experimental value. To tackle these questions, we aim at analyzing the RG-improvement of the effective potential including the running of the quartic coupling induced by the light degrees of freedom present in the Twin Higgs paradigm. Our starting point is the low-energy Lagrangian at the scale m_* generated after integrating out the UV physics together with the heavy mirror copy of the Higgs doublet. We consider a non-linear implementation of the Twin Higgs symmetries, so that also the radial mode of the linear realization is integrated out. We will be completely agnostic as regards the particular UV completion of the theory, which could be a strongly interacting composite dynamics [118, 119], a weakly coupled supersymmetric sector [129, 132] or the linear model itself, and as regards any possible UV mechanism that softly breaks the discrete symmetry. At the same time, we will not specify any particular symmetry breaking coset; as long as it delivers seven GB's, it could be $SU(4)/SU(3)$ as in the original model [125] or $SO(8)/SO(7)$ as in the minimal composite UV completion [118, 119]. We will also neglect the tree-level contribution of all the higher-dimensional operators, like current-current or four fermions operators, that could be originated after integrating out heavy bosonic or fermionic resonances. Their Wilson coefficients at the scale m_* are in fact model-dependent and moreover they are suppressed both by the weak coupling between the light degrees of freedom and the new dynamics and by inverse powers of m_* . Supposing this scale to be in the multi-TeV range, as in the spirit of the Twin Higgs paradigm, the initial conditions for these type of higher-dimensional operators can be safely taken to be zero. Our Lagrangian will however take into account the two basic elements of the twin Higgs construction, namely the presence of non-linear Higgs interactions due to the pNGB nature of the Higgs boson

and the existence of extra light degrees of freedom charged under the $\widetilde{\text{SM}}$. The remaining non-renormalizable terms that we neglected at the tree-level will be seeded at one-loop by the non-linear Higgs dynamics. We will consider just the most relevant contributions to the potential, originating from the G -breaking gauge and Yukawa interactions. We neglect the weak gauge couplings, whose effects are much smaller than those in the quark sector, and we keep only the terms proportional to the top Yukawa coupling, which generates the most important corrections to the potential. Under all these assumptions, the effective Lagrangian at the scale m_* is:

$$\begin{aligned} \mathcal{L}(m_*) = & (D^\mu H^\dagger)(D_\mu H) - V(H^\dagger H, m_*) + \\ & \bar{Q}_L i \not{D} Q_L + \bar{t}_R i \not{D} t_R - y_t(m_*) \left[f \bar{Q}_L \frac{H'}{\sqrt{2H^\dagger H}} \sin\left(\frac{\sqrt{2H^\dagger H}}{f}\right) t_R + \text{h.c.} \right] + \\ & \bar{\tilde{t}} i \not{D} \tilde{t} - \frac{\tilde{y}_t(m_*)}{\sqrt{2}} f \cos\left(\frac{\sqrt{2H^\dagger H}}{f}\right) \bar{\tilde{t}} \tilde{t}. \end{aligned} \quad (4.1)$$

In the previous equation, y_t and \tilde{y}_t denote the SM top Yukawa coupling and its twin; they are initially equal due to the approximate Z_2 symmetry: $y_t(m_*) = \tilde{y}_t(m_*)$. The twin tops \tilde{t} are not charged under the SM and therefore do not form any doublet with the corresponding twin bottom. This latter can then be neglected since its contribution to the RG flow of the Higgs potential would be proportional to \tilde{y}_b and is thus sub-leading. The covariant derivatives of the fermion fields contain the strong interactions with coupling g_S for the $SU(3)$ SM gauge groups and \tilde{g}_S for its twin. Because of the twin symmetry, we have again $g_S(m_*) = \tilde{g}_S(m_*)$. H is instead the SM Higgs doublet,

$$H = \frac{1}{\sqrt{2}} \begin{pmatrix} \pi_1 + i\pi_2 \\ h + i\pi_3 \end{pmatrix}; \quad (4.2)$$

we define $H' = i\sigma_2 H^*$ and $V(H^\dagger H, m_*)$ is the Higgs effective potential at the scale m_* :

$$V(H^\dagger H, m_*) = L(m_*) \sin^2\left(\frac{\sqrt{2H^\dagger H}}{f}\right) + F(m_*) \left[\sin^4\left(\frac{\sqrt{2H^\dagger H}}{f}\right) + \cos^4\left(\frac{\sqrt{2H^\dagger H}}{f}\right) \right]. \quad (4.3)$$

The mass term L is generated by the Z_2 breaking interactions, whereas the function F arises at the tree-level after integrating out the UV sector; their explicit form at m_* is model-dependent and provides an $O(1)$ initial condition for the running of the effective potential.

The low-energy Lagrangian fully takes into account the pNGB nature of the Higgs scalar by introducing the non-linear trigonometric interactions between the Higgs doublet and fermions. The effective potential has also the specific trigonometric dependence that is dictated by the existence of a non-linearly realized spontaneous symmetry breaking coset. It is convenient to make a field redefinition in order to recover the SM Lagrangian supplemented

by higher-dimensional operators and to simplify the initial conditions at the scale m_* for the relevant Wilson coefficients. We therefore redefine the Higgs doublet as

$$H \rightarrow f \frac{H}{\sqrt{2H^\dagger H}} \sin\left(\frac{\sqrt{2H^\dagger H}}{f}\right) \quad (4.4)$$

and recast the Lagrangian in Eq. (4.1) in the following form:

$$\begin{aligned} \mathcal{L}(m_*) = & (D^\mu H^\dagger)(D_\mu H) + \frac{1}{2f^2} \left[c_H(m_*) + d_H(m_*) \frac{H^\dagger H}{4f^2} \right] \mathcal{O}_H + \frac{c'_H(m_*)}{f^2} \mathcal{O}'_H - V(H^\dagger H, m_*) + \\ & \bar{Q}_L i \not{D} Q_L + \bar{t}_R i \not{D} t_R + \bar{\tilde{t}} i \not{D} \tilde{t} - \left[y_t(m_*) \bar{Q}_L H' t_R + \frac{\tilde{y}_t(m_*) f}{\sqrt{2}} \sqrt{1 - \frac{2H^\dagger H}{f^2}} \bar{\tilde{t}} \tilde{t} + \text{h.c.} \right], \end{aligned} \quad (4.5)$$

where the potential can now be written as

$$V(H^\dagger H, m_*) = 2\mu^2(m_*) H^\dagger H + 4\lambda(m_*) (H^\dagger H)^2 + 8 \frac{c_6(m_*)}{f^2} \mathcal{O}_6. \quad (4.6)$$

Using the notation of [25], we have introduced the following dimension-6 operators: $\mathcal{O}_H = \partial^\mu (H^\dagger H) \partial_\mu (H^\dagger H)$ and $\mathcal{O}'_H = H^\dagger H (D^\mu H^\dagger)(D_\mu H)^1$. It is straightforward to verify that $c_H(m_*) = 1$, whereas \mathcal{O}'_H is not generated at the tree-level with our choice of basis, $c'_H(m_*) = 0$.² Only the RG-evolution will seed this operator at loop-level. Notice also the presence of the dimension-8 operator $\mathcal{O}_D = H^\dagger H \partial^\mu (H^\dagger H) \partial_\mu (H^\dagger H)$, with $d_H(m_*) = 8$, which is necessary to capture all the effects due to the running in the Twin sector, as we shall see. The Wilson coefficients in the Higgs potential can be expressed as functions of L and F at the scale m_* , although the explicit relation is not relevant for the analysis of the IR contributions to the Higgs mass. However, one can check that the initial condition for c_6 is simply $c_6(m_*) = 0$, so that the operator $\mathcal{O}_6 = (H^\dagger H)^3$ is generated only through the running. All the contributions to the Higgs mass or to other observables due to the higher-dimensional operators in the SM sector are suppressed by powers of ξ , which measures the degree of tuning between the EW scale and the GB decay constant. The parameter ξ is also constrained to be small by electroweak precision tests (EWPT) which set a bound $\xi \leq 0.2$. As regards the Twin sector, notice finally that the non-renormalizable interactions generated at the tree-level are all collected in the

¹Notice that the operators \mathcal{O}_H and \mathcal{O}'_H are already present in the Lagrangian of Eq. (4.1), but the initial conditions for their Wilson coefficients in that basis are such that the Higgs kinetic term is canonical. We have therefore omitted to report them

²The operator \mathcal{O}'_H corrects the W boson mass at order ξ , whereas in the basis (4.4) no correction to the gauge boson masses is induced. We did not report the low-energy Lagrangian in the gauge sector, but it can be found in [118], for instance. As a consequence, this operator is absent at the tree-level. For the same reason, the eight-dimensional companion operator of \mathcal{O}_D , $\mathcal{O}'_D = (H^\dagger H)^2 |D_\mu H^\dagger|^2$, has vanishing boundary conditions when matching with the Twin Higgs Lagrangian in our basis. Since only the tree-level initial conditions for the eight-dimensional operators can affect the RG-improvement of the potential at cubic order, we can completely neglect \mathcal{O}'_D from our Lagrangian.

function of the Higgs field which accompanies \tilde{y}_t . From the Lagrangian in Eq. (4.5), we can also derive the expressions of the top masses and their scale separation. After EWSB, we have in fact $m_t = y_t v / \sqrt{2}$ for the SM tops and $\tilde{m}_t = \tilde{y}_t f \sqrt{1 - \xi} / \sqrt{2}$ for their twins.

4.1.1 The Higgs mass and the LL result

The potential at the scale m_* gives rise to a first small UV contribution to the Higgs mass. This is a model-dependent tree-level effect that arises after integrating out the heavy physics. We have:

$$(M_H^2)_{UV} \sim \lambda(m_*) v^2. \quad (4.7)$$

The RG evolution of the potential induced by the light degrees of freedom generates other log-enhanced IR corrections due to the running from m_* down to the low-energy scale where the Higgs mass is experimentally measured, for instance m_t , the top mass scale. The Higgs mass receives then a second contribution, $(M_H^2)_{IR}$, which is model-independent and proper to any possible UV completion of the Twin Higgs paradigm. Our full prediction for this observable is therefore:

$$M_H^2 = (M_H^2)_{UV} + (M_H^2)_{IR}, \quad (4.8)$$

where $(M_H^2)_{IR}$ can be expressed at a generic renormalization scale μ as a function of the renormalized Wilson coefficients appearing in Eq. (4.5). At first order in ξ , we have:

$$(M_H^2)_{IR}(\mu) = 8 \left[\lambda(\mu) + 3 c_6(\mu) \xi \right] \left[1 - (c_H(\mu) + c'_H(\mu)) \xi \right] v^2. \quad (4.9)$$

Once the RG flow to the IR scale has been computed to the desired level of accuracy, one can match with the UV mass term so as to reproduce the observed value of the Higgs mass, $(M_H^2)_{Exp} = (125 \text{ GeV})^2$. We aim at deriving an expression for the IR RG evolution in order to judge how important the running effects are and to analyze which value of the UV threshold correction is more suitable. This will in turn give information on what kind of UV completion can be imagined to generate $(M_H^2)_{UV}$ of the right size.

The computation of the RG evolution of the Higgs potential can be carried out at different orders in an expansion in logarithms. The leading contribution is obtained by neglecting the running of the top Yukawas and the strong couplings and retaining only the first power in the logarithmic expansion. We call this order leading logarithm (LL) result. Using the standard Coleman-Weinberg technique, one finds that only λ can be generated at the leading order,

whereas c_6 is still vanishing; the Higgs mass is then [118]:

$$(M_H^2)_{IR}^{LL}(m_t) = \frac{3}{8\pi^2} \left[y_t^4(m_*) \log\left(\frac{m_*^2}{m_t^2}\right) + \tilde{y}_t^4(m_*) \log\left(\frac{m_*^2}{\tilde{m}_t^2}\right) \right] (1 - \xi) v^2, \quad (4.10)$$

which is the sum of two different contributions. The first one is proportional to y_t^4 and is induced by the running of the quartic coupling due to loops of SM fermions, while the second is of order \tilde{y}_t^4 and results from analogous loops of twin tops. Notice also that we have included the first correction to the leading logarithm, proportional to ξ . This effect is usually smaller and parametrically belongs to the next class of contributions. By setting y_t to the experimental value at the scale m_t , we can estimate the value of the Higgs mass generated by the IR physics. For $\xi = 0.1$ and $m_* = 10$ TeV, we predict $(M_H)_{IR} \sim 150$ GeV, which is far above the experimental observations. A more accurate analysis that takes into account the running of the Yukawas, the strong couplings and the higher-dimensional operators can drastically change this prediction and the consequent necessary size of the UV threshold correction.

In this Chapter we will study the RG-improvement of the potential and derive the first two corrections of the LL Higgs mass, up to effects that are cubic in the logarithmic series. Indicating with $t = \log(m_*^2/\mu^2)$ the expansion parameter, where μ is again the renormalization scale, we shall consider first of all the next-to-leading logarithmic contribution to the potential (NLL), which incorporates all the effects proportional to t^2 . We will include in this class also the smaller ξt^2 contributions to the Higgs mass, that would belong to the next class of corrections; for simplicity of exposition we classify them in the same category as the other t^2 terms. We will neglect all the other powers of ξ , which are much smaller due to the constraint from EWPT. The second correction we shall compute is the next-to-NLL (NNLL), which contains only the t^3 effects. We will not compute the smaller ξt^3 corrections, which are part of the next class of contributions.

4.2 The NLL effective potential

The RG-improvement of the Higgs effective potential is the result of all the physical effects that induce an evolution of the Wilson coefficients when changing the energy scale of a process. While running down from m_* to m_t , the high energy - or equivalently short distance - degrees of freedom are integrated out and the initial parameters in the Lagrangian must be redefined to properly describe the physics at low-energy and to eliminate the loop divergences. In particular, in order to fully capture the NLL corrections to the potential, we have to take into account three important effects. First of all, the top Yukawa couplings in the SM and $\widetilde{\text{SM}}$ sectors evolve along the RG flow because of the strong interactions and the coupling with the Higgs field. The adequate inclusion of this running contributes to the potential at order t^2 .

Secondly, the dimension-6 operators \mathcal{O}_H and \mathcal{O}'_H are corrected with respect to their tree-level initial values due to loops of fermions, thus affecting the Higgs mass at order ξt^2 . Finally, also the Higgs wave function receives a non-vanishing correction from top loops resulting in a non-canonical scalar field; the wave function renormalization will affect the whole NLL result, both at t^2 and ξt^2 level.

We will derive the NLL effective potential using the background field method, as developed in standard textbooks of quantum field theory [21, 22]. This technique proves to be extremely powerful for theories like the Twin Higgs model while at the same time being perfectly equivalent to the diagrammatic approach. Due to the presence of non-renormalizable interactions, in fact, new operators are generated along the RG-flow at each step of the running, so that using a more conventional diagrammatic procedure one would need to keep track of all them and compute an increasing number of diagrams. The application of the background technique, instead, treats the Higgs field as an external spectator and re-sums automatically a huge class of diagrams without much increasing the effort as more powers of t are included. At the quadratic level, this method is so powerful that the sole renormalization of the twin top propagator is equivalent to the computation of an order of ten loops with the diagrammatic approach. We shall devote this Section to the presentation of the background field method and its usage to derive a general RG-improved Coleman-Weinberg formula for the effective potential. This latter will be applied to the Twin Higgs Lagrangian in order to compute the NLL correction to the Higgs mass.

4.2.1 The background field

The background field method is based on the idea that one can explicitly integrate out the short distance degrees of freedom after separating them from the low-energy modes. Since we are interested in computing the effective potential for the Higgs boson, our starting point is to split the scalar doublet in two parts, a background spectator field and a quantum fluctuation:

$$H = H_c + \hat{\eta}. \quad (4.11)$$

H_c indicates the classical field configuration for the Higgs doublet; it comprises all the low-energy modes that we will keep in the spectrum and for which we will find a potential. $\hat{\eta}$ denotes instead the dynamical fluctuations over the classical field; these are the high-energy modes we seek to integrate out. Notice that we are keeping the full Higgs doublet as a classical spectator field; the $SU(2)$ symmetry therefore allows us to apply the background field method in successive steps, without needing to classify from the beginning all the operators containing the classical configuration, the quantum fluctuation and their derivatives. Instead, we will first integrate out a layer of high-energy modes and generate a series of operators that were

absent at the tree-level. These will be function of the background H_c , which we consider as a dynamical space-time dependent field. After the first step, we will again separate H_c into a low-energy part and a short distance component and in this way we will recollect also the contributions to the effective potential generated by operators involving derivatives of η . These latter would be naively lost if considering H_c as a non-dynamical field and would be kept only with a full classification of the operators allowed by the symmetry of the theory at the scale m_* . This is an alternative approach that guarantees full generality, but for the simple case of the computation of the Higgs effective potential our procedure of successive divisions and integrations proves to be simpler and faster. We will apply this approach especially in the last part of this Chapter when considering the operators involving derivatives of the quantum fluctuation and contributing to the potential. H_c can be always viewed as a dynamical field still containing a high-energy part that we can integrate out to keep only lower energy terms. In this sense, our application of the background field method is somewhat similar to a Wilsonian renormalization where different layers of degrees of freedom are integrated out in successive steps.

After separating the first layer of short distance modes from the large distance degrees of freedom, we can recast the top and twin top sectors of the Lagrangian in Eq (4.5) as follows:

$$\mathcal{L}^F(m_*) = \mathcal{L}_{Kin}^F(m_*) - \bar{Q}_L m(H_c)' t_R - \hat{y}_t(H_c) \bar{Q}_L \hat{\eta}' t_R - \tilde{m}_t(H_c) \tilde{t} \tilde{t} + \frac{\hat{\tilde{y}}_t(H_c)^\dagger \hat{\eta}}{\sqrt{2}} \tilde{t} \tilde{t} + \text{h.c.}, \quad (4.12)$$

where $\mathcal{L}_{Kin}^F(m_*)$ collectively indicates the kinetic terms of the fermion fields. Expanding the Lagrangian in powers of $\hat{\eta}$, we kept only the linear interactions of the high-frequency modes with the top quarks, since the remaining non-linear interactions do not contribute at the NLL order. The coupling between the $\hat{\eta}$ fields and fermions is in general a background-dependent function; in the SM, it is trivially equivalent to the top Yukawa, but in the Twin sector it has a specific functional form. Promoting the Yukawa couplings to spurions of the spectator Higgs field, we have introduced the following background-dependent quantities:

$$\hat{y}_t(H_c) \equiv y_t, \quad \hat{\tilde{y}}_t(H_c) \equiv \tilde{y}_t \frac{H_c}{f} \frac{1}{\sqrt{1 - \frac{2H_c^\dagger H_c}{f^2}}}. \quad (4.13)$$

Also the fermion masses at the tree-level can be considered as functions of the spectator H_c and treated formally as spurions; one easily finds:

$$m_t(H_c) = y_t H_c, \quad \tilde{m}_t(H_c) = \frac{\tilde{y}_t f}{\sqrt{2}} \sqrt{1 - \frac{2H_c^\dagger H_c}{f^2}}. \quad (4.14)$$

The physical value of the mass parameters is obtained by setting the background doublet to

its EW vacuum expectation value, thus recovering the standard expressions.³

Let us now consider the scalar sector of the theory. After separating the short distance modes from the long-distance ones, a set of new interactions between the background field and the quantum fluctuation is generated. Of these, only a few are relevant for the NLL computation; in practice, we just have to take into account that the kinetic term for $\hat{\eta}$ becomes non-canonical and acquires a background dependence. We have in fact:

$$\mathcal{L}^S(m_*) \supset |D^\mu H_c|^2 + \frac{1}{2f^2} \left(c_H + d_H \frac{H_c^\dagger H_c}{4f^2} \right) \mathcal{O}_H(H_c) + \frac{1}{2} Z_{\hat{\eta}_4}(H_c) (D^\mu \hat{\eta}_4)^2 + \frac{1}{2} \sum_{i=1}^3 Z_{\hat{\eta}_i}(H_c) (D^\mu \hat{\eta}_i)^2, \quad (4.15)$$

with

$$Z_{\hat{\eta}_4}(H_c) = 1 + 2c_H \frac{H_c^\dagger H_c}{f^2} + c'_H \frac{H_c^\dagger H_c}{f^2} + d_H \frac{(H_c^\dagger H_c)^2}{2f^4}, \quad Z_{\hat{\eta}_1}(H_c) = Z_{\hat{\eta}_2}(H_c) = Z_{\hat{\eta}_3}(H_c) = 1 + c'_H \frac{H_c^\dagger H_c}{f^2}. \quad (4.16)$$

As for the fermionic sector, the previous equation serves as an initial condition for the wave function of the high-energy modes, which will be modified along the flow by quantum corrections. Notice that the operators \mathcal{O}_H and \mathcal{O}_D break the $SU(2)$ invariance of the Higgs field, contributing only to the wave function renormalization of the scalar fluctuation corresponding to the real Higgs boson. We have therefore divided $\hat{\eta}$ into two parts: η_4 , describing the high-energy modes of the Higgs, and η_i , the three fluctuations of the Goldstone modes. At the scale m_* , given that $c'_H = 0$, the wave function of these latter does not get renormalized, but it will be affected by the running at higher orders in the loop expansion, as we shall see later.

One could choose to perform a proper field redefinition in order to eliminate the background dependence and render the fluctuation canonical. We will work, instead, with a non-canonical basis and integrate out the high-energy degrees freedom without redefining the $\hat{\eta}$ fields. As a consequence, we will have to write down a separate evolution equation for the wave function which will be coupled to the β -functions of the Yukawa couplings. Despite this additional feature, choosing a non-canonical basis has many advantages and allows to efficiently re-sum all the diagrams generated by insertions of the higher-dimensional operators \mathcal{O}_H , \mathcal{O}'_H and \mathcal{O}_D . Only after deriving the effective potential will we perform the field redefinition and find the Higgs mass in the canonical basis.

³The top Yukawas in Eqs. (4.14) and (4.13) are both evaluated at the scale m_* ; from now on, we will omit to specify the scale where the initial condition of the bare parameters originates, unless differently stated they will all be considered at the cut-off.

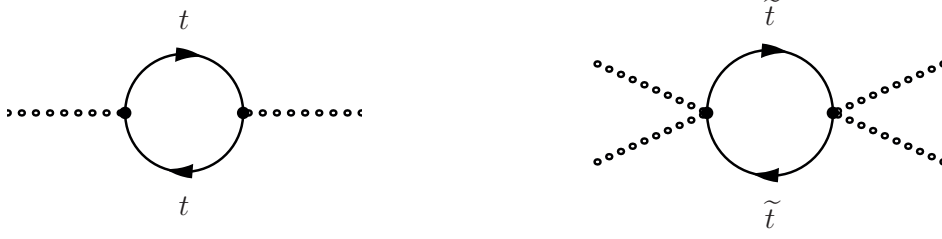


Figure 4.1 – One loop diagrams contributing to the wave function renormalization (on the left) and to the running of c'_H (on the right). The external dotted lines denote the background field H_c .

4.2.2 β -functions in the Higgs background

After separating the quantum fluctuation from the long distance modes and finding the background-dependent couplings and fermion masses, the short distance degrees of freedom must be integrated out to derive the effective action at low energies. In the scalar sector, this process generates a quantum contribution to the wave function of H_c and $\hat{\eta}$ and also renormalizes c_H and c'_H . In the fermionic sector, the integration of the high-frequency modes results in the redefinition of the background-dependent Yukawa couplings and masses, which start evolving with the energy scale. In this section, we will derive a set of coupled differential equations for the Higgs wave function and the Yukawas in the classical background. They are the generalization of the usual β -functions for a general theory with a non-canonical Higgs and field-dependent Wilson coefficients.

We start our study with the scalar sector. The running of the wave function and of the other Lagrangian parameters is induced in this case by loops of fermions; one would formally need to split also the top fields into long distance and short distance modes and integrate out these latter. This is completely equivalent to computing the one-loop diagrams in Fig. (4.1) with $N_c = 3$ colors circulating for both SM and $\widetilde{\text{SM}}$ quarks. The coupling between the background field and the fermionic fluctuation is obtained by expanding the mass terms in Eq. (4.12) in powers of the spectator H_c . For the SM, only the usual linear coupling proportional to y_t exists and therefore loops of tops can only renormalize the wave function of the Higgs. For the Twin sector, instead, the first non-trivial coupling is quadratic in the Higgs background, so that no contribution to the wave function can be obtained from the mirror tops. One-loop diagrams of twin fermions will however renormalize the higher-dimensional operator \mathcal{O}'_H . At first order

in the expansion parameter t , the Lagrangian at a generic renormalization scale μ becomes:

$$\begin{aligned} \mathcal{L}(t)^S \supset & Z_H(t) |D^\mu H_c|^2 + \frac{1}{2} Z_{\hat{\eta}_4}(H_c, t) (D^\mu \hat{\eta}_4)^2 + \frac{1}{2} \sum_{i=1}^3 Z_{\hat{\eta}_i}(H_c, t) (D^\mu \hat{\eta}_i)^2 + \\ & \frac{c_H(t)}{2f^2} \mathcal{O}_H + \frac{c'_H(t)}{f^2} \mathcal{O}'_H + \frac{d_H}{8f^4} \mathcal{O}_D, \end{aligned} \quad (4.17)$$

where

$$\begin{aligned} Z_H(t) &= 1 + \frac{N_c \gamma_t^2}{16\pi^2} t, \quad c_H(t) = c_H, \quad c'_H(t) = \frac{N_c \tilde{\gamma}_t^2}{16\pi^2} t, \\ Z_{\hat{\eta}_4}(H_c, t) &= Z_H(t) + (2c_H(t) + c'_H(t)) \frac{H_c^\dagger H_c}{f^2} + d_H \frac{(H_c^\dagger H_c)^2}{2f^4} \\ Z_{\hat{\eta}_1}(H_c, t) &= Z_{\hat{\eta}_2}(H_c, t) = Z_{\hat{\eta}_3}(H_c, t) = Z_H(t) + c'_H(t) \frac{H_c^\dagger H_c}{f^2}. \end{aligned} \quad (4.18)$$

The one-loop integration of the high-energy fermionic modes also induces a renormalization of d_H which however we can neglect. Only the tree-level value of this parameter, in fact, contributes to the Higgs effective potential at the NLL because \mathcal{O}_D can only renormalize \mathcal{O}_6 which in turn can be first generated at order t^2 . Finally, since the wave functions for the three GBs are always equal, for simplicity we will refer only to $Z_{\hat{\eta}_1}$ in the following, implying that the other two wave functions behave in the same way.

Let us now consider the fermionic sector of the Twin Higgs theory. The process of integrating out the high energy modes of the Higgs field translates in this case into a renormalization of the top quarks propagator, as in Fig. (4.2). Together with the scalar fluctuations, a contribution to the running of the Yukawas is also generated by QCD gluons, both in the SM and in the $\widetilde{\text{SM}}$. The computation of these effects is standard and leads to a background-dependent quantum correction to the quarks wave functions and their mass. After rescaling the fermion fields⁴ we

⁴Notice that, integrating out the quantum fluctuation, a field-dependent wave function renormalization for the fermions is induced. When re-scaling the fermion fields to go in the canonical basis, a derivative interaction with the external classical background may be generated, which in turn could induce an additional correction to the Higgs effective potential. However, the most generic expression for the wave function renormalization of the fermion kinetic term takes the form:

$$\mathcal{L}_{wave} \supset i Z_\psi(H_c) \bar{\psi} \gamma^\mu (\vec{\partial}_\mu - \overleftarrow{\partial}_\mu) \psi, \quad (4.19)$$

where ψ collectively indicates the top quarks or their twins. A general field redefinition like

$$\psi \rightarrow (1 + a Z_\psi(H_c)) \psi \quad (4.20)$$

can make the fermions canonical with a suitable choice of the free parameter a . Since the kinetic term contains two derivatives acting on the fermion field and its conjugate with opposite sign, any derivative interaction with the external classical Higgs cancels out and no additional contribution to the effective potential is generated.



Figure 4.2 – One-loop diagrams displaying the renormalization of the top quark propagator due to the interaction with the Higgs quantum fluctuations (on the left) and with gluons (on the right). The solid black lines denote the fermion field, either the SM tops or their SM mirrors, whereas the curly line stands both for the $SU(3)$ and the $\widetilde{SU}(3)$ gluons. The dashed line stands for the quantum fluctuation.

find:

$$y_t(t) = y_t + \frac{y_t}{64\pi^2} \left(16g_S^2 - 3 \frac{\hat{y}_t^2(H_c)}{Z_{\hat{\eta}_4}(H_c)} \right) t, \quad \tilde{y}_t(t) = \tilde{y}_t + \frac{\tilde{y}_t}{64\pi^2} \left(16\tilde{g}_S^2 - 3 \frac{\hat{\tilde{y}}_t^2(H_c)}{Z_{\hat{\eta}_4}(H_c)} \right) t. \quad (4.21)$$

Since the scalar fluctuation is still non-canonical in our basis, every propagator of the $\hat{\eta}$ fields is accompanied by an inverse power of $Z_{\hat{\eta}}(H_c)$, which in turn must appear explicitly in the evolution of the Yukawa couplings. This is why it is convenient to keep the short distance modes non-canonical: all the contributions to the running proportional to c_H , c'_H and d_H will be automatically re-summed in the denominator of the beta functions without any need of computing additional diagrams. The sole renormalization of the top quark propagator in the background field language is enough to consistently keep track of all the higher-dimensional operators that will be generated along the flow.

The RG evolution of the Yukawa couplings and of the Higgs wave functions can be elegantly described by a set of background-dependent coupled differential equations that take into account the physical effects we have encountered so far. These β -functions will re-sum all the leading logarithms in the energy flow; for a general Wilson coefficient c they can be defined as:

$$\beta_c = \frac{dc(t)}{dt}. \quad (4.22)$$

From the previous results, we then easily find the following RG-equations:

$$\begin{aligned} \beta_{y_t} &= \frac{y_t(H_c, t)}{64\pi^2} \left(16g_S^2(t) - 3 \frac{y_t^2(H_c, t)}{Z_{\hat{\eta}_4}(H_c, t)} \right), \quad \beta_{Z_{\hat{\eta}_4}} = \beta_{Z_{\hat{\eta}_1}} = \frac{3y_t^2(H_c, t)}{16\pi^2} + \frac{3\tilde{y}_t^2(H_c, t)}{16\pi^2} \frac{H_c^\dagger H_c}{f^2}, \\ \beta_{\tilde{y}_t} &= \frac{\tilde{y}_t(H_c, t)}{64\pi^2} \left(16\tilde{g}_S^2(t) - 3 \frac{\tilde{y}_t^2(H_c, t)}{Z_{\hat{\eta}_4}(H_c, t)} \frac{2H_c^\dagger H_c}{f^2} \frac{1}{1 - \frac{2H_c^\dagger H_c}{f^2}} \right), \quad \beta_{Z_H} = \frac{3y_t^2(H_c, t)}{16\pi^2} \Big|_{H_c=0}. \end{aligned}$$

(4.23)

The β -functions we have just derived are valid in a non-canonical basis; once they are solved, we need to redefine the background field H_c in order to compute the RG-improved physical quantities. For instance, the SM top Yukawa in the canonical basis is obtained with the simple combination

$$y_t^{phys}(t) = \frac{y_t(0, t)}{\sqrt{Z_H(t)}}, \quad (4.24)$$

with $y_t(0, t)$ being the running Yukawa coupling evaluated at zero spectator field; analogous relations hold for the remaining parameters. Notice that we do not need an explicit β -function for c_H and c'_H since their RG-evolution is already absorbed in the running of the wave function for the fluctuation $\hat{\eta}$. This is another reason why it is advantageous to keep the Higgs field non-canonical. Finally, the running of the top quark masses, which are the quantities we will need in the Coleman-Weinberg formula, is directly related to the evolution of the Yukawas. We have:

$$m_t(H_c, t) = y_t(H_c, t) H_c, \quad \tilde{m}_t(H_c, t) = \frac{\tilde{y}_t(H_c, t) f}{\sqrt{2}} \sqrt{1 - \frac{2H_c^\dagger H_c}{f^2}}, \quad (4.25)$$

where $y_t(H_c, t)$ and $\tilde{y}_t(H_c, t)$ denote the solution of the β -functions in the Higgs background. This is the starting point for the computation of the RG-improved effective potential.

4.2.3 RG-improved Coleman-Weinberg formula and Higgs mass

The Coleman-Weinberg procedure to compute the effective potential is an efficient way of re-summing all the one-loop diagrams contributing to the low-energy action with a generic number of external scalar legs. This formally corresponds to calculate the vacuum energy, or cosmological constant, of the theory in an external background. In order to improve the LL result and include all the leading logarithms that are generated during the running, we can use an evolution equation for the cosmological constant itself that serves as a β -function for the vacuum energy. We introduce therefore the RG-improved Coleman-Weinberg formula as follows:

$$\frac{d}{dt} V_{CW}^F(H_c, t) = \frac{N_c}{16\pi^2} (m_t^4(H_c, t) + \tilde{m}_t^4(H_c, t)), \quad (4.26)$$

where only the fermionic loops have been considered, the scalar loops giving contributions from the NNLL correction. In order to improve the potential up to the t^2 terms, we need to solve Eqs. (4.23) and find the renormalized top at twin top masses of Eq. (4.25) at the LL. The initial conditions for the Wilson coefficients are fixed at the scale m_* ; in particular, the wave

function $Z_{\hat{\eta}}$ has the field-dependent starting value of Eq. (4.16) and automatically re-sums the contribution to the Higgs mass induced by the higher-dimensional operators \mathcal{O}_H , \mathcal{O}'_H and \mathcal{O}_D . After re-scaling the Higgs field to pass in the canonical basis,

$$H_c \rightarrow \frac{H_c}{\sqrt{Z_H(t)}}, \quad (4.27)$$

we can derive $\lambda(t)$ and $c_6(t)$ at order t^2 from the RG-improved Coleman-Weinberg formula. We also need to compute the physical value of $c_H(t)$, which appears in the external correction of order ξ to the Higgs mass:

$$c_H(t) \rightarrow \frac{c_H(t)}{Z_H^2(t)} = c_H - \frac{3c_H y_t^2}{8\pi^2} t. \quad (4.28)$$

Notice that $c'_H(t)$ does not receive contributions from the wave function of the Higgs field at order t since it is only generated at one-loop.

From Eq. (4.9), it is finally straightforward to find the IR correction to the Higgs boson mass at the NLL:

$$\begin{aligned} (M_H^2)_{IR}^{NLL}(t) = & \frac{3v^2}{256\pi^4} \left[(16g_S^2 y_t^4 + 16\tilde{g}_S^2 \tilde{y}_t^4 - 15y_t^6 + 3(c_H + 1)\tilde{y}_t^6 - 12y_t^2 \tilde{y}_t^4) t^2 + \right. \\ & \left(36c_H y_t^6 + \tilde{y}_t^6 \left(\frac{9}{8} d_H - 12c_H - 12c_H^2 - 6 \right) - 6y_t^4 \tilde{y}_t^2 + 24c_H y_t^2 \tilde{y}_t^4 - \right. \\ & \left. \left. 16c_H g_S^2 y_t^4 - 16c_H \tilde{g}_S^2 \tilde{y}_t^4 \right) \xi t^2 \right]. \end{aligned} \quad (4.29)$$

This is our final result for the model-independent RG evolution of the Higgs mass in a low-energy Twin Higgs theory. The renormalization scale μ encoded in the expansion parameter t is taken to be a generic scale bigger than the physical twin top mass. When explicitly evaluating the Higgs mass, we will fix $\mu = m_t$ and match at the scale \tilde{m}_t where the twin tops need to be integrated out. Finally notice that the result in Eq. (4.29) agrees with the same solution derived with a more conventional diagrammatic approach in Appendix G.

4.3 The NNLL effective potential

Since our Twin Higgs extension of the SM is a non-renormalizable theory, the RG-improvement of the Higgs effective potential is not completely exhausted by the β -functions we have just computed. These latter cannot capture all the physical effects coming into play at the next orders in t . Other higher-dimensional operators are in fact generated along the flow that contribute to the Higgs mass and that cannot be included in our previous background-dependent renormalization of the fermion masses. In order to fully capture the NNLL correction to the potential, we then need to classify a series of new quantum contributions to the twin top

masses that are only present from the t^3 terms. Together with these effects, we have to take into account the RG-evolution of the strong couplings, whose running is negligible at the NLL order, and the scalar part of the Coleman-Weinberg potential. In this Section, we analyze the cubic correction to the low-energy action in the background field language studying in detail the contributions in each category. We will supplement the field-dependent β -functions with another set of RG-evolution equations for the twin top masses and solve them to systematically re-sum the leading logarithms. The expression of the Higgs mass at the NNLL order will be our final result.

4.3.1 Running of the strong couplings and scalar contribution to the Coleman-Weinberg potential

The first important correction to the NLL effective potential comes from the RG-evolution of the strong couplings, both in the SM and in the $\widetilde{\text{SM}}$. The Twin $\widetilde{SU}(3)$ strong interactions are an exact mirror copy of the $SU(3)$ gauge theory. They are both external to the whole mechanism that protects the Higgs mass from radiative corrections so that we can assume the Z_2 symmetry to be unbroken in this sector. The runnings of g_S and \widetilde{g}_S are therefore identical and both described by the standard QCD β -function with $n_f = 6$ flavors. From our initial conditions at the scale m_* , we find:

$$g_S(t) = g_S + \frac{7g_S^3}{32\pi^2}t, \quad \widetilde{g}_S(t) = \widetilde{g}_S + \frac{7\widetilde{g}_S^3}{32\pi^2}t, \quad (4.30)$$

which give the strong couplings at the renormalization scale $\mu \ll m_*$.

The second non-trivial contribution comes from the scalar part of the Coleman-Weinberg potential, which re-sums all the vacuum energy loops involving the Higgs and the GB's. The generalization of Eq. (4.26) is straightforward:

$$\frac{d}{dt} V_{CW}^S(H_c, t) = -\frac{1}{64\pi^2} \left(\sum_{i=1}^3 (\widehat{m}_{GB}^i)^4(H_c, t) + \widehat{m}_H^4(H_c, t) \right), \quad (4.31)$$

where \widehat{m}_{GB}^i and \widehat{m}_H are respectively the masses of the quantum fluctuations for the three SM GB's and for the Higgs in the background field. They can be found by diagonalizing the mass term for the high-energy modes; from the general form of the potential in Eq. (4.6), in fact, after splitting as in Eq. (4.11), we find a non-diagonal mass matrix for $\widehat{\eta}$,

$$\mathcal{L}_M(H_c) = -\widehat{M}_{ij}^2(H_c) \widehat{\eta}^i \widehat{\eta}^j, \quad (4.32)$$

where each of the $\widehat{\eta}^i$ denotes a component of the full high-frequency doublet. The diagonal-

ization of \widehat{M} leads to the following expressions in the spectator background:

$$\begin{aligned} (\widehat{m}_{GB}^1)^2 &= (\widehat{m}_{GB}^2)^2 = (\widehat{m}_{GB}^3)^2(H_c, t) = \frac{1}{Z_{\widehat{\eta}_1}(H_c, t)} \left(\mu^2(t) + 8\lambda(t)H_c^\dagger H_c + 24c_6(t) \frac{(H_c^\dagger H_c)^2}{f^2} \right), \\ \widehat{m}_H^2(H_c, t) &= \frac{1}{Z_{\widehat{\eta}_4}(H_c, t)} \left(\mu^2(t) + 24\lambda(t)H_c^\dagger H_c + 120c_6(t) \frac{(H_c^\dagger H_c)^2}{f^2} \right). \end{aligned} \quad (4.33)$$

The presence of the wave function for $\widehat{\eta}$ is again a feature of our non-canonical basis. When finding the masses for the physical fields, we need to redefine the fluctuation thus getting an explicit dependence from $Z_{\widehat{\eta}}$ in the scalar masses.

The correction to the low-energy action from the scalar Coleman-Weinberg potential can only arise at cubic order in the logarithmic expansion. This is because λ in our theory is first generated at one-loop, so that when integrating Eq. (4.31) we cannot find a lower contribution. For the NNLL result, we do not need to compute c_6 , since it gives an effect suppressed by ξ . We reported, however, the full expression of the scalar masses for completeness. Finally, also in the scalar sector, the computation of the running of the Higgs quartic coupling through the background field method is perfectly equivalent to the diagrammatic approach. At the NNLL, it is in one-to-one correspondence only with the one-loop diagram generated by the Higgs self-interaction. With the background technique, however, one has the advantage to avoid deriving any symmetry factor, that can be cumbersome in the standard procedure.

4.3.2 Renormalization of the twin top mass in the Higgs background

The second class of effects that contribute to the Higgs mass at the NNLL order is related to the renormalization of the twin top mass induced by the non-linear interactions between the quarks and the scalar fluctuation and by new higher-dimensional operators. Let us start considering how the twin propagator is affected by the non-linear coupling with $\widehat{\eta}$. After splitting the high-energy modes from the long-distance degrees of freedom, the Lagrangian in Eq. (4.12) develops an additional background-dependent quadratic interaction as follows:

$$\mathcal{L}^F(m_*) \supset \frac{\widehat{y}_2^{GB}(H_c)}{2\sqrt{2}f} \sum_{i=1}^3 \bar{t} \tilde{t} \widehat{\eta}_i^2 + \frac{\widehat{y}_2^H(H_c)}{2\sqrt{2}f} \bar{t} \tilde{t} \widehat{\eta}_4^2. \quad (4.34)$$

In the previous equation, we have again explicitly written the quantum fluctuation in components,

$$\widehat{\eta} = \frac{1}{\sqrt{2}} \begin{pmatrix} \widehat{\eta}_1 + i\widehat{\eta}_2 \\ \widehat{\eta}_4 + i\widehat{\eta}_3 \end{pmatrix}, \quad (4.35)$$

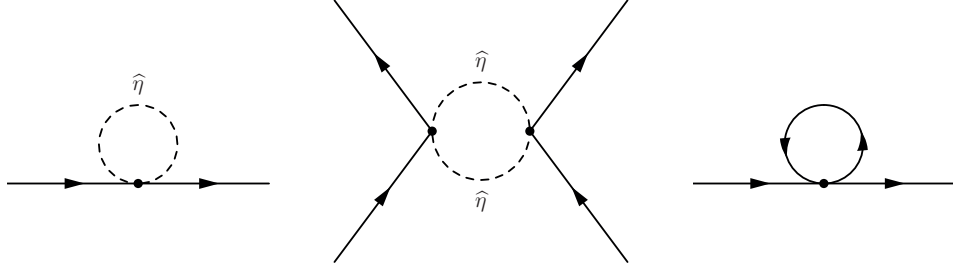


Figure 4.3 – One-loop diagrams displaying the renormalization of the twin top quark mass. On the left, the diagram correcting the twin top propagator with loops of scalars; in the middle the one generating the four-fermion operator of Eq. (4.38); on the right, the renormalization of the twin top propagator due to the four-fermion interaction. Solid lines indicate the twin quarks, dashed lines the scalar fluctuation.

indicating with η_4 the high-energy modes of the physical Higgs and with the remaining η_i those of the three GB's. The twin tops interact differently with the various types of scalar fluctuations and we have introduced two field-dependent couplings:

$$\hat{y}_2^{GB}(H_c) = \frac{\tilde{y}_t}{\sqrt{1 - \frac{2H_c^\dagger H_c}{f^2}}}, \quad \hat{y}_2^H(H_c) = \frac{\tilde{y}_t}{\left(1 - \frac{2H_c^\dagger H_c}{f^2}\right)^{3/2}}. \quad (4.36)$$

The first one denotes the interaction with the three GB's, which are all coupled identically with fermions. The physical Higgs, instead, picks up an additional term after expanding the doublet and it is coupled differently with respect to the other scalars.

The existence of these quadratic interactions induces a renormalization of the twin top propagator due to scalar tadpoles, as in Fig. (4.3). In particular, no correction to the fermion wave function can be generated and we find only a quantum contribution to the twin mass:

$$\delta \tilde{m}_t^S(H_c, t) = 3 \frac{\hat{y}_2^{GB}(H_c)}{32\sqrt{2}\pi^2} \frac{(\hat{m}_{GB}^1)^2(H_c, t)}{f} t + \frac{\hat{y}_2^H(H_c)}{32\sqrt{2}\pi^2} \frac{\hat{m}_H^2(H_c, t)}{f} t. \quad (4.37)$$

The renormalization of \tilde{m}_t is proportional to the field-dependent scalar masses, which originate first at the LL. The correction to the Higgs effective potential must then arise at cubic order, as expected.

We consider now the class of physical effects due to the generation of new higher-dimensional operators that are not captured by the field-dependent β -functions of the top Yukawas. The first of these operators is the six-dimensional four-fermions interaction obtained by integrating out the high-frequency scalar modes, as shown in the median diagram of Fig. (4.3). At one-loop, the Lagrangian in the fermionic sector receives the following additional contribution:

$$\mathcal{L}^F(t) \supset \frac{c_{4t}(H_c, t)}{4f^2} (\tilde{t} \tilde{t})^2, \quad (4.38)$$

with

$$c_{4t}(H_c, t) = 3 \frac{\hat{y}_2^{GB}(H_c)^2}{16\pi^2 Z_{\hat{\eta}_1}^2(H_c)} t + \frac{\hat{y}_2^H(H_c)^2}{16\pi^2 Z_{\hat{\eta}_4}^2(H_c)} t. \quad (4.39)$$

In the background field language, this operator affects the Higgs potential by renormalizing the twin top propagator, as it can be seen again in the last diagram of Fig. (4.3). It is straightforward to derive a second correction to the fermion mass which reads:

$$\delta \tilde{m}_t^F(H_c, t) = -\frac{N_c}{4\pi^2} c_{4t}(H_c, t) \frac{\tilde{m}_t^3(H_c)}{f^2} t. \quad (4.40)$$

The joint quantum correction to the four fermion interaction and to the twin mass implies a contribution to the low-energy action only at NNLL.

There is a second kind of higher-dimensional operators renormalizing the twin top mass which are seeded along the flow by \mathcal{O}_H , \mathcal{O}'_H and \mathcal{O}_D and which are distinct from the ones captured by the wave function renormalization of $\hat{\eta}$. After splitting the high-energy modes from the low-energy degrees of freedom, in fact, not only do those operators induce a non-canonical kinetic term for $\hat{\eta}$, but they also generate other interactions involving derivatives of the external background field. These latter were previously neglected since their contribution to the Higgs mass is first encountered at the NNLL. For instance, according to the notation of [25], in the SM sector one would get at one-loop the current-current operators $\mathcal{O}_L^t = i(H_c^\dagger \overleftrightarrow{D}_\mu H_c) \bar{Q}_L \gamma^\mu Q_L$, $\mathcal{O}_L^{(3)t} = i(H_c^\dagger \sigma^a \overleftrightarrow{D}_\mu H_c) \bar{Q}_L \gamma^\mu \sigma^a Q_L$ and $\mathcal{O}_R^t = i(H_c^\dagger \overleftrightarrow{D}_\mu H_c) \bar{t}_R \gamma^\mu t_R$. These latter can only renormalize the effective potential at order ξ , since they contribute to the running of c_6 . They therefore do not belong to the NNLL order and we neglect them. Analogous current-current operators in the $\widetilde{\text{SM}}$ sector cannot be generated. The Higgs currents $H_c^\dagger \overleftrightarrow{D}_\mu H_c$ and $H_c^\dagger \sigma^a \overleftrightarrow{D}_\mu H_c$ transform in fact as a $(\mathbf{3}, \mathbf{1})$ and a $(\mathbf{1}, \mathbf{3})$, respectively, under the custodial group $SO(4) \sim SU(2)_L \times SU(2)_R$, whereas the twin tops are global singlets under this symmetry. In the SM, the Yukawa coupling transforms as a $(\mathbf{2}, \mathbf{1})$; it is then possible to form an $SU(2)_L$ total singlet proportional to y_t^2 and the current-current operators are allowed by selection rules. In the twin sector, these latter are instead forbidden by the quantum numbers, since the twin top Yukawa transforms as $(\mathbf{1}, \mathbf{1})$; an operator of the type $i(H_c^\dagger \overleftrightarrow{D}_\mu H_c) \bar{\tilde{t}} \gamma^\mu \tilde{t}$ is therefore absent because of selection rules.

The only type of higher-dimensional operator involving derivatives of the external field that is

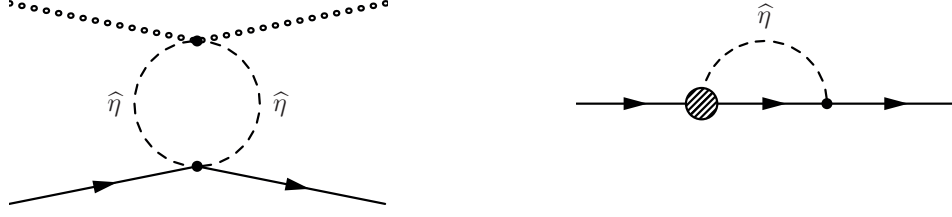


Figure 4.4 – The one loop-diagrams displaying the generation of the operator \mathcal{O}_\square (on the left) and the renormalization of the twin top mass (one the right). The blob in the last diagram denotes insertions of \mathcal{O}_\square . The external dotted lines indicate the background field, the internal dashed ones the dynamical fluctuation; the solid lines indicate again the twin tops.

generated in the twin top sector has dimension seven and is of the form:

$$\mathcal{O}_\square = -H_c^\dagger \square H_c \tilde{t} \tilde{t} + \text{h.c.} \quad (4.41)$$

It is made up of total singlets and is allowed by the symmetries of our theory. From the original Lagrangian (4.1), after the redefinition in Eq. (4.11), one finds the following interaction between the scalar fluctuations and the background field that seeds exactly this operator:

$$\mathcal{L}(m_*) \supset -\frac{1}{2f^2} \left(2c_H + c'_H + d_H \frac{H_c^\dagger H_c}{2f^2} \right) \eta_4^2 H_c^\dagger \square H_c - \frac{c'_H}{2f^2} \left(\sum_{i=1}^3 \eta_i^2 \right) H_c^\dagger \square H_c + \text{h.c.} \quad (4.42)$$

After integrating out the short-distance degrees of freedom, we can generate at order t the following contribution to the Lagrangian,

$$\mathcal{L}(t) \supset \frac{c_\square(H_c, t)}{f^3} \mathcal{O}_\square; \quad (4.43)$$

the background-dependent Wilson coefficient is obtained by computing the diagram on the left in Fig. (4.4). We find:

$$c_\square(H_c, t) = \left(2c_H + c'_H + d_H \frac{H_c^\dagger H_c}{2f^2} \right) \frac{\hat{y}_2^H(H_c)}{16\sqrt{2}\pi^2 Z_{\eta_4}^2(H_c)} t + c'_H \frac{3\hat{y}_2^{GB}(H_c)}{16\sqrt{2}\pi^2 Z_{\eta_1}^2(H_c)} t. \quad (4.44)$$

Notice that c'_H is zero at the scale m_* and it is first generated at one-loop, so that it will not give a contribution to the NNLL effective potential through the operator \mathcal{O}_\square . We reported its correction to c_\square for completeness.

The operator \mathcal{O}_\square contributes to the Higgs potential by renormalizing the twin top mass, as depicted in the last diagram of Fig. (4.4). We formally need to split the high-energy modes a second time and keep only the interactions with the box operator acting on the fluctuating

field. We have:

$$\mathcal{L}(t) \supset - \left(c_{\square}(H_c, t) \frac{H_c^\dagger}{f} \right) \frac{\square \hat{\eta} \tilde{t} \tilde{t}}{f^2} + \text{h.c.} \quad (4.45)$$

The field-dependent correction to the twin masses is then found to be:

$$\delta \tilde{m}_t^{\square}(H_c, t) = -c_{\square}(H_c, t) \frac{2H_c^\dagger}{f} \frac{\hat{y}_t(H_c)}{8\sqrt{2}\pi^2 Z_{\hat{\eta}_4}(H_c)} \frac{\tilde{m}_t^3(H_c)}{f^2} t, \quad (4.46)$$

where we used the notation of Eq. (4.13) for the coupling $\hat{y}_t(H_c)$. Together with the previous two quantum contributions, this formula gives the last renormalization of the fermion masses entering the effective action at the NNLL order.

We finally summarize the results obtained in this Section with a set of β -functions for the higher-dimensional operators and the twin top masses. They will supplement the evolution equations we already have for the Yukawa couplings and re-sum all the leading logarithms appearing in the Higgs mass. From our previous expressions, we immediately find:

$$\begin{aligned} \beta_{c_{4t}} &= \frac{3\hat{y}_2^{GB}(H_c, t)^2}{16\pi^2 Z_{\hat{\eta}_1}^2(H_c, t)} + \frac{\hat{y}_2^H(H_c, t)^2}{16\pi^2 Z_{\hat{\eta}_4}^2(H_c, t)}, \\ \beta_{c_{\square}} &= \left(2c_H(t) + c'_H(t) + d_H \frac{H_c^\dagger H_c}{2f^2} \right) \frac{\hat{y}_2^H(H_c, t)}{16\sqrt{2}\pi^2 Z_{\hat{\eta}_4}^2(H_c, t)} + c'_H(t) \frac{3\hat{y}_2^{GB}(H_c, t)}{16\sqrt{2}\pi^2 Z_{\hat{\eta}_1}^2(H_c, t)}, \\ \beta_{\tilde{m}_t^S} &= \frac{3\hat{y}_2^{GB}(H_c, t)(\tilde{m}_{GB}^1)^2(H_c, t) + \hat{y}_2^H(H_c, t)\tilde{m}_H^2(H_c, t)}{32\sqrt{2}\pi^2 f}, \quad \beta_{\tilde{m}_t^F} = -\frac{3}{4\pi^2} c_{4t}(H_c, t) \frac{\tilde{m}_t^3(H_c, t)}{f^2}, \\ \beta_{\tilde{m}_t^{\square}} &= -c_{\square}(H_c, t) \frac{2H_c^\dagger H_c}{f^2} \frac{\tilde{y}_t(H_c, t)}{\sqrt{1 - \frac{2H_c^\dagger H_c}{f^2}}} \frac{1}{8\sqrt{2}\pi^2 Z_{\hat{\eta}_4}(H_c, t)} \frac{\tilde{m}_t^3(H_c, t)}{f^2}. \end{aligned} \quad (4.47)$$

The quadratic couplings \hat{y}_2^{GB} and \hat{y}_2^H acquire in general a dependence on the expansion parameter through the evolution of the twin Yukawa. The background-dependent twin top mass at a generic order in t is now defined as:

$$\tilde{m}_t(H_c, t) = \frac{\tilde{y}_t(H_c, t)f}{\sqrt{2}} \sqrt{1 - \frac{2H_c^\dagger H_c}{f^2}} + \tilde{m}_t^S(H_c, t) + \tilde{m}_t^F(H_c, t) + \tilde{m}_t^{\square}(H_c, t), \quad (4.48)$$

where the last three additional terms correspond to the solution of the previous β -functions in the Higgs spectator field. This formula together with the RG equations are the basic elements to compute the Higgs potential at NNLL.

4.3.3 Higgs mass at the NNLL

In order to find the Higgs effective potential at the NNLL, we solve the β -functions in Eqs. (4.23) and (4.47) up to order t^2 and use Eqs. (4.25) and (4.48) to derive the renormalized background-dependent fermionic masses. Adding the running of the strong couplings and the scalar contribution in Eq. (4.31), we have in the canonical basis:

$$(M_H^2)_{IR}^{NNLL}(t) = \frac{v^2}{8192\pi^6} [736g_S^4 y_t^4 - 1104g_S^2 y_t^6 + 387y_t^8 + \tilde{y}_t^4 (736\tilde{g}_S^4 - 288g_S^2 y_t^2 - 576\tilde{g}_S^2 y_t^2 + 18(3 - 2c_H)y_t^4) + \tilde{y}_t^6 (240(1 + c_H)\tilde{g}_S^2 - 18(7 + 8c_H)y_t^2) - 4\tilde{y}_t^8 \left(72 + 7c_H + 30c_H^2 - \frac{11}{4}d_H\right)] t^3. \quad (4.49)$$

All the parameters are again evaluated at m_* , which sets the scale where the RG-evolution of the Wilson coefficients starts.

4.4 Results

The background field method proved to be a useful technique to automatically re-sum a whole series of diagrams, compute the renormalized effective potential and derive an expression for the Higgs mass valid up to the NNLL. Our final prediction for the IR RG-evolution of this observable is the sum of three different contributions:

$$(M_H^2)_{IR}(\mu) = (M_H^2)_{IR}^{LL}(\mu) + (M_H^2)_{IR}^{NLL}(\mu) + (M_H^2)_{IR}^{NNLL}(\mu), \quad (4.50)$$

which are given respectively in Eqs. (4.10), (4.29) and (4.49). The renormalization scale μ is encoded in the expansion parameter $t = \log(m_*^2/\mu^2)$ and is chosen to be the energy scale where the Higgs mass is measured, for instance the top mass. From our analytic result, we can now obtain a numerical estimate of $(M_H^2)_{IR}(m_t)$ and compare it with the experimental observations. This in turn will give us an idea of the capability of the low-energy Twin Higgs construction to predict the Higgs mass in the correct range only through the IR physics. We will also try to estimate the UV correction that would be needed in order to match with experiments. The prediction of the Higgs mass at cubic precision is therefore an important test of the Twin Higgs scenario as a new paradigm for understanding physics at the EW scale.

In order to derive a numerical estimate of the Higgs mass, we have first to assign a value to all the Wilson coefficients appearing in the final formula. The initial conditions for their RG-evolution are fixed at the scale m_* ; we know already that $c_H = 1$ and $d_H = 8$ due to the pNGB nature of the Higgs field. Because of Twin parity, which is still approximately a good symmetry

at m_* , we can set $\tilde{g}_S = g_S$ and $\tilde{y}_t = y_t$; the strong and the Yukawa couplings, however, are measured at the IR scale m_t and we must solve their RG evolution equation to run their value up to the UV. We need to derive g_S at first order in the logarithmic expansion, whereas y_t must be known up to the quadratic contributions. We have:

$$\begin{aligned} g_S = \tilde{g}_S &= g_E - \frac{7g_E^3}{32\pi^2} \log\left(\frac{m_*^2}{m_t^2}\right), \\ y_t = \tilde{y}_t &= y_E + \frac{y_E(9y_E^2 - 16g_E^2)}{64\pi^2} \log\left(\frac{m_*^2}{m_t^2}\right) + \frac{y_E(704g_E^4 - 576g_E^2y_E^2 + 243y_E^4)}{8192\pi^4} \log^2\left(\frac{m_*^2}{m_t^2}\right), \end{aligned} \quad (4.51)$$

where y_E and g_E indicate the experimental value of these couplings at the scale m_t . For the Yukawa, we use the $\overline{\text{MS}}$ value of the top quark mass, $m_t^{\overline{\text{MS}}} = 160$ GeV, from which we derive $y_E \sim 0.92$. For the strong interaction, we run the parameter measured at the scale of the Z boson mass, $g_S(M_Z) \sim 1.22$, to the top mass scale, so we have $g_E \sim 1.17$. Notice that the RG evolution of the top Yukawa in Eq. (4.51) coincides with the solution of the β -functions in Eqs. (4.23) for vanishing external field after re-scaling the Higgs spectator as in Eq. (4.27).

The last aspect we must take care of when estimating the Higgs mass is the existence of the twin top mass threshold. We have previously derived all our results at a generic scale $\mu \gg \tilde{m}_t$; if we want to fix $\mu = m_t$, we need to integrate out the Twin partners at the scale \tilde{m}_t and resume the purely SM running from this scale down to the top quark mass. Our Higgs mass is then the sum of two pieces: a first evolution from m_* to \tilde{m}_t which serves as the initial condition for a second contribution from \tilde{m}_t to m_t . This latter is obtained by switching off the twin parameters and keeping only the SM supplemented by dimension-six operators. The twin mass is evaluated at the scale \tilde{m}_t using Eq. (4.48), setting the external background to its physical vacuum expectation value and expanding at first order in ξ .

Our final results are shown in Fig. (4.5), where we plot the value of the Higgs mass at the scale m_t as function of the cut-off m_* for the fixed value of $\xi = 0.1$. We choose this latter in agreement with the general constraint due to EWPT. Fig. (4.5) shows two different sets of curves, a first one in black for the full prediction in the Twin Higgs low-energy model and a second one in red for the pure SM quartic coupling evolution. In each of the two cases, we reported the Higgs mass at the LL, the NLL and the NNLL. For both results, the LL solution appears to be quite an overestimation of the logarithmic series, indicating the importance of extending the computation to the higher orders including the effects of the top Yukawa running. At the NLL, the Higgs mass reduces drastically because y_t and \tilde{y}_t become considerably smaller along the flow from m_t to m_* due to QCD effects. For the Twin Higgs model we get $(M_H^2)_{IR}^{NLL}(m_t) \sim (105 \text{ GeV})^2$ with a cut-off at 10 – 20 TeV, which is considerably bigger than the SM value of $(80 \text{ GeV})^2$ due to the presence of the extra light degrees of freedom. The truncation of the logarithmic series to quadratic order, however, is

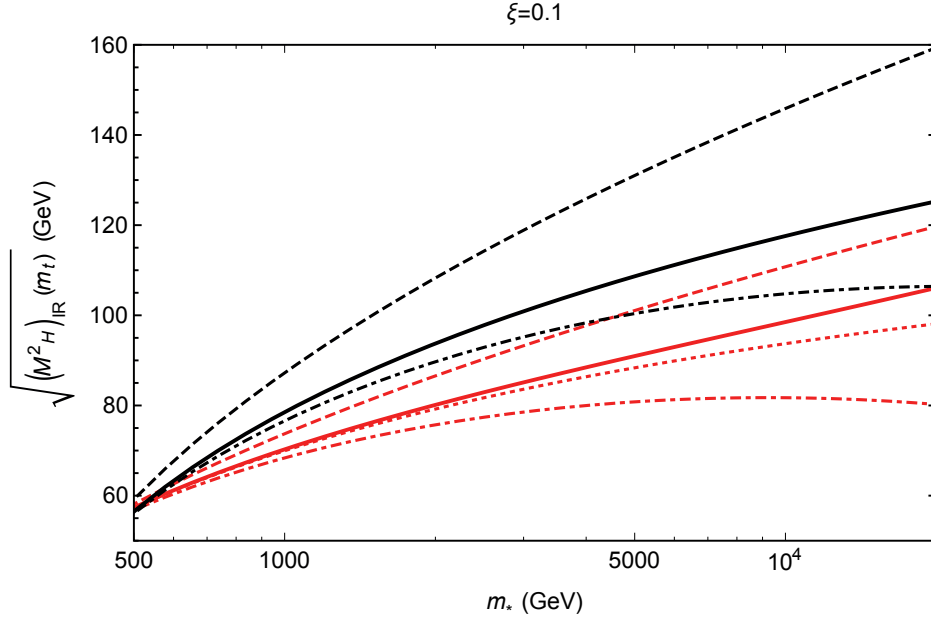


Figure 4.5 – IR contributions to the Higgs mass in logarithmic scale, both in the full Twin Higgs theory and in the pure SM: LL contribution (dashed black curve), NLL contribution (dashed dotted black curve), NNLL contribution (thick black curve), LL SM contribution (dashed red curve), NLL SM contribution (dashed dotted red curve), NNLL SM contribution (thick red curve), re-summed total SM contribution (dotted red curve).

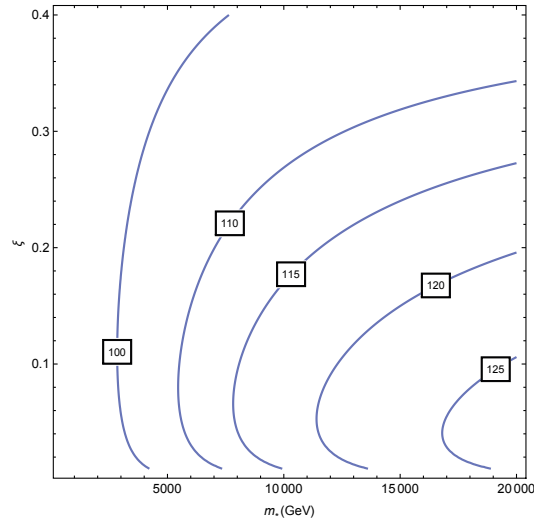


Figure 4.6 – Contour plots of the renormalized Higgs mass (in GeV) at NNLL in the plane (m_*, ξ) .

still a rude approximation of the re-summed solution; we see in fact that the NNLL introduces non-negligible effects already for $m_* \sim 2 - 3$ TeV and for bigger values of the cut-off the NLL

solution becomes less reliable. At cubic order, the prediction for the Higgs mass increases in both cases, mostly due to QCD effects that tend to rise the value of y_t , as in Eq. (4.51), and of its corresponding twin. The growth of M_H^2 in the Twin Higgs model is however less sharp than in the SM, because of non-renormalizable effects. In particular, the contributions to the effective potential from four fermions interactions and from the operator \mathcal{O}_\square are both negative and tend to reduce the Higgs mass with respect to QCD. We may wonder if the NNLL solution is a reliable approximation for values of the cut-off scale of 10 – 20 TeV or if quartic effects will still give non-negligible corrections. We do not have a result at this order in the logarithmic series for the Twin Higgs model, but we can estimate its behavior studying the SM. We reported in Fig. (4.5) also the re-summed SM solution for the Higgs mass obtained after solving numerically the β -function for the quartic coupling. The comparison of this latter with the NNLL prediction shows that the cubic approximation in the SM can be considered reliable up to $m_* \sim 20$ TeV, for which value the difference between the two solutions is indicatively 5%. We can expect that something similar will happen also in the Twin Higgs case. Despite the presence of non-renormalizable corrections, in fact, the QCD effects are still the dominant ones and they must behave exactly as in the SM. The full solution must then decrease with respect to the NNLL correction and we expect our NNLL solution to be a reliable approximation for $m_* \sim 20$ TeV. Beyond this value for the cut-off, the quartic contributions must necessarily be taken into account and our computation cannot be trusted any longer.

After discussing the validity of our approximation, we can now specifically consider the prediction of the Higgs mass that we get in the Twin Higgs model up to the NNLL order. From Fig. (4.5), we see that $(M_H^2)_{IR}^{NNLL} \sim 120 \text{ GeV}$ for $m_* \sim 10 - 20 \text{ TeV}$, a value which is in the perfect range to match with the experimental observations, $(M_H^2)_{Exp} = 125 \text{ (GeV)}^2$. We also show in Fig. (4.6) the contour plots for the renormalized Higgs mass at NNLL in the plane (m_*, ξ) , so as to visualize the effects of the fine-tuning parameter as the cut-off scale changes. We find again that with a moderate tuning, $\xi \sim 0.1 - 0.2$, and a value of m_* around 20 TeV it is possible to reproduce the experimental results. The IR physics alone can therefore generate an acceptable value for the Higgs mass through the RG-evolution. The remaining part that is missing to agree with observations could be supplemented by a small UV contribution. For example, with $\xi = 0.1$ and $m_* \sim 10 \text{ TeV}$, a value of the cut-off for which our computation is more reliable, a modest $(M_H^2)_{UV} \sim (5 \text{ GeV})^2$ is enough for the Twin Higgs paradigm to be matched perfectly with experiments. The smallness of the UV effect together with the possibility of pushing m_* up to $\sim 20 \text{ TeV}$ are also necessary for the whole mechanism to make sense. On one side, the fact the $(M_H^2)_{UV}$ can be small confirms that the Higgs boson is not sensitive to the UV physics. On the other side, if m_* can be very large, in the multi-TeV range, it is reasonable to neglect all the tree-level initial conditions for the higher-dimensional operators generated after integrating out the new physics. Their Wilson coefficients at the scale m_* are model-

dependent and suppressed by inverse powers of the cut-off; we expect them to give only a very small contribution to the Higgs mass. It is therefore approximately correct to set them to zero at m_* and consider only their one-loop value seeded by the six-dimensional operator present at the tree-level, \mathcal{O}_H , and automatically captured by the background field method. Our prediction is then consistently model-independent and results only from the IR physics.

The lesson we can learn from the Twin Higgs mechanism is that it is possible to construct models with a natural light Higgs in the spectrum without necessarily requiring the existence of new light colored top partners. The Higgs can be insensitive to the UV scale of the heavy resonances charged under the SM, which can be pushed up to ~ 20 TeV for the experimental value of M_H to be almost exactly reproduced by the IR physics through RG effects. The UV contribution must be small and any UV completion that can be imagined must be able to generate a modest value of the quartic coupling at the cut-off scale. Composite UV completions, for instance, can be easily realized that fulfill this requirement, [118].

4.5 Discussion

In this Chapter, we have computed the RG-improved Higgs effective potential and mass in the Twin Higgs model up to third order in logarithmic accuracy. We have carried out the calculation in the most general setting, writing an effective Lagrangian comprising only the IR degrees of freedom, namely the Higgs doublet, the SM quarks and their twins. In this way, our prediction for the Higgs mass is completely model-independent and proper to any possible UV completion, supersymmetric or composite, of the Twin Higgs paradigm. We have discussed the validity of our approximation. First of all, the Higgs potential is insensitive to the UV physics and we expect that the most important contributions to the mass come from the RG evolution due to loops of the IR degrees of freedom. Secondly, we have neglected the initial conditions for the higher-dimensional operators generated at the tree level after integrating out the UV physics. Their Wilson coefficients at m_* are in fact suppressed by the weak coupling between the elementary and the UV sectors as well as by inverse powers of the cut-off m_* , which is reasonably of the order of $10 - 20$ TeV. Their contribution to the running of the potential, which is model-dependent, is therefore safely negligible.

We showed how to carry out the renormalization of the potential in the most efficient way using the background field method. This technique proved to be extremely useful in order to re-sum the one-loop diagrams contributing to the running without necessarily classifying all the non-renormalizable operators in the Twin sector. We applied this method to our low-energy Lagrangian and we systematically included all the physical effects that are relevant up to the NNLL order. The final result can be obtained by solving a simple set of background-dependent β -functions from which we find the top and twin top masses in the spectator field.

The Coleman-Weinberg formula for the effective action can then be easily applied to derive the Higgs mass at cubic order in the logarithmic expansion.

Our final prediction for the Higgs mass is summarized in Figs. (4.5) and (4.6) where we plot this observable as a function of the cut-off of the theory. At the NNLL, we get a value of the order of $M_H \sim 120$ GeV for $m_* \sim 10 - 20$ TeV, which is in the perfect range to match with the experimental observations without requiring a big UV contribution. The IR degrees of freedom are then enough to account for the measured value of the Higgs mass through the RG-evolution of the effective potential.

The background field computation developed in this Chapter can be improved in order to re-sum the whole logarithmic series and possibly get a numerical solution valid at all orders in the expansion parameter. For this purpose, a classification of the operators in the Twin sector seems unavoidable. Writing in full generality the Lagrangian at the scale m_* including all the possible gauge invariant operators, we can again split the low-energy degrees of freedom from the short distance modes and integrate out these latter. After computing the most general β -functions for the running of the top mass and its twin, one could easily find the potential using the RG-improved Coleman-Weinberg formula without needing to specify which operators are generated at each order in the expansion in logarithms. From this point of view, our application of the background field method is not the most efficient one, since we had to understand for the NNLL solution which operators we expected to produce at one-loop that were not already captured in the background-dependent β -functions for the NLL result. Such a procedure would make it even more cumbersome to compute the quartic correction to the effective potential, because one would need to separately derive the evolution of \mathcal{O}_D , for instance, and again individuate the operators that were not previously included and that could give new contributions to the Higgs mass. A complete classification of the gauge invariant operators in the Twin sector together with the six-dimensional ones already listed for the SM would then provide the best way to systematically apply the background field method to the Twin Higgs model. This could be a very interesting extension of our results and could give more information on the stability of the effective potential with respect to the UV physics.

5 Precision Tests and Fine Tuning in Twin Higgs models

The principle of naturalness offers arguably the main motivation for exploring physics at around the weak scale. According to naturalness, the plausibility of specific parameter choices in quantum field theory must be assessed using symmetries and selection rules, as we saw in the Introduction. Let us briefly recall what symmetries and selection rules imply in the SM. When viewing the SM as an effective field theory valid below a physical cut-off scale and considering only the known interactions of the Higgs boson, we expect the following corrections to its mass¹

$$\delta m_h^2 = \frac{3y_t^2}{4\pi^2} \Lambda_t^2 - \frac{9g^2}{32\pi^2} \Lambda_g^2 - \frac{3g'^2}{32\pi^2} \Lambda_{g'}^2 - \frac{3\lambda_h}{8\pi^2} \Lambda_h^2 + \dots, \quad (5.1)$$

where each Λ represents the physical cut-off scale in a different sector of the theory. The above equation is simply dictated by symmetry: dilatations (dimensional analysis) determine the scale dependence and the broken shift symmetry of the Higgs field sets the coupling dependence. Unsurprisingly, these contributions arise in any explicit UV completion of the SM, although in some cases they may be larger. According to Eq. (5.1), any given (large) value of the scale of new physics can be associated with a (small) number ϵ , which characterizes the accuracy at which the different contributions to the mass must cancel among themselves, in order to reproduce the observed value $m_h \simeq 125$ GeV. As the largest loop factor is due to the top Yukawa coupling, according to Eq. (5.1) the scale Λ_{NP} where new states must first appear is related to m_h^2 and ϵ via

$$\Lambda_{NP}^2 \sim \frac{4\pi^2}{3y_t^2} \times \frac{m_h^2}{\epsilon} \implies \Lambda_{NP} \sim 0.45 \sqrt{\frac{1}{\epsilon}} \text{ TeV}. \quad (5.2)$$

¹We take $m_h^2 = 2m_H^2 = \lambda_h v^2/2$ with $\langle H \rangle = v/\sqrt{2} = 174$ GeV, which corresponds to a potential

$$V = -m_H^2 |H|^2 + \frac{\lambda_h}{4} |H|^4.$$

The dimensionless quantity $1/\epsilon$ measures how finely-tuned m_h^2 is, given Λ_{NP} , and can therefore be regarded as a measure of the tuning. Notice that the contributions from g^2 and λ_h in Eq. (5.1) correspond to $\Lambda_{NP} = 1.1 \text{ TeV}/\sqrt{\epsilon}$ and $\Lambda_{NP} = 1.3 \text{ TeV}/\sqrt{\epsilon}$, respectively. Although not significantly different from the relation in the top sector, these are still large enough to push new states out of direct LHC reach for $\epsilon \sim 0.1$.

Indeed, for a given ϵ , Eq. (5.2) only provides an upper bound for Λ_{NP} ; in the more fundamental UV theory, there can in principle exist larger corrections to m_h^2 which are not captured by Eq. (5.1). For instance, in the Minimal Supersymmetric SM (MSSM) with high-scale mediation of the soft terms, δm_h^2 in Eq. (5.1) is logarithmically enhanced by RG evolution above the weak scale. In that case, Eq. (5.2) is modified as follows:

$$\Lambda_{NP}^2 \sim \frac{2\pi^2}{3y_t^2} \times \frac{1}{\ln \Lambda_{UV}/\Lambda_{NP}} \times \frac{m_h^2}{\epsilon}, \quad (5.3)$$

where Λ_{NP} corresponds to the overall mass of the stops and $\Lambda_{UV} \gg \Lambda_{NP}$ is the scale of mediation of the soft terms. However, for generic composite Higgs (CH) models, as well as for supersymmetric models with low-scale mediation, Eq. (5.2) provides a fair estimate of the relation between the scale of new physics and the amount of tuning. If the origin of m_h is normally termed *soft* in the MSSM with large Λ_{UV} , it should then be termed *supersoft* in models respecting Eq. (5.2). The essential feature of these supersoft models is that the Higgs mass is fully generated by quantum corrections at around the weak scale, whereas in the MSSM with large Λ_{UV} it is well-known (and shown by Eq. (5.3), for $\Lambda_{UV} \gtrsim 100 \text{ TeV}$) that the natural expectation is $\Lambda_{NP} \sim m_Z \sim m_h$. In view of this, the soft scenarios were already somewhat constrained by direct searches at LEP and Tevatron. Instead, the natural range of the scale of supersoft models is only now being probed at the LHC.

Equation (5.2) sets an absolute upper bound on Λ_{NP} for a given fine tuning $1/\epsilon$, but does not give any details on its nature. In particular it does not specify the quantum numbers of the new states that enter the theory at or below this scale. Indeed, the most relevant states associated with the top sector, the so-called top partners, are bosonic (fermionic) in standard supersymmetric models (CH models). Nonetheless, one common feature of these standard scenarios is that the top partners carry SM quantum numbers, color in particular. They are thus copiously produced in hadronic collisions, making the LHC a good probe of these scenarios. Yet there remains the logical possibility that the states that are primarily responsible for the origin of the Higgs mass at or below Λ_{NP} are not charged under the SM, and thus much harder to produce and detect at the LHC. The Twin Higgs (TH) is probably the most interesting of the (few) ideas that take this approach [118–121, 125–129, 132–142]. This is primarily because the TH mechanism can, at least in principle, be implemented in a SM extension valid up to ultra-high scales. The structure of TH models is such that the states at

the threshold Λ_{NP} in Eq. (5.2) carry quantum numbers under the gauge group of a copy, a twin, of the SM, but are neutral under the SM gauge group. These twin states, of which the twin tops are particularly relevant, are thus poorly-produced at the LHC. The theory must also contain states with SM quantum numbers, but their mass m_* is boosted with respect to Λ_{NP} roughly by a factor g_*/g_{SM} , where g_* describes the coupling strength of the new dynamics, while g_{SM} represents a generic SM coupling. As discussed in the next section, depending on the structure of the model, g_{SM} can be either the top Yukawa or the square root of the Higgs quartic. As a result, given the tuning $1/\epsilon$, the squared mass of the new colored and charged states is roughly given by

$$m_*^2 \sim \frac{4\pi^2}{3y_t^2} \times \frac{m_h^2}{\epsilon} \times \left(\frac{g_*}{g_{SM}} \right)^2. \quad (5.4)$$

For $g_* > g_{SM}$, we could define these model as effectively *hypersoft*, in that, for fixed fine tuning, the gap between the SM-charged states and the weak scale is even larger than that in supersoft models. In practice the above equation implies that, for strong $g_* \sim 4\pi$, the new states are out of reach of the LHC even for mild tuning, $\epsilon \gtrsim 0.1$. Eq. (5.4) synthesizes the potential relevance of the TH mechanism, and makes it clear that the new dynamics must be rather strong for the mechanism to work. Given the hierarchy problem, it then seems almost inevitable to make the TH a Composite TH (although it could also be a Supersymmetric Composite TH). Realizations of the TH mechanism within the paradigm of CH models with fermion partial compositeness [13] have already been proposed, both in the holographic and effective theory set-ups [118–120, 133].

It is important to recognize that the factor that boosts the mass of the states with SM gauge quantum numbers in Eq. (5.4) is the coupling g_* itself. Because of this, strong-dynamics effects in the Higgs sector, which are described in the low-energy theory by non-renormalizable operators with coefficients proportional to powers of g_*/m_* , do not “decouple” when these states are made heavier, at fixed fine tuning ϵ . In the standard parametrics of the CH, m_*/g_* is of the order of f , the decay constant of the σ -model within which the Higgs doublet emerges as a pseudo Nambu-Goldstone Boson (pNGB). Then $\xi \equiv v^2/f^2$, as well as being a measure of the fine tuning through $\epsilon = 2\xi$, also measures the relative deviation of the Higgs couplings from the SM ones, in the TH like in any CH model.² Recent Higgs coupling measurements roughly constrain $\xi \lesssim 10 - 20\%$ [99], and a sensitivity of order 5% is expected in the high-luminosity phase of the LHC [54]. However Higgs loop effects in precision Z -pole observables measured at LEP already limit $\xi \lesssim 5\%$ [57, 59]. Having to live with this few percent-level tuning would somewhat undermine the motivation for the clever TH construction. In ordinary CH models this strong constraint on ξ can in principle be relaxed thanks to compensating corrections

²The factor of two difference between the fine tuning ϵ and ξ is due to the Z_2 symmetry of the Higgs potential in the TH models, as shown in section 5.1.1.

to the \hat{T} parameter coming from the top partners. In the most natural models, these are proportional to $y_t^4 v^2 / m_*^2$ and thus, unlike the Higgs-sector contribution, decouple when m_* is increased. This makes it hard to realize such a compensatory effect in the most distinctive range of parameters for TH models, where $m_* \sim 5 - 10$ TeV. Alternatively one could consider including custodial-breaking couplings larger than y_t in the top-partner sector. Unfortunately these give rise to equally-enhanced contributions to the Higgs potential, which would in turn require further ad-hoc cancellations.

As already observed in the literature [118, 119] another important aspect of TH models is that calculable IR-dominated contributions to the Higgs quartic coupling almost saturate its observed value. Though a welcome property in principle, this sets even stronger constraints on additional UV contributions, such as those induced by extra sources of custodial breaking. In this Chapter we study the correlation between these effects, in order to better assess the relevance of the TH construction as a valid alternative to more standard ideas about EW-scale physics. Several such studies already exist for standard composite Higgs scenarios [107, 108, 110]. In extending these to the TH we shall encounter an additional obstacle to gaining full benefit from the TH boost in Eq. (5.4): the model structure requires rather “big” multiplets, implying a large number of degrees of freedom. This results in a naive dimensional analysis (NDA) upper bound for the coupling that is parametrically smaller than 4π , and hence so is the boost factor. We shall discuss in detail how serious and unavoidable a limitation this is.

This Chapter is organized as follows: in section 5.1 we discuss the general structure and parametrics of TH models, followed by section 5.2 where we describe the more specific class of composite TH models we focus on for the purpose of our study. In sections 5.3 and 5.4 we present our computations of the basic physical quantities: the Higgs potential and precision electroweak parameters $(\hat{S}, \hat{T}, \delta g_{Lb})$. Section 5.5 is devoted to a discussion of the resulting constraints on the model and an appraisal of the whole TH scenario. Our conclusions are presented in section 5.6.

5.1 A classification of Twin Higgs scenarios

5.1.1 Structure and Parametrics

In this section we outline the essential aspects of the TH mechanism. Up to details and variants which are not crucial for the present discussion, the TH scenario involves an exact duplicate, $\widetilde{\text{SM}}$, of the SM fields and interactions, underpinned by a Z_2 symmetry. In practice this Z_2 must be explicitly broken in order to obtain a realistic phenomenology, and perhaps more importantly, a realistic cosmology [140, 142]. However the sources of Z_2 breaking can have a

structure and size that makes them irrelevant in the discussion of naturalness in electroweak symmetry breaking, which is the main goal in this section.

Our basic assumption is that the SM and its twin emerge from a more fundamental Z_2 -symmetric theory at the scale m_* , at which new states with SM quantum numbers, color in particular, first appear. In order to get a feeling for the mechanism and its parametrics, it is sufficient to focus on the most general potential for two Higgs doublets H and \tilde{H} , invariant under the gauge group $G_{SM} \times \tilde{G}_{SM}$, with $G_{SM} = SU(3)_c \times SU(2)_L \times U(1)_Y$, as well as a Z_2 :

$$V(H, \tilde{H}) = -m_{\mathcal{H}}^2(|H|^2 + |\tilde{H}|^2) + \frac{\lambda_{\mathcal{H}}}{4}(|H|^2 + |\tilde{H}|^2)^2 + \frac{\hat{\lambda}_h}{8}(|H|^4 + |\tilde{H}|^4). \quad (5.5)$$

Strictly speaking, the above potential does not have minima with realistic “tunable” $\langle H \rangle$. This goal can be achieved by the simple addition of a naturally small Z_2 -breaking mass term, which does not affect the estimates of fine tuning, and hence will be neglected for the purposes of this discussion. Like for the SM Higgs, the most general potential is accidentally invariant under a custodial $SO(4) \times \tilde{SO}(4)$. Notice however that in the limit $\hat{\lambda}_h \rightarrow 0$, the additional Z_2 enhances the custodial symmetry to $SO(8)$, where $\mathcal{H} \equiv H \oplus \tilde{H} \equiv \mathbf{8}$. In this exact limit, if \tilde{H} acquired an expectation value $\langle \tilde{H} \rangle \equiv f/\sqrt{2}$, all 4 components of the ordinary Higgs H would remain exactly massless NGBs. Of course the SM and \tilde{SM} gauge and Yukawa couplings, along with $\hat{\lambda}_h$, explicitly break $SO(8)$, changing the nature of H . Consider however the scenario where these other couplings, which are known to be weak, can be treated as small $SO(8)$ -breaking perturbations of a stronger $SO(8)$ -preserving underlying common dynamics, of which the quartic coupling $\lambda_{\mathcal{H}}$ is a manifestation. In this situation we can reconsider the relation between the SM Higgs mass, the amount of tuning and the scale m_* where new states charged under the SM are first encountered, treating $\hat{\lambda}_h$ as a small perturbation of $\lambda_{\mathcal{H}}$. At zeroth order, i.e. neglecting $\hat{\lambda}_h$, we can expand around the vacuum $\langle \tilde{H} \rangle^2 = 2m_{\mathcal{H}}^2/\lambda_{\mathcal{H}} \equiv f^2/2$, $\langle H \rangle = 0$. The spectrum consists of a heavy scalar σ , with mass $m_\sigma = \sqrt{2}m_{\mathcal{H}} = \sqrt{\lambda_{\mathcal{H}}}f/\sqrt{2}$, corresponding to the radial mode, 3 NGBs eaten by the twin gauge bosons, which get masses $\sim gf/2$ and the massless H . When turning on $\hat{\lambda}_h$, $SO(8)$ is broken explicitly and H acquires a potential. At leading order in a $\hat{\lambda}_h/\lambda_{\mathcal{H}}$ expansion the result is simply given by substituting $|\tilde{H}|^2 = f^2/2 - |H|^2$ in Eq. (5.5).³ The quartic coupling and the correction to the squared mass are then given by

$$\lambda_h \simeq \hat{\lambda}_h \quad \delta m_H^2 \sim -\hat{\lambda}_h f^2/8 \simeq -(\lambda_h/2\lambda_{\mathcal{H}})m_{\mathcal{H}}^2. \quad (5.6)$$

As mentioned above, we assume that m_H^2 also receives an independent contribution from a Z_2 -breaking mass term, which can be ignored in the estimates of tuning. Note that in terms of the physical masses of the Higgs, m_h , and of its heavy twin, m_σ , we have precisely the same

³Notice that the effective Higgs quartic receives approximately equal contributions from $|H|^4$ and $|\tilde{H}|^4$. This is a well-known and interesting property of the TH.

numerical relation $\delta m_h^2 = (\lambda_h/2\lambda_{\mathcal{H}})m_\sigma^2$. The amount of tuning ϵ , defined as $m_h^2/\delta m_h^2$, is given by $\epsilon = 2\xi = 2v^2/f^2$.

Our estimate of δm_H^2 in Eq. (5.6) is based on a simplifying approximation where the $SO(8)$ -breaking quartic is taken Z_2 -symmetric. In general we could have allowed different couplings $\hat{\lambda}_h$ and $\hat{\lambda}_{\tilde{h}}$ for $|H|^4$ and $|\tilde{H}|^4$ respectively, constrained by the requirement $\hat{\lambda}_h + \hat{\lambda}_{\tilde{h}} \simeq 2\lambda_h$. As the estimate of δm_H^2 in Eq. (5.6) is determined by the $|\tilde{H}|^4$ term, it is clear that a reduction of $\hat{\lambda}_{\tilde{h}}$, with λ_h fixed, would improve the tuning, as emphasized in ref. [139]. As discussed in section 4, however, a significant fraction of the contribution to $\hat{\lambda}_h$ and $\hat{\lambda}_{\tilde{h}}$ is coming from RG evolution due to the top and twin top. According to our analysis, $\hat{\lambda}_h/\hat{\lambda}_{\tilde{h}}$ varies between 1.5 in the simplest models to 3 in models where $\hat{\lambda}_{\tilde{h}}$ is purely IR-dominated as in in ref. [139]. Though interesting, this gain does not change our parametric estimates.

The ratio $\lambda_h/\lambda_{\mathcal{H}}$ is the crucial parameter in the game. Indeed it is through Eq. (5.6) that m_H is sensitive to quantum corrections to the Lagrangian mass parameter $m_{\mathcal{H}}$, or, equivalently, that the physical Higgs mass m_h is sensitive to the physical mass of the radial mode m_σ . In particular, what matters is the correlation of m_σ with, and its sensitivity to, m_* , where new states with SM quantum numbers appear. One can think of three basic scenarios for that relation, which we now illustrate, ordering them by increasing level of model building cleverness. Beyond these scenarios there is the option of tadpole dominated electroweak symmetry breaking, which we shall briefly discuss at the end.

Sub-Hypersoft Scenario

The simplest option is given by models with $m_\sigma \sim m_*$. Supersymmetric TH models with medium- to high-scale soft-term mediation belong to this class [132], with m_* representing the soft mass of the squarks. Like in the MSSM, $m_{\mathcal{H}}$, and therefore m_σ , is generated via RG evolution: two decades of running are sufficient to obtain $m_\sigma \sim m_*$. Another example is composite TH models [118, 119]. In their simplest incarnation they are characterized by one overall mass scale m_* and coupling g_* [24], so that by construction one has $m_\sigma \sim m_*$ and $\lambda_{\mathcal{H}} \sim g_*^2$. As discussed below Eq. (5.6), in both these scenarios one then expects $\delta m_h^2 \sim (\lambda_h/2\lambda_{\mathcal{H}})m_\sigma^2$. It is interesting to compare this result to the leading top-sector contribution in Eq. (5.1). For that purpose it is worth noticing that, as discussed in section 5.3, in TH models the RG-induced contribution to the Higgs quartic coupling $\Delta\lambda_h|_{RG} \sim (3y_t^4/\pi^2) \ln m_*/m_t$ nearly saturates its experimental value $\lambda_h \sim 0.5$ for $m_* \sim 3 - 10$ TeV.⁴ We can thus write

$$\delta m_h^2 \sim (\lambda_h/2\lambda_{\mathcal{H}})m_\sigma^2 \sim \frac{3y_t^4}{2\pi^2} \frac{1}{\lambda_{\mathcal{H}}} \ln(m_*/m_t) m_\sigma^2 \equiv \frac{3y_t^2}{2\pi^2} \times \frac{y_t^2}{g_*^2} \times \ln(m_*/m_t) \times m_*^2 \quad (5.7)$$

⁴For this naive estimate we have taken the twin-top contribution equal to the top one, so that the result is just twice the SM one. For a more precise statement see section 5.3.

which should be compared to the first term on the right-hand side of Eq. (5.1). Accounting for the possibility of tuning we then have

$$m_* \sim 0.45 \times \frac{g_*}{\sqrt{2}y_t} \times \sqrt{\frac{1}{\ln(m_*/m_t)}} \times \sqrt{\frac{1}{\epsilon}} \text{ TeV}. \quad (5.8)$$

Compared to Eq. (5.2), the mass of colored states is on one hand parametrically boosted by the ratio $g_*/(\sqrt{2}y_t)$, and on the other it is mildly decreased by the log. The gain and the motivation in the ongoing work on the simplest realization of the TH idea are then clinging to the above g_*/y_t . The basic question is how big g_* can be with the overall description still making sense, at least qualitatively. One of the goals of this Chapter is also to investigate to what extent one can realistically gain from this parameter by focusing on slightly more explicit CH realizations. Applying naive dimensional analysis (NDA) one would be tempted to say that g_* as big as $\sim 4\pi$ makes sense, in which case $m_* \sim 10$ TeV would only cost a mild $\epsilon \sim 0.1$ tuning. However such an estimate seems quantitatively too naive. For instance, by focusing on the simple toy model whose potential is given by Eq. (5.5), we can associate the upper bound on $\lambda_{\mathcal{H}} \equiv g_*^2$, to the point where perturbation theory breaks down. One possible way to proceed is to consider the one loop beta function

$$\mu \frac{d\lambda_{\mathcal{H}}}{d\mu} = \frac{N+8}{32\pi^2} \lambda_{\mathcal{H}}^2, \quad (5.9)$$

and to estimate the maximum value of the coupling $\lambda_{\mathcal{H}}$ as the one for which $\Delta\lambda_{\mathcal{H}}/\lambda_{\mathcal{H}} \sim O(1)$ through one e-folding of RG evolution. One finds

$$\lambda_{\mathcal{H}} = \frac{2m_\sigma^2}{f^2} \lesssim \frac{32\pi^2}{N+8} \implies \frac{m_\sigma}{f} \lesssim \pi, \text{ for } N=8, \quad (5.10)$$

which also gives $g_* \sim \sqrt{\lambda_{\mathcal{H}}} \lesssim \sqrt{2}\pi$, corresponding to a significantly smaller maximal gain in Eq. (5.8) with respect to the NDA estimate. In section 5.2.2 we shall perform alternative estimates in more specific CH constructions, obtaining similar results. However it is perhaps too narrow minded to stick to such estimates to precisely decide the boost that $g_*/(\sqrt{2}y_t)$ can give to m_* . What is parametrically true is that the stronger the coupling g_* , the heavier the colored partners can be at fixed tuning. However as we are debating on factors of a few, it is hard to be sharper. In any case the gain offered by Eq. (5.8) is probably less than one would naively have hoped and it is thus fair to question the motivation for the TH, at least in its “sub-hypersoft” realization. We will keep this doubt in our hearts, but continue the exploration of TH with the belief that the connection between naturalness and LHC signatures is so important that it must be analyzed in all its possible facets.

Concerning in particular composite TH scenarios one last important model building issue concerns the origin of the Higgs quartic λ_h . In generic CH it is known that the contribution to

λ_h that arises at $O(y_t^2)$ is too large when g_* is strong. Given that the TH mechanism demands g_* as strong as possible then composite TH models must ensure that the leading $O(y_t^2)$ is absent so that λ_h arises at $O(y_t^4)$. As discussed in ref. [118], this property is not guaranteed but it can be easily ensured provided the couplings that give rise to y_t via partial compositeness respect specific selection rules.

Hypersoft scenario

The second option corresponds to the structurally robust situation where m_σ^2 is one loop factor smaller than m_*^2 . This is for instance achieved if \mathcal{H} is a PNG-boson octet multiplet associated to the spontaneous breaking $SO(9) \rightarrow SO(8)$ in a model with fundamental scale m_* . Another option would be to have a supersymmetric model where supersymmetric masses of order m_* are mediated to the stops at the very scale m_* at which \mathcal{H} is massless. Of course in both cases a precise computation of m_σ^2 would require the full theory. However a parametrically correct estimate can be given by considering the quadratically divergent 1-loop corrections in the low energy theory, in the same spirit of Eq. (5.1). As y_t and $\lambda_{\mathcal{H}}$ are expectedly the dominant couplings the analogue of Eq. (5.1) and (5.6) imply

$$\delta m_h^2 \sim \frac{\lambda_h}{2\lambda_{\mathcal{H}}} \left(\frac{3y_t^2}{4\pi^2} + \frac{5\lambda_{\mathcal{H}}}{16\pi^2} \right) m_*^2 = \left(\frac{y_t^2}{\lambda_{\mathcal{H}}} + \frac{5}{12} \right) \frac{3\lambda_h}{8\pi^2} m_*^2. \quad (5.11)$$

Very roughly, for $\lambda_{\mathcal{H}} \gtrsim y_t^2$, top effects become sub-dominant and the natural value for m_h becomes controlled by λ_h , similarly to the term induced by the Higgs quartic in Eq. (5.1). In the absence of tuning this roughly corresponds to the technicolor limit $m_* \sim 4\pi v$, while allowing for fine tuning we have

$$m_* \sim 1.4 \times \sqrt{\frac{1}{\epsilon}} \text{ TeV}. \quad (5.12)$$

It should be said that in this scenario there is no extra boost of m_* at fixed tuning by taking $\lambda_{\mathcal{H}} > y_t^2$. Indeed the choice $\lambda_{\mathcal{H}} \sim y_t^2$ is preferable as concerns electroweak precision tests (EWPT). Indeed, as it is well known, RG evolution in the effective theory below m_σ gives rise to the corrections to the \hat{S} and \hat{T} parameters that will be discussed in section 5.4 [102]. In view of the relation $\epsilon = 2v^2/f^2$ this gives a direct connection between fine tuning, EWPT and the mass of the twin Higgs m_σ . At fixed v^2/f^2 , EWPT then favor the smallest possible $m_\sigma = \sqrt{\lambda_{\mathcal{H}}} f / \sqrt{2}$, that is the smallest $\lambda_{\mathcal{H}} \sim y_t^2$. The most plausible spectrum in this class of models is roughly the following: the twin scalar σ and the twin tops appear around the same scale $\sim y_t f / \sqrt{2}$ below the colored partners who live at m_* . The presence of the somewhat light scalar σ is one of interesting features of this class of models.

Super-Hypersoft Scenario

This option is a clever variant of the previous one, where below the scale m_* approximate supersymmetry survives in the Higgs sector in such a way that the leading contribution proportional to $\lambda_{\mathcal{H}}$ to $\delta m_{\mathcal{H}}^2$ is purely due to the top sector. In that way Eq. (5.11) reduces to

$$\delta m_h^2 \sim \frac{\lambda_h}{2\lambda_{\mathcal{H}}} \left(\frac{3y_t^2}{4\pi^2} \right) m_*^2 = \frac{y_t^2}{\lambda_{\mathcal{H}}} \times \frac{3\lambda_h}{8\pi^2} m_*^2. \quad (5.13)$$

so that by choosing $g_* > y_t$ one can push the scale m_* further up with fixed fine tuning ϵ

$$m_* \sim 1.4 \times \frac{g_*}{\sqrt{2}y_t} \times \sqrt{\frac{1}{\epsilon}} \text{ TeV}. \quad (5.14)$$

In principle even under the conservative assumption that $g_* \sim \sqrt{2}\pi$ is the maximal allowed value, this scenario seemingly allows $m_* \sim 14$ TeV with a mild $\epsilon \sim 0.1$ tuning.

It should be said that in order to realize this scenario, along the lines of ref. [132], one would need to complete \mathcal{H} into a pair of chiral superfield octets \mathcal{H}_u and \mathcal{H}_d as well as add a singlet superfield S in order to generate the Higgs quartic via the superpotential trilinear $g_* S \mathcal{H}_u \mathcal{H}_d$. Obviously this is a very far fetched scenario featuring all possible ideas to explain the weak scale: supersymmetry, compositeness and the Twin Higgs mechanism.

Alternative vacuum dynamics: tadpole induced EWSB

In all the scenarios discussed so far the tuning of the Higgs vacuum expectation value (VEV) and that of the Higgs mass coincided: ϵ , which controls the tuning of m_h^2 according to eqs. (5.8), (5.12) and (5.14), is equal to $2v^2/f^2$, which measures the tuning of the VEV. This was because the only tuning in the Higgs potential was associated with the small quadratic term, while the quartic was assumed to be of the right size without the need for further cancellations (see e.g. the discussion in ref. [7]). Experimentally however, one can distinguish between the need for tuning that originates from measurements of Higgs and electroweak observables, which are controlled by v^2/f^2 , and that coming from direct searches for top partners. Currently, with bounds on colored top partners at just around 1 TeV [97, 98], but with Higgs couplings already bounded to lie within 10 – 20% of their SM value [99], the only reason for tuning in all TH scenarios is to achieve a small v^2/f^2 . It is then fair to consider options that reduce or eliminate only the tuning of v^2/f^2 . As argued in ref. [141], this can be achieved by modifying the H scalar vacuum dynamics, and having its VEV induced instead by a tadpole mixing with an additional electroweak-breaking technicolor (TC) sector [130, 131]. In order to preserve the Z_2 symmetry one adds two twin TC sectors, both characterized by a mass scale m_{TC} and a decay constant $f_{TC} \sim m_{TC}/4\pi$ (i.e. it is parametrically convenient to assume $g_{TC} \sim 4\pi$). Below the

TC scale the dynamics in the visible and twin sectors is complemented by Goldstone triplets π_a and $\tilde{\pi}_a$ which can be embedded into doublet fields according to

$$\Sigma = f_{TC} e^{i\pi_a \sigma_a} \begin{pmatrix} 0 \\ 1 \end{pmatrix}, \quad \tilde{\Sigma} = f_{TC} e^{i\tilde{\pi}_a \sigma_a} \begin{pmatrix} 0 \\ 1 \end{pmatrix}, \quad (5.15)$$

and are assumed to mix with H and \tilde{H} via the effective potential terms

$$V_{\text{tadpole}} = M^2 (H^\dagger \Sigma + \tilde{H}^\dagger \tilde{\Sigma}) + \text{h.c.} \quad (5.16)$$

Assuming $m_{TC} \ll m_{\mathcal{H}}$ the \tilde{H} vacuum dynamics is not significantly modified, but, for $m_{TC} > m_h$, V_{tadpole} acts like a rigid tadpole term for H . The expectation value $\langle H \rangle$ is thus determined by balancing such a tadpole against the gauge-invariant $|H|^2$ mass term; the latter will then roughly coincide with m_h^2 . In order for this to work, by Eq. (5.6) the $SO(8)$ -breaking quartic $\hat{\lambda}_h$ should be negative, resulting in $v \sim (M^2/m_h^2) f_{TC}$. It is easy to convince oneself that the corrections to Higgs couplings are $O(f_{TC}^2/v^2)$: present bounds can then be satisfied for $f_{TC} \sim v/\sqrt{10} \simeq 80$ GeV. In turn, the value of v/f is controlled by f and can thus be naturally small. The TC scale is roughly $m_{TC} \sim 4\pi f_{TC} \sim 600 - 800$ GeV, while the non-eaten pNGB π in Eq. (5.15) have a mass $m_\pi^2 \sim M^2 v/f_{TC} \sim m_h^2 (v/f_{TC})^2 \sim 400$ GeV. The latter value, although rather low, is probably large enough to satisfy constraints from direct searches. In our opinion, what may be more problematic are EWPT, in view of the effects from the TC sector, which shares some of the vices of ordinary TC. The IR contributions to \hat{S} and \hat{T} , associated with the splitting $m_{\pi_a} < m_{TC}$, are here smaller than the analogues of ordinary technicolor (there associated with the splitting $m_W \ll m_{TC}$). However the UV contribution to \hat{S} is parametrically the same as in ordinary TC, in particular it is enhanced at large N_{TC} . Even at $N_{TC} = 2$, staying within the allowed (\hat{S}, \hat{T}) ellipse still requires a correlated contribution from $\Delta\hat{T}$, which in principle should also be counted as tuning. In spite of this, models with tadpole-induced EWSB represent a clever variant where, technically, the dynamics of EWSB does not currently appear tuned. A thorough analysis of the constraints is certainly warranted.

5.2 The Composite Twin Higgs: a comprehensive construction

In this section and in the remainder of the Chapter, we will focus on the CH realization of the TH, which belongs to the sub-hypersoft class of models. In this simple and well-motivated context we shall discuss EWPT, fine tuning and structural consistency of the model.

Our basic structural assumption is that at a generic UV scale $\Lambda_{UV} \gg m_*$, our theory can be decomposed into two sectors: a strongly-interacting Composite Sector and a weakly-interacting Elementary Sector. The Composite Sector is assumed to be endowed with the global symmetry $G = SO(8) \times U(1)_X \times Z_2$ and to be approximately scale- (conformal) invariant

5.2. The Composite Twin Higgs: a comprehensive construction

down to the scale m_* , at which it develops a mass gap. We assume the overall interaction strength at the resonance mass scale m_* to be roughly described by one parameter g_* [24]. The large separation of mass scales $\Lambda_{UV} \gg m_*$ is assumed to arise naturally, in that the occurrence of the mass gap m_* is controlled by either a marginally-relevant deformation, or by a relevant deformation whose smallness is controlled by some global symmetry. At the scale m_* , $SO(8) \times U(1)_X \times Z_2$ is spontaneously broken to the subgroup $H = SO(7) \times U(1)_X$, giving rise to seven NGBs in the **7** of $SO(7)$ with decay constant $f \sim m_*/g_*$. The subgroup $U(1)_X$ does not participate to the spontaneous breaking, but its presence is needed to reproduce the hypercharges of the SM fermions, similarly to CH models. The Elementary Sector consists in turn of two separate weakly-interacting sectors: one containing the visible SM fermions and gauge bosons, corresponding to the SM gauge group $G_{SM} = SU(3)_c \times SU(2)_L \times U(1)_Y$; the other containing the twin SM with the same fermion content and a \widetilde{SM} gauge group $\widetilde{G}_{SM} = \widetilde{SU}(3)_c \times \widetilde{SU}(2)_L$. The external Z_2 symmetry, or twin parity, interchanges these two copies. For simplicity, and following [118], we choose not to introduce a mirror hypercharge field. This is our only source of explicit Twin-parity breaking, and affects neither our discussion of fine tuning, nor that of precision electroweak measurements.

The Elementary and Composite sectors are coupled according to the paradigm of partial compositeness [13]. The elementary EW gauge bosons couple to the strong dynamics as a result of the weak gauging of the $SU(2)_L \times U(1)_Y \times \widetilde{SU}(2)_L$ subgroup of the global $SO(8) \times U(1)_X$. A linear mixing with the global conserved currents is thus induced:

$$\mathcal{L}_{\text{mix}}^V \supset g_2 W_\mu^\alpha J_\alpha^\mu + g_1 B_\mu J_B^\mu + \tilde{g}_2 \widetilde{W}_\mu^\alpha \tilde{J}_\alpha^\mu, \quad (5.17)$$

where $g_{1,2}$ and \tilde{g}_2 denote the SM and twin weak gauge couplings, $J_B^\mu \equiv J_{3R}^\mu + J_X^\mu$ and J^μ, \tilde{J}^μ and J_X^μ are the currents associated respectively to the $SU(2)_L, \widetilde{SU}(2)_L$ and $U(1)_X$ generators. The elementary fermions mix analogously with various operators transforming as linear representations of $SO(8)$ that are generated in the far UV by the strongly-interacting dynamics. The mixing Lagrangian takes the schematic form:

$$\mathcal{L}_{\text{mix}}^F \supset \tilde{q}_L^\alpha \Delta_{\alpha A} \mathcal{O}_R^A + \tilde{t}_R \Theta_A \mathcal{O}_L^A + \tilde{q}_L^\alpha \tilde{\Delta}_{\alpha A} \tilde{\mathcal{O}}_R^A + \tilde{t}_R \tilde{\Theta}_A \tilde{\mathcal{O}}_L^A + \text{h.c.}, \quad (5.18)$$

where, following e.g. ref. [38], we introduced spurions $\Delta_{\alpha A}, \tilde{\Delta}_{\alpha A}, \Theta_A$ and $\tilde{\Theta}_A$ in order to uplift the elementary fields to linear representations of $SO(8)$, and match the quantum numbers of the composite operators. The left-handed mixings $\Delta_{\alpha A}, \tilde{\Delta}_{\alpha A}$ necessarily break $SO(8)$ since q_L only partially fills a multiplet of $SO(8)$. The right-handed mixings, instead, may or may not break $SO(8)$. The breaking of $SO(8)$ gives rise to a potential for the NGBs at one loop and the physical Higgs is turned into a pNGB. We conclude by noticing that $g_{1,2}$ and \tilde{g}_2 correspond to quasi-marginal couplings which start off weak in the UV, and remain weak down to m_* . The fermion mixings could be either relevant or marginal, and it is possible

that some may correspond to interactions that grow as strong as g_* at the IR scale m_* [18]. In particular, as is well known, there is some advantage as regards tuning in considering the right mixings Θ_A and $\tilde{\Theta}_A$ to be strong. In that case one may even imagine the IR scale to be precisely generated by the corresponding deformation of the fixed point. While this latter option may be interesting from a top-down perspective, it would play no appreciable role in our low-energy phenomenological discussion.

5.2.1 A simplified model

In order to proceed we now consider a specific realization of the composite TH and introduce a concrete simplified effective Lagrangian description of its dynamics. Our model captures the most important features of this class of theories, like the pNGB nature of the Higgs field, and provides at the same time a simple framework for the interactions between the elementary fields and the composite states, vectors and fermions. We make use of this effective model as an example of a specific scenario in which we can compute EW observables, and study the feasibility of the TH idea as a new paradigm for physics at the EW scale.

We write down an effective Lagrangian for the Composite TH model using the Callan-Coleman-Wess-Zumino (CCWZ) construction [9, 10], and generalizing the simpler case of a two-site model developed in ref. [118]. According to the CCWZ technique, a Lagrangian invariant under the global $SO(8)$ group can be written following the rules of a local $SO(7)$ symmetry. The basic building blocks are the Goldstone matrix $\Sigma(\Pi)$, which encodes the seven NGBs, Π , present in the theory, and the operators $d_\mu(\Pi)$ and $E_\mu(\Pi)$ resulting from the Maurer-Cartan form constructed with the Goldstone matrix. An external $U(1)_X$ group is also added to the global invariance in order to reproduce the correct fermion hypercharges [118]. The CCWZ approach is reviewed and applied to the $SO(8)/SO(7)$ coset in Appendix A.

Before proceeding, we would like to recall the simplified model philosophy of ref. [8], which we essentially employ. In a generic composite theory, the mass scale m_* would control both the cut-off of the low energy σ -model and the mass of the resonances. In that case no effective Lagrangian method is expected to be applicable to describe the resonances. So, in order to produce a manageable effective Lagrangian we thus consider a Lagrangian for resonances that can, at least in principle, be made lighter than m_* . One more structured way to proceed could be to consider a deconstructed extra-dimension where the mass of the lightest resonances, corresponding to the inverse compactification length, is parametrically separated from the 5D cut-off, interpreted as m_* . Here we do not go that far and simply consider a set of resonances that happen to be a bit lighter than m_* . We do so to give a structural dignity to our effective Lagrangian, though at the end, for our numerical analysis, we just take the resonances a factor of 2 below m_* . We believe that is a fair procedure given our purpose of estimating the

5.2. The Composite Twin Higgs: a comprehensive construction

parametric consistency of the general TH scenario.

We start our analysis of the effective Lagrangian with the bosonic sector. Together with the elementary SM gauge bosons, the W 's and B , we introduce the twin partners \widetilde{W} to gauge the $\widetilde{SU}(2)_L$ group. As representative of the composite dynamics, we restrict our interest to the heavy spin-1 resonances transforming under the adjoint of $SO(7)$ and to a vector singlet. We therefore introduce a set of vectors ρ_μ^a which form a **21** of $SO(7)$ and the gauge vector associated with the external $U(1)_X$, which we call ρ_μ^X . The Lagrangian for the bosonic sector can be written as

$$\mathcal{L}_{\text{bosonic}} = \mathcal{L}_\pi + \mathcal{L}_{\text{comp}}^V + \mathcal{L}_{\text{elem}}^V + \mathcal{L}_{\text{mix}}^V. \quad (5.19)$$

The first term describes the elementary gauge bosons masses and the NGBs dynamics and is given by

$$\mathcal{L}_\pi = \frac{f^2}{4} \text{Tr} [d_\mu d^\mu]. \quad (5.20)$$

The second term, $\mathcal{L}_{\text{comp}}^V$, is a purely composite term, generated at the scale m_* after confinement; it reduces to the kinetic terms for the ρ vectors, namely:

$$\mathcal{L}_{\text{comp}}^V = -\frac{1}{4g_\rho^2} \rho_{\mu\nu}^a \rho^{\mu\nu a} - \frac{1}{4g_{\rho^X}^2} \rho_{\mu\nu}^X \rho^{X\mu\nu}, \quad (5.21)$$

where $\rho_{\mu\nu}^a = \partial_\mu \rho_\nu^a - \partial_\nu \rho_\mu^a - f_{abc} \rho_\mu^b \rho_\nu^c$, $\rho_{\mu\nu}^X = \partial_\mu \rho_\nu^X - \partial_\nu \rho_\mu^X$ and g_ρ and g_{ρ^X} are the coupling strengths for the composite spin-1 bosons. The third term in Eq. (5.19), $\mathcal{L}_{\text{elem}}^V$, is a purely elementary interaction, produced at the scale Λ_{UV} where the elementary fields are formally introduced. Also this Lagrangian can contain only the kinetic terms for the elementary fields:

$$\mathcal{L}_{\text{elem}}^V = -\frac{1}{4g_1^2} B_{\mu\nu} B^{\mu\nu} - \frac{1}{4g_2^2} W_{\mu\nu}^a W^{a\mu\nu} - \frac{1}{4\widetilde{g}_2^2} \widetilde{W}_{\mu\nu}^a \widetilde{W}^{a\mu\nu}, \quad (5.22)$$

where g_1 , g_2 and \widetilde{g}_2 denote the weak gauge couplings. The last term in the Lagrangian (5.19), $\mathcal{L}_{\text{mix}}^V$, is a mixing term between the elementary and composite sectors originating from partial compositeness. We have:⁵

$$\mathcal{L}_{\text{mix}}^V = \frac{M_\rho^2}{2g_\rho^2} \left(\text{Tr} \left[\rho_\mu^a T_a^{21} - E_\mu \right] \right)^2 + \frac{M_{\rho^X}^2}{2g_{\rho^X}^2} (\rho_\mu^X - B_\mu)^2, \quad (5.23)$$

where T_a^{21} are the $SO(8)$ generators in the adjoint of $SO(7)$ (see Appendix A).

⁵Notice that in the Lagrangian (5.23), the parameters f , M_ρ , M_{ρ^X} , g_ρ and g_{ρ^X} are all independent. It is common to define the parameters $a_\rho = M_\rho / (g_\rho f)$ and $a_{\rho^X} = M_{\rho^X} / (g_{\rho^X} f)$, which are expected to be $O(1)$. In our analysis we set $a_\rho = 1/\sqrt{2}$ corresponding to the two-site model value (see the last paragraph of this section) and $a_{\rho^X} = 1$.

We now introduce the Lagrangian for the fermionic sector. This depends on the choice of quantum numbers for the composite operators in Eq. (5.18). The minimal option is to choose \mathcal{O}_R and $\tilde{\mathcal{O}}_R$ to be in the fundamental representation of $SO(8)$, whereas the operators \mathcal{O}_L and $\tilde{\mathcal{O}}_L$ are singlets of the global group. Therefore, the elementary SM doublet and its twin must be embedded into fundamental representations of $SO(8)$, whereas the t_R and the \tilde{t}_R are complete singlets under the global $SO(8)$ invariance. This choice is particularly useful to generalize our discussion to the case of a fully-composite right-handed top. From the low-energy perspective, the linear mixing between composite operators and elementary fields translates into a linear coupling between the latter and a layer of fermionic resonances excited from the vacuum by the operators in the fundamental and singlet representations of the global group. Decomposing the $\mathbf{8}$ of $SO(8)$ as $\mathbf{8} = \mathbf{7} + \mathbf{1}$ under $SO(7)$, we introduce a set of fermionic resonances filling a complete fundamental representation of $SO(7)$ and another set consisting of just one singlet.⁶ We denote with Ψ_7 the fermionic resonances in the septuplet and with Ψ_1 the singlet, both charged under $SU(3)_c$. Together with them, we must introduce analogous composite states charged under $\widetilde{SU}(3)_c$; we use the corresponding notation $\tilde{\Psi}_7$ and $\tilde{\Psi}_1$. We refer to Appendix F for the complete expression of Ψ_7 and $\tilde{\Psi}_7$ in terms of the constituent fermions.

The fermionic effective Lagrangian is split into three parts, which have the same meaning as the analogous distinctions we made for the bosonic sector of the theory:

$$\mathcal{L}_{\text{fermionic}} = \mathcal{L}_{\text{comp}}^F + \mathcal{L}_{\text{elem}}^F + \mathcal{L}_{\text{mix}}^F. \quad (5.24)$$

The fully composite term is given by:

$$\begin{aligned} \mathcal{L}_{\text{comp}}^F = & \bar{\Psi}_7(iD_7 - M_\Psi)\Psi_7 + \bar{\Psi}_1(iD_1 - M_S)\Psi_1 + \bar{\tilde{\Psi}}_7(i\tilde{D} - \tilde{M}_\Psi)\tilde{\Psi}_7 + \bar{\tilde{\Psi}}_1(i\tilde{D} - \tilde{M}_S)\tilde{\Psi}_1 \\ & + \left(i c_L \bar{\Psi}_{7L}^i d_i \Psi_{1L} + i c_R \bar{\Psi}_{7R}^i d_i \Psi_{1R} + i \tilde{c}_L \bar{\tilde{\Psi}}_{7L}^i d_i \tilde{\Psi}_{1L} + i \tilde{c}_R \bar{\tilde{\Psi}}_{7R}^i d_i \tilde{\Psi}_{1R} + \text{h.c.} \right), \end{aligned} \quad (5.25)$$

where $D_{7\mu} = \nabla_\mu + iXB_\mu$, $D_{1\mu} = \partial_\mu + iXB_\mu$, and $\nabla_\mu = \partial_\mu + iE_\mu$. We have introduced two sets of $O(1)$ coefficients, c_L and c_R and their twins, for the interactions mediated by the d_μ operator. Considering the elementary part of the Lagrangian, it comprises just the kinetic terms for the doublets and right-handed tops:

$$\mathcal{L}_{\text{elem}}^F = \bar{q}_L i \not{D} q_L + \bar{t}_R i \not{D} t_R + \bar{\tilde{q}}_L i \not{D} \tilde{q}_L + \bar{\tilde{t}}_R i \not{D} \tilde{t}_R. \quad (5.26)$$

The final term in our classification is the elementary/composite mixing that we write again

⁶Notice that in general we should introduce two different singlets in our Lagrangian. One corresponds to a full $SO(8)$ singlet, while the other is the $SO(7)$ singlet appearing in the decomposition $\mathbf{8} = \mathbf{7} + \mathbf{1}$ of the fundamental of $SO(8)$ under the $SO(7)$ subgroup. We will further simplify our study identifying the two singlets with just one composite particle.

5.2. The Composite Twin Higgs: a comprehensive construction

following the prescription of partial compositeness. With our choice of quantum numbers for the composite operators, the spurions in Eq. (5.18) can be matched to dimensionless couplings according to

$$\Delta_{\alpha A} = \begin{pmatrix} 0 & 0 & i y_L & -y_L & 0 \times 4 \\ i y_L & y_L & 0 & 0 & 0 \times 4 \end{pmatrix}, \quad \Theta_A = y_R, \quad (5.27)$$

and

$$\tilde{\Delta}_{\alpha A} = \begin{pmatrix} 0 \times 4 & 0 & 0 & i \tilde{y}_L & -\tilde{y}_L \\ 0 \times 4 & i \tilde{y}_L & \tilde{y}_L & 0 & 0 \end{pmatrix}, \quad \tilde{\Theta}_A = \tilde{y}_R, \quad (5.28)$$

where we have introduced the elementary/composite mixing parameters y_L , y_R and their twin counterparts. These dimensionless y 's control the strength of the interaction between the elementary and composite resonance fields, according to the Lagrangian:

$$\begin{aligned} \mathcal{L}_{\text{mix}}^F = & f \left(\tilde{q}_L^\alpha \Delta_{\alpha A} \Sigma_{Ai} \Psi_7^i + \tilde{q}_L^\alpha \Delta_{\alpha A} \Sigma_{A8} \Psi_1 + y_R \tilde{t}_R \Psi_1 + \text{h.c.} \right) \\ & + f \left(\tilde{\tilde{q}}_L^\alpha \tilde{\Delta}_{\alpha A} \Sigma_{Ai} \tilde{\Psi}_7^i + \tilde{\tilde{q}}_L^\alpha \tilde{\Delta}_{\alpha A} \Sigma_{A8} \tilde{\Psi}_1 + \tilde{y}_R \tilde{\tilde{t}}_R \tilde{\Psi}_1 + \text{h.c.} \right). \end{aligned} \quad (5.29)$$

Depending on the UV boundary condition and the relevance or marginality of the operators appearing in Eq. (5.18), the y 's can vary from weak to $O(g_*)$. Correspondingly the light fermions vary from being completely elementary (for y weak) to effectively fully composite (for $y \sim g_*$). For reasons that will become clear, given $y_t \sim y_L y_R / g_*$, it is convenient to take $y_L \simeq \tilde{y}_L \sim y_t$, i.e. weak left mixing, and $y_R \simeq \tilde{y}_R \sim g_*$. For such strong right-handed mixing the right-handed tops can be practically considered part of the strong sector.

The last term that we need to introduce in the effective Lagrangian describes the interactions between the vector and fermion resonances and originates completely in the Composite Sector. We have:

$$\begin{aligned} \mathcal{L}_{\text{comp}}^{VF} = & \sum_{i=L,R} \left[\alpha_i \bar{\Psi}_{7i} (\not{p} - E) \Psi_{7i} + \alpha_{7i} \bar{\Psi}_{7i} (\not{p}^X - B) \Psi_{7i} + \alpha_{1i} \bar{\Psi}_{1i} (\not{p}^X - B) \Psi_{1i} \right. \\ & \left. + \tilde{\alpha}_i \bar{\tilde{\Psi}}_{7i} (\not{p} - E) \tilde{\Psi}_{7i} + \tilde{\alpha}_{7i} \bar{\tilde{\Psi}}_{7i} (\not{p}^X - B) \tilde{\Psi}_{7i} + \tilde{\alpha}_{1i} \bar{\tilde{\Psi}}_{1i} (\not{p}^X - B) \tilde{\Psi}_{1i} \right], \end{aligned} \quad (5.30)$$

where all the coefficients α_i appearing in the Lagrangian are $O(1)$ parameters.

We conclude the discussion of our effective Lagrangian by clarifying its two-site model limit [117] (see also ref. [111]). This is obtained by combining the singlet and the septuplet into a complete representation of $SO(8)$, so that the model enjoys an enhanced $SO(8)_L \times SO(8)_R$ global symmetry. This is achieved by setting $c_L = c_R = \tilde{c}_L = \tilde{c}_R = 0$ and all the α_i equal to 1. Moreover, we have to impose $M_\rho = g_\rho f / \sqrt{2}$, so that the heavy vector resonances can be reinterpreted as gauge fields of $SO(7)$. As shown in ref. [117], with this choice of the free

parameters the Higgs potential becomes calculable up to only a logarithmic divergence, that one can regulate by imposing just one renormalization condition. In the subsequent sections, we will extensively analyze the EW precision constraints in the general case, as well as in the two-site limit.

5.2.2 Perturbativity of the simplified model

In section 5.1.1 it was noted that a TH construction typically involves large multiplicities of states and, as a consequence, the dynamics responsible for its UV completion cannot be maximally strongly coupled. This in turn limits the improvement in fine tuning that can be achieved compared to standard scenarios of EWSB. In our naive estimates of eqs. (5.7), (5.11) and (5.13) the interaction strength of the UV theory was controlled by the σ -model quartic coupling $\lambda_{\mathcal{H}}$ or, equivalently, by m_σ/f . By considering the $\lambda_{\mathcal{H}}$ one-loop β -function (Eq. (5.9)) we estimated the maximal value of $\lambda_{\mathcal{H}}$ as the one corresponding to an $O(1)$ relative change through one e-folding of RG evolution. For an $SO(8)/SO(7)$ σ -model this led to $\sqrt{\lambda_{\mathcal{H}}} \lesssim \sqrt{2}\pi$, or, equivalently, $m_\sigma/f \lesssim \pi$.

Alternatively, the limit set by perturbativity on the UV interaction strength may also be estimated in the effective theory described by the non-linear σ -model by determining the energy scale at which tree-level scattering amplitudes become non-perturbative. For concreteness, we considered the following two types of scattering processes: $\pi\pi \rightarrow \pi\pi$ and $\pi\pi \rightarrow \bar{\psi}\psi$, where π are the NGBs and $\psi = \{\Psi_7, \tilde{\Psi}_7\}$ denotes a composite fermion transforming in the fundamental of $SO(7)$. Other processes can (and should) be considered, with the actual bound being given by the strongest of the constraints obtained in this way.

Requiring that the process $\pi\pi \rightarrow \pi\pi$ stay perturbative up the cutoff scale m_* gives the bound

$$\frac{M_\rho}{f} \sim \frac{M_\Psi}{f} \lesssim \frac{m_*}{f} < \frac{4\pi}{\sqrt{N-2}} \simeq 5.1, \quad (5.31)$$

where the second inequality is valid in a generic $SO(N)/SO(N-1)$ non-linear σ -model, and we have set $N = 8$ in the last step. More details on how this result was obtained can be found in Appendix L. Equation (5.31) in fact corresponds to a limit on the interaction strength of the UV theory, given that the couplings among fermion and vector resonances are of order M_Ψ/f and M_ρ/f , respectively. Perturbativity of the scattering amplitude for $\pi\pi \rightarrow \bar{\psi}\psi$ instead gives (see Appendix L for details)

$$\frac{M_\rho}{f} \sim \frac{M_\Psi}{f} \lesssim \frac{m_*}{f} < \frac{\sqrt{12\sqrt{2}}\pi}{\sqrt{N_f}} \simeq \frac{4\pi}{\sqrt{N_f}}, \quad (5.32)$$

where N_f is the multiplicity of composite fermions (including the number of colors and

families). Our simplified model with one family of composite fermions has $N_f = 6$, which gives a limit similar to Eq. (5.31): $M_\Psi/f \lesssim 5.3$. A model with three families of composite quarks and leptons has instead $N_f = 24$, from which follows the stronger bound $M_\Psi/f \lesssim 2.6$.

As a third alternative, one could analyze when 1-loop corrections to a given observable become of the same order as its tree-level value. We applied this criterion to our simplified model by considering the \hat{S} parameter, the new physics contribution to which includes a tree-level correction from heavy vectors given by Eq. (5.48), and a one-loop correction due to heavy fermions, which can be found in Appendix J. By requiring that the one-loop term be smaller than the tree-level correction, we obtain a bound on the strong coupling constant g_ρ . As an illustration, we consider the two-site model limit $c_L = c_R = 0$ and $M_\rho = g_\rho f/\sqrt{2}$ and keep the dominant UV contribution to \hat{S} in Eq. (J.19) which is logarithmically sensitive to the cut-off. By setting $m_* = 2M_\Psi$, we find:

$$\frac{\Delta\hat{S}_{1\text{-loop}}}{\Delta\hat{S}_{\text{tree}}} < 1 \implies \frac{M_\rho}{f} = \frac{g_\rho}{\sqrt{2}} < \frac{\pi}{\sqrt{2\log 2}} \simeq 2.7. \quad (5.33)$$

The perturbative limits obtained from eqs. (5.31), (5.32) and (5.33) are comparable to that on $\lambda_{\mathcal{H}}$ derived in Sec. 5.1.1. As already discussed there, one could take any of these results as indicative of the maximal interaction strength in the underlying UV dynamics, though none of them should be considered as a sharp exclusion condition. In our analysis of EW observables we will make use of Eq. (5.31) with $N = 8$ and of Eq. (5.32) with $N_f = 24$ to highlight the regions of parameter space where our perturbative calculation is less reliable. We use both limits as a measure of the intrinsic uncertainty which is inevitably associated with this type of estimation.

5.3 Higgs Effective Potential: a brief reminder

As anticipated in the general discussion of section 5.1.1, a potential for the Higgs boson is generated at the scale m_* by loops of heavy states through the $SO(8)$ -breaking couplings of the elementary fields to the strong sector. Once written in terms of the Higgs boson h (where $H^\dagger H = f^2 \sin^2(h/f)/2$, $\tilde{H}^\dagger \tilde{H} = f^2 \cos^2(h/f)/2$), at 1-loop this UV threshold contribution has the form [118]:

$$\frac{V(m_*)}{f^4} = \frac{3}{32\pi^2} \left[\frac{1}{16} g_1^2 g_\rho^2 L_1 + (y_L^2 - \tilde{y}_L^2) g_\Psi^2 L_2 \right] \sin^2 \frac{h}{f} + \frac{3y_L^4}{64\pi^2} F_1 \left(\sin^4 \frac{h}{f} + \cos^4 \frac{h}{f} \right), \quad (5.34)$$

where $g_\Psi \equiv M_\Psi/f$, L_1, L_2, F_1 are $O(1)$ dimensionless functions of the masses and couplings of the theory and the explicit expression of the function F_1 is reported in Eq. (G.4) of Appendix G.

The first term in the above equation originates from Z_2 -breaking effects.⁷ The second term, generated by loops of fermions, is Z_2 symmetric and explicitly violates the $SO(8)$ invariance; it thus corresponds to the (UV part of the) last term of Eq. (5.5). Upon electroweak symmetry breaking, Eq. (5.34) contributes to the physical Higgs mass an amount equal to

$$\delta m_h^2|_{UV} = \frac{3y_1^4}{4\pi^2} F_1 f^2 \xi (1 - \xi), \quad (5.35)$$

where ξ controls the degree of vacuum misalignment:

$$\xi \equiv \sin^2 \frac{\langle h \rangle}{f} = \frac{v^2}{f^2}. \quad (5.36)$$

Below the scale m_* an important contribution to the potential arises from loops of light states, in particular from the top quark and from its twin. The bulk of this IR contribution is captured by the RG evolution of the Higgs potential from the scale m_* down to the electroweak scale. As noted in previous studies (see e.g. ref. [118]), for sufficiently large m_* this IR effect dominates over the UV threshold correction and can reproduce the experimental Higgs mass almost entirely. An analogous IR correction to the Higgs quartic arises in SUSY theories with large stop masses, from loops of top quarks. The distinctive feature of any TH scenario, including our model, is the additional twin top contribution.

The Higgs effective action, including the leading $O(\xi)$ corrections associated with operators of dimension 6, was computed at 1-loop in ref. [118]; the resulting IR contribution to m_h^2 was found to be

$$\delta m_h^2|_{IR}^{1\text{-loop}} = \frac{3y_1^4}{8\pi^2} f^2 \xi (1 - \xi) \left(\log \frac{m_*^2}{m_t^2} + \log \frac{m_*^2}{\tilde{m}_t^2} \right), \quad (5.37)$$

where y_1 denotes the top Yukawa coupling (see Eq. (G.8) in Appendix G). The two single log terms in parentheses correspond to the IR contributions to the effective Higgs quartic λ_h from the top quark and twin top respectively. Leading-logarithmic corrections of the form $(\alpha \log)^n$, arising at higher loops have however an important numerical impact.⁸ For example, $(\alpha \log)^2$ corrections generated by 2-loop diagrams (mostly due to the running of the top and twin top Yukawa couplings, that are induced by respectively QCD and twin QCD) are expected to give a $\sim 30\%$ reduction in the Higgs mass for $m_* \simeq 5$ TeV,

We have computed the $(\alpha \log)^2$ correction through an effective operator approach by matching with the low-energy effective theory at the scale m_* and running down the Higgs quartic cou-

⁷Sub-leading Z_2 -breaking terms have been neglected for simplicity. The complete expressions are given in ref. [118].

⁸Here $\alpha = g_{SM}^2/4\pi$, with g_{SM} being any large SM coupling, i.e. g_S and y_t .

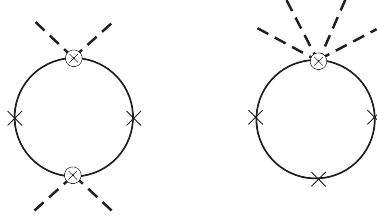


Figure 5.1 – Diagrams with loops of twin tops contributing to the β -function of λ_h . Crosses denote mass insertions. The first diagram features two insertions of a dimension-5 operator, while the interaction vertex in the second diagram arises from a dimension-7 operator.

pling. A suitable redefinition of fields makes the form of the effective Lagrangian particularly compact at the scale m_* . In particular, the only dimension 6 operator in the Higgs + SM sector with non-vanishing coefficient at the relevant loop order is the kinetic Higgs quadrilinear O_H . We report the details in Appendix G. In this operator basis the RG-improved Higgs mass also acquires a simple form:

$$m_h^2 = \delta m_h^2|_{UV} + \delta m_h^2|_{IR} = \frac{\lambda_h(\mu)}{2\sqrt{2}G_F}(1 - \xi), \quad (5.38)$$

where the Higgs quartic coupling is evaluated at $\mu = m_h$ and the Fermi constant is given by

$$G_F = \frac{1}{\sqrt{2}f^2\xi} \equiv \frac{1}{\sqrt{2}v^2}. \quad (5.39)$$

Formula (5.38) is valid up to $O[\xi(\alpha \log)^2]$ and $O[(\alpha \log)^3]$ contributions, which we did not include. Our result is thus valid at next-to-leading order (NLO) in a combined perturbative expansion in $(\alpha \log)$ and ξ . An interesting peculiarity characterizing the RG contribution of the twin top is the fact that the latter couples to the Higgs boson only through higher-dimensional operators suppressed by the scale f (see Appendix). Insertions of the twin top mass, which is also of order f , can however compensate for such suppression. This is an example of a situation where a marginal coupling can get renormalized by irrelevant ones in the presence of a relevant operator in the theory [11]. For an NLO calculation it is sufficient to include up to dimension-7 operators, as shown in figure 5.1 and discussed in the Appendix. The RG equation for λ_h is coupled to those of the other couplings of the theory, in particular the couplings of the top and twin top to the Higgs boson. We have solved this system of coupled equations perturbatively by making an expansion in powers of the logarithms and of ξ and working at second order. The initial conditions at the scale m_* are fixed by matching to the full theory. In particular, the initial value of λ_h is obtained from Eq. (5.37),

$$\lambda_h(m_*) = \frac{3y_L^4}{2\pi^2}F_1, \quad (5.40)$$

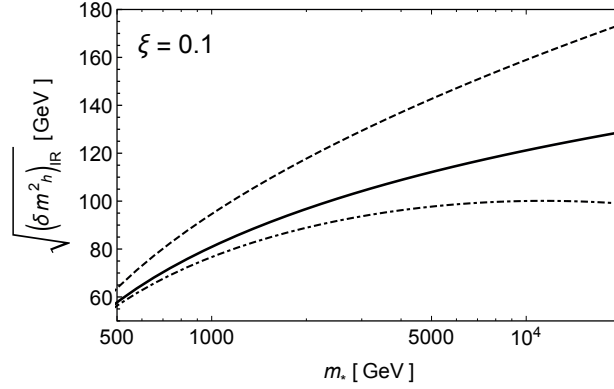


Figure 5.2 – IR contribution to the Higgs mass as a function of the scale m_* for $\xi = 0.1$. The dashed and dot-dashed curves denote respectively the LO and NLO result in a combined perturbative expansion in $(\alpha \log)$ and ξ . The continuous curve corresponds to the NNLO calculation of ref. [122].

the top Yukawa coupling is given by

$$y_1(m_*) = \frac{y_L y_R f}{\sqrt{M_S^2 + y_R^2 f^2}}. \quad (5.41)$$

while the higher dimensional Higgs-top couplings, in particular y_3 , vanish in our chosen field parametrization and are not generated by RG evolution at the order at which we are working (see Appendix G). The couplings of the twin top are instead fixed assuming (approximate) Z_2 invariance at the matching scale. Our final expression for $\lambda_h(\mu)$ is reported in Eq. (G.13) of the Appendix and agrees with the result found in ref. [122] using a background field method.⁹

A numerical determination of the IR contribution $\delta m_h^2|_{IR}$ can be obtained by making use of the experimental value of the top quark mass to fix $y_1(m_*)$. In fact, the 1-loop RG equation for y_1 is decoupled from the twin sector and can be easily solved. We find:

$$y_1(m_*) = y_1(m_t) + \left(\frac{9y_1^3}{64\pi^2} - \frac{g_S^2 y_1}{4\pi^2} \right) \log \frac{m_*^2}{m_t^2}, \quad (5.42)$$

which fixes $y_1(m_*)$ in terms of $y_1(m_t)$.¹⁰ The value of $\delta m_h^2|_{IR}$ is shown in figure 5.2 as a function of m_* for $\xi = 0.1$. The naive expectation is confirmed, as the NLO correction decreases the

⁹Notice that our normalization of the Higgs quartic λ_h differs with respect to ref. [122], where the Higgs potential is written as $V(H) = 2\mu^2 H^\dagger H + 4\lambda(H^\dagger H)^2$.

¹⁰As an input to our numerical analysis we use the PDG combination for top quark pole mass $m_t^{\overline{\text{MS}}}(m_t) = 173.21 \pm 0.51 \pm 0.71$ GeV [100]. This is converted into the top Yukawa coupling in the $\overline{\text{MS}}$ scheme $y_1^{\overline{\text{MS}}}(m_t) = 0.936 \pm 0.005$ by making use of Eq. (62) of ref. [124].

Higgs mass by $\sim 32\%$ for $m_* = 5$ TeV. The plot also shows the curve obtained in ref. [122] with an NNLO calculation including effects up to order $\xi(\alpha \log)^2$ and $(\alpha \log)^3$. Performing this calculation with an operator approach would be rather complicated, since the number of effective operators to include grows considerably. The background field technique adopted in ref. [122] is instead particularly effective and greatly simplifies the calculation. The NNLO terms are found to increase the Higgs mass, for example they give a 15% enhancement for $m_* = 5$ TeV and $\xi = 0.1$. Higher-order logs are expected to have a smaller impact and can be neglected. Indeed, corrections of order $(\alpha \log)^4$ are naively smaller than the 2-loop finite corrections (including those from UV thresholds) that are not captured by the RG-improvement.¹¹

The plot of figure 5.2 illustrates one of the characteristic features of TH models: the IR contribution to the Higgs mass largely accounts for its experimental value and is completely predicted by the theory in terms of the low-energy particle content (SM plus Twin states). Threshold effects arising at the UV matching scale, on the other hand, are model dependent but give a sub-leading correction. An accurate prediction of the Higgs mass and an assessment of the plausibility of the model thus requires a precise determination of its IR contribution. Indeed the difference between the IR contribution of figure 5.2 and the measured value $m_h = 125$ GeV, must be accounted for by the UV threshold contribution in Eq. (5.35). That translates into a generic constraint of the size of y_L^4 , a parameter upon which electroweak precision observables (EWPO) crucially depend, thus creating a non-trivial correlation between the Higgs mass, EWPO and naturalness.

Even though our discussion was here based on a NLO computation of the Higgs potential, in our numerical analysis presented in section 5.5 we use the NNLO computation of ref. [122].

5.4 Electroweak Precision Observables

In this section we compute the contribution of the new states described by our simplified model to the electroweak precision observables (EWPO). Although it neglects the effects of the heavier resonances, our calculation is expected to give a fair assessment of the size of the corrections due to the full strong dynamics, and in particular to reproduce the correlations among different observables.

It is well known that, under the assumption of quark and lepton universality, short-distance corrections to the electroweak observables due to heavy new physics can be expressed in terms of four parameters, \hat{S} , \hat{T} , W , Y , defined in ref. [56] (see also ref. [58] for an equivalent analysis) as a generalization of the parametrization introduced by Peskin and Takeuchi in refs. [55]. Two additional parameters, δg_{Lb} and δg_{Rb} , can be added to account for the modified couplings of

¹¹A complete numerical re-summation of the leading logs can be performed in the SM, and one can check a posteriori that N³LO terms are indeed small, see ref. [122].

the Z boson to left- and right-handed bottom quarks respectively.¹² A naive estimate shows that in CH theories, including our TH model, W and Y are sub-dominant in an expansion in the weak couplings [24] and can thus be neglected. The small coupling of the right-handed bottom quark to the strong dynamics makes also δg_{Rb} small and negligible in our model. We thus focus on \hat{S} , \hat{T} and δg_{Lb} , and compute them by including effects from the exchange of vector and fermion resonances, and from Higgs compositeness.

We work at the 1-loop level and at leading order in the electroweak couplings and perform an expansion in inverse powers of the new physics scale. In this limit, the twin states do not affect the EWPO as a consequence of their being neutral under the SM gauge group. Deviations from the SM predictions arise only from heavy states with SM quantum numbers and are parametrically the same as in ordinary CH models with singlet t_R . This can be easily shown by means of naive dimensional analysis and symmetries as follows. Twin tops interact with the SM fields only through higher-dimensional operators. The operators relevant for the EWPO are those involving either a SM current or a derivative of the hypercharge field strength:

$$O_{B\tilde{t}} = \frac{g'}{m_W^2} \partial^\mu B_{\mu\nu} \tilde{t} \gamma^\nu \tilde{t}, \quad O_{q\tilde{t}} = \frac{1}{v^2} \bar{q}_L \gamma_\mu q_L \tilde{t} \gamma^\mu \tilde{t}, \quad O_{H\tilde{t}} = \frac{i}{v^2} H^\dagger \overleftrightarrow{D}_\mu H \tilde{t} \gamma^\mu \tilde{t}, \quad (5.44)$$

where \tilde{t} indicates either a right- or left-handed twin top.¹³ The first two operators of Eq. (5.44) are generated at the scale m_* by the tree-level exchange of the ρ_X . Their coefficients (in a basis with canonical kinetic terms) are respectively of order $(m_W^2/m_*^2)(\tilde{y}/g_*)^2$ and $(y_L^2 v^2/m_*^2)(\tilde{y}/g_*)^2$, where \tilde{y} equals either \tilde{y}_L or \tilde{y}_R depending on the chirality of \tilde{t} . The third operator breaks custodial isospin and the only way it can be generated is via the exchange of weakly coupled elementary fields at loop level. Given that the contribution to EWPO is further suppressed by \tilde{t} loops, the third operator can affect EWPO only at, at least, two loops and is thus clearly negligible. By closing the \tilde{t} loops the first two operators can give rise to effects that are schematically of the form BB , $B\bar{q}q$ or $(\bar{q}q)^2$. The formally quadratically divergent piece of the loop integral renormalizes the corresponding dimension-6 operators. For instance the second structure gives

$$C \frac{g'}{16\pi^2} \frac{y_L^2}{m_*^2} \left(\frac{\tilde{y}}{g_*} \right)^4 \partial_\nu B^{\mu\nu} \bar{q}_L \gamma_\mu q_L \quad (5.45)$$

with C an $O(1)$ coefficient which depends on the details of the physics at the scale m_* . Using

¹²We define δg_{Lb} and δg_{Rb} in terms of the following effective Lagrangian in the unitary gauge:

$$\mathcal{L}_{eff} \supset \frac{g_2}{2c_W} Z_\mu \bar{b} \gamma^\mu \left[(g_{Lb}^{SM} + \delta g_{Lb})(1 - \gamma_5) + (g_{Rb}^{SM} + \delta g_{Rb})(1 + \gamma_5) \right] b + \dots \quad (5.43)$$

where the dots stand for higher-derivative terms and $g_{Lb}^{SM} = -1/2 + s_W^2/3$, $g_{Rb}^{SM} = s_W^2/3$.

¹³Notice that $O_{H\tilde{t}}$ can be rewritten in terms of the other two operators by using the equations of motion, but it is still useful to consider it in our discussion.

the equations of motion for B , the above operator gives rise to a correction to the Zbb vertex of relative size

$$\frac{\delta g_{Lb}}{g_{Lb}} = \frac{g'^2}{16\pi^2} \frac{y_L^2 v^2}{m_*^2} \left(\frac{\tilde{y}}{g_*} \right)^4 \quad (5.46)$$

which, even assuming $\tilde{y} \sim g_*$, is $O(g'/y_t)^2$ suppressed with respect to the leading visible sector effect we discuss below. Aside the quadratically divergent piece there is also a logarithmic divergent piece whose overall coefficient is calculable. The result is further suppressed with respect to the above contribution by a factor $(m_t^2/m_*^2) \ln(m_t^2/m_*^2)$.

An additional contribution could in principle come from loops of the extra three “twin” NGBs contained in the coset $SO(8)/SO(7)$. Simple inspection however shows that there is no corresponding 1-loop diagram contributing to the EWPO. In the end we conclude that the effect of twin loops is negligible.

Since the effects from the twin sector can be neglected, the corrections to \hat{S} , \hat{T} and δg_{Lb} are parametrically the same as in ordinary CH models. We now give a concise review of the contributions to each of these quantities, distinguishing between the threshold correction generated at the scale m_* and the contribution arising from the RG evolution down to the electroweak scale. For recent analyses of the EWPO in the context of $SO(5)/SO(4)$ CH models see for example Refs. [108, 110, 111].

5.4.1 \hat{S} parameter

The leading contribution to the \hat{S} parameter arises at tree level from the exchange of spin-1 resonances. Since only the (3, 1) and (1, 3) components of the spin-1 multiplet contribute, its expression is the same as in $SO(5)/SO(4)$ composite-Higgs theories.¹⁴

$$\Delta \hat{S}_\rho = \frac{g_2^2}{2g_\rho^2} \xi. \quad (5.47)$$

In our numerical analysis presented in section 5.5 we use the two-site model relation $M_\rho = g_\rho f / \sqrt{2}$ to rewrite

$$\Delta \hat{S}_\rho = \frac{m_W^2}{M_\rho^2}. \quad (5.48)$$

The 1-loop contribution from loops of spin-1 and fermion resonances is sub-dominant (by a factor $g_*^2/16\pi^2$) and will be neglected for simplicity in the following. Nevertheless, we

¹⁴We neglect for simplicity a contribution from the operator $E_{\mu\nu}\rho^{\mu\nu}$, which also arises at tree level. See for example the discussion in Refs. [111, 112].

explicitly computed the fermionic contribution (see Appendix J) to monitor the validity of the perturbative expansion and estimate the limit of strong coupling in our model (a discussion on this aspect was given in section 5.2.2). An additional threshold correction to \hat{S} , naively of the same order as Eq. (5.48), arises from the exchange of cutoff modes at m_* . As already anticipated, we neglect this correction in the following. In this respect our calculation is subject to an $O(1)$ uncertainty and should rather be considered as an estimate, possibly more refined than a naive one, which takes the correlations among different observables into account.

Besides the UV threshold effects described above, \hat{S} gets an IR contribution from RG evolution down to the electroweak scale. The leading effect of this type comes from the compositeness of the Higgs boson, and is the same as in $SO(5)/SO(4)$ CH models [102]:

$$\Delta\hat{S}_h = \frac{g_2^2}{192\pi^2} \xi \log \frac{m_*^2}{m_h^2}. \quad (5.49)$$

In the effective theory below m_* this corresponds to the evolution of the dimension-6 operators

$$O_W = \frac{ig}{2m_W^2} H^\dagger \sigma^i \overleftrightarrow{D}^\mu H D^\nu W_{\mu\nu}^i, \quad O_B = \frac{ig'}{2m_W^2} H^\dagger \overleftrightarrow{D}^\mu H \partial^\nu B_{\mu\nu} \quad (5.50)$$

induced by a 1-loop insertion of

$$O_H = \frac{1}{2v^2} \partial^\mu (H^\dagger H) \partial_\mu (H^\dagger H). \quad (5.51)$$

Denoting with \bar{c}_i the coefficients of the effective operators and working at leading order in the SM couplings, the RG evolution can be expressed as

$$\bar{c}_i(\mu) = \left(\delta_{ij} + \gamma_{ij} \log \frac{\mu}{M} \right) \bar{c}_j(M), \quad (5.52)$$

where γ_{ij} is the anomalous dimension matrix (computed at leading order in the SM couplings). The \hat{S} parameter gets a correction $\Delta\hat{S} = (\bar{c}_W(m_Z) + \bar{c}_B(m_Z))\xi$, and one has $\gamma_{W,H} + \gamma_{B,H} = -g_2^2/(96\pi^2)$. An additional contribution to the running arises from insertions of the current-current operators

$$O_{Hq} = \frac{i}{v^2} \bar{q}_L \gamma^\mu q_L H^\dagger \overleftrightarrow{D}_\mu H, \quad O'_{Hq} = \frac{i}{v^2} \bar{q}_L \gamma^\mu \sigma^i q_L H^\dagger \sigma^i \overleftrightarrow{D}_\mu H, \quad O_{Ht} = \frac{i}{v^2} \bar{t}_R \gamma^\mu t_R H^\dagger \overleftrightarrow{D}_\mu H \quad (5.53)$$

in a loop of top quarks. This is however suppressed by a factor y_L^2/g_*^2 compared to Eq. (5.49) and will be neglected. The suppression arises because the current-current operators are generated at the matching scale with coefficients proportional to y_L^2 .

The total correction to the \widehat{S} parameter in our model is $\Delta\widehat{S} = \Delta\widehat{S}_\rho + \Delta\widehat{S}_h$, with the two contributions given by eqs. (5.48) and (5.49).

5.4.2 \widehat{T} parameter

Tree-level contributions to the \widehat{T} parameter are forbidden in our model by the $SO(3)$ custodial symmetry preserved by the strong dynamics, and can only arise via loops involving the elementary states. A non-vanishing effect arises at the 1-loop level corresponding to a violation of custodial isospin by two units. The leading contribution comes from loops of fermions and is proportional to y_L^4 , given that the spurionic transformation rule of y_L is that of a doublet, while y_R is a singlet. We find:

$$\Delta\widehat{T}_\Psi = a_{UV} N_c \frac{y_L^2}{16\pi^2} \frac{y_L^2 v^2}{M_\Psi^2} + a_{IR} N_c \frac{y_t^2}{16\pi^2} \frac{y_L^2 v^2}{M_\Psi^2} \log \frac{M_1^2}{m_t^2}, \quad (5.54)$$

where $a_{UV,IR}$ are $O(1)$ coefficients whose values are reported in Appendix J and we have defined $M_1 \equiv \sqrt{M_S^2 + y_R^2 f^2}$. The result is finite and does not depend on the cutoff scale m_* . The first term corresponds to the UV threshold correction generated at the scale $\mu = M_1 \sim M_\Psi$. The second term instead encodes the IR running from the threshold scale down to low energy, due to loops of top quarks. In the effective theory below M_1 it corresponds to the RG evolution of the dimension-6 operator

$$O_T = \frac{1}{2v^2} (H^\dagger \overleftrightarrow{D}^\mu H)^2 \quad (5.55)$$

due to insertions of the current-current operators of Eq. (5.53). In particular, $\Delta\widehat{T} = \widehat{c}_T(m_Z)\xi$ and one has $\gamma_{T,Ht} = -\gamma_{T,Hq} = 3y_t^2/4\pi^2$, $\gamma_{T,Hq'} = 0$. Notice that the size of the second contribution with respect to the first is $O[(y_t/y_L)^2 \log(M_1^2/m_t^2)]$: for $y_t \sim y_L$, that is for fully composite t_R , the IR dominated contribution is formally logarithmically enhanced and dominant.

Further contributions to \widehat{T} come from loops of spin-1 resonances, the exchange of cutoff modes and Higgs compositeness. The latter is due to the modified couplings of the composite Higgs to vector bosons and reads [102]:

$$\Delta\widehat{T}_h = -\frac{3g_1^2}{64\pi^2} \xi \log \frac{m_*^2}{m_h^2}. \quad (5.56)$$

In the effective theory it corresponds to the running of O_T due to the insertion of the operator O_H in a loop with hypercharge. The contribution is of the form of Eq. (5.52) with $\gamma_{T,H} = 3g_1^2/32\pi^2$. The exchange of spin-1 resonances gives a UV threshold correction which is also proportional to g_1^2 (as a spurion, the hypercharge coupling transforms as an isospin triplet), but without any log enhancement. It is thus subleading compared to Eq. (5.56) and we will neglect

it for simplicity (see ref. [111] for the corresponding computation in the context of $SO(5)/SO(4)$ models). Finally, we also omit the effect of the cutoff modes because it is incalculable, although naively this is of the same order as the contribution from states included in our simplified model. Our result is thus subject to an $O(1)$ uncertainty.

The total contribution to the \hat{T} parameter in our model is therefore $\Delta\hat{T} = \Delta\hat{T}_h + \Delta\hat{T}_\Psi$ with the two contributions given by eqs. (5.54) and (5.56).

5.4.3 δg_{Lb}

In the limit of vanishing transferred momentum, tree-level corrections to δg_{Lb} are forbidden by the P_{LR} parity of the strong dynamics that exchanges $SU(2)_L$ with $SU(2)_R$ in the visible $SO(4)$ and $\widetilde{SU}(2)_L$ with $\widetilde{SU}(2)_R$ in the twin $\widetilde{SO}(4)$ (see Appendix A for details). This is a simple extension of the P_{LR} symmetry of CH models which protects the $Zb\bar{b}$ coupling from large corrections [39]. In our case P_{LR} is an element of the unbroken $SO(7)$ and keeps the vacuum unchanged. It is thus an exact invariance of the strong dynamics, differently from $SO(5)/SO(4)$ models where it is accidental at $O(p^2)$. The gauge couplings $g_{1,2}$ and y_L explicitly break it, while y_R preserves it. At finite external momentum δg_{Lb} gets a non-vanishing tree-level contribution:

$$(\delta g_{Lb})_{\text{tree}} = \frac{f^2 \xi}{8M_\rho^2} [g_1^2(\alpha_L + \alpha_{7L}) - g_2^2 \alpha_L] \frac{y_L^2 f^2}{M_\Psi^2 + y_L^2 f^2}. \quad (5.57)$$

In the effective theory below M_1 , this correction arises from the dimension-6 operators

$$O_{Bq} = \frac{g'}{m_W^2} \partial^\mu B_{\mu\nu} \bar{q}_L \gamma^\nu q_L, \quad O_{Wq} = \frac{g}{m_W^2} D^\mu W_{\mu\nu}^a \bar{q}_L \gamma^\nu \sigma^a q_L. \quad (5.58)$$

It is of order $(y_L^2/g_*^2)(g^2/g_*^2)\xi$, hence a factor g^2/g_*^2 smaller than the naive expectation in absence of the P_{LR} protection.

At the 1-loop level, corrections to δg_{Lb} arise from the virtual exchange of heavy fermion and vector states. The leading effect comes at $O(y_L^4)$ from loops of heavy fermions (the corresponding diagrams are those of figs. J.2 and J.3) and reads

$$(\delta g_{Lb})_\Psi = \frac{y_L^2}{16\pi^2} N_c \frac{y_L^2 v^2}{M_\Psi^2} \left(b_{UV} + c_{UV} \log \frac{m_*^2}{M_\Psi^2} \right) + b_{IR} \frac{y_t^2}{16\pi^2} N_c \frac{y_L^2 v^2}{M_\Psi^2} \log \frac{M_1^2}{m_t^2}. \quad (5.59)$$

The expressions of the $O(1)$ coefficients $b_{UV,IR}$ and c_{UV} are reported in Appendix J. The first term is logarithmically divergent and encodes the UV threshold correction at the matching scale. The divergence comes, in particular, from diagrams where the fermion loop is connected to the b -quark current through the exchange of a spin-1 resonance [108]. A simple operator

analysis shows that the threshold contribution from the vector resonances in the adjoint of $SO(7)$ identically vanishes in our model (see Appendix I for details). An additional UV threshold contribution to δg_{Lb} arises from diagrams where the spin-1 resonances circulate in the loop. For simplicity we will not include such effect in our analysis (see ref. [110] for the corresponding computation in the context of $SO(5)/SO(4)$ models). It is however easy to show that there is no possible diagram with ρ_X circulating in the loop as a consequence of its quantum numbers, while the corresponding contribution from vector resonances in the adjoint of $SO(7)$ is non-vanishing in this case.

The second term in Eq. (5.59) accounts for the IR running down to the electroweak scale. In the effective theory below M_1 one has $\delta g_{Lb} = -(\bar{c}_{Hq}(m_Z) + \bar{c}'_{Hq}(m_Z))/2$, hence the IR correction arises from the evolution of the operators O_{Hq} and O'_{Hq} due to loops of top quarks. In this case the operators that contribute to the running via their 1-loop insertion are those of Eq. (5.53) as well as the following four-quark operators [25]:

$$O_{LR} = (\bar{q}_L \gamma^\mu q_L) (\bar{t}_R \gamma_\mu t_R), \quad O_{LL} = (\bar{q}_L \gamma^\mu q_L) (\bar{q}_L \gamma_\mu q_L), \quad O'_{LL} = (\bar{q}_L \sigma^a \gamma^\mu q_L) (\bar{q}_L \sigma^a \gamma_\mu q_L). \quad (5.60)$$

In fact, the operators contributing at $O(y_L^2 y_t^2)$ to Eq. (5.52) are only those generated at $O(y_L^2)$ at the matching scale; these are O_{Ht} , the linear combination $O_{Hq} - O'_{Hq}$ (even under P_{LR}), and O_{LR} (generated via the exchange of ρ_X).¹⁵ Notice finally that the relative size of the IR and UV contributions to δg_{Lb} is $O[(y_t/y_L)^2 \log(M_1^2/m_t^2)]$ precisely like in the case of $\Delta \hat{T}_\Psi$.

It is interesting that in our model the fermionic corrections to δg_{Lb} and \hat{T} are parametrically of the same order and their signs tend to be correlated. It is for example well known that a heavy fermion with the quantum numbers of t_R gives a positive correction to both quantities [105–107, 109]. We have verified that this is also the case in our model for $M_S \ll M_\Psi \sim M_\rho$ (light singlet).¹⁶ Conversely, a light septuplet ($M_\Psi \ll M_S \sim M_\rho$) gives a negative contribution to both δg_{Lb} and \hat{T} .¹⁷ Although in general the expressions for $\Delta \hat{T}_\Psi$ and $(\delta g_{Lb})_\Psi$ are uncorrelated, their signs tend to be the same whenever the contribution from ρ_X to Eq. (5.59) is subleading. When also the operator O_{Ht} is not generated at the scale m_* , the two observables are exactly correlated and one can show that $a_{IR} = b_{IR}$ (see Appendix H for a detailed discussion of this point). The sign correlation can instead be broken if ρ_X contributes significantly to δg_{Lb} (in particular, $(\delta g_{Lb})_\Psi$ can be negative for $\alpha_{iL} = -\alpha_{iR}$). The importance of the above considerations lies in the fact that EW precision data prefer a positive \hat{T} and a negative δg_{Lb} . Situations when both quantities have the same sign are thus experimentally disfavored.

¹⁵The operators O_{LL} and O'_{LL} are generated at $O(y_L^4)$ by the tree-level exchange of both ρ_X and ρ .

¹⁶In this limit one has $\Delta \hat{T}_\Psi \simeq 3(\delta g_{Lb})_\Psi$.

¹⁷The existence of a similar sign correlation in the limit of a light (2,2) has been pointed out in the context of $SO(5)/SO(4)$ CH models, see ref. [108].

Considering that no additional correction to δg_{Lb} arises from Higgs compositeness, and that we neglect as before the incalculable effect due to cutoff states, the total contribution in our model is $\delta g_{Lb} = (\delta g_{Lb})_{\text{tree}} + (\delta g_{Lb})_{\Psi}$, with the two contributions given by eqs. (5.57) and (5.59).

5.5 Results

We are now ready to translate the prediction for the Higgs mass and the EWPO into bounds on the parameter space of our simplified model and for the composite TH in general. We are interested in quantifying the degree of fine tuning that our construction suffers when requiring the mass scale of the heavy fermions to lie above the ultimate experimental reach of the LHC. As made evident by the discussion in section 2, the parameter region where the TH mechanism boosts this scale up without increasing the fine tuning of the Higgs mass corresponds to a fully strongly coupled QFT where no quantitatively precise EFT description is allowed. Our computations of physical quantities in this most relevant regime should then be interpreted as an *educated Naive Dimensional Analysis* (eNDA) estimate, where one hopes to capture the generic size of effects beyond the naivest 4π counting, and including factors of a few related to multiplet size, to spin and to numerical accidents. In the limit where M_ρ/f and M_Ψ/f are significantly below their perturbative upper bound our computations are well defined. eNDA then corresponds to assuming that the results do not change by more than $O(1)$ (i.e. less than $O(5)$ to be more explicit) when extrapolating to a scenario where the resonance mass scale sits at strong coupling. In practice we shall consider the resonant masses up to their perturbativity bound and vary the α_i and c_i within an $O(1)$ range¹⁸. In view of the generous parameter space that we shall explore our analysis should be viewed as conservative, in the sense that a realistic TH model will never do better.

Let us now describe the various pieces of our analysis. Consider first the Higgs potential where the dependence on physics at the resonance mass scale is encapsulated in the function F_1 (Eq. (5.35)) which controls the UV threshold correction to the Higgs quartic. It is calculable in our simplified model and the result is $O(1)$ (its expression is reported in Eq. (G.4)), but it can easily be made a bit smaller at the price of some mild tuning by varying the field content or the representations of the heavy fermions. In order to account for these options and thus broaden the scope of our analysis we will thus treat F_1 as a free $O(1)$ parameter. The value of F_1 has a direct impact in determining the size of the left-handed top mixing y_L , since $\delta m_h^2|_{UV} \sim y_L^4 F_1$, and controls the interplay between the Higgs potential and EWPO. Specifically, as we already stressed, a smaller F_1 implies a larger value of y_L , which in turn gives a larger $\Delta \hat{T} \propto y_L^4 v^2 / M_\Psi^2$: this can help improve the compatibility with the EWPT even for large M_Ψ . Of course that is at the cost of a mild additional tuning, both considering the need for a clever maneuver in the

¹⁸Notice indeed that $(\alpha = 1, c = 0)$ and $(\alpha = 0, c = 1/\sqrt{2})$ correspond to specific limits at weak coupling, respectively the two-site model and the linear sigma model. This suggests that their natural range is $O(1)$.

\hat{S}, \hat{T} plane to get back into the ellipse and the fact that F is generically expected to be $O(1)$. In the following we will thus treat F_1 as an input parameter and use eqs. (5.35) and (5.41) to fix y_L and y_R in terms of the Higgs and top quark experimental masses. Our final results will be shown for two different choices of F_1 , namely $F_1 = 1$ and $F_1 = 0.3$, in order to illustrate how the bounds are affected by changing the size of the UV threshold correction to the Higgs potential.

The EWPO and the Higgs mass computed in the previous sections depend on several parameters, in particular on the mass spectrum of resonances (see Appendix F), the parameters c_i, α_i of eqs. (5.25), (5.30), and the parameter F_1 discussed above. In order to focus on the situation where resonances can escape detection at the LHC, we will assume that their masses are all comparable and that they lie at or just below the cutoff scale. In order to simplify the numerical analysis we thus set $M_\Psi = M_S = \widetilde{M}_\Psi = \widetilde{M}_S = M_\rho = M_{\rho^x} = m_*/2$. The factor of two difference between M_Ψ and m_* is chosen to avoid all UV logarithms of the form $\log(m_*/M_\Psi)$ to vanish, while preventing the appearance of artificially large enhancements. As a further simplification we set $c_L = c_R \equiv c$, $\alpha_{7L} = \alpha_{1L}$ and $\alpha_{7R} = \alpha_{1R}$. The parameter α_L appears only in the tree-level contribution to δg_{Lb} , see Eq. (5.57), and we fix it equal to 1 for simplicity. Even though the above parameter choices represent a significant reduction of the whole available parameter space, for the purpose of our analysis they represent a sufficiently reach set where EWPT can be successfully passed.

Let us now discuss the numerical bounds on the parameter space of our simplified model. They have been obtained by fixing the top and Higgs masses to their experimental value and performing the numerical fit described in Appendix K. As experimental inputs, we use the PDG values of the top quark pole mass $m_t = 173.21 \pm 0.51 \pm 0.71$ (see footnote 10), and of the Higgs mass, $m_h = 125.09 \pm 0.24 \text{ GeV}$ [100]. Figure 5.3 shows the results of the fit in the (M_Ψ, ξ) plane for $F_1 = 0.3$ (left panel) and $F_1 = 1$ (right panel). In both panels we have set $c = 0$, which corresponds to the two-site model limit of our simplified Lagrangian. The yellow regions correspond to the points that pass the χ^2 test at 95% confidence level (CL), see Appendix K for details. Solid black contours denote the regions for which $\alpha_{1L} = -\alpha_{1R} = 1$, while dashed contours surround the regions obtained with $\alpha_{1L} = \alpha_{1R} = 1$. The areas in blue are theoretically inaccessible. The lower left region in dark blue, in particular, corresponds to $M_\Psi/f \equiv g_\Psi < y_L$. The upper dark and light blue regions correspond instead to points violating the perturbative limits on g_Ψ given by respectively Eq. (5.31) with $N = 8$ and Eq. (5.32) with $N_f = 24$ (see section 5.2.2 for a discussion). The difference between these two regions can be taken as an indication of the uncertainty related to such perturbative bound.

In the left panel of figure 5.3 the allowed (lighter yellow) region extends up to $\xi \simeq 0.2$ for masses M_Ψ in the 2 – 3 TeV range. Values of ξ so large are possible in this case because the fermionic contribution $\Delta \hat{T}_\Psi$ turns out to be positive and sufficiently large to compensate for both the negative $\Delta \hat{T}_h$ in Eq. (5.56) and the positive $\Delta \hat{S}_\rho$ and $\Delta \hat{S}_h$ in eqs. (5.48), (5.49). For larger M_Ψ

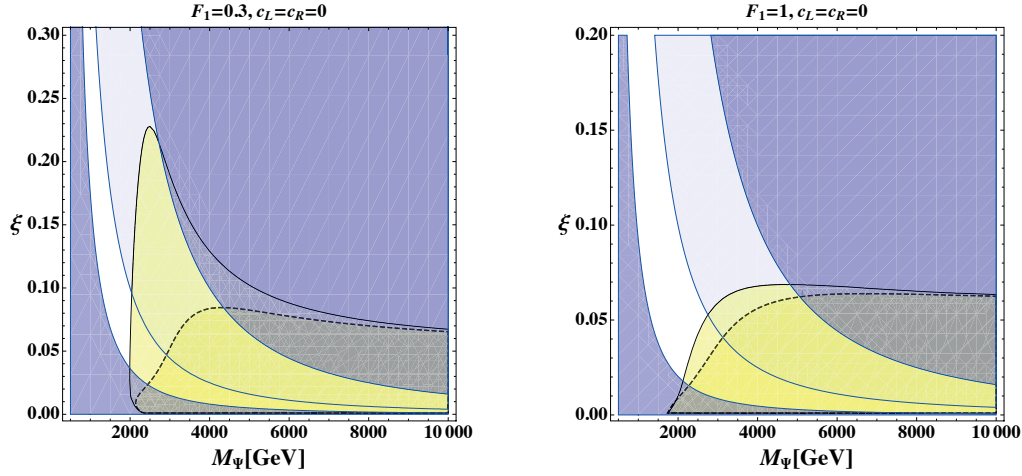


Figure 5.3 – Allowed regions in the (M_Ψ, ξ) plane for $F_1 = 0.3$ (left panel) and $F_1 = 1$ (right panel). See the text for an explanation of the different regions and of the choice of parameters.

the fermionic contribution $\Delta \hat{T}_\Psi$ becomes too small and such compensation fails. In this case, however, the strongest bound comes from the perturbativity limit (blue region), which makes points with large M_Ψ at fixed ξ theoretically inaccessible. Notice that large values of ξ become excluded if one considers the choice $\alpha_{1L} = \alpha_{1R} = 1$ leading to the dashed contour. The large difference between the solid and dashed curves (i.e. lighter and darker yellow regions) depends on the sign correlation between $\Delta \hat{T}_\Psi$ and δg_{Lb} . In the case of the solid line, the two parameters turn out to be anti-correlated (e.g. positive $\Delta \hat{T}_\Psi$ and negative δg_{Lb}), allowing for the compensation effect by $\Delta \hat{T}_\Psi$. In the case of the dashed line, instead, the signs of the two parameters are correlated (both positive), so that when $\Delta \hat{T}_\Psi$ is large, δg_{Lb} is also large and positive. This makes it more difficult to pass the χ^2 test, since data prefer a negative δg_{Lb} .

In the right panel of figure 5.3, obtained with $F_1 = 1$, the allowed yellow region shrinks because the larger value of F_1 implies a smaller y_L hence a smaller $\Delta \hat{T}_\Psi$. In this case the χ^2 test is passed only for $\xi < 0.06$, and the difference between the solid and dashed lines is small since the large and positive $\Delta \hat{S}$ always dominates the fit. Masses M_Ψ larger than ~ 5 TeV are excluded by the perturbative bound, unless one considers smaller values of ξ .

The results of figure 5.3 can significantly change if the parameter c is allowed to be different from zero. In particular, as one can verify from our formulae in Appendix J, positive values of c increase $\Delta \hat{T}$ and as a result the allowed regions in figure 5.3 shift to the right towards larger values of M_Ψ . In this case the perturbative bound excludes a large portion of the region passing the χ^2 test. The effect of varying c is illustrated by figure 5.4, which shows the 95% CL allowed regions in the plane (c, α) for $F_1 = 0.3$ (left panel) and $F_1 = 1$ (right panel). In both panels we have set $\alpha \equiv \alpha_{1L} = -\alpha_{1R}$ (ensuring positive $\Delta \hat{T}_\Psi$ and negative δg_{Lb}). The yellow,

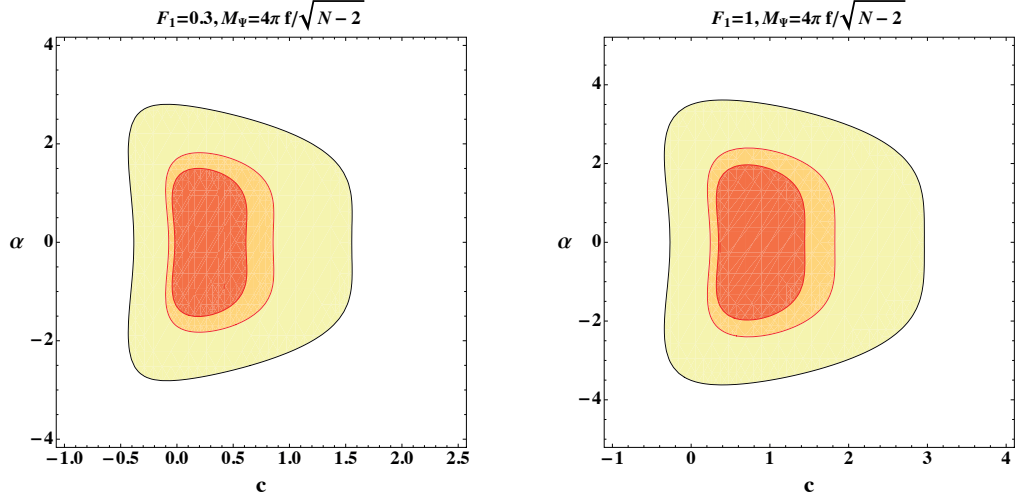


Figure 5.4 – Allowed regions in the (c, α) plane, with $c = c_L = c_R$, for $F_1 = 0.3$ (left panel) and $F_1 = 1$ (right panel). The yellow, orange and red regions correspond to $\xi = 0.05, 0.1$ and 0.15 respectively. See the text for an explanation of the choice of the other parameters.

orange and red regions are obtained respectively for $\xi = 0.05$, $\xi = 0.1$ and $\xi = 0.15$, with the masses of the resonances fixed at their perturbative upper bound $M_\rho = M_\Psi = 4\pi f/\sqrt{N-2}$ which for $N = 8$ gives respectively $\sim 6/4/3.2$ TeV. Notice that when increasing the value of F_1 , which corresponds to reducing y_L , the allowed region shifts towards positive values of c . As already mentioned, this is because for smaller y_L a larger positive value of c is needed to get a large enough $\Delta\hat{T}_\Psi$. Obviously, larger values of ξ correspond to smaller allowed regions, as already clear from figure 5.3. Finally, notice that the vertically symmetric structure of the allowed regions is due to the quadratic dependence of δg_{Lb} on α . From these plots, one can see that for resonances conceivably out of direct LHC reach and for $\xi \sim 0.1$, corresponding to about 20% tuning of the Higgs mass, both α and c are allowed to span a good fraction of their expected $O(1)$ range. No dramatic extra tuning in these parameters seems therefore needed to meet the constraints of EWPT. In particular, considering the plot for $F_1 = 1$ (at the right), one notices that the bulk of the allowed region is at positive c . For instance by choosing $c \sim 0.2 - 0.5$ the plot in the (ξ, M_Ψ) plane for $F_1 = 1$ becomes quite similar to the one at the left of figure 3 valid for $F_1 = 0.3$: there exists a “peak” centered at $M_\Psi \sim 2 - 4$ TeV and extending up to $\xi \sim 0.2$. The specific choice $c = 0$ is thus particularly reductive for $F_1 = 1$ (right panel of figure 5.3), but this reduction disappears for positive c . Overall we conclude that for $\xi \sim 0.1$ and for resonances a bit above safe LHC reach, the correct value of the Higgs quartic can be obtained and EWPT passed with only a mild additional tuning associated with a sign correlation $\alpha_{1L} = -\alpha_{1R}$, and a correlation between c and F_1 (ex. $c > 0$ for $F_1 = 1$). These correlations allow for compensation among the various contributions to \hat{T} and δg_{Lb} : it is clear that EWPT are not passed beautifully, but they are passed. If forced to quote an extra

figure of tuning we could say it is about $1/4 = (1/2) \times (1/2)$, given about $1/2$ of the plausible choices for both α_i and c_i are allowed.

5.6 Discussion

In this Chapter we tried to assess how plausible a scenario yielding no new particles at the LHC can be provided using the TH construction. We distinguished three possible classes of models: sub-hypersoft, hypersoft and super-hypersoft, with increasing degree of technical complexity and decreasing (technical) fine tuning. We then focused on the CH incarnation of the simplest option, the sub-hypersoft scenario. The marriage of twinning and compositeness is practically obligatory, especially as concerns sub-hypersoft models, where the boost factor for the mass of colored partners (Eq. (5.8)) at fixed tuning is roughly given by

$$\frac{g_*}{\sqrt{2}y_t} \times \frac{1}{\sqrt{\ln(m_*/m_t)}} \quad (5.61)$$

and hence the gain rests entirely on the relative coupling strength $g_*/\sqrt{2}y_t$. We attempted a more precise estimate of the upper bound on $g_*/\sqrt{2}y_t$, as compared with previous studies (e.g. Ref. [118]). We found, by independent but consistent estimates based on a toy sigma model (Section 5.1.1) and on a simplified CH model (Section 5.2.2), that the upper bound ranges between ~ 3 , in Eq. (5.10), and ~ 5 , in Eq. (5.31). These numbers are somewhat below the NDA estimate $4\pi \sim 12$. Consequently for a mild tuning $\epsilon \sim 0.1$ the upper bound on the mass of the resonances with SM quantum numbers is closer to the 3 – 5 TeV range than it is to 10 TeV. This gain, despite being less spectacular than naively expected, is still sufficient to push these states out of direct reach of the LHC, at the cost of resorting to full strong coupling. One practical implication of this is that, unlike in ordinary CH models, there is no real computational gain in considering holographic realizations: the boost factor is controlled by the KK coupling, and in the most interesting region the KK coupling is strong and the whole 5D description breaks down. In this situation an explicit 5D construction, such as the ones studied in Refs. [120, 121] for instance, would be just as good as our simplified model when used to obtain rough numerical estimates, but may not be pushed further. Indeed, using a simplified model, we have checked that EWPT can be satisfied in a sizable portion of parameter space, given some interplay among the various contributions. In particular the IR corrections to \hat{T} and \hat{S} are enhanced by $\ln(m_*/m_h)$, and for $\xi > 0.1$ the compensating contribution to \hat{T} , which decreases like $1/m_*^2$, is necessary. Given that perturbativity limits m_* to be below 5 TeV for $\xi > 0.1$ (see the upper blue exclusion region in Fig. 5.3) this compensation in EWPT can still take place at the price of a moderate extra tuning. For ξ of order a few percent on the other hand, EWPT would be passed without any additional tuning, while the masses of SM-charged resonances would be pushed up to the 10 TeV range, where nothing less than a

100 TeV collider would be required to discover them, and barely so [36, 101].

Although EWPT work similarly in the CH and composite TH frameworks, the two are crucially different when it comes to contributions to the Higgs quartic. In the CH these are enhanced when g_* , i.e. m_*/f , is strong and, as discussed for instance in Ref. [7], in order to avoid additional tuning of the Higgs quartic, g_* cannot be too strong. According to the study in Refs. [30, 34] the corresponding upper bound on the mass of the colored top partners in CH reads roughly $m_*/f \lesssim 1.5$, which should be compared to the upper bound $m_*/f \lesssim 5$ from strong coupling we found in Eq. (5.31). The Higgs quartic protection operated by the TH mechanism allows us to take m_*/f as large as possible, allowing the colored partners to be heavier at fixed f , hence at fixed fine tuning ξ . In the end the gain is about a factor of $5/1.5 \sim 3$, not impressive, but sufficient to place the colored partners outside of LHC reach at moderate tuning $\xi \sim 0.1$.

Finally, we comment on the classes of models not covered in this Chapter: the hypersoft and super-hypersoft scenarios. The latter requires combining supersymmetry and compositeness with the TH mechanism, which, while logically possible, does not correspond to any existing construction. Such a construction would need to be rather ingenious, and we currently do not feel compelled to provide it, given the already rather epicyclic nature of the TH scenario. The simpler hypersoft scenario, though also clever, can by contrast be implemented in a straightforward manner, via e.g. a tumbling $SO(9) \rightarrow SO(8) \rightarrow SO(7)$ pattern of symmetry breaking. The advantage of this approach is that it allows us to remain within the weakly-coupled domain, due to the presence of a relatively light twin Higgs scalar mode σ , whose mass can be parametrically close to that of the twin tops, $\sim y_t f$ (around 1 TeV for $\xi \sim 0.1$). As well as giving rise to distinctive experimental signatures due to mixing with the SM Higgs [103], the mass of the light σ acts as a UV cut-off for the IR contributions to \hat{S} and \hat{T} in Eqs. (5.49) and (5.56) [137]. For sufficiently light σ then, less or no interplay between the various contributions is required in order to pass EWPT. Together with calculability, this property singles out the hypersoft scenario as one of the more promising TH constructions.

6 Conclusion

In this thesis, we explored two different roads to stabilize the EW scale against quantum radiative corrections. The first, more conventional possibility is a natural extension of the SM endowed with a protection mechanism to dynamically explain the lightness of the Higgs particle. Along this direction, we analyzed Composite Higgs models, theories that conceive the Higgs as a bound state of a new strongly interacting dynamics which is not concerned by any problem of hierarchies. As an example, we constructed the minimal scenario with a $SO(5)/SO(4)$ coset and studied in detail the phenomenology of heavy vector resonances. In order to both have a light Higgs and comply with precision tests, we naturally expect that the spectrum of this class of models is characterized by two different scales, a lower one related to the top partner mass and a higher one for the composite spin-1 resonances. These latter are assumed to be heavier, due to the constraints from \hat{S} parameter measurements, with a mass of ~ 2 TeV. We presented a recast of the LHC direct searches of new heavy vectors and translated the experimental data into bounds on the parameter space of the minimal CH model. Interestingly enough, this procedure offers a re-interpretation of the existing measurements as a test of the notion of naturalness and as a mean of quantifying how natural the Higgs sector is expected to be. We found that several portions of parameter space are already excluded by the combination of direct and indirect constraints and that naturalness should have a quite elusive character in composite extensions of the SM, due to the apparent difficulty to detect any new state at the LHC, be that a top partner or a vector.

Motivated by the rising tension between experiments and theoretical expectations, we studied a second more elaborate road which implies that the particles responsible for making the Higgs light are uncolored and therefore almost un-discoverable at the LHC. This is the general paradigm of neutral naturalness, which can be efficiently incarnated in the Twin Higgs scenario. We presented a general UV completion of the original model into a composite setting and we gave an effective low-energy description of its features, showing that, differently from what we could have expected, the TH symmetry protection mechanism cannot automatically be

uplifted to the UV theory. Using symmetry and selection rules, one can easily show that the original symmetry breaking pattern cannot protect the Higgs from large quadratic corrections due to loops of heavy composite resonances, contributions which are sizable and as important as those arising from the loops of elementary particles considered in the original model. The minimal possibility for a consistent realization of the Twin Higgs paradigm into a composite theory is to have a $SO(8)/SO(7)$ spontaneous symmetry breaking coset which is the basic ingredient of the Composite Twin Higgs (CTH) model introduced in this thesis. We also explored the implications of a strongly interacting UV completion of the TH on the cut-off scale of the theory, namely the energy scale where the SM-charged resonances are expected. One could naively imagine that, due to the strongly coupled nature of the CTH, the parametric gain in fine-tuning granted by the TH mechanism can be maximized so as to push m_* far up in the UV, to values of order ~ 10 TeV, as we saw in Chapter 3. This conclusion would also be supported by an exact computation of the Higgs boson mass in these scenarios. We carried out this estimate up to three loops order in Chapter 4 and found with a model-independent procedure that a 125 GeV Higgs can be easily reproduced in TH theories only with RG effects if m_* reaches 10 – 20 TeV. For lower values of the cut-off, the experimental measurement can be predicted with an increasingly bigger, but still in a natural $\mathcal{O}(1)$ range, UV correction, which makes the result more dependent on the specific higher energy physics. Despite the naive estimate that m_* may be pushed way out of the LHC reach, however, a closer inspection to the properties of CTH models shows that several requirements bring the cut-off scale much closer to the TeV threshold. A first obvious observation is related to the perturbativity of the effective field theory construction under scrutiny: since the CTH is strongly interacting, any computation is valid only in the window of parameter space where the strong coupling is small enough to allow a perturbative treatment. Roughly, we expect the perturbative limit to be

$$g_* \lesssim \frac{4\pi}{\sqrt{N}}, \quad (6.1)$$

where N specifies the symmetry breaking pattern $SO(N)/SO(N-1)$. Since the coset $SO(8)/SO(7)$ demands the existence of big multiplets which are invariant under the global symmetry, the coupling is constrained to be no bigger than $g_* \sim 4$, pointing towards a less promising scenario. The scale $m_* \sim g_* f$, in fact, must lie at ~ 5 TeV, still out of the LHC reach but making this model falsifiable and therefore discoverable in a future post-LHC machine. Another important requirement, the agreement with EWPT, was extensively analyzed showing that lighter top partners are nevertheless required also in CTH constructions to compensate the large negative correction to the \hat{T} parameter due to the compositeness of the Higgs particle. In general, light fermionic resonances must be present already at ~ 2 TeV, in this case not because of their role to cancel the large quadratic contributions to the Higgs mass term, but because of their positive enhancement of the \hat{T} parameter. This result furthermore confirms that, even though the CTH construction may escape detection at the present 14 TeV machine, it will

definitely be testable at a future 100 TeV collider.

An interesting question remains open to further future investigations, namely whether it is possible to discover neutral naturalness and probe CTH models already at the LHC and with the center of mass energy at our disposal. One possibility would be to find a striking evidence of the uncolored mirror states, which are a necessary element of any theory incarnating neutral naturalness. The light colorless top partners are, however, way more difficult to produce at the LHC than their colored version in natural theories. The twin partners can be generated through the mixing between the Higgs and its mirror, which exists as a consequence of the TH mechanism to stabilize the EW scale. This results in a Higgs portal production: the colliding protons emit a Higgs which mixes, even modestly, with a heavier singlet, this latter decaying to uncolored resonances. The production rate is expected to be small and the final states would evade detection, appearing only as missing transverse energy, thus posing difficulties for a clear LHC detection. Another possibility would be the discovery of the heavier twin Higgs, a SM-neutral scalar singlet. Again, this direction does not seem to be the best strategy: this kind of particles have low cross-sections and may be too wide to appear as a resonance. Furthermore, they are present in many other extensions of the SM, so that a potential discovery of a heavy scalar with properties similar to the Higgs does not necessarily confirm the TH constructions.

A more interesting alternative exists to make the neutral natural scenario falsifiable at the LHC, namely the production of twin gluons hadronizing into meta-stable bound states which can decay into SM particles. The mirror glueballs thus formed may decay preferentially to SM states because in most of the realistic neutral natural scenarios they are expected to be the lightest hadronic compounds in the twin sector. Cosmological considerations, in fact, suggests that, if the twin quarks were lighter compared to the mirror QCD confinement scale, than an unacceptably big contribution to the dark radiation would be generated, see for instance [140, 142]. Given the present constraints on the effective number of neutrino species due to the Planck collaboration [143], $N_{eff} = 3.2 \pm 0.5$, the existence of new light species is severely constrained. We can avoid any difficulty by supposing that the Z_2 symmetry breaking, necessary to give rise to the right amount of EWSB, takes place in the Yukawa sector of the theory, so that the twin quarks are much heavier than the twin QCD confinement scale. In the early universe, the SM and its mirror are in equilibrium and interact with each other through the Higgs portal, so that they have the same temperature. At some decoupling temperature T_d , the interaction between the two sectors becomes inefficient and they evolve independently; the twin particles eventually decay into dark photons and neutrinos giving an extra contribution to the dark radiation. To satisfy the present bound, the SM colored states should generate the usual effective number of degrees of freedom, but their twin counterparts should contribute very little to the number of mirror degrees of freedom. This can happen

if the twin quarks are heavy with respect to the twin QCD confinement scale and the strong phase transition is purely gluonic, differently to the case of the SM [142]. In this condition, TH models can evade the bound on N_{eff} and provide a realistic cosmology, implying at the same time that the lightest hadronic states must be the glueballs. The production of this latter mirror hadron at the LHC would finally generate striking confining hidden valley signatures, discussed for instance in [137]. As an example, we can think about a gluon fusion process that generates a Higgs through top loops; the SM Higgs mixes with its heavier mirror, which can decay into twin gluons through a loop of twin fermions. The branching fraction for this event is around 0.1%. After production, the twin gluons hadronize forming glue-balls; most of them will escape detection again as missing transverse energy, but the lightest state has the right quantum numbers to mix with the Higgs and decay back to SM particles, which can be detected at the LHC. The detection of the decay products of this light twin hadron depends on the glue-ball mass. If it is very heavy, its decay is fast and its production rate through the Higgs mixing may be too rare to be significantly observed. For lower masses, instead, the lightest glue-ball can have a bigger lifetime, so that its decay is displaced with respect to the interaction point. The displaced vertex decay may provide a good signature at the LHC, capable of compensating the low production rate and give un-disputable proof of the mirror gluon states. Overall, this scenario would offer the possibility to probe TH theories and similar models before the advent of a futuristic collider. The precise implications of displaced vertex decays and consequent hidden valley phenomenology require a better understanding of both the experimental methods of detection and a precise theoretical estimate of twin glue-ball production rates in Higgs decay, which is complicated due to our poor understanding of hadronization, especially in the mirror sector. A complete assessment of the LHC coverage of neutral natural models requires therefore deeper studies on the experimental as well as on the theoretical side. Our brief discussion shows, however, that, although seeming very elaborate constructions to provide a last refuge to the naturalness paradigm, Twin Higgs theories and their UV-completions may provide a falsifiable alternative for physics at the EW scale.

Whether realized as a conventional extension with colored new light resonances or as a neutral theory with only uncolored states at the TeV scale, naturalness remains the most important paradigm to expect and model new physics at the LHC. Its role as a leading principle for particle physics may be disputed and new approaches may be needed in the future to revitalize our understanding of nature at its deepest structural level and to understand the very concrete possibility of no discoveries contradicting the SM at the intensity frontier. The upcoming experimental data collected in the second run of the LHC are therefore of crucial importance to understand to what extent naturalness or neutral naturalness can be realistic paradigms for high energy physics, fueling our quest for a deep understanding of matter at its most fundamental level.

A CCWZ variables

In this Appendix, we give some details about the CCWZ construction and generators for both the $SO(5)/SO(4)$ and $SO(8)/SO(7)$ cosets. We refer to [9] and [10] for a detailed analysis of this procedure and we closely follow [7] and [118] for establishing our notation.

A.1 CCWZ construction for the $SO(5)/SO(4)$ coset

We indicate with $T^{\hat{a}}$ ($\hat{a} = 1, \dots, 4$) the broken generators parametrizing the coset $SO(5)/SO(4)$ and with T^{a_L/a_R} ($a_L/a_R = 1, 2, 3$) the $SO(4)$ unbroken generators, whose expressions can be found in [7]. The 5×5 Goldstone boson matrix, $U(\Pi) = e^{i\sqrt{2}/f\Pi^{\hat{a}}T^{\hat{a}}}$, has the following form in the unitary gauge:

$$U = \left(\begin{array}{c|cc} \mathbb{I}_3 & & \\ \hline & \cos\left(\theta + \frac{h}{f}\right) & \sin\left(\theta + \frac{h}{f}\right) \\ & -\sin\left(\theta + \frac{h}{f}\right) & \cos\left(\theta + \frac{h}{f}\right) \end{array} \right), \quad (\text{A.1})$$

with the $d_{\mu}^{\hat{a}}$, $E_{\mu}^{a_L}$ and $E_{\mu}^{a_R}$ variables defined by the relation:

$$-iU^{\dagger}D_{\mu}U = d_{\mu}^{\hat{a}}T^{\hat{a}} + E_{\mu}^{a_L}T_L^{a_L} + E_{\mu}^{a_R}T^{a_R}. \quad (\text{A.2})$$

D_{μ} is the SM covariant derivative containing the elementary gauge fields,

$$D_{\mu} = \partial_{\mu} - ig_{el}\frac{W_{\mu}^i}{2}\sigma^i - ig'_{el}YB_{\mu}, \quad (\text{A.3})$$

where $i = 1, 2, 3$ and σ^i are the Pauli matrices.

The d and E symbols, on the other hand, can be easily computed once $U(\Pi)$ is known; up to

Appendix A. CCWZ variables

quadratic order in the unitary gauge their expression is given by:

$$\begin{aligned} d_\mu^{\hat{a}} &= A_\mu^{\hat{a}} + \frac{\sqrt{2}}{f} \partial_\mu h + \frac{\sqrt{2}}{2f} h (\delta^{a_L \hat{a}} A_\mu^{a_L} - \delta^{a_R \hat{a}} A_\mu^{a_R}), \\ E_\mu^{a_L} &= A_\mu^{a_L} - \delta^{a_L \hat{a}} \frac{\sqrt{2}}{2f} h A_\mu^{\hat{a}}, \\ E_\mu^{a_R} &= A_\mu^{a_R} - \delta^{a_R \hat{a}} \frac{\sqrt{2}}{2f} h A_\mu^{\hat{a}}, \end{aligned} \quad (\text{A.4})$$

where we have defined the Kronecker $\delta^{\hat{a}i}$, for a generic index $i = 1, 2, 3$, as:

$$\delta^{i\hat{a}} = \begin{cases} 1 & \text{if } \hat{a} = i \\ 0 & \text{if } \hat{a} \neq i \end{cases} \quad \text{or} \quad \hat{a} = 4.$$

The external gauge fields appearing in the formulae for the d and E symbols, for a given value of the angle θ , have the following forms:

$$\begin{aligned} A_\mu^{\hat{a}} &= \frac{\sin \theta}{\sqrt{2}} (\delta^{\hat{a}i} g_{el} W_\mu^i - \delta^{\hat{a}3} g'_{el} B_\mu), \quad A_\mu^{\hat{4}} = 0, \\ A_\mu^{a_L} &= \delta^{a_L i} \left(\frac{1 + \cos \theta}{2} \right) g_{el} W_\mu^i + \delta^{a_L 3} \left(\frac{1 - \cos \theta}{2} \right) g'_{el} B_\mu, \\ A_\mu^{a_R} &= \delta^{a_R i} \left(\frac{1 - \cos \theta}{2} \right) g_{el} W_\mu^i + \delta^{a_R 3} \left(\frac{1 + \cos \theta}{2} \right) g'_{el} B_\mu, \end{aligned} \quad (\text{A.5})$$

where g_{el} and g'_{el} are the weak coupling of the elementary sector.

Under a global transformation $g \in SO(5)$, the Goldstone boson matrix transforms as:

$$U(\Pi) \rightarrow g U(\Pi) h^\dagger(\Pi, g), \quad (\text{A.6})$$

where $h(\Pi, g) \in SO(4)$. As a consequence of Eq. (A.2), the previous relation implies the following transformation rules for d and E :

$$\begin{aligned} d_\mu^{\hat{a}} &\rightarrow h(\Pi, g) d_\mu^{\hat{a}} h^\dagger(\Pi, g) \\ E_\mu^{a_{L/R}} &\rightarrow h(\Pi, g) E_\mu^{a_{L/R}} h^\dagger(\Pi, g) - i h(\Pi, g) \partial_\mu h^\dagger(\Pi, g), \end{aligned} \quad (\text{A.7})$$

showing that both these variables transform under a local $SO(4)$ symmetry when acted upon with g . Since in particular $E_\mu^{a_{L/R}}$ behaves like a gauge field under $h(\Pi, g)$, we can introduce the covariant derivative

$$\nabla_\mu = \partial_\mu - i E_\mu^{a_L} T^{a_L} - i E_\mu^{a_R} T^{a_R} \quad (\text{A.8})$$

and a field strength

$$\begin{aligned} E_{\mu\nu}^{L/R} &= \partial_\mu E_\nu^{L/R} - \partial_\nu E_\mu^{L/R} + i[E_\mu^{L/R}, E_\nu^{L/R}] \\ E_{\mu\nu}^{L/R} &\rightarrow h(\Pi, g) E_{\mu\nu}^{L/R} h^\dagger(\Pi, g), \end{aligned} \tag{A.9}$$

where $E_\mu^{L/R} = E_\mu^{a_{L/R}} T^{a_{L/R}}$.

A.2 CCWZ construction for the $SO(8)/SO(7)$ coset

We define now the generators of the $SO(8)$ algebra and describe the $SO(8)/SO(7)$ symmetry breaking pattern, introducing the CCWZ variables for this coset.

Generators and Σ matrix

We start by listing the twenty-eight generators of $SO(8)$ decomposing them into irreducible representations of the unbroken subgroup $SO(7)$, $\mathbf{28} = \mathbf{7} \oplus \mathbf{21}$. They can compactly be written as:

$$(T_{ij})_{kl} = \frac{i}{\sqrt{2}} (\delta_{ik} \delta_{jl} - \delta_{il} \delta_{jk}), \tag{A.10}$$

with $i, j, k, l = 1, \dots, 8$. The seven broken generators transform in the $\mathbf{7}$ of $SO(7)$ and they can be chosen to be the following ones:

$$(T_a^7)_{\beta\gamma} = \frac{i}{\sqrt{2}} (\delta_{8\beta} \delta_{a\gamma} - \delta_{8\gamma} \delta_{a\beta}), \tag{A.11}$$

with $\alpha = 1 \dots 7$ and $\beta, \gamma = 1, \dots, 8$. With this choice, the vacuum expectation value for the spontaneous breaking of the approximate global symmetry points in the direction:

$$v = f(0, 0, 0, 0, 0, 0, 0, 1)^t. \tag{A.12}$$

The remaining unbroken generators transform in the ad-joint representation of $SO(7)$; we collectively call them:

$$(T_{\alpha\beta}^{21})_{\gamma\rho} = \frac{i}{\sqrt{2}} (\delta_{\alpha\gamma} \delta_{\beta\rho} - \delta_{\alpha\rho} \delta_{\beta\gamma}), \tag{A.13}$$

with $\alpha, \beta = 1 \dots 7$ and $\gamma, \rho = 1 \dots, 8$.

The generators that are gauged in the Twin Higgs model are obtained by taking linear combinations of the broken and unbroken ones in order to reconstruct the orthogonal subgroups $SO(4) \sim SU(2)_L \times SU(2)_R$ and $\widetilde{SO}(4) \sim \widetilde{SU}(2)_L \times \widetilde{SU}(2)_R$ contained in $SO(8)$. We choose them

Appendix A. CCWZ variables

to be

$$(T_{\mathbf{L}})^\alpha = \begin{pmatrix} T_{\mathbf{L}}^\alpha & 0 \\ 0 & 0 \end{pmatrix}, (T_{\mathbf{R}})^\alpha = \begin{pmatrix} T_{\mathbf{R}}^\alpha & 0 \\ 0 & 0 \end{pmatrix}, (\tilde{T}_{\mathbf{L}})^\alpha = \begin{pmatrix} 0 & 0 \\ 0 & T_{\mathbf{L}}^\alpha \end{pmatrix}, (\tilde{T}_{\mathbf{R}})^\alpha = \begin{pmatrix} 0 & 0 \\ 0 & T_{\mathbf{R}}^\alpha \end{pmatrix}, \quad (\text{A.14})$$

where $T_{\mathbf{L}}^\alpha$ and $T_{\mathbf{R}}^\alpha$ are the 4×4 generators of $SO(4)$:

$$(T_{\mathbf{L},\mathbf{R}}^\alpha)_{ij} = -\frac{i}{2} \left[\frac{1}{2} \epsilon^{\alpha\beta\gamma} (\delta_i^\beta \delta_j^\gamma - \delta_j^\beta \delta_i^\gamma) \pm (\delta_i^\alpha \delta_j^4 - \delta_j^\alpha \delta_i^4) \right] \quad (\text{A.15})$$

with $\alpha = 1, \dots, 3$ and $i, j = 1, \dots, 4$.

The spontaneous breaking of $SO(8)$ to $SO(7)$ delivers seven Goldstone bosons, that we collect in the vector $\Pi = (\pi_1, \dots, \pi_7)^t$. They can be arranged in the Goldstone matrix in the usual way,

$$\Sigma(\Pi) = e^{i \frac{\sqrt{2}}{f} \Pi \cdot T^7} = \begin{pmatrix} \mathbb{I}_7 - \frac{\Pi \Pi^t}{\Pi^t \cdot \Pi} \left(1 - \cos \left(\frac{\sqrt{\Pi^t \cdot \Pi}}{f} \right) \right) & \frac{\Pi}{\sqrt{\Pi^t \cdot \Pi}} \sin \left(\frac{\sqrt{\Pi^t \cdot \Pi}}{f} \right) \\ -\frac{\Pi}{\sqrt{\Pi^t \cdot \Pi}} \sin \left(\frac{\sqrt{\Pi^t \cdot \Pi}}{f} \right) & \cos \left(\frac{\sqrt{\Pi^t \cdot \Pi}}{f} \right) \end{pmatrix}; \quad (\text{A.16})$$

this latter transforms non-linearly under the action of an $SO(8)$ group element, g , according to the standard relation:

$$\Sigma(\Pi) \rightarrow g \cdot \Sigma(\Pi) \cdot h^\dagger(\Pi, g), \quad (\text{A.17})$$

where $h(\Pi, g) \in SO(7)$ and implicitly depends on the global group transformation. We choose the Higgs particle to be the Goldstone boson aligned with the generator T_4^7 ; in the unitary gauge, all the remaining Goldstones are non-propagating fields and the Π vector becomes

$$\Pi = (0, \dots, H = \langle h \rangle + h, \dots, 0), \quad (\text{A.18})$$

so that the Σ matrix simplifies to:

$$\Sigma(\Pi) = e^{i \frac{\sqrt{2}}{f} H T_4^7} = \begin{pmatrix} \mathbb{I}_3 & 0 & 0 & 0 \\ 0 & \cos \frac{H}{f} & 0 & \sin \frac{H}{f} \\ 0 & 0 & \mathbb{I}_3 & 0 \\ 0 & -\sin \frac{H}{f} & 0 & \cos \frac{H}{f} \end{pmatrix}. \quad (\text{A.19})$$

The CCWZ variables

We introduce now the d_μ and E_μ symbols of the $SO(8)/SO(7)$ coset structure. The external weak gauging of the $SU(2)_L \times U(1)_{R_3}$ subgroup of $SO(4)$ introduces the SM vector bosons, whereas the external weak gauging of the $\widetilde{SU}(2)_L$ subgroup of $\widetilde{SO}(4)$ serves for the analogous description of their Twin counterparts. As a consequence, the covariant derivative can be

written as:

$$D_\mu = \partial_\mu - i A_\mu^A T^A, \quad (\text{A.20})$$

with

$$A_\mu^A T^A = g_2 W_\mu^\alpha (T_L)^\alpha + g_1 B_\mu (T_R)^3 + \tilde{g}_2 \tilde{W}_\mu^\alpha (\tilde{T}_L)^\alpha, \quad (\text{A.21})$$

where g_2 , g_1 and \tilde{g}_2 are the gauge couplings corresponding the the three different gauged subgroups. The CCWZ symbols are consequently derived through the Maurer-Cartan form,

$$\Sigma^\dagger(\Pi) D_\mu \Sigma(\Pi) = i d_\mu^i(\Pi) T_i^7 + i E_\mu^a(\Pi) T_a^{21}, \quad (\text{A.22})$$

with d_μ^i and E_μ^a corresponding respectively to the decomposition of this latter under the broken and unbroken generators of the global group $SO(8)$. It can be shown that these two symbols transform under $SO(8)$ following the rules of a local $SO(7)$ transformation,

$$d_\mu \equiv d_\mu^i T_i^7 \rightarrow h(\Pi, g) d_\mu h^\dagger(\Pi, g), \quad E_\mu \equiv E_\mu^a T_a^{21} \rightarrow h(\Pi, g) (E_\mu - i \partial_\mu) h^\dagger(\Pi, g), \quad (\text{A.23})$$

where g and h are the group elements previously defined.

The d_μ and E_μ terms are in general a function of all the seven Goldstone bosons which are present in our model. We report here their simplified expression in the unitary gauge after EWSB:

$$d_\mu = - \begin{pmatrix} \frac{g_2}{\sqrt{2}} \left(\sqrt{\xi} + \frac{h}{f} \sqrt{1-\xi} \right) W_\mu^1 \\ \frac{g_2}{\sqrt{2}} \left(\sqrt{\xi} + \frac{h}{f} \sqrt{1-\xi} \right) W_\mu^2 \\ \frac{1}{\sqrt{2}} \left(\sqrt{\xi} + \frac{h}{f} \sqrt{1-\xi} \right) (g_2 W_\mu^3 - g_1 B_\mu) \\ -\sqrt{2} \frac{\partial_\mu h}{f} \\ \frac{\tilde{g}_2}{\sqrt{2}} \left(\sqrt{1-\xi} - \frac{h}{f} \sqrt{\xi} \right) \tilde{W}_\mu^1 \\ \frac{\tilde{g}_2}{\sqrt{2}} \left(\sqrt{1-\xi} - \frac{h}{f} \sqrt{\xi} \right) \tilde{W}_\mu^2 \\ \frac{\tilde{g}_2}{\sqrt{2}} \left(\sqrt{1-\xi} - \frac{h}{f} \sqrt{\xi} \right) \tilde{W}_\mu^3 \end{pmatrix}, \quad (\text{A.24})$$

and

$$E_\mu = -i \begin{pmatrix} E_\mu^1 & 0_{3 \times 3} \\ 0_{3 \times 3} & E_\mu^2 \end{pmatrix}, \quad (\text{A.25})$$

Appendix A. CCWZ variables

with

$$E_\mu^1 = \begin{pmatrix} 0 & \frac{1}{2}(-g_2 W_\mu^3 - B_\mu g_1) & \frac{1}{2}g_2 W_\mu^2 & \frac{(h\sqrt{\xi} - f\sqrt{1-\xi})g_2 W_\mu^1}{2f} \\ \frac{1}{2}(g_2 W_\mu^3 + B_\mu g_1) & 0 & -\frac{1}{2}g_2 W_\mu^1 & \frac{(h\sqrt{\xi} - f\sqrt{1-\xi})g_2 W_\mu^2}{2f} \\ -\frac{1}{2}g_2 W_\mu^2 & \frac{1}{2}g_2 W_\mu^1 & 0 & \frac{(h\sqrt{\xi} - f\sqrt{1-\xi})(g_2 W_\mu^3 - B_\mu g_1)}{2f} \\ \frac{(f\sqrt{1-\xi} - h\sqrt{\xi})g_2 W_\mu^1}{2f} & \frac{(f\sqrt{1-\xi} - h\sqrt{\xi})g_2 W_\mu^2}{2f} & \frac{(f\sqrt{1-\xi} - h\sqrt{\xi})(g_2 W_\mu^3 - B_\mu g_1)}{2f} & 0 \end{pmatrix} \quad (\text{A.26})$$

and

$$E_\mu^2 = \begin{pmatrix} 0 & -\frac{(\sqrt{\xi}f + h\sqrt{1-\xi})\tilde{g}_2 \tilde{W}_\mu^1}{2f} & -\frac{(\sqrt{\xi}f + h\sqrt{1-\xi})\tilde{g}_2 \tilde{W}_\mu^2}{2f} & -\frac{(\sqrt{\xi}f + h\sqrt{1-\xi})\tilde{g}_2 \tilde{W}_\mu^3}{2f} \\ \frac{(\sqrt{\xi}f + h\sqrt{1-\xi})\tilde{g}_2 \tilde{W}_\mu^1}{2f} & 0 & -\frac{1}{2}\tilde{g}_2 \tilde{W}_\mu^3 & \frac{1}{2}\tilde{g}_2 \tilde{W}_\mu^2 \\ \frac{(\sqrt{\xi}f + h\sqrt{1-\xi})\tilde{g}_2 \tilde{W}_\mu^2}{2f} & \frac{1}{2}\tilde{g}_2 \tilde{W}_\mu^3 & 0 & -\frac{1}{2}\tilde{g}_2 \tilde{W}_\mu^1 \\ \frac{(\sqrt{\xi}f + h\sqrt{1-\xi})\tilde{g}_2 \tilde{W}_\mu^3}{2f} & -\frac{1}{2}\tilde{g}_2 \tilde{W}_\mu^2 & \frac{1}{2}\tilde{g}_2 \tilde{W}_\mu^1 & 0 \end{pmatrix}. \quad (\text{A.27})$$

In the previous formulae, we have explicitly introduced the fine-tuning parameter ξ , which is related to the EW scale ν and the Higgs VEV f by the usual relation

$$\xi = \left(\frac{\nu}{f}\right)^2 = \sin^2\left(\frac{\langle h \rangle}{f}\right); \quad (\text{A.28})$$

we can then obviously identify $\frac{\langle h \rangle}{f}$ with the misalignment angle between the direction of the vector ν , Eq.(A.12), and the preferred orientation in the coset space induced by the external gauging.

We finally consider how to write down an effective Lagrangian description for composite fermions, Ψ , in the CCWZ notation. These latter can be classified according to the representation of the unbroken group $SO(7)$ they belong to. Under the non-linearly realized global $SO(8)$ they therefore transform as

$$\Psi \rightarrow h(\Pi, g)\Psi, \quad (\text{A.29})$$

so that in order to write an invariant kinetic term we must introduce the covariant derivative

$$\nabla_\mu \Psi = (\partial_\mu + i E_\mu)\Psi. \quad (\text{A.30})$$

B Heavy vector contribution to the Electroweak Precision Observables

In this Appendix, we briefly study the contribution to the Electroweak Precision Observables generated by integrating out at tree level the vectors in our models. In general, the deviations from the SM in the vector boson vacuum polarization amplitudes can be described by four effective form factors: \hat{S} , \hat{T} , W and Y . New physics contributions to the four parameters can be expressed as a function of the Wilson coefficients of the leading dimension-6 operators obtained by integrating out the BSM sector. If the BSM sector respects the custodial symmetry, as in the case of the minimal composite Higgs model, \hat{T} is vanishing and we are left with the remaining three oblique parameters. In the SILH basis, [24], \hat{S} comes from the linear combination of $O_W + O_B$, W and Y on the other hand are generated by O_{2W} and O_{2B} respectively. In order to get the Wilson coefficients of these dimension-6 operators, we integrate out the ρ resonances using the EOM at $O(p^3)$:

$$\rho_\mu^{a_L/a_R} = E_\mu^{a_L/a_R} - \frac{1}{M_{\rho_{L/R}}^2} \nabla_\mu E^{a_L/a_R \mu\nu} + O(p^5), \quad \rho_\mu^X = B_\mu - \frac{\partial_\mu B^{\mu\nu}}{M_{\rho_X}^2} + O(p^5); \quad (\text{B.1})$$

we have to keep up to three derivative terms in the EOM, because the operators O_{2W} and O_{2B} include six derivatives according to the SILH power counting (gauge fields count as one derivative). Once evaluated on the equation of motions, we obtain from the \mathcal{L}_ρ term in Eqs. (2.14), (2.30), (2.36), the following low-energy Lagrangian:

$$\begin{aligned} \mathcal{L}_6 = & -\frac{1}{4g_{\rho_L}^2} (E_{\mu\nu}^{a_L})^2 - \frac{1}{4g_{\rho_R}^2} (E_{\mu\nu}^{a_R})^2 - \frac{1}{4g_{\rho_X}^2} B^{\mu\nu} B_{\mu\nu} - \frac{1}{2} \frac{1}{M_{\rho_L}^2 g_{\rho_L}^2} \nabla_\mu E^{a_L \mu\nu} \nabla_\rho E^{a_L \rho}_\nu \\ & - \frac{1}{2} \frac{1}{M_{\rho_R}^2 g_{\rho_R}^2} \nabla_\mu E^{a_R \mu\nu} \nabla_\rho E^{a_R \rho}_\nu - \frac{1}{2} \frac{1}{M_{\rho_X}^2 g_{\rho_X}^2} \partial_\mu B^{\mu\nu} \partial_\rho B^\rho_\nu + \dots, \end{aligned} \quad (\text{B.2})$$

where the dots imply terms more than quadratic in the field strength and with at least four partial derivatives. The first two terms will give rise to O_W and O_B and the last two terms will instead lead to O_{2W} , O_{2B} . To see this explicitly, we rewrite the formulae for the E_μ connections

Appendix B. Heavy vector contribution to the Electroweak Precision Observables

in terms of the Higgs current; the relevant terms are

$$\begin{aligned} E_\mu^{a_L} &= \delta^{a_L i} g_{el} W_\mu^i + \frac{i}{f^2} H^\dagger \frac{\sigma^a}{2} \overleftrightarrow{D}_\mu H + \dots, \\ E_\mu^{3_R} &= g'_{el} B_\mu + \frac{i}{f^2} H^\dagger \frac{1}{2} \overleftrightarrow{D}_\mu H + \dots, \end{aligned} \quad (\text{B.3})$$

and, after substituting in B.2, we get:

$$\begin{aligned} \mathcal{L}_6 &= \frac{ig}{g_{\rho_L}^2 f^2} H^\dagger \frac{\sigma^a}{2} \overleftrightarrow{D}^\mu H D^\nu W_{\mu\nu}^a + \frac{ig'}{g_{\rho_R}^2 f^2} H^\dagger \frac{1}{2} \overleftrightarrow{D}_\mu H \partial_\nu B^{\mu\nu} - \frac{1}{2} \frac{g^2}{g_{\rho_L}^2 M_{\rho_L}^2} D^\mu W_{\mu\nu}^a D_\rho W^{a\rho\nu} \\ &\quad - \frac{1}{2} \frac{g'^2}{g_{\rho_R}^2 M_{\rho_R}^2} \partial^\mu B_{\mu\nu} \partial_\rho B^{\rho\nu} - \frac{1}{2} \frac{g'^2}{g_{\rho_X}^2 M_{\rho_X}^2} \partial^\mu B_{\mu\nu} \partial_\rho B^{\rho\nu}. \end{aligned} \quad (\text{B.4})$$

From the previous formulae, we can immediately find the expression of the three oblique parameters:

$$\hat{S} = c_W + c_B = a_{\rho_L}^2 \frac{m_W^2}{M_{\rho_L}^2} + a_{\rho_R}^2 \frac{m_W^2}{M_{\rho_R}^2}, \quad W = \frac{g^2 m_W^2}{g_{\rho_L}^2 M_{\rho_L}^2}, \quad Y = \frac{g'^2 m_W^2}{g_{\rho_R}^2 M_{\rho_R}^2} + \frac{g'^2 m_W^2}{g_{\rho_X}^2 M_{\rho_X}^2}. \quad (\text{B.5})$$

C Heavy vector couplings

In this Appendix, we give some technical details on the structure of the Lagrangian in the mass eigenstate basis, for the case of a heavy vector triplet and a heavy vector singlet. We will focus on trilinear interactions, neglecting for simplicity the quartic vertices.

We start considering the Lagrangian of a vector triplet with top partners in the fourplet, \mathcal{L}_ρ^T . Without making explicit reference to the representation under which the spin-1 resonances fall, we can rewrite in full generality the Lagrangian after rotation to the mass eigenstate basis as a set of three fields, the charged ρ_μ^\pm and the neutral ρ_μ^0 , interacting with the SM particles and the top partners. The couplings between the heavy vectors and the other bosons and fermions are in general a function of all the free parameters of the theory and they explicitly depend on the model under consideration; we will name them $g_{\rho^+ ij}$, for the couplings of the charged pair, and $g_{\rho^0 ij}$, for the couplings of the neutral state, where i and j generically stand for two particles the resonance interacts with. We can therefore introduce the following decomposition for \mathcal{L}_ρ^T :

$$\mathcal{L}_\rho^T = \mathcal{L}_{gbh}^T + \mathcal{L}_{ef}^T + \mathcal{L}_{tb}^T + \mathcal{L}_{TPtb}^T + \mathcal{L}_{TP}^T, \quad (\text{C.1})$$

where \mathcal{L}_{gbh}^T contains the interactions between the ρ 's and the gauge bosons and between the ρ 's, the Higgs and a gauge boson, whereas \mathcal{L}_{ef}^T , \mathcal{L}_{tb}^T , \mathcal{L}_{TPtb}^T and \mathcal{L}_{TP}^T comprise, respectively, the couplings of the spin-1 heavy states to fully elementary fermions, to top and bottom quarks, to one top partner and one heavy quarks and finally to two top partners. It is straightforward to derive the form of the different contributions in the mass eigenstate basis and in the unitary

Appendix C. Heavy vector couplings

gauge; we find:¹

$$\begin{aligned}\mathcal{L}_{gbh}^T = & i g_{\rho^0 WW} \left[(\partial_\mu W_\nu^+ - \partial_\nu W_\mu^+) W^{\mu-} \rho^{0\nu} + \frac{1}{2} (\partial_\mu \rho_\nu^0 - \partial_\nu \rho_\mu^0) W^{\mu+} W^{\nu-} + \text{h.c.} \right] \\ & + i g_{\rho^+ WZ} \left[(\partial_\mu \rho_\nu^+ - \partial_\nu \rho_\mu^+) W^{\mu-} Z^\nu - (\partial_\mu W_\nu^- - \partial_\nu W_\mu^-) \rho^{\mu+} Z^\nu \right. \\ & \left. + (\partial_\mu Z_\nu - \partial_\nu Z_\mu) \rho^{\mu+} W^{\nu-} + \text{h.c.} \right] + g_{\rho^0 ZH} h \rho_\mu^0 Z^\mu + g_{\rho^+ WH} (h \rho_\mu^+ W_\mu^- + \text{h.c.}),\end{aligned}\quad (\text{C.2})$$

$$\begin{aligned}\mathcal{L}_{ef}^T = & \frac{1}{\sqrt{2}} g_{\rho^+ ffL} (\rho_\mu^+ \bar{\psi}_u \gamma^\mu P_L \psi_d + \text{h.c.}) \\ & + \rho_\mu^0 \bar{\psi}_u \gamma^\mu \left[\frac{1}{2} (g_{\rho^0 ffL} - g_{\rho^0 ffY}) P_L + g_{\rho^0 ffY} Q[\psi_u] \right] \psi_u \\ & + \rho_\mu^0 \bar{\psi}_d \gamma^\mu \left[-\frac{1}{2} (g_{\rho^0 ffL} - g_{\rho^0 ffY}) P_L + g_{\rho^0 ffY} Q[\psi_d] \right] \psi_d,\end{aligned}\quad (\text{C.3})$$

$$\begin{aligned}\mathcal{L}_{tb}^T = & \frac{1}{\sqrt{2}} g_{\rho^+ tb} (\rho_\mu^+ \bar{t}_L \gamma^\mu b_L + \text{h.c.}) \\ & + g_{\rho^0 t_L t_L} \rho_\mu^0 \bar{t}_L \gamma^\mu t_L + g_{\rho^0 t_R t_R} \rho_\mu^0 \bar{t}_R \gamma^\mu t_R + g_{\rho^0 b_L b_L} \rho_\mu^0 \bar{b}_L \gamma^\mu b_L,\end{aligned}\quad (\text{C.4})$$

$$\begin{aligned}\mathcal{L}_{TPtb}^T = & \frac{1}{\sqrt{2}} \left[\rho_\mu^+ \left(g_{\rho^+ T_L b_L} \bar{T}_L \gamma^\mu b_L + g_{\rho^+ X_{\frac{2}{3}L} b_L} \bar{X}_{\frac{2}{3}L} \gamma^\mu b_L + g_{\rho^+ B_L t_L} \bar{t}_L \gamma^\mu B_L \right. \right. \\ & \left. + g_{\rho^+ X_{\frac{5}{3}L} t_L} \bar{X}_{\frac{5}{3}L} \gamma^\mu t_L + g_{\rho^+ B_R t_R} \bar{t}_R \gamma^\mu B_R + g_{\rho^+ X_{\frac{5}{3}R} t_R} \bar{X}_{\frac{5}{3}R} \gamma^\mu t_R \right) + \text{h.c.} \left. \right] \\ & + \rho_\mu^0 \left(g_{\rho^0 T_L t_L} \bar{T}_L \gamma^\mu t_L + g_{\rho^0 X_{\frac{2}{3}L} t_L} \bar{X}_{\frac{2}{3}L} \gamma^\mu t_L + g_{\rho^0 B_L b_L} \bar{B}_L \gamma^\mu b_L \right. \\ & \left. + g_{\rho^0 T_R t_R} \bar{T}_R \gamma^\mu t_R + g_{\rho^0 X_{\frac{2}{3}R} t_R} \bar{X}_{\frac{2}{3}R} \gamma^\mu t_R + \text{h.c.} \right),\end{aligned}\quad (\text{C.5})$$

$$\begin{aligned}\mathcal{L}_{TP}^T = & \frac{1}{\sqrt{2}} \left[\rho_\mu^+ \left(g_{\rho^+ T_L B_L} \bar{T}_L \gamma^\mu B_L + g_{\rho^+ X_{\frac{2}{3}L} B_L} \bar{X}_{\frac{2}{3}L} \gamma^\mu B_L + g_{\rho^+ X_{\frac{5}{3}L} T_L} \bar{X}_{\frac{5}{3}L} \gamma^\mu T_L \right. \right. \\ & \left. + (L \leftrightarrow R) + g_{\rho^+ X_{\frac{5}{3}L} X_{\frac{2}{3}L}} \bar{X}_{\frac{5}{3}L} \gamma^\mu X_{\frac{2}{3}L} \right) + \text{h.c.} \left. \right] \\ & + \rho_\mu^0 \left(g_{\rho^0 T_L T_L} \bar{T}_L \gamma^\mu T_L + g_{\rho^0 X_{\frac{2}{3}L} T_L} (\bar{X}_{\frac{2}{3}L} \gamma^\mu T_L + \text{h.c.}) + g_{\rho^0 B_L B_L} \bar{B}_L \gamma^\mu B_L + (L \leftrightarrow R) \right. \\ & \left. + g_{\rho^0 X_{\frac{2}{3}L} X_{\frac{2}{3}L}} \bar{X}_{\frac{2}{3}L} \gamma^\mu X_{\frac{2}{3}L} + g_{\rho^0 X_{\frac{5}{3}L} X_{\frac{5}{3}L}} \bar{X}_{\frac{5}{3}L} \gamma^\mu X_{\frac{5}{3}L} \right).\end{aligned}\quad (\text{C.6})$$

We make some comments on the parametrization chosen in the previous formulae. As regards the couplings to fully elementary fermions, we have collectively indicated with ψ_u (ψ_d) any

¹All interaction terms between SM fermions and spin-1 resonances in this Lagrangian are flavor diagonal. This follows from assuming that all the lightest fermions are fully elementary: in absence of elementary-composite fermion mixings one can always make fields rotations to diagonalize the fermionic kinetic terms in flavor space. By allowing for some degrees of compositeness for leptons and the first two quark families and thus for non-vanishing elementary-composite couplings λ , the Lagrangian C.1 is valid up to $O(\lambda)$ in the weak interaction eigenbasis for the fermions. In this basis the fermion masses are not diagonal in flavor space. After rotating the fermion fields to diagonalize the mass matrices, a V_{CKM} matrix appear in the vertex $\rho_\mu^+ \bar{\psi}_u \psi_d$, while the interactions of ρ^0 remain diagonal.

of the SM up-type quarks and neutrinos (down-type quarks and charged leptons) and we have introduced their charge through the function $Q[\psi_u]$ ($Q[\psi_d]$). The form chosen for \mathcal{L}_{ef}^T is convenient for the implementation of the models in a `Mathematica` code, since the couplings to different kinds of leptons and quarks can be easily and unambiguously derived from the universal functions $g_{\rho^{+10}ffL}$ and $g_{\rho^{+10}ffY}$. The top-bottom doublet and the t_R are instead treated differently, as seen in equation C.4; we introduce specific couplings for every vertex between the heaviest quarks and the spin-1 resonances, in order to take into account the enhancement in the interactions due to partial compositeness. Finally, in the last term of the Lagrangian, \mathcal{L}_{TP}^T , we have differentiated the couplings of the heavy vectors to left-handed and right-handed top partners, because they are in general expected to be different. The only exceptions are the interactions involving only the exotic $X_{\frac{5}{3}}$ and the top-like $X_{\frac{2}{3}}$, namely $g_{\rho^0 X_{\frac{2}{3}} X_{\frac{2}{3}}}$, $g_{\rho^0 X_{\frac{5}{3}} X_{\frac{5}{3}}}$ and $g_{\rho^+ X_{\frac{5}{3}} X_{\frac{2}{3}}}$; in this case the couplings to states of different chirality are equal since these $X_{5/3}$ top partner is left invariant by the rotation in the fermionic sector, whereas the $X_{2/3L}$ and $X_{2/3R}$ fields transforms in the same way under the fermionic rotation, [7].

We finally consider the Lagrangian for the singlets: a neutral vector resonance interacting with a fermionic heavy state, both being invariant under the unbroken $SO(4)$. The Lagrangian can be decomposed analogously to the previous formulae as:

$$\mathcal{L}_{\rho}^S = \mathcal{L}_{gbh}^S + \mathcal{L}_{ef}^S + \mathcal{L}_{tb}^S + \mathcal{L}_{TPtb}^S + \mathcal{L}_{TP}^S. \quad (C.7)$$

The first three terms have the same expressions as the Lagrangian for the neutral heavy state, ρ_{μ}^0 , in \mathcal{L}_{ρ}^T . The last two contributions can be instead easily rewritten after rotations to the mass eigenstate basis and specifically depend on the choice of the representation for the top partner; we find:

$$\mathcal{L}_{TPtb}^S = \rho_{\mu}^0 \left(g_{\rho^0 \tilde{T}_L t_L} \tilde{T}_L \gamma^{\mu} t_L + g_{\rho^0 \tilde{T}_R t_R} \tilde{T}_R \gamma^{\mu} t_R + \text{h.c.} \right), \quad (C.8)$$

$$\mathcal{L}_{TP}^S = \rho_{\mu}^0 \left(g_{\rho^0 \tilde{T}_L \tilde{T}_L} \tilde{T}_L \gamma^{\mu} \tilde{T}_L + g_{\rho^0 \tilde{T}_R \tilde{T}_R} \tilde{T}_R \gamma^{\mu} \tilde{T}_R \right). \quad (C.9)$$

As before, the couplings are a function of all the free input parameters of the theory and we find different expressions if the t_R is fully composite or only partially composite.

D Effects of a degenerate vector spectrum

In this Appendix, we clarify the phenomenological effects of relaxing the assumption that one vector resonance is much lighter and the other two belong to the tower of states that are integrated out. We want to analyse the possible consequences of having an almost degenerate spectrum and, for simplicity, we will not consider the most complicated case in which all the three heavy states are present together. We will only analyse, instead, the simpler situation in which two resonances are degenerate and the other one is heavier and is thus integrated out. We therefore introduce the three following cases,

$$\begin{aligned}
 \text{(I)} \quad & (\rho_L, \rho_R) \text{ with Lagrangian } \mathcal{L}_{L+R} = \mathcal{L}_{light} + \mathcal{L}_\Psi + \mathcal{L}_{\rho_L} + \mathcal{L}_{\rho_R}, \\
 \text{(II)} \quad & (\rho_L, \rho_X) \text{ with Lagrangian } \mathcal{L}_{L+X} = \mathcal{L}_{light} + \mathcal{L}_\Psi + \mathcal{L}_{\tilde{T}^1} + \mathcal{L}_{\rho_L} + \mathcal{L}_{\rho_X^1}, \\
 \text{(III)} \quad & (\rho_R, \rho_X) \text{ with Lagrangian } \mathcal{L}_{R+X} = \mathcal{L}_{light} + \mathcal{L}_\Psi + \mathcal{L}_{\tilde{T}^1} + \mathcal{L}_{\rho_R} + \mathcal{L}_{\rho_X^1};
 \end{aligned} \tag{D.1}$$

in all combinations the t_R quark arises as a singlet of the composite dynamics, so that we have considered only the interference with model \mathbf{M}_X^1 in (II) and (III).

When considering the degeneracy of the particle spectrum, there are different effects on our analysis of direct searches that we must take into account with respect to the situations studied in the main text. First of all, we expect that the expressions of the couplings in the mass eigenstate basis will be corrected and that the more degenerate the spectrum is, the stronger these corrections will be. Secondly, the branching ratios will change as well, due to the opening of new decay channels, a heavy-light one, with a vector resonance decaying to a second heavy vector and a gauge boson, and a heavy-heavy one, which involves a vector state decaying to other two heavy spin-1 resonances. These two classes of modifications could significantly alter the results concerning the bounds on the free parameters of our models; we will analyse them in the following, showing that considering only one resonance at a time and integrating out the other two is a good basic approximation for interpreting the experimental data.

Appendix D. Effects of a degenerate vector spectrum

Let us start considering how the couplings change in case (I). The spectrum now contains two charged and two neutral heavy vector particles. The mass matrix is given by a 3×3 charged block and a 4×4 neutral block, whose expressions is not reported here, but can be found in [52], where also some of the modified couplings in the mass eigenstate basis are given. Since the ρ_μ^R and ρ_μ^L resonances belong to different representations of the unbroken $SO(4)$, all the corrections to the couplings in Appendix C must arise after EWSB and are therefore suppressed. As a consequence, we do not expect that the degeneracy of the resonances masses will induce important differences on the branching ratios that have already been analysed in this work, so that no relevant modifications on the bounds can be induced by the changes in the couplings.

In case (II) and (III), on the other hand, one charged and two neutral vector resonances are present. The charged block of the mass matrix is not affected by the interference with the singlet, which mixes only with the B_μ boson, so that no modification is induced on the couplings of the charged vector. The neutral block, on the other hand, becomes now a 4×4 matrix and, after rotation to the mass eigenstate basis, the couplings of the neutral resonances will be indeed modified with respect to the situation considered in the main text. In particular, in model (II) these corrections must be suppressed by ξ , since ρ_μ^L mixes with B_μ only after EWSB, whereas in model (III) both ρ_R^3 and ρ^X mix with B_μ before EWSB, therefore inducing interference effects that can have important consequences on their phenomenology. We conclude that the approximate description adopted in the main text works well for case (II), even with a degenerate spectrum, whereas in case (III) the bounds and branching ratios should be corrected if the two resonances have comparable masses.

We now study more quantitatively the effects of the spectrum degeneracy on the branching ratios, analysing, as illustration, the cascade decay of one heavy vector to a second spin-1 resonance and a gauge boson. We want to estimate the branching ratio of this process in the three cases, so as to understand how much the decay widths analysed in this work can be altered by the opening of this new decay channel. From triple vector couplings in the kinetic terms of the Lagrangians in (D.1), an additional interaction between two heavy vectors is generated; we can write it as follows:

$$\begin{aligned} \mathcal{L}_{XYM} = & ig_{X^+Y^-M^0} [(\partial_\mu X_\nu^+ - \partial_\nu X_\mu^+) Y^{\mu-} M^{0\nu} - (\partial_\mu X_\nu^- - \partial_\nu X_\mu^-) Y^{\mu+} M^{0\nu} \\ & + (\partial_\mu Y_\nu^+ - \partial_\nu Y_\mu^+) X^{\mu-} M^{0\nu} - (\partial_\mu Y_\nu^- - \partial_\nu Y_\mu^-) X^{\mu+} M^{0\nu} \\ & + (\partial_\mu M_\nu^0 - \partial_\nu M_\mu^0)(X^{\mu+} Y^{\nu-} - X^{\mu-} Y^{\nu+})], \end{aligned} \quad (D.2)$$

when X is different from Y , and

$$\begin{aligned} \mathcal{L}_{XXM} = i g_{X^+ X^- M^0} [(\partial_\mu X_\nu^+ - \partial_\nu X_\mu^+) X^{\mu-} M^{0\nu} - (\partial_\mu X_\nu^- - \partial_\nu X_\mu^-) X^{\mu+} M^{0\nu} \\ + \frac{1}{2} (\partial_\mu M_\nu^0 - \partial_\nu M_\mu^0) (X^{\mu+} X^{\nu-} - X^{\mu-} X^{\nu+})], \end{aligned} \quad (\text{D.3})$$

when $X = Y$. We have indicated with X , Y and M any of $(W/Z, \rho^+, \rho_0)$. As a result, when one of the two vectors is relatively heavier than the other one, the channels $\rho_1^+ \rightarrow \rho_2^0 W^+$, $\rho_1^0 \rightarrow \rho_2^+ W^-$ and $\rho_1^+ \rightarrow \rho_2^+ Z$ open up (ρ_1 and ρ_2 stand for the vectors in different representations for each of the three cases considered). In order to illustrate the relevance of these cascade decays, we focus on the two following sets of benchmark values

$$\begin{aligned} (\text{I}) \quad m_{\rho_L} = 1.5 m_{\rho_R} = 1.5 g_{\rho_R} f, \quad g_{\rho_L} = g_{\rho_R} \equiv g_\rho, \\ (\text{III}) \quad m_{\rho_R} = 1.5 m_{\rho_X} = 1.5 g_{\rho_X} f, \quad g_{\rho_R} = g_{\rho_X} \equiv g_\rho, \end{aligned} \quad (\text{D.4})$$

and we show in Fig. (D.1) the relative branching ratios as a function of the resonant mass, for illustration, fixing to 1 all the $O(1)$ parameters controlling the couplings to top partners. The results in case (II) are very similar to case (I) and the corresponding branching ratios are not shown. We see that the branching ratios are very tiny for cases (I), due to the fact that the mixing between a charged and a neutral state or between two charged states belonging to different representation of H arises at $O(\xi)$ after EWSB. The situation is different for case (III); the branching ratio is now considerably bigger, even if the coupling between two different heavy vectors arises again at $O(\xi)$. This is a consequence of the small couplings of the charged right-handed resonance to SM fermions: since the branching ratios for its decay to both elementary and partially composite fermions are strongly suppressed, the decay channel to the lighter vector and a W boson is much more competitive. As expected, in case (III) the corrections to the branching ratios are therefore more important. However, these corrections will not have relevant consequences on the exclusion plots we derived in the main text. These latter are in fact obtained for the neutral right-handed vector which is not affected by the presence of the relatively lighter ρ_μ^X since no couplings involving two neutral heavy vectors can be induced in our models. We thus conclude that our estimate of the branching ratios and relative bounds on the parameter space of the models is a good approximation for all the resonances, even neglecting their possible degeneracy.

Appendix D. Effects of a degenerate vector spectrum

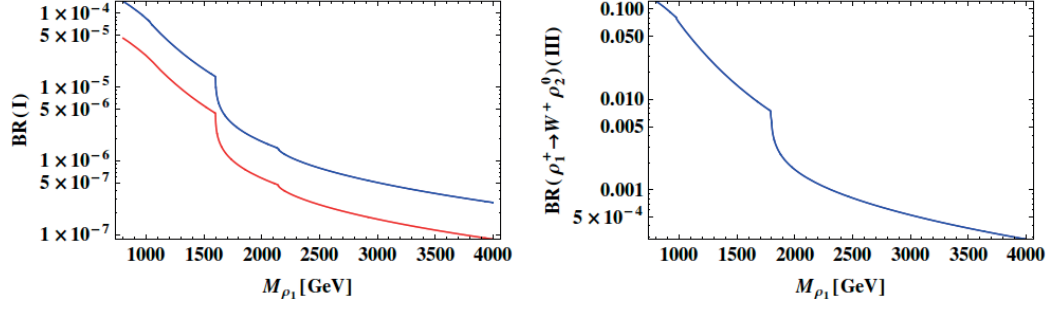


Figure D.1 – Cascade decay branching ratios as a function of the heavier resonance mass, for the benchmark value $g_\rho = 3$, for case (I) (left plot) and case (III) (right plot) of Eq. (D.4). The blue line corresponds to $BR(\rho_1^+ \rightarrow W^+ \rho_2^0)$ and the red curve corresponds to $BR(\rho_1^+ \rightarrow \rho_2^+ Z)$.

E A MadGraph5 model for heavy vector phenomenology

The four models discussed in Chapter 2 have been implemented in the parton level generator MadGraph5 for the simulation of Monte Carlo events. All the trilinear interaction vertices involving vector resonances, SM particles and top partners have been introduced in the UFO file, following the conventions of Appendix C.

A `Mathematica` calculator is also provided, which performs a numerical diagonalization of the vector mass matrix and computes all the physical quantities, masses and trilinear couplings between heavy vectors and SM particles, after the input parameters are specified. This code also implements the numerical diagonalization of the fermionic mass matrices in the top partner sector and computes the trilinear couplings between heavy resonances, top partners and partially composite SM fermions to full order in ξ . The semi-analytical formulae for the computation of the cross sections and the partial decay widths described in the main text can be also derived with this program.

We also stress that our numerical code has been designed not only to simulate the production and decay of vector resonances, but also to study WW scattering processes at the LHC and at future colliders. In order for these processes to be suitably simulated in the presence of vector resonances, also the modifications to the couplings g_{HWW} , g_{HZZ} , g_{HHWW} , g_{HHZZ} and g_{HHH} after rotation to the mass eigenstate basis must be properly taken into account. The corrections to the first four couplings are numerically calculated by the `Mathematica` file and in particular the vertices g_{HHWW} and g_{HHZZ} are the only four-particles interactions that are numerically derived by the calculator. On the other hand, the modification of the trilinear Higgs coupling g_{HHH} for the minimal model with elementary fermions embedded in the vector representation of $SO(5)$ (MCHM5) has been derived analytically in [50] to all orders in ξ and it is implemented in the code accordingly.

All the available software can be downloaded in a single package from the HEPMDB website

Appendix E. A MadGraph5 model for heavy vector phenomenology

[66] and the instruction on how to run the calculator can be found in the README file which is provided with the program.

F Fermionic spectrum of the $SO(8)/SO(7)$ Twin Higgs model

The heavy fermion multiplets in the minimal Composite Twin Higgs model form complete fundamental representations of $SO(8)$ and decompose under $SO(7)$ as described in the main text. The first multiplet, which is colored under the SM gauge group $SU(3)$ and is charged under $U(1)_X$ with X -charge $2/3$, contains eight heavy fermions which are organized as follows:

$$\Psi_7 = \frac{1}{\sqrt{2}} \begin{pmatrix} iB - iX_{5/3} \\ B + X_{5/3} \\ iT + iX_{2/3} \\ -T + X_{2/3} \\ \sqrt{2}S_{2/3}^1 \\ \sqrt{2}S_{2/3}^2 \\ \sqrt{2}S_{2/3}^3 \end{pmatrix}, \quad \Psi_1 = S_{2/3}^4. \quad (\text{E1})$$

The second multiplet, colored under the twin group $\widetilde{SU}(3)$ and charged under $\widetilde{U(1)}_X$ with \tilde{X} -charge $2/3$, contains another set of eight heavy fermions; they are organized in a fundamental of $SO(8)$, related to the previous representation by Twin symmetry, as follows:

$$\tilde{\Psi}_7 = \frac{1}{\sqrt{2}} \begin{pmatrix} i\tilde{D}_{-1} - i\tilde{D}_1 \\ \tilde{D}_{-1} + \tilde{D}_1 \\ i\tilde{D}_0^1 + i\tilde{D}_0^2 \\ -\tilde{D}_0^1 + \tilde{D}_0^2 \\ \sqrt{2}\tilde{U}_0^1 \\ \sqrt{2}\tilde{U}_0^2 \\ \sqrt{2}\tilde{U}_0^3 \end{pmatrix}, \quad \tilde{\Psi}_1 = \tilde{U}_0^4. \quad (\text{E2})$$

Appendix F. Fermionic spectrum of the $SO(8)/SO(7)$ Twin Higgs model

In this notation, it is easy to decompose these heavy particles under the SM weak gauge groups. The fermions T , B , $X_{2/3}$ and $X_{5/3}$ carry all the SM quantum numbers, both in the weak and in the color sector; they decompose into two heavy doublets, $(X_{5/3}, X_{2/3})$, with electric charges $5/3$ and $2/3$ respectively, and (T, B) , with electric charges $2/3$ and $-1/3$ respectively. These two doublets can be therefore identified with the usual heavy fermions that we expect to exist also in conventional composite Higgs models. The remaining components of the vector Ψ , the $S_{2/3}^1, \dots, S_{2/3}^4$ fields, carry mixed quantum numbers since they participate both to the SM and the Twin sector gauge interactions. In particular, they are charged under the twin weak gauge group, but they are colored under the SM $SU(3)$ and they all have electric charge equal to $2/3$. Thus they decompose as four electrically charged singlets under the SM weak gauge group. The decomposition of the Twin vector $\tilde{\Psi}$ under the SM is quite similar. The first four components participate to the SM weak interactions, but they carry twin color quantum numbers. They decompose into two heavy doublets under the SM weak gauge group, $(\tilde{D}_1, \tilde{D}_0^2)$, with electric charges 1 and 0 respectively, and $(\tilde{D}_0^1, \tilde{D}_{-1})$, with electric charges 0 and -1 respectively. Finally, the fields $\tilde{U}_0^1, \dots, \tilde{U}_0^4$ are charged under the Twin weak and strong gauge groups and they do not carry any electric charge. They decompose therefore as four electrically neutral singlets under the SM gauge groups.

The action of Twin symmetry on these two vectors of heavy fermions can be easily described. It can be in general decomposed as the product of two discrete symmetries. The first one can be identified as a Z_2 which is external to the strong sector and that rigidly interchanges Ψ_7 with $\tilde{\Psi}_7$ and Ψ_1 with $\tilde{\Psi}_1$. For the singlet, this is all we need to implement the Twin symmetry and we can easily identify \tilde{U}_0^4 as the Twin partner of $S_{2/3}^4$. For the remaining component in the **7**, we need to make the convolution of the external discrete symmetry with an element of the unbroken symmetry group $SO(7)$, $h(\Pi)$, so that the complete Twin symmetry takes the form:

$$\Psi_7 \rightarrow h(\Pi)\tilde{\Psi}_7. \quad (\text{E3})$$

The matrix $h(\Pi)$ is an explicit function of the Goldstone boson fields and in general it is quite complicated to work out; we expect to have a highly non-linear relation between the heavy fields in the two representations. In the limit when the Goldstone bosons are all set to zero, however, we can find a simple expression for h which we can write as follows:

$$h = \begin{pmatrix} 0 & 0 & \mathbb{I}_3 \\ 0 & -1 & 0 \\ \mathbb{I}_3 & 0 & 0 \end{pmatrix}. \quad (\text{E4})$$

By combining the action of this matrix with the external Z_2 , we have thus an illustrative example of the action of Twin symmetry in a simple case.

We now briefly discuss the mass matrices of the different charged sectors in the Composite Twin Higgs model and the related particle spectrum. We start considering the fields that do not have the right quantum numbers to mix with the elementary SM and Twin quarks and whose mass is therefore independent on the mixing parameters $y_{L/R}$ and $\tilde{y}_{L/R}$. These are the composite fermions $X_{5/3}$, \tilde{D}_1 and \tilde{D}_{-1} , with charges 5/3, 1 and -1 respectively; their mass is exactly given by the Lagrangian parameters M_Ψ , for the first one, and \tilde{M}_Ψ for the last two ones.

The remaining sectors have charge $-1/3$, 0 and $2/3$ and because of the elementary/composite mixing the associated mass matrices are in general non-diagonal and must be diagonalised by a proper field rotation. The simplest case is the $-1/3$ -charged sector, containing the bottom quark and the heavy B field; the mass matrix in the $\{b, B\}$ basis is

$$M_{-1/3} = \begin{pmatrix} 0 & f y_L \\ 0 & -M_\Psi \end{pmatrix}. \quad (\text{E5})$$

After rotation, we find the massless bottom quark, which acquires no mass since we are not including the b_R in the model, and a massive B particle with $m_B^2 = M_\Psi^2 + y_L^2 f^2$.

As regards the sector of charge $2/3$, it contains seven different particles, the top quark, the top-like heavy states T and $X_{2/3}$ and four composite fermions that do not participate to the SM weak interactions, $S_{2/3}^1, \dots, S_{2/3}^4$. In the $\{t, T, X_{2/3}, S_{2/3}^1, \dots, S_{2/3}^4\}$ basis, the mass matrix is in this case given by:

$$M_{2/3} = \begin{pmatrix} 0 & \frac{1}{2} f y_L (\sqrt{1-\xi} + 1) & -\frac{1}{2} f y_L (\sqrt{1-\xi} - 1) & 0 & -\frac{f y_L \sqrt{\xi}}{\sqrt{2}} \\ 0 & -M_\Psi & 0 & 0 & 0 \\ 0 & 0 & -M_\Psi & 0 & 0 \\ 0 & 0 & 0 & -M_\Psi \times \mathbb{I}_3 & 0 \\ f y_R & 0 & 0 & 0 & -M_S \end{pmatrix}. \quad (\text{E6})$$

We see immediately that the three particles $S_{2/3}^1 \dots S_{2/3}^4$ completely decouple from the elementary sector and they do not mix with the top quark. Their mass is therefore exactly given by the Lagrangian parameter M_Ψ . The remaining 4×4 matrix is in general complicated to be analytically diagonalised, but we can easily find the spectrum in perturbation theory expanding $M_{2/3}$ for $\xi \ll 1$, which is in general the phenomenologically viable constraint. The leading order

Appendix F. Fermionic spectrum of the SO(8)/SO(7) Twin Higgs model

expression for the masses is then:

$$\begin{aligned}
 m_t^2 &\simeq \frac{f^4}{2} \frac{y_L^2 y_R^2}{M_S^2 + y_R^2 f^2} \xi + \mathcal{O}(\xi^2), \quad m_{X_{2/3}}^2 = M_\Psi^2 \\
 m_T^2 &\simeq M_\Psi^2 + y_L^2 f^2 \left(1 - \frac{\xi}{2}\right) + \mathcal{O}(\xi^2), \\
 m_{S_{2/3}^4}^2 &\simeq M_S^2 + y_R^2 f^2 + \frac{y_L^2 f^2 M_S^2}{2(M_S^2 + y_R^2 f^2)} \xi + \mathcal{O}(\xi^2).
 \end{aligned} \tag{E7}$$

We see that the $X_{2/3}$ fermion can be also decoupled and it has an exact mass equal to M_Ψ . On the contrary, the other three particles mix with each other and their mass gets corrected after EWSB, the top mass being in particular generated only for non-zero values of ξ .

We finally analyze the neutral sector of our model. It comprises eight fields, the Twin top and bottom quarks, and six of the composite fermions contained in the $\tilde{\Psi}_7$ multiplet. In the basis $\{\tilde{t}, \tilde{b}, \tilde{D}_0^1, \tilde{D}_0^2, \tilde{U}_0^1, \dots, \tilde{U}_0^4\}$, the mass matrix reads:

$$M_0 = \begin{pmatrix} 0 & 0 & -\frac{1}{2}f\sqrt{\xi}\tilde{y}_L & \frac{1}{2}f\sqrt{\xi}\tilde{y}_L & 0 & 0 & -\frac{if\tilde{y}_L}{\sqrt{2}} & -\frac{f\sqrt{1-\xi}\tilde{y}_L}{\sqrt{2}} \\ 0 & 0 & 0 & 0 & -\frac{if\tilde{y}_L}{\sqrt{2}} & \frac{f\tilde{y}_L}{\sqrt{2}} & 0 & 0 \\ 0 & 0 & -\tilde{M}_\Psi & 0 & 0 & 0 & 0 & 0 \\ 0 & 0 & 0 & -\tilde{M}_\Psi & 0 & 0 & 0 & 0 \\ 0 & 0 & 0 & 0 & -\tilde{M}_\Psi & 0 & 0 & 0 \\ 0 & 0 & 0 & 0 & 0 & -\tilde{M}_\Psi & 0 & 0 \\ 0 & 0 & 0 & 0 & 0 & 0 & -\tilde{M}_\Psi & 0 \\ f\tilde{y}_R & 0 & 0 & 0 & 0 & 0 & 0 & -\tilde{M}_S \end{pmatrix}. \tag{E8}$$

After diagonalisation, we find one exactly massless eigenvalue corresponding to the Twin bottom quark, which does not acquire mass since we are not introducing the \tilde{b}_R particle. Four of the neutral heavy fermions completely decouple and acquire the following exact masses

$$m_{\tilde{U}_0^1} = m_{\tilde{U}_0^3} = m_{\tilde{D}_0^2} = \tilde{M}_\Psi, \quad m_{\tilde{U}_0^2}^2 = \tilde{M}_\Psi^2 + \tilde{y}_L^2 f^2. \tag{E9}$$

The elementary/composite mixing induces instead corrections to the masses of the remaining

neutral particles; at leading order in ξ we find:

$$\begin{aligned}
m_{\tilde{t}}^2 &\simeq \frac{f^4}{2} \frac{\tilde{y}_L^2 \tilde{y}_R^2}{\widetilde{M}_S^2 + \tilde{y}_R^2 f^2} (1 - \xi) + \mathcal{O}(\xi^2), \\
m_{\tilde{D}_0^1}^2 &\simeq \widetilde{M}_\Psi^2 + \frac{1}{2} \tilde{y}_L^2 f^2 (1 + \xi) + \mathcal{O}(\xi^2), \\
m_{\tilde{U}_0^4}^2 &\simeq \widetilde{M}_S^2 + \tilde{y}_R^2 f^2 + \frac{\tilde{y}_L^2 f^2 \widetilde{M}_S^2}{2(\widetilde{M}_S^2 + \tilde{y}_R^2 f^2)} (1 - \xi) + \mathcal{O}(\xi^2).
\end{aligned} \tag{E10}$$

We conclude by noticing that the masses of the particles in the different charged sectors are not unrelated to each other, but must be connected according to the action of the Twin Symmetry. In particular, it is obvious that the two singlets $S_{2/3}^4$ and \tilde{U}_0^4 form an exact twin pair, as it is the case for each SM quark and the corresponding twin partner. The remaining pairs can be easily found from the spectrum and correspond to the implementation of the Twin Symmetry in the Composite Sector that we have previously described.

G Diagrammatic renormalization of the Twin Higgs effective potential

This Appendix is devoted to briefly giving some technical details concerning the derivation of the Higgs effective potential in the Twin Higgs model. We will provide the explicit form of the function F_1 appearing in the UV correction, Eq (3.33), and give an alternative derivation of the RG-improved effective action at NLL with a diagrammatic approach.

We start considering the UV contributions, which can be derived with a standard Coleman-Weinberg procedure, [115]. We have:

$$V(H) = -\frac{2N_C}{16\pi^2} \int d^4p \, p^2 \{ \text{Tr} \log [p^2 \times \mathbb{1} + M^\dagger(H, y_L)_c M(H, y_L)_c] + \text{Tr} \log [p^2 \times \mathbb{1} + \widetilde{M}^\dagger(H, \tilde{y}_L)_c \widetilde{M}(H, \tilde{y}_L)_c] \}, \quad (\text{G.1})$$

where $M(H)_c$ and $\widetilde{M}(H)_c$ indicate the fermionic mass matrices of a sector with charge c . $M_c(H)$ corresponds to the sector of particles mixing with the SM quarks embedded in Q_L , whereas $\widetilde{M}_c(H)$ is derived only from the mixing of heavy fermions with the Twin quarks in \widetilde{Q}_L . The trace is understood as a sum over all the degrees of freedom, including all possible charges in the model. Since we are looking for the potential at order $O(y_L^4)$ and $O(\tilde{y}_L^4)$, we can expand the mass matrices for $y_L \sim \tilde{y}_L \ll g_*$ and decompose them in the following way:

$$M_c(H, y_L)^\dagger M_c(H, y_L) = M_c^0 + y_L M_c^1(H), \quad \widetilde{M}^\dagger(H) \widetilde{M}_c(H) = \widetilde{M}_c^0 + \tilde{y}_L \widetilde{M}_c^1(H), \quad (\text{G.2})$$

where M_c^0 and \widetilde{M}_c^0 do not depend on the Higgs field. Keeping only the terms that explicitly depend on H , the integral in Eq.(G.1) can be simplified to:

$$V(H) = -\frac{2N_C}{16\pi^2} \int d^4p \, p^2 \left\{ \text{Tr} \log \left[\mathbb{1} + y_L \frac{M_c^1(H)}{p^2 \times \mathbb{1} + M_c^0} \right] + \text{Tr} \log \left[\mathbb{1} + \tilde{y}_L \frac{\widetilde{M}_c^1(H)}{p^2 \times \mathbb{1} + \widetilde{M}_c^0} \right] \right\}; \quad (\text{G.3})$$

the trace may be now easily computed and the result expanded at the order in the symmetry breaking parameters we are interested in.

Appendix G. Diagrammatic renormalization of the Twin Higgs effective potential

It is now straightforward to replace the mass matrices in Appendix F into Eq.(G.3) and derive the expression of the Higgs potential as reported in the main text. All possible quadratic divergences in the final result must cancel out due to the two-side structure of our model, [117]; the explicit form of the function F_1 retains therefore only a logarithmic dependence on the cut-off scale m_* . We get:

$$F_1 = \frac{1}{4} \left[-1 - \frac{M_S^4}{(M_S^2 + f^2 y_R^2)^2} + \frac{M_S^2 + M_\Psi^2 - f^2 y_R^2}{M_S^2 - M_\Psi^2 + f^2 y_R^2} \log \frac{m_*^2}{M_\Psi^2} - \frac{M_S^2 (M_S^2 (M_\Psi^2 + f^2 y_R^2) + 2 f^2 y_R^2 M_\Psi^2 + M_S^4)}{(M_S^2 + f^2 y_R^2)^2 (M_S^2 - M_\Psi^2 + f^2 y_R^2)} \log \frac{m_*^2}{M_S^2 + f^2 y_R^2} \right]. \quad (\text{G.4})$$

Regarding the RG-improvement of the effective potential, as explained in the text, we use a simple diagrammatic approach to re-sum the leading logarithms up to two loops. We start by writing the TH effective action in two parts, a renormalizable term plus a sum over all the higher-dimensional operators that are relevant for our computation:

$$\mathcal{L} = \mathcal{L}_{d=4} + \sum_i c_i(\mu) O_i^{d_i}, \quad (\text{G.5})$$

where $O_i^{d_i}$ are the operators with dimension d_i and $c_i(\mu)$ are their coefficients evaluated at the renormalization scale μ (in this Appendix we follow the notation of ref. [24] to define the effective operators). We further divide the action into three parts, one describing the Higgs sector of the theory, \mathcal{L}_H , a second part for the top sector, \mathcal{L}_t , and a final piece for the interactions in the twin sector, $\mathcal{L}_{\tilde{t}}$.

The term \mathcal{L}_H contains the renormalizable operators of the SM Lagrangian involving the Higgs field, namely the Higgs kinetic term and its potential, plus a set of three dimension-6 operators, \mathcal{O}_H , \mathcal{O}'_H and \mathcal{O}_6 . The Lagrangian takes the form:

$$\mathcal{L}_H = (D^\mu H^\dagger)(D_\mu H) + \frac{c_H}{2f^2} \partial_\mu (H^\dagger H) \partial^\mu (H^\dagger H) + \frac{c'_H}{f^2} H^\dagger H (D^\mu H^\dagger)(D_\mu H) - V(H^\dagger H), \quad (\text{G.6})$$

$$V(H^\dagger H) = -m_H^2 H^\dagger H + \frac{\lambda_h}{4} (H^\dagger H)^2 + \frac{c_6}{f^2} (H^\dagger H)^3. \quad (\text{G.7})$$

The top sector consists of the renormalizable Yukawa term plus the dimension-6 operator \mathcal{O}_{y_t} ; we have:

$$\mathcal{L}_t = -y_1 \bar{q}_L H^c t_R + \frac{y_3}{3f^2} (H^\dagger H) \bar{q}_L H^c t_R, \quad (\text{G.8})$$

where $H^c = i\sigma_2 H^*$. All the remaining gauge-invariant operators in the top sector do not give contributions to the Higgs mass at NLO because they do not renormalize the Higgs quartic. On the other hand, the coupling y_3 in general renormalizes c_6 and enters in the NLO definition of the top mass, which is one of our input parameters.

Considering finally the Twin top sector, it contains a relevant operator of dimension 3, the Twin top mass term, $\mathcal{O}_{\tilde{y}_0} = \tilde{t} \tilde{t}$, plus a set of non-renormalizable interactions of odd dimension. The Lagrangian takes the form:

$$\mathcal{L}_{\tilde{t}} = -\frac{\tilde{y}_0 f}{\sqrt{2}} \tilde{t} \tilde{t} + \frac{\tilde{y}_2}{\sqrt{2} f} (H^\dagger H) \tilde{t} \tilde{t} - \frac{\tilde{y}_4}{6\sqrt{2} f^3} (H^\dagger H)^2 \tilde{t} \tilde{t} + \frac{\tilde{c}_2}{f^2} (H^\dagger H) \tilde{t} i \not{\partial} \tilde{t} + \frac{\tilde{c}_4}{6f^4} (H^\dagger H)^2 \tilde{t} i \not{\partial} \tilde{t}, \quad (\text{G.9})$$

where the combinatorial factors have been chosen for convenience.

The initial conditions for all the Wilson coefficients in the previous Lagrangians are given at the scale m_* and can be easily found by matching eqs. (G.6), (G.7), (G.8) and (G.9) with the simplified model of Sec. 5.2.1. We can select a convenient basis where many of the $c_i(m_*)$ vanish, simplifying considerably the computation. This is found by redefining the Higgs doublet as

$$H \rightarrow \hat{H} \equiv f \frac{H}{\sqrt{2H^\dagger H}} \sin\left(\frac{\sqrt{2H^\dagger H}}{f}\right) \quad (\text{G.10})$$

and rewriting accordingly the effective action and the Higgs potential of Sec. 5.2.1. It is immediate to verify that in this basis $c_6 = c'_H = y_3 = 0$ and $c_H = 1$. Since these coefficients do not evolve along the RG flow at NLO, their value is fixed once for all after matching. The higher-dimensional operators involving the twin top kinetic terms are absent at tree-level in our effective model and are generated at loop level as a result of their RG evolution. The UV boundary conditions for their coefficients are then $\tilde{c}_2(m_*) = \tilde{c}_4(m_*) = 0$. The top and twin top Yukawa couplings are instead generated at tree level at m_* ; since at this scale the theory respects an approximate Z_2 symmetry, we have: $y_1(m_*) = \tilde{y}_0(m_*) = \tilde{y}_2(m_*) = \tilde{y}_4(m_*)$.

The RG evolution of the quartic coupling in eq. (5.38) can be derived by a one-loop computation that takes into account the running of the SM and twin top Yukawas. We define the β -functions of a generic coefficient c_i as:

$$\beta_{c_i} = \mu \frac{\partial}{\partial \mu} c_i(\mu), \quad (\text{G.11})$$

where μ is the renormalization scale. All the β -functions are computed at one loop in the basis obtained by redefining the Higgs doublet as in eq. (G.10) and accordingly re-scaling $y_4 \rightarrow -3y_4$ and $c_4 \rightarrow 3c_4$. We neglect both the running of all the dimension-6 operators that would give a contribution proportional to the third power in our logarithmic expansion, and the diagrams

Appendix G. Diagrammatic renormalization of the Twin Higgs effective potential

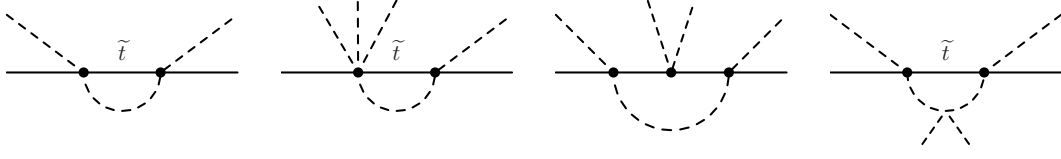


Figure G.1 – Topology of the diagrams inducing the running of the Wilson coefficients in the Twin sector. The last diagram on the right contains an insertion of c_H in the four-scalars vertex.

with only virtual NGBs and Higgs boson circulating in the loop, which also contribute at NNLO. The topology of the diagrams we need to compute in the Twin sector of the model is shown in figure G.1. The result is the following set of coupled differential equations, where $C_F = 4/3$ is one of the $SU(3)$ Casimirs:.

$$\begin{aligned}
 \beta_{y_1} &= \frac{1}{8\pi^2} \left(\frac{9}{4} y_1^3 - 3g_S^2 C_F y_1 \right), \\
 \beta_{\tilde{y}_0} &= -\frac{3\tilde{g}_S^2 C_F}{8\pi^2} \tilde{y}_0, \\
 \beta_{\tilde{y}_2} &= \frac{1}{8\pi^2} (-\tilde{y}_0 \tilde{y}_2^2 + 3y_1^2 \tilde{y}_2 - 3\tilde{g}_S^2 C_F \tilde{y}_2), \\
 \beta_{\tilde{y}_4} &= \frac{1}{8\pi^2} (-4\tilde{y}_0 \tilde{y}_2 \tilde{y}_4 + 2\tilde{y}_2^3 + 4\tilde{y}_0 \tilde{y}_2^2 c_H + 6y_1^2 \tilde{y}_4 - 3\tilde{g}_S^2 C_F \tilde{y}_4), \\
 \beta_{\tilde{c}_2} &= \frac{1}{8\pi^2} \left(-\frac{\tilde{y}_2^2}{2} \right), \\
 \beta_{\tilde{c}_4} &= \frac{1}{8\pi^2} (-2\tilde{y}_2 \tilde{y}_4 + 2\tilde{y}_2^2 c_H), \\
 \beta_{\lambda_h} &= \frac{1}{8\pi^2} (6y_1^2 \lambda - 12y_1^4 - 18\tilde{y}_0^2 \tilde{y}_2^2 + 6\tilde{y}_4 \tilde{y}_0^3 - 48\tilde{y}_2 \tilde{y}_0^3 \tilde{c}_2 + 6\tilde{y}_0^4 \tilde{c}_4).
 \end{aligned} \tag{G.12}$$

By solving eq. (G.11) at NLO, we find the following expression for $\lambda(\mu)$, where μ is an arbitrary scale larger than $m_{\tilde{t}}$:

$$\begin{aligned}
 \lambda_h(\mu) &= \frac{3}{4\pi^2} (y_1^4 + \tilde{y}_0^4) \log \frac{m_*^2}{\mu^2} \\
 &+ \frac{3}{128\pi^4} [-15y_1^6 + 3(c_H + 1)\tilde{y}_0^6 - 12y_1^2 \tilde{y}_0^4 + 16g_S^2 y_1^4 + 16\tilde{g}_S^2 \tilde{y}_0^4] \log^2 \frac{m_*^2}{\mu^2}.
 \end{aligned} \tag{G.13}$$

Here y_1 and \tilde{y}_0 are the top and twin top Yukawa couplings evaluated at the cutoff scale m_* . By virtue of Twin Parity we have written the solution imposing $\tilde{y}_0(m_*) = \tilde{y}_2(m_*) = \tilde{y}_4(m_*)$. From the general solution in eq. (G.13), we can find the NLO contribution to the running of the Higgs mass by matching at the scale $m_{\tilde{t}}$ where the Twin degrees of freedom are integrated out.

H Correlation between the IR contributions to $\Delta\hat{T}_\Psi$ and to δg_{Lb}

We show in this Appendix that the IR contributions to $\Delta\hat{T}_\Psi$ and to δg_{Lb} are always connected with one another in any Composite Higgs model whose strong sector enjoys both the P_{LR} and the custodial symmetries. We can in fact interpret the IR corrections to these EW observables as an effect due to the running of the Wilson coefficients of the dimension-six operators generated at the cut-off scale after integrating out the heavy fermionic resonances. The operators that are relevant for our analysis are those that give contributions to \hat{T} and δg_{Lb} . Following [25], we must consider four operators:

$$\begin{aligned}\mathcal{O}_T &= \frac{1}{2}(H^\dagger \overleftrightarrow{D}_\mu H)^2, & \mathcal{O}_L^t &= (iH^\dagger \overleftrightarrow{D}_\mu H)\bar{q}_L\gamma^\mu q_L, \\ \mathcal{O}_L^{t(3)} &= (iH^\dagger \sigma^a \overleftrightarrow{D}_\mu H)\bar{q}_L\gamma^\mu \sigma^a q_L, & \mathcal{O}_R^t &= (iH^\dagger \overleftrightarrow{D}_\mu H)\bar{t}_R\gamma^\mu t_R,\end{aligned}\tag{H.1}$$

where $H^\dagger \overleftrightarrow{D}_\mu H = H^\dagger D_\mu H - (D_\mu H)^\dagger H$. The corrections to \hat{T} and to δg_{Lb} can be parametrized in terms of the Wilson coefficients of three of these operators as follows [25]:

$$\Delta\hat{T} = c_T\xi, \quad \delta g_{Lb} = -\frac{1}{2}\left(c_L^t + c_L^{t(3)}\right)\xi,\tag{H.2}$$

so that the IR corrections can be obtained by running each of the three coefficients down from the scale m_* to the scale m_{top} . The operator \mathcal{O}_R , despite not appearing explicitly in the definition of the two observables, affects the running of the Wilson coefficients through the anomalous dimensions and it is thus relevant to our analysis.

In order to study the RG evolution of each operator, we start considering the UV boundary conditions, namely the value of the three Wilson coefficients contributing to \hat{T} and δg_{Lb} at the scale m_* . Since the strong sector respects the custodial symmetry, all tree-level corrections to \hat{T} vanish and as a result the operator \mathcal{O}_T cannot be generated after integrating out the BSM physics, so that $c_T(m_*) = 0$. On the other hand, the new dynamics also respects the P_{LR} symmetry, which forbids the existence of any tree-level contribution to δg_{Lb} . As

a consequence, only one combination of the remaining two operators can originate at the scale m_* , precisely the one that does not induce any correction to this coupling; we call this combination $\mathcal{O}_- = \mathcal{O}_L^t - \mathcal{O}_L^{t(3)}$. The second linearly independent combination, $\mathcal{O}_+ = \mathcal{O}_L^t + \mathcal{O}_L^{t(3)}$, that contributes to δg_{Lb} , is not produced at the scale m_* , but it will eventually be generated by the running together with \mathcal{O}_T .¹ The UV boundary conditions for the Wilson coefficients parametrizing δg_{Lb} are therefore: $c_L^{t(3)}(m_*) = -c_L^t(m_*)$. Due to the structure of the mixing Lagrangian in our model, these latter coefficients are generated at the scale m_* at order $\mathcal{O}(y_L^2)$.

Having derived the initial values of the Wilson coefficients, we can study their RG evolution from the cut-off to the EW scale using the corresponding β functions reported in [25]. Let us start considering the operator \mathcal{O}_T . Neglecting the effects proportional to g_1^2 , its RG evolution is induced by two operators, \mathcal{O}_L^t and \mathcal{O}_R^t . The β -function is:

$$\frac{\partial c_T}{\partial \log \mu} = \frac{3}{4\pi^2} y_t^2 (c_R^t(\mu) - c_L^t(\mu)), \quad (\text{H.3})$$

from which we find:

$$c_T(m_{top}) = \frac{3}{8\pi^2} y_t^2 (c_L^t(m_*) - c_R^t(m_*)) \log \left(\frac{m_*^2}{m_{top}^2} \right). \quad (\text{H.4})$$

The presence of a non-vanishing tree-level UV boundary value for c_L^t and c_R^t therefore generates a contribution to \hat{T} in the IR due to the running of \mathcal{O}_T .

We study now the evolution of the remaining two operators, \mathcal{O}_L^t and $\mathcal{O}_L^{t(3)}$. Their β -functions are much more complicated and, beside the running induced by \mathcal{O}_L^t , $\mathcal{O}_L^{t(3)}$ and \mathcal{O}_R^t , they contain the contributions of all the four fermions operators that are generated by integrating out the heavy vectors [25]. These latter can be neglected, since we are focusing only on the operators that arise after integrating out the fermionic resonances; neglecting also the running due to the gauge couplings and considering again that the only combination generated at the tree-level is \mathcal{O}_- , we can write simply two coupled equations:

$$\begin{cases} \frac{\partial c_L^t}{\partial \log \mu} = \frac{y_t^2}{8\pi^2} \left(\frac{9}{2} c_L^t(\mu) - 3 c_L^{t(3)}(\mu) - \frac{1}{2} c_R^t(\mu) \right), \\ \frac{\partial c_L^{t(3)}}{\partial \log \mu} = \frac{y_t^2}{8\pi^2} \left(\frac{5}{2} c_L^{t(3)}(\mu) - c_L^t(\mu) \right). \end{cases} \quad (\text{H.5})$$

¹Notice that the P_{LR} symmetry interchanges the left-handed and right-handed generators, T_L^α and T_R^α (see Appendix A), with each other. The symmetry therefore acts on the neutral Higgs currents in the following way: $H^\dagger \overleftrightarrow{D}_\mu H \leftrightarrow -H^\dagger \sigma^3 \overleftrightarrow{D}_\mu H$. The combination \mathcal{O}_- , generated at the scale m_* , is consequently even under P_{LR} , whereas \mathcal{O}_+ is odd under this symmetry and as a result it cannot be produced at tree-level after integrating out the composite dynamics.

It is then straightforward to solve and apply our UV boundary conditions to find:

$$c_L^t(m_{top}) = -\frac{y_t^2}{16\pi^2} \left(\frac{15}{2} c_L^t(m_*) - \frac{1}{2} c_R^t(m_*) \right) \log \left(\frac{m_*^2}{m_{top}^2} \right), \quad c_L^{t(3)}(m_{top}) = \frac{y_t^2}{16\pi^2} \frac{7}{2} c_L^t(m_*) \log \left(\frac{m_*^2}{m_{top}^2} \right). \quad (\text{H.6})$$

Similarly to what happened for \mathcal{O}_T , also in this case the combination \mathcal{O}_+ , that was absent at the scale m_* , gets generated after running the Wilson coefficients down to m_{top} , so that it can only contribute to δg_{Lb} with an IR correction.

We can finally study the correlation between the two IR effects on $\Delta \hat{T}$ and on δg_{Lb} . From Eq. (H.2), we find in fact:

$$\begin{aligned} \Delta \hat{T}_\Psi^{IR} &= \frac{3\xi}{8\pi^2} y_t^2 (c_L^t(m_*) - c_R^t(m_*)) \log \left(\frac{m_*^2}{m_{top}^2} \right), \\ \delta g_{Lb\Psi}^{IR} &= \frac{\xi}{8\pi^2} y_t^2 \left(c_L^t(m_*) - \frac{1}{8} c_R^t(m_*) \right) \log \left(\frac{m_*^2}{m_{top}^2} \right), \end{aligned} \quad (\text{H.7})$$

which, following our parametrization in Eqs. (5.54) and (5.59), immediately implies $a_{IR} = b_{IR}$ for vanishing α 's and $c_R = 0$. The operator \mathcal{O}_R can only be generated at the tree-level from the interaction mediated by the d_μ symbol proportional to c_R ; in absence of this latter, the two observables would be exactly correlated. Taking into account that the UV boundary values are of order $\mathcal{O}(y_L^2)$, these IR terms generate contributions that go like $\mathcal{O}(y_L^2 y_t^2 / g_*^2)$, in agreement with what we find with a direct computation. We can then conclude that, starting only from the assumption that the strong sector respects the custodial and P_{LR} symmetries, the contributions to \hat{T} and to the $Z\bar{b}_L b_L$ coupling due to the running of the dimension-six operators generated after integrating out the heavy fermions must always be correlated and, in particular, they always have the same sign.

For completeness, we finally report also the expressions of c_L^t , $c_L^{t(3)}$ and c_R^t at the scale m_* as obtained at the tree-level after integrating out the UV physics:

$$\begin{aligned} c_L^t(m_*) &= -c_L^{t(3)}(m_*) = \frac{f^2 y_L^2 (f^4 y_R^4 + M_S^2 (2f^2 y_R^2 + M_\Psi^2) + M_S^4)}{4M_\Psi^2 (M_S^2 + y_R^2 f^2)^2} - c_L y_L^2 \frac{f^2 M_S}{\sqrt{2} M_\Psi (M_S^2 + y_R^2 f^2)}, \\ c_R^t(m_*) &= \sqrt{2} c_R \frac{f^4 y_L^2 y_R^2}{M_\Psi^2 (M_S^2 + y_R^2 f^2)}. \end{aligned} \quad (\text{H.8})$$

I Operator analysis of the heavy-vector contribution to δg_{Lb}

In this Appendix we discuss the UV threshold contribution to δg_{Lb} generated by the tree-level exchange of the composite vectors ρ (adjoint of $SO(7)$) and ρ^X (singlet of $SO(7)$) at zero transferred momentum. This effect arises at leading order from diagrams with a loop of heavy fermions, as in figure J.3. Our simple effective operator analysis will show that the contribution of the ρ identically vanishes, in agreement with the explicit calculation in the simplified model.

An adjoint of $SO(7)$ decomposes under the custodial $SU(2)_L \times SU(2)_R$ as:

$$\mathbf{21} = (\mathbf{3}, \mathbf{1}) + (\mathbf{1}, \mathbf{3}) + 3 \times (\mathbf{2}, \mathbf{2}) + 3 \times (\mathbf{1}, \mathbf{1}). \quad (\text{I.1})$$

The first two representations contain the vector resonances that are typically predicted by ordinary CH models, namely ρ_L and ρ_R . They mix at tree-level with the Z boson and in general contribute to δg_{Lb} . The remaining resonances do not have the right quantum numbers to both mix with the Z boson and couple to the left-handed bottom quark due to isospin conservation. As a result, only the components ρ_L and ρ_R inside the $\mathbf{21}$ can give a contribution to δg_{Lb} at the 1-loop level.

In order to analyze such effect, we make use of an operator approach. We classify the operators that can be generated at the scale m_* by integrating out the composite states, focusing on those which can modify the $Zb\bar{b}$ vertex at zero transferred momentum. In general, since an exact P_{LR} invariance implies vanishing correction to g_{Lb} at zero transferred momentum, any δg_{Lb} must be generated proportional to some spurionic coupling breaking this symmetry. In our model, the only coupling breaking P_{LR} in the fermion sector is y_L , and a non-vanishing δg_{Lb} arises at order y_L^4 . The effective operators can be constructed using the CCWZ formalism in terms of the covariant spurion

$$\chi_L = \Sigma^\dagger \Delta^\dagger \Delta \Sigma, \quad (\text{I.2})$$

Appendix I. Operator analysis of the heavy-vector contribution to δg_{Lb}

where Δ is defined in eq. (5.27). By construction χ_L is an hermitian complex matrix. Under the action of an element $g \in SO(8)$, it transforms as a $2\mathbf{1}_a + 2\mathbf{7}_s + \mathbf{7} + \mathbf{1} + \mathbf{1}$ of $SO(7)$ (where the $\mathbf{7}$ is complex), and its formal transformation rule is

$$\chi_L \rightarrow h(\Pi, g) \chi_L h^\dagger(\Pi, g), \quad h \in SO(7). \quad (\text{I.3})$$

As a second ingredient to build the effective operators, we uplift the elementary doublet q_L into a $\mathbf{7} + \mathbf{1}$ representation of $SO(7)$ by dressing it with NGBs:

$$Q_L = (\Sigma^\dagger \Delta^\dagger q_L). \quad (\text{I.4})$$

We will denote with $Q_L^{(7)}$ and $Q_L^{(1)}$ respectively the septuplet and singlet components of Q_L . Since $Q_L^{(1)}$ does not contain b_L (it depends only on t_L), only $Q_L^{(7)}$ is of interest for the present analysis. Under an $SO(8)$ transformation

$$Q_L^{(7)} \rightarrow h(\Pi, g) Q_L^{(7)}. \quad (\text{I.5})$$

The effective operators contributing to δg_{Lb} can be thus constructed in terms of χ_L , d_μ and $Q_L^{(7)}$. We find that the exchange of ρ_μ in the diagram of figure J.3 can generate two independent operators,

$$O_{21} = \bar{Q}_L^{(7)} \gamma^\mu T^a Q_L^{(7)} \text{Tr}(d_\mu \chi_L T^a), \quad O'_{21} = \bar{Q}_L^{(7)} \gamma^\mu T^a Q_L^{(7)} (d_\mu T^a \chi_L)_{88}, \quad (\text{I.6})$$

where T^a is an $SO(8)$ generator in the adjoint of $SO(7)$; the exchange of ρ_μ^X gives rise to other two:¹

$$O_1 = \bar{Q}_L^{(7)} \gamma^\mu Q_L^{(7)} \text{Tr}(d_\mu \chi_L), \quad O'_1 = \bar{Q}_L^{(7)} \gamma^\mu Q_L^{(7)} (d_\mu \chi_L)_{88}. \quad (\text{I.7})$$

Simple inspection reveals that only the septuplet component of χ_L contributes in the above equations. One can easily check that the operators of eq. (I.6) give a vanishing contribution to δg_{Lb} . In particular, the terms generated by the exchange of the (2,2) and (1,1) components of the ρ give (as expected) an identically vanishing contribution. Those arising from ρ_L and ρ_R (obtained by setting T^a in eq. (I.6) equal to respectively one of the (3,1) and (1,3) generators) give instead an equal and opposite correction to g_{Lb} . This is in agreement with the results of a direct calculation in the simplified model, from which one finds that the contributions

¹Additional structures constructed in terms of d_μ and χ_L can be rewritten in terms of those appearing in eqs. (I.6) and (I.7), hence they do not generate new linearly independent operators. Notice that $\text{Tr}(d_\mu \chi_L T^a) \propto f^{a\hat{a}\hat{b}} d_\mu^{\hat{a}} (\chi_L^{(7)})^{\hat{b}}$, $(d_\mu T^a \chi_L)_{88} \propto f^{a\hat{a}\hat{b}} d_\mu^{\hat{a}} (\chi_L^{(7)*})^{\hat{b}}$, $(d_\mu \chi_L)_{88} = -d_\mu^{\hat{a}} (\chi_L^{(7)})^{\hat{a}}$, $\text{Tr}(d_\mu \chi_L) = -d_\mu^{\hat{a}} (\chi_L^{(7)})^{\hat{a}} + d_\mu^{\hat{a}} (\chi_L^{(7)*})^{\hat{a}}$, where $\chi_L^{(7)}$ denotes the component of χ_L transforming as a (complex) fundamental of $SO(7)$. A similar classification in the context of $SO(5)/SO(4)$ models in ref. [108] found only one operator, corresponding to the linear combination $O'_1 - O_1$.

from ρ_L and ρ_R cancel each other. Finally, a non-vanishing δg_{Lb} arises from the operators of eq. (I.7) generated by the exchange of ρ^X . Upon expanding in powers of the Higgs doublet, O_1 and O'_1 both match the dimension-6 operator O_{Hq} of eq. (5.53) and differ only by higher-order terms.

J Explicit formulae for the EWPO

In this Appendix we report the results of our calculation of the electroweak precision observables, in particular we collect here the explicit expression of the coefficients a_{UV} , a_{IR} of eq. (5.54) and b_{UV} , c_{UV} , b_{IR} of eq. (5.59).

J.1 Computation of the \hat{S} and \hat{T} parameters

Let us start considering the \hat{S} and \hat{T} parameters. Following [56], we define these EW observables as

$$\begin{aligned}\hat{T} &= \frac{\Pi_{W_3 W_3}(0) - \Pi_{W^+ W^-}(0)}{m_W^2}, \\ \hat{S} &= \frac{g_2}{g_1} \Pi'_{W_3 B}(0),\end{aligned}\tag{J.1}$$

where the different Π functions can be computed by expanding the vacuum polarization amplitudes in powers of the external momentum, q^2 , as it is customary:

$$\Pi_{ab}^{\mu\nu}(q^2) = -i g^{\mu\nu} [\Pi_{ab}(0) + q^2 \Pi'_{ab}(0)] + q^\mu q^\nu \text{ terms}.\tag{J.2}$$

The indices a and b now run from one to four and denote one of the SM gauge bosons; we can set in general $W_\mu^a = \{W_\mu^+, W_\mu^-, W_\mu^3, B_\mu\}$.

We will be concerned only with the computation of the oblique contributions to \hat{S} and \hat{T} , the non-oblique terms involving vertex and box corrections being in general negligible. As a consequence, we must focus on one-loop diagrams of the type shown in Fig. (J.1), where fermions with different masses circulate in the loop.

In order to evaluate the contributions of the fermions in our model, we start by writing down

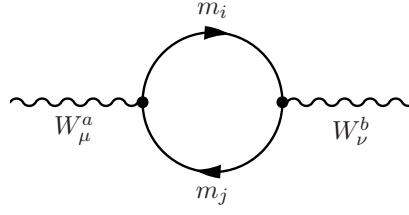


Figure J.1 – The one-loop diagram displaying the fermion contribution to the gauge boson vacuum polarization amplitude. Two virtual fermions with generically different masses, m_i and m_j , circulate in the loop.

in full generality the Lagrangian describing their couplings to gauge vectors:

$$\mathcal{L} = W_\mu^a (C_{L,a}^{ij} \bar{f}_L^i \gamma^\mu f_L^j + C_{R,a}^{ij} \bar{f}_R^i \gamma^\mu f_R^j), \quad (\text{J.3})$$

where $f_{L/R}^i$ are the left-handed and right-handed fermions in the theory, including the light quarks, and $C_{L/R}^{i,j}$ denote the coupling matrices.

Let us consider first of all the \hat{T} parameter. We carry out the computation in the mass eigenstate basis and we indicate with m_i and m_j the masses of the two different fermions in the loop. In order to rotate the coupling matrices in the new basis, we compute the standard rotation matrices U_c and W_c for the left-handed and right-handed fields, respectively, in each sector of charge c . We finally calculate the loop integrals in dimensional regularization and we encode the divergent part in the parameter

$$\Delta = \frac{1}{\epsilon} - \gamma + \log(4\pi), \quad (\text{J.4})$$

where ϵ is defined by $d = 4 - 2\epsilon$ and γ is the Euler-Mascheroni constant. The resulting expression for $\Pi_{ab}(0)$ is therefore:

$$\begin{aligned} \Pi_{ab}(0) = & -\frac{3}{8\pi^2} \sum_{i,j,c} \left\{ \left[\left(U_c^\dagger C_{L,a} U_c \right)_{ij} \cdot \left(U_c^\dagger C_{L,b} U_c \right)_{ij} + \left(W_c^\dagger C_{R,a} W_c \right)_{ij} \cdot \left(W_c^\dagger C_{R,b} W_c \right)_{ij} \right] \cdot \right. \\ & \left[\frac{1}{2} (m_i^2 + m_j^2) \Delta - G_1(m_i, m_j) \right] - \left[\left(U_c^\dagger C_{L,a} U_c \right)_{ij} \cdot \left(W_c^\dagger C_{R,b} W_c \right)_{ij} + \right. \\ & \left. \left. \left(W_c^\dagger C_{R,a} W_c \right)_{ij} \cdot \left(U_c^\dagger C_{L,b} U_c \right)_{ji} \right] \cdot [m_i m_j \Delta - G_2(m_i, m_j)] \right\} \end{aligned} \quad (\text{J.5})$$

where we have introduced the functions

$$G_1(m_i, m_j) = \frac{m_i^4 \log\left(\frac{m_i^2}{\mu^2}\right) - m_j^4 \log\left(\frac{m_j^2}{\mu^2}\right)}{2(m_i^2 - m_j^2)} - \frac{1}{2}(m_i^2 + m_j^2),$$

$$G_2(m_i, m_j) = m_i m_j \frac{m_i^2 \log\left(\frac{m_i^2}{\mu^2}\right) - m_j^2 \log\left(\frac{m_j^2}{\mu^2}\right)}{m_i^2 - m_j^2} - m_i m_j.$$
(J.6)

In the previous formulae, μ is to be identified with a generic renormalization scale. Once the Π factors have been computed for the W^+ and W_3 propagators, it is then straightforward to infer the expression of \hat{T} from Eq. (J.1).

As regards the \hat{S} parameter, we find the following expression for $\Pi'_{ab}(0)$:

$$\begin{aligned} \Pi'_{ab}(0) = & -\frac{3}{8\pi^2} \sum_{i,j,c} \left\{ \left[\left(U_c^\dagger C_{L,a} U_c \right)_{ij} \cdot \left(U_c^\dagger C_{L,b} U_c \right)_{ij} + \left(W_c^\dagger C_{R,a} W_c \right)_{ij} \cdot \left(W_c^\dagger C_{R,b} W_c \right)_{ij} \right] \cdot \right. \\ & \left[-\frac{1}{3} \Delta + H_1(m_i, m_j) \right] - \left[\left(U_c^\dagger C_{L,a} U_c \right)_{ij} \cdot \left(W_c^\dagger C_{R,b} W_c \right)_{ij} + \right. \\ & \left. \left. \left(W_c^\dagger C_{R,a} W_c \right)_{ij} \cdot \left(U_c^\dagger C_{L,b} U_c \right)_{ij} \right] \cdot H_2(m_i, m_j) \right\}, \end{aligned}$$
(J.7)

with

$$\begin{aligned} H_1(m_i, m_j) = & \frac{1}{36(m_i^2 - m_j^2)^3} \left(-12m_j^4(m_j^2 - 3m_i^2) \log\left(\frac{m_j^2}{\mu^2}\right) + 12(m_i^6 - 3m_i^4 m_j^2) \log\left(\frac{m_i^2}{\mu^2}\right) \right. \\ & \left. + 45m_i^4 m_j^2 - 45m_i^2 m_j^4 - 7m_i^6 + 7m_j^6 \right), \\ H_2(m_i, m_j) = & \frac{m_i m_j}{2(m_i^2 - m_j^2)^3} \left(m_i^4 - m_j^4 - 2m_i^2 m_j^2 \log\left(\frac{m_i^2}{m_j^2}\right) \right). \end{aligned}$$
(J.8)

The previous formula gives directly the \hat{S} parameter for a theory with a generic number of fermions, once evaluated for the $W_3 - B$ propagator.

J.2 Computation of δg_{Lb}

We derive now a general formula for computing δg_{Lb} in a theory with a generic number of new heavy fermions, under reasonable assumptions. We proceed in fact by setting all the gauge couplings to zero and considering only the interactions mediated by the Yukawa couplings. This approximation can be justified by noticing that, as in the SM, the most relevant contributions to this EW observable are those arising from the top sector, the gauge sector giving in general only a smaller correction. This is indeed the well known *gaugeless limit*, firstly introduced in [116];¹ in this latter reference, the gauge vectors are treated as external non-propagating fields and δg_{Lb} is then extracted from the one-loop renormalization of the $\partial_\mu \pi^0 \rightarrow b_L \bar{b}_L$ vertex, π^0 being the neutral Goldstone boson in the Higgs doublet. We will follow, however, a different procedure, considering the Z boson as a propagating gauge field and calculating the one-loop corrections to the $Z b_L \bar{b}_L$ vertex in the Feynman gauge. Having set all the gauge couplings to zero, all the one-loop diagrams with internal vector lines do not give any contribution and the final number of total diagrams considerably reduces to four, as shown in Fig. (J.2). We will therefore be concerned in finding a general expression for δg_{Lb} arising from these one-loop diagrams for a general composite Higgs theory with new fermionic resonances.

We start our computation by writing down the most general Lagrangian describing the interactions involving Z_μ , a generic pair of fermions and the SM charged Goldstone bosons:

$$\begin{aligned} \mathcal{L} = & \frac{g_2^2}{c_W} Z_\mu (g_{b_L} \bar{b}_L \gamma^\mu b_L + g_{b_R} \bar{b}_R \gamma^\mu b_R + C_L^{ij} \bar{f}_L^i \gamma^\mu f_L^j + C_R^{ij} \bar{f}_R^i \gamma^\mu f_R^j) \\ & + i \lambda_i (\pi^- \bar{b}_L f_R^i - \pi^+ \bar{f}_R^i b_L) + i \frac{g_2^2}{2c_W} Z_\mu (\pi^- \partial^\mu \pi^+ - \pi^+ \partial^\mu \pi^-) \\ & + i \frac{g_2^2}{c_W} \rho_i Z_\mu (\pi^- \bar{b}_L \gamma^\mu f_L^i - \pi^+ \bar{f}_L^i \gamma^\mu b_L) + \eta_i (\partial_\mu \pi^- \bar{b}_L \gamma^\mu f_L^i + \partial_\mu \pi^+ \bar{f}_L^i \gamma^\mu b_L), \end{aligned} \quad (\text{J.9})$$

where, as before, $f_{L/R}$ denotes a left-handed or right-handed fermion in the theory and, in terms of the Goldstone fields in Eq.(A.16), we have set $\pi^+ = (\pi_1 - i\pi_2)/\sqrt{2}$ and $\pi^- = (\pi_1 + i\pi_2)/\sqrt{2}$. Notice that in our model there are no interactions between the neutral Goldstone boson and fermions or the Z vector, so that only one-loop diagrams involving the charged Goldstone bosons must be taken into account. As a consequence, only the top-like particles will give a non-zero correction to g_{b_L} and we must in the end focus on the sector of charge

¹See however [107] for a discussion of the effects of the gauge couplings to δg_{Lb} .

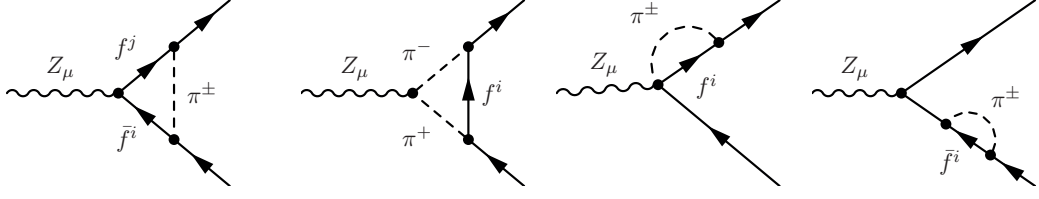


Figure J.2 – The four one-loop diagrams displaying the fermion contribution to the $Z \rightarrow b_L \bar{b}_L$ vertex.

$c = 2/3$. The final result reads:

$$\begin{aligned}
 \delta g_{Lb} = & -\frac{1}{32\pi^2} \sum_i \lambda_i^2 \left(g_{b_L} + \frac{1}{2} \right) \left(\Delta + \frac{3}{2} - \log \left(\frac{m_i^2}{\mu^2} \right) \right) \\
 & + \frac{1}{16\pi^2} \sum_{ij} \lambda_i \lambda_j \left[\frac{A_{Rij}}{2} \left(\Delta + \frac{1}{2} - J_1(m_i, m_j) \right) + A_{Lij} J_2(m_i, m_j) \right] \\
 & + \frac{1}{16\pi^2} \sum_{ij} \left[2\rho_i m_i (\lambda_i + \eta_i m_i) \left(\Delta + 1 - \log \left(\frac{m_i^2}{\mu^2} \right) \right) + \frac{1}{2} \eta_i^2 m_i^2 g_{b_L} \left(3\Delta + \frac{5}{2} - 3 \log \left(\frac{m_i^2}{\mu^2} \right) \right) \right. \\
 & \left. - \frac{\eta_i m_i}{2} (\lambda_i + \frac{1}{2} \eta_i m_i) \left(\Delta + \frac{3}{2} - \log \left(\frac{m_i^2}{\mu^2} \right) \right) + \eta_i \lambda_i m_i g_{b_L} \left(\Delta + \frac{1}{2} - \log \left(\frac{m_i^2}{\mu^2} \right) \right) \right. \\
 & \left. + \eta_i \eta_j \left(\frac{A_{Rij}}{2} m_i m_j \left(\Delta + \frac{1}{2} - J_1(m_i, m_j) \right) - A_{Lij} \left((m_i^2 + m_j^2)(\Delta + 1) - K(m_i, m_j) \right) \right) \right. \\
 & \left. + 2\eta_i \lambda_j \left(\frac{A_{Rij}}{2} m_i \left(\Delta + \frac{1}{2} - J_1(m_i, m_j) \right) - A_{Lij} m_j (\Delta + 1 - J_1(m_i, m_j)) \right) \right],
 \end{aligned} \tag{J.10}$$

with $A_L = U_{2/3}^\dagger C_L U_{2/3}$, $A_R = W_{2/3}^\dagger C_R W_{2/3}$ and

$$\begin{aligned}
 J_1(m_i, m_j) &= \frac{1}{m_i^2 - m_j^2} \left(m_i^2 \log \left(\frac{m_i^2}{\mu^2} \right) - m_j^2 \log \left(\frac{m_j^2}{\mu^2} \right) \right), \\
 J_2(m_i, m_j) &= \frac{m_i m_j}{m_i^2 - m_j^2} \log \left(\frac{m_i^2}{m_j^2} \right), \\
 K(m_i, m_j) &= \frac{1}{m_i^2 - m_j^2} \left(m_i^4 \log \left(\frac{m_i^2}{\mu^2} \right) - m_j^4 \log \left(\frac{m_j^2}{\mu^2} \right) \right).
 \end{aligned} \tag{J.11}$$

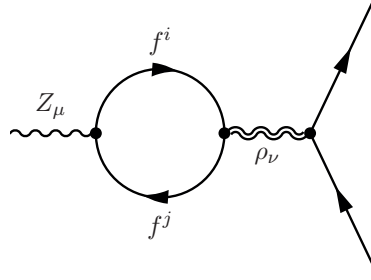


Figure J.3 – The one-loop diagram displaying the divergent contribution to the $Z \rightarrow b_L \bar{b}_L$ vertex originating from the renormalization of the Z boson propagator.

The last contribution to δg_{Lb} comes from the Feynman diagrams containing a tree-level exchange of a vector resonance, specifically ρ_μ^X in our construction (see Fig. (J.3)). A logarithmically divergent correction to the $Z b_L \bar{b}_L$ vertex is introduced in this case, together with additional contributions to the remaining finite parts, as explained in Chapter 4.

In order to take into account the presence of the heavy vectors, we need to renormalize the Z boson propagator resulting from the tree-level exchange of the neutral composite states and adding the one-loop contribution coming from all the fermions in the model. After diagonalizing the mixing between the gauge and heavy bosons in Eq. (5.23) at leading order in ξ , we can find the couplings between the Z gauge boson and the neutral resonances with the heavy fermions in the mass eigenstate basis. Once this is done, it is straightforward to compute the renormalized $Z - \rho$ propagator using the result of the previous sections; in particular, we can easily derive the renormalization function $\Pi_{Z\rho_0}(0)$. Indicating finally with $A_{\rho_0}^{b_L}$ the coupling between the neutral heavy vectors and the left-handed bottom quark, we find:

$$\delta g_{Lb} = \frac{\Pi_{Z\rho_0}(0)}{m_{\rho_0}^2} A_{\rho_0}^{b_L}. \quad (\text{J.12})$$

J.3 Results

We finally collect the explicit results for the EW observables in our models. Let us start considering the \hat{T} parameter. For convenience, we split the UV contribution into two parts, re-defining a_{UV} as:

$$a_{UV} = a_{UV}^{Fin} + a_{UV}^{Log} \log \left(\frac{M_\Psi^2}{M_S^2 + f^2 y_R^2} \right). \quad (\text{J.13})$$

The coefficients a_{UV}^{Fin} and a_{UV}^{Log} are obtained through a straightforward calculation, but their expressions are complicated functions of the Lagrangian parameters. We thus show them only

in the limit $c_L = c_R \equiv c$ and $M_\Psi = M_S \equiv M$, for simplicity. For a_{IR} we give instead the complete expression. We find:

$$\begin{aligned}
 a_{UV}^{Fin} &= \frac{1}{12} \left(-\frac{12M^4}{f^4 y_R^4} + \frac{6f^2 M^2 y_R^2}{(f^2 y_R^2 + M^2)^2} + \frac{9M^6}{(f^2 y_R^2 + M^2)^3} - 8 \right) \\
 &\quad + \frac{c(-5f^8 y_R^8 - 2f^6 M^2 y_R^6 + 7f^4 M^4 y_R^4 + 12f^2 M^6 y_R^2 + 4M^8)}{\sqrt{2} f^4 y_R^4 (f^2 y_R^2 + M^2)^2} \\
 &\quad + \frac{c^2 (f^2 y_R^2 + 2M^2)^2 (3f^2 y_R^2 - 5M^2)}{2f^4 y_R^4 (f^2 y_R^2 + M^2)}, \\
 a_{UV}^{Log} &= \frac{f^6 y_R^6 - f^4 M^2 y_R^4 - f^2 M^4 y_R^2 - 2M^6}{2f^6 y_R^6} \\
 &\quad + \frac{\sqrt{2}c(2f^6 y_R^6 - 3f^4 M^2 y_R^4 + 3f^2 M^4 y_R^2 + 2M^6)}{f^6 y_R^6} + \frac{c^2(f^2 M^4 y_R^2 - 10M^6)}{f^6 y_R^6}, \\
 a_{IR} &= \frac{1}{2} + \frac{M_S^2 M_\Psi^2}{2(M_S^2 + f^2 y_R^2)^2} + \sqrt{2} \frac{c_L M_S M_\Psi + 2c_R f^2 y_R^2}{M_S^2 + f^2 y_R^2}.
 \end{aligned} \tag{J.14}$$

The derivation of δg_{Lb} at 1-loop level is more involved and requires the computation of a series of diagrams. As explained in the text, we focus on those featuring a loop of fermions and NGBs (see figure J.2), and that one with a loop of fermion and the tree-level exchange of a heavy vector (see figure J.3).

The coefficients c_{UV} is generated only by the latter diagram; we find:

$$c_{UV} = \alpha_{7L}(\alpha_{1R} + \alpha_{7R})(1 + \sqrt{2}c_R) \frac{g_{\rho^x}^2 f^2}{M_{\rho^x}^2} \frac{M_\Psi^2}{2(M_\Psi^2 + y_L^2 f^2)}. \tag{J.15}$$

We remind the reader that in our numerical analysis we use $M_{\rho^x}/(g_{\rho^x} f) = 1$, see footnote 5. We re-define the other two coefficients as

$$\begin{aligned}
 b_{IR} &= \delta_{IR} + \bar{\delta}_{IR} \\
 b_{UV} &= \left(\delta_{UV}^{Fin} + \bar{\delta}_{UV}^{Fin} \right) + \left(\delta_{UV}^{Log} + \bar{\delta}_{UV}^{Log} \right) \log \left(\frac{M_\Psi^2}{M_S^2 + f^2 y_R^2} \right),
 \end{aligned} \tag{J.16}$$

where δ_{IR} , δ_{UV}^{Fin} and δ_{UV}^{Log} are generated by the diagrams in figure J.2 only, whereas $\bar{\delta}_{IR}$, $\bar{\delta}_{UV}^{Fin}$ and $\bar{\delta}_{UV}^{Log}$ parametrize the correction due to the tree-level exchange of a heavy spin-1 singlet in figure J.3. As before, we report the expression of the UV parameters in the limit $c_L = c_R \equiv c$, $M_\Psi = M_S \equiv M$, for simplicity; in the case of the coefficients with a bar, generated by the

Appendix J. Explicit formulae for the EWPO

diagram of figure J.3, we further set $\alpha_{7L} = \alpha_{1L}$ and $\alpha_{7R} = \alpha_{1R}$. We find:

$$\begin{aligned}
\delta_{UV}^{Fin} &= \frac{-2f^6 y_R^6 - 4f^4 M^2 y_R^4 - 4f^2 M^4 y_R^2 + M^6}{12(f^2 y_R^2 + M^2)^3} - \frac{c(f^6 y_R^6 + 4f^4 M^2 y_R^4 - 2f^2 M^4 y_R^2 + M^6)}{6\sqrt{2}f^2 y_R^2 (f^2 y_R^2 + M^2)^2} \\
&\quad + \frac{1}{6}c^2 M^2 \left(\frac{3}{f^2 y_R^2 + M^2} - \frac{2}{f^2 y_R^2} \right) - \frac{c^3 M^2}{3\sqrt{2}f^2 y_R^2}, \\
\delta_{UV}^{Log} &= \frac{1}{6} - \frac{M^2}{6f^2 y_R^2} - \frac{c^3 M^4}{3\sqrt{2}f^4 y_R^4} - \frac{c^2 M^4}{3f^4 y_R^4} - \frac{c(-f^4 y_R^4 + 2f^2 M^2 y_R^2 + M^4)}{6\sqrt{2}f^4 y_R^4}, \\
\bar{\delta}_{UV}^{Fin} &= \frac{f^2 M^2 \alpha_{1L} g_{\rho^x}^2 (f^4 y_R^4 (\alpha_{1L} + 2\alpha_{1R}) + f^2 M^2 y_R^2 (3\alpha_{1L} + 8\alpha_{1R}) + 2M^4 (\alpha_{1L} + \alpha_{1R}))}{4M_{\rho^x}^2 (f^2 y_L^2 + M^2) (f^2 y_R^2 + M^2)^2} \\
&\quad + \frac{c f^2 M^2 \alpha_{1L} g_{\rho^x}^2 (f^2 y_R^2 (2\alpha_{1L} + \alpha_{1R}) + 2M^2 \alpha_{1L})}{\sqrt{2}M_{\rho^x}^2 (f^2 y_L^2 + M^2) (f^2 y_R^2 + M^2)}, \\
\bar{\delta}_{UV}^{Log} &= \frac{cM^4 \alpha_{1L} g_{\rho^x}^2 (\alpha_{1L} - \alpha_{1R})}{\sqrt{2}y_R^2 M_{\rho^x}^2 (f^2 y_L^2 + M^2)} + \frac{f^2 M^2 \alpha_{1L} \alpha_{1R} g_{\rho^x}^2}{2M_{\rho^x}^2 (f^2 y_L^2 + M^2)}.
\end{aligned} \tag{J.17}$$

For the IR coefficients we give instead the full expressions. We find:

$$\begin{aligned}
\delta_{IR} &= \frac{1}{6} + \frac{M_S^2 M_\Psi^2}{6(M_S^2 + f^2 y_R^2)^2} + \sqrt{2} \frac{c_L M_S M_\Psi}{3(M_S^2 + f^2 y_R^2)} + \sqrt{2} \frac{c_R f^2 y_R^2}{12(M_S^2 + f^2 y_R^2)}, \\
\bar{\delta}_{IR} &= \alpha_{7L} \alpha_{1R} \frac{g_{\rho^x}^2}{M_{\rho^x}^2} \frac{f^4 M_\Psi^2 y_R^2}{2(f^2 y_L^2 + M_\Psi^2) (f^2 y_R^2 + M_S^2)}.
\end{aligned} \tag{J.18}$$

Notice that the IR corrections a_{IR} and b_{IR} are related to each other and parametrize the running of the effective coefficients \bar{c}_{Hq} , \bar{c}'_{Hq} and \bar{c}_{Ht} , as explained in the main text.

Finally, we report the contribution to \hat{S} generated in our simplified model by loops of heavy fermions. We do not include this correction in our electroweak fit, because in the perturbative region of the parameter space it is sub-dominant with respect to the tree-level shift of eq. (5.48). Rather, we use this computation as an additional way to estimate the perturbativity bound, as discussed in Sec. 5.2.2. Analogously to what we did for \hat{T} and δg_{Lb} , we parametrize the

fermionic contribution to \widehat{S} as:

$$\begin{aligned}\Delta\widehat{S}_\Psi &= \frac{g_2^2}{8\pi^2}\xi \left[(1 - c_L^2 - c_R^2) \log \frac{m_*^2}{M_\Psi^2} + (1 - \tilde{c}_L^2 - \tilde{c}_R^2) \log \frac{m_*^2}{\tilde{M}_\Psi^2} \right] \\ &+ \frac{g_2^2}{16\pi^2}\xi \left[s_{UV}^{Fin} + s_{UV}^{Log} \log \left(\frac{M_\Psi^2}{M_S^2 + f^2 y_R^2} \right) + \tilde{s}_{UV}^{Fin} + \tilde{s}_{UV}^{Log} \log \left(\frac{\tilde{M}_\Psi^2}{\tilde{M}_S^2 + f^2 \tilde{y}_R^2} \right) \right] \\ &+ \frac{g_2^2}{16\pi^2}\xi s_{IR} \frac{y_L^2 f^2}{M_\Psi^2} \log \frac{M_1^2}{m_t^2}.\end{aligned}\quad (\text{J.19})$$

Terms in the first line are logarithmically sensitive to the UV cut-off, the second line contains the UV threshold corrections, while the IR running appears in the third line. The UV thresholds include a contribution from the twin composites $\tilde{\Psi}_7$ and $\tilde{\Psi}_1$, parametrized by \tilde{s}_{UV}^{Fin} and \tilde{s}_{UV}^{Log} . At leading order in y_L , by virtue of the twin parity invariance of the strong sector, such contribution can be obtained from that of Ψ_7 and Ψ_1 (i.e. from s_{UV}^{Fin} and s_{UV}^{Log}) by simply interchanging the tilded quantities with the un-tilded ones. Higher orders in y_L break this symmetry and generate different corrections in the two sectors. We performed the computation of the UV coefficients for $y_L = 0$, whereas s_{IR} is derived up to order y_L^2 . We find:

$$\begin{aligned}s_{UV}^{Fin} &= \frac{1}{2} - \frac{6c_L c_R M_S M_\Psi (f^2 y_R^2 + M_S^2 + M_\Psi^2)}{(f^2 y_R^2 + M_S^2 - M_\Psi^2)^2} + \frac{(c_R^2 + c_L^2)}{6} \left(\frac{24M_S^2 M_\Psi^2}{(f^2 y_R^2 + M_S^2 - M_\Psi^2)^2} - 7 \right), \\ s_{UV}^{Log} &= - \frac{2(M_S^2 + f^2 y_R^2)}{(M_S^2 - M_\Psi^2 + f^2 y_R^2)^3} \left[6c_L c_R M_S M_\Psi^3 + c_R^2 M_S^2 (f^2 y_R^2 + M_S^2 - 3M_\Psi^2) \right. \\ &\quad \left. + c_L^2 (f^2 y_R^2 + M_S^2) (f^2 y_R^2 + M_S^2 - 3M_\Psi^2) \right], \\ s_{IR} &= \frac{M_S^2 M_\Psi^4 - f^2 y_L^2 ((f^2 y_R^2 + M_S^2)(M_S^2 - f^2 y_R^2) + M_S^2 M_\Psi^2) + M_\Psi^2 (f^2 y_R^2 + M_S^2)^2}{6M_\Psi^2 (f^2 y_R^2 + M_S^2)^2} \\ &\quad - c_R \frac{2\sqrt{2}f^2 y_R^2 (M_\Psi^2 - f^2 y_L^2)}{3M_\Psi^2 (f^2 y_R^2 + M_S^2)} - c_L \frac{\sqrt{2}M_S (M_\Psi^2 - f^2 y_L^2)}{3M_\Psi (f^2 y_R^2 + M_S^2)}.\end{aligned}\quad (\text{J.20})$$

K The EW fit

For our analysis of the electroweak observables we make use of the fit to the parameters $\epsilon_{1,2,3,b}$ [61–63] performed in ref. [60] (see also ref. [57]). The central values there obtained for the shifts $\Delta\epsilon_i \equiv \epsilon_i - \epsilon_i^{SM}$ and the corresponding correlation matrix are:

$$\begin{aligned} \Delta\epsilon_1 &= 0.0007 \pm 0.0010 \\ \Delta\epsilon_2 &= -0.0001 \pm 0.0009 \\ \Delta\epsilon_3 &= 0.0006 \pm 0.0009 \\ \Delta\epsilon_b &= 0.0003 \pm 0.0013 \end{aligned} \quad \rho = \begin{pmatrix} 1 & 0.8 & 0.86 & -0.33 \\ 0.8 & 1 & 0.51 & -0.32 \\ 0.86 & 0.51 & 1 & -0.22 \\ -0.33 & -0.32 & -0.22 & 1 \end{pmatrix}. \quad (\text{K.1})$$

We can directly relate $\Delta\epsilon_1$ to $\Delta\hat{T}$ and $\Delta\epsilon_3$ to $\Delta\hat{S}$ by using the results of Ref. [111], and furthermore $\Delta\epsilon_b = -2\delta g_{Lb}$. We set $\Delta\epsilon_2 = 0$ in our study, since its effect is sub-dominant in our model as well as in CH models [111]. We thus make use of eq. (K.1) to perform a χ^2 test of the compatibility of our predictions with the experimental constraints. The χ^2 function is defined as customary:

$$\chi^2 = \sum_{ij} (\Delta\epsilon_i - \mu_i) (\sigma^2)_{ij}^{-1} (\Delta\epsilon_j - \mu_j), \quad (\sigma)_{ij}^2 = \sigma_i \rho_{ij} \sigma_j, \quad (\text{K.2})$$

where μ_i and σ_i denote respectively the mean values and the standard deviations of eq. (K.1), while $\Delta\epsilon_i$ indicates the theoretical prediction for each EW observable computed in terms of the Lagrangian parameters. After deriving the χ^2 , we perform a fit by scanning over the points in our parameter space keeping only those for which $\Delta\chi^2 \equiv \chi^2 - \chi_{min}^2 < 7.82$, the latter condition corresponding to the 95% Confidence Level with 3 degrees of freedom. Using this procedure, we convert the experimental constraints into bounds over the plane (M_Ψ, ξ) .

L Estimates of the perturbativity bound

This Appendix contains details on the derivation of the perturbative limits discussed in Sec. 5.2.2. As there explained, we considered the processes $\pi^a \pi^b \rightarrow \pi^c \pi^d$ and $\pi^a \pi^b \rightarrow \bar{\psi}^c \psi^d$, where $\psi = \{\Psi_7, \tilde{\Psi}_7\}$ and all indices transform under the fundamental representation of the unbroken $SO(7)$. In order to better monitor how the results depend on the multiplicity of NGBs and fermions, we performed the calculation for a generic $SO(N)/SO(N-1)$ coset with N_f composite fermions ψ in the fundamental of $SO(N-1)$. Taking $N = 8$ and $N_f = 2 \times 3 = 6$ thus reproduces the simplified model of Sec. 5.2.1.

The perturbative limits are obtained by first expressing the scattering amplitudes in terms of components with definite $SO(N-1)$ quantum numbers. In the case of $SO(7)$ the product of two fundamentals decomposes as $\mathbf{7} \otimes \mathbf{7} = \mathbf{1} \oplus \mathbf{21}_a \oplus \mathbf{27}_s$, where the indices a and s label respectively the anti-symmetric and symmetric two-index representations. A completely analog decomposition holds in the general case of $SO(N)/SO(N-1)$,¹ but for simplicity we will use the $SO(7)$ notation in the following to label the various components. The tree-level leading contributions to the scattering amplitudes arise from the contact interaction generated by the expansion of the NGB kinetic term of eq. (5.20) and from the NGB-fermion interactions of eq. (5.25). The structure of the corresponding vertices implies that the four-NGB amplitude has components in all the three irreducible representations of $SO(N-1)$ and contains all partial waves. The amplitude with two NGBs and two fermions, instead, has only the anti-symmetric component of $SO(N-1)$ and starts with the p -wave. At energies much larger than

¹One has $\mathbf{N} \otimes \mathbf{N} = \mathbf{1} \oplus [\mathbf{N}(\mathbf{N}-1)/2]_a \oplus [\mathbf{N}(\mathbf{N}+1)/2-1]_s$.

Appendix L. Estimates of the perturbativity bound

all masses the amplitudes read

$$\begin{aligned}
\mathcal{M}(\pi^a \pi^b \rightarrow \pi^c \pi^d) &= \frac{s}{f^2} \delta^{ab} \delta^{cd} + \frac{t}{f^2} \delta^{ac} \delta^{bd} + \frac{u}{f^2} \delta^{ad} \delta^{bc}, \\
\mathcal{M}(\pi^a \pi^b \rightarrow \bar{\Psi}_{7_L}^c \Psi_{7_L}^d) &= \frac{s}{2f^2} \sin \theta (\delta^{ac} \delta^{bd} - \delta^{ad} \delta^{bc}), \\
\mathcal{M}(\pi^a \pi^b \rightarrow \bar{\Psi}_{7_R}^c \Psi_{7_R}^d) &= \frac{s}{2f^2} \sin \theta (\delta^{ac} \delta^{bd} - \delta^{ad} \delta^{bc}).
\end{aligned} \tag{L.1}$$

They decompose into irreducible representations of $SO(N-1)$ as follows:

$$\begin{aligned}
\mathcal{M}^{(1)}(\pi^a \pi^b \rightarrow \pi^c \pi^d) &= (N-2) \frac{s}{f^2}, & \mathcal{M}^{(21)}(\pi^a \pi^b \rightarrow \bar{\Psi}_{7_L}^c \Psi_{7_L}^d) &= \frac{s}{2f^2} \sin \theta, \\
\mathcal{M}^{(21)}(\pi^a \pi^b \rightarrow \pi^c \pi^d) &= \frac{s}{f^2} \cos \theta, & \mathcal{M}^{(21)}(\pi^a \pi^b \rightarrow \bar{\Psi}_{7_R}^c \Psi_{7_R}^d) &= \frac{s}{2f^2} \sin \theta. \\
\mathcal{M}^{(27)}(\pi^a \pi^b \rightarrow \pi^c \pi^d) &= -\frac{s}{f^2},
\end{aligned} \tag{L.2}$$

Performing a partial wave decomposition we get

$$\mathcal{M}^{(\mathbf{r})} = \sum_{\lambda_i, \lambda_f} \mathcal{M}_{\lambda_i, \lambda_f}^{(\mathbf{r})} = 16\pi k^{(i)} k^{(f)} \sum_{j=0}^{\infty} a_j^{(\mathbf{r})} (2j+1) \sum_{\lambda_i, \lambda_f} D_{\lambda_i, \lambda_f}^j(\theta), \tag{L.3}$$

where λ_i, λ_f are the initial and final state total helicities, and $k^{(i)} (k^{(f)})$ is equal to either 1 or $\sqrt{2}$ depending on whether the two particles in the initial (final) state are distinguishable or identical respectively. In the above equation $\mathcal{M}^{(\mathbf{r})}$ should be considered as a matrix acting on the space of different channels. The coefficients $a_j^{(\mathbf{r})}$ are given by

$$a_j^{(\mathbf{r})} = \frac{1}{32\pi k^{(i)} k^{(f)}} \int_0^\pi d\theta \sum_{\lambda_i, \lambda_f} \mathcal{D}_{\lambda_i, \lambda_f}^j(\theta) \mathcal{M}_{\lambda_i, \lambda_f}^{(\mathbf{r})}. \tag{L.4}$$

and act as matrices on the space of (elastic and inelastic) channels with total angular momentum j and $SO(N-1)$ irreducible representations \mathbf{r} . They can be rewritten as a function of the scattering phase as

$$a_j^{(\mathbf{r})} = \frac{e^{2i\delta_j^{(\mathbf{r})}} - 1}{2i} \sim \delta_j^{(\mathbf{r})}. \tag{L.5}$$

Our NDA estimate of the perturbativity bound is derived by requiring this phase to be smaller than maximal:

$$|\delta_j^{(\mathbf{r})}| < \frac{\pi}{2} \quad \Rightarrow \quad |a_j^{(\mathbf{r})}| < \frac{\pi}{2} \tag{L.6}$$

Let us consider first the case $\mathbf{r} = \mathbf{1}$, corresponding to the amplitude singlet of $SO(N-1)$. The

only contribution comes from the four-NGB channel. Since the helicities of the initial and final states are all zeros, in this particular case the Wigner functions $\mathcal{D}_{\lambda_i, \lambda_f}^j(\theta)$ reduce to the Legendre polynomials:

$$a_j^{(1)} = \frac{1}{64\pi} \int_0^\pi d\theta P_j(\cos\theta) \mathcal{M}^{(1)}. \quad (\text{L.7})$$

The first and strongest perturbativity constraint comes from the s -wave amplitude, which corresponds to $j = 0$. We find:

$$a_0^{(1)} = \frac{N-2}{32\pi} \frac{s}{f^2}, \quad (\text{L.8})$$

where $N = 8$ in our case. From eqs. (L.6) and (L.8), one obtains the constraint of eq. (5.31).

We analyze now the constraint from the scattering in the anti-symmetric representation, $\mathbf{r} = \mathbf{21}$. In this case, both the NGB and the fermion channels contribute; the process $\pi\pi \rightarrow \pi\pi$ is however independent of the fermion and Goldstone multiplicities and can be neglected in the limit of N and N_f . The process involving fermions is a function of N_f and generates a perturbative limit which is comparable and complementary to the previous one. We have:

$$a_j^{(21)} = \sum_{\lambda_f = \pm 1} \frac{1}{32\pi} \int_0^\pi d\theta \mathcal{D}_{0, \lambda_f}^j(\theta) \mathcal{M}_{0, \lambda_f}^{(21)}. \quad (\text{L.9})$$

As anticipated, this equation vanishes for $j = 0$, so that the strongest constraint is now derived for p -wave scattering, with $j = 1$. We have

$$a_1^{(21)} = \frac{N_f}{24\sqrt{2}\pi} \frac{s}{f^2}. \quad (\text{L.10})$$

From eqs. (L.6) and (L.10) it follows the constraint of eq. (5.32).



Bibliography

- [1] G. 't Hooft, NATO Sci. Ser. B **59**, 135 (1980).
- [2] S. R. Coleman and J. Mandula, Phys. Rev. **159**, 1251 (1967). doi:10.1103/PhysRev.159.1251
- [3] R. Haag, J. T. Lopuszanski and M. Sohnius, Nucl. Phys. B **88**, 257 (1975). doi:10.1016/0550-3213(75)90279-5
- [4] A. Arvanitaki, M. Baryakhtar, X. Huang, K. van Tilburg and G. Villadoro, JHEP **1403** (2014) 022 doi:10.1007/JHEP03(2014)022 [arXiv:1309.3568 [hep-ph]].
- [5] R. Barbieri and G. F. Giudice, Nucl. Phys. B **306**, 63 (1988). doi:10.1016/0550-3213(88)90171-X
- [6] S. Dimopoulos and G. F. Giudice, Phys. Lett. B **357**, 573 (1995) doi:10.1016/0370-2693(95)00961-J [hep-ph/9507282].
- [7] A. De Simone, O. Matsedonskyi, R. Rattazzi and A. Wulzer, JHEP **1304** (2013) 004 [arXiv:1211.5663 [hep-ph]].
- [8] R. Contino, D. Marzocca, D. Pappadopulo and R. Rattazzi, JHEP **1110** (2011) 081 [arXiv:1109.1570 [hep-ph]].
- [9] S. R. Coleman, J. Wess and B. Zumino, Phys. Rev. **177** (1969) 2239.
- [10] C. G. Callan, Jr., S. R. Coleman, J. Wess and B. Zumino, Phys. Rev. **177** (1969) 2247.
- [11] S. Weinberg, Phys. Lett. **91B**, 51 (1980). doi:10.1016/0370-2693(80)90660-7
- [12] M. Bando, T. Kugo, S. Uehara, K. Yamawaki and T. Yanagida, Phys. Rev. Lett. **54** (1985) 1215.
- [13] D. B. Kaplan, Nucl. Phys. B **365** (1991) 259.
- [14] D. B. Kaplan and H. Georgi, Phys. Lett. B **136** (1984) 183.
- [15] R. Contino, T. Kramer, M. Son and R. Sundrum, JHEP **0705** (2007) 074 [hep-ph/0612180].

Bibliography

- [16] Y. Grossman and M. Neubert, Phys. Lett. B **474** (2000) 361 [hep-ph/9912408].
- [17] T. Gherghetta and A. Pomarol, Nucl. Phys. B **586** (2000) 141 [hep-ph/0003129].
- [18] R. Contino and A. Pomarol, JHEP **0411** (2004) 058 [hep-th/0406257].
- [19] K. Agashe, R. Contino and A. Pomarol, Nucl. Phys. B **719** (2005) 165 [hep-ph/0412089].
- [20] R. Contino, arXiv:1005.4269 [hep-ph].
- [21] S. Weinberg, *The quantum theory of fields. Vol. 2: Modern applications*.
- [22] M. E. Peskin and D. V. Schroeder, *An Introduction to quantum field theory*, Reading, USA: Addison-Wesley (1995) 842 p.
- [23] M. Schmaltz and D. Tucker-Smith, Ann. Rev. Nucl. Part. Sci. **55** (2005) 229 doi:10.1146/annurev.nucl.55.090704.151502 [hep-ph/0502182].
- [24] G. F. Giudice, C. Grojean, A. Pomarol and R. Rattazzi, JHEP **0706** (2007) 045 [hep-ph/0703164].
- [25] J. Elias-Miro, J. R. Espinosa, E. Masso and A. Pomarol, JHEP **1311** (2013) 066 doi:10.1007/JHEP11(2013)066 [arXiv:1308.1879 [hep-ph]].
- [26] E. E. Jenkins, A. V. Manohar and M. Trott, JHEP **1310** (2013) 087 doi:10.1007/JHEP10(2013)087 [arXiv:1308.2627 [hep-ph]].
- [27] E. E. Jenkins, A. V. Manohar and M. Trott, JHEP **1401** (2014) 035 doi:10.1007/JHEP01(2014)035 [arXiv:1310.4838 [hep-ph]].
- [28] R. Alonso, E. E. Jenkins, A. V. Manohar and M. Trott, JHEP **1404** (2014) 159 doi:10.1007/JHEP04(2014)159 [arXiv:1312.2014 [hep-ph]].
- [29] G. Panico, M. Redi, A. Tesi and A. Wulzer, JHEP **1303** (2013) 051 [arXiv:1210.7114 [hep-ph]].
- [30] O. Matsedonskyi, G. Panico and A. Wulzer, JHEP **1301** (2013) 164 [arXiv:1204.6333 [hep-ph]].
- [31] M. Redi and A. Tesi, JHEP **1210** (2012) 166 [arXiv:1205.0232 [hep-ph]].
- [32] A. Pomarol and F. Riva, JHEP **1208** (2012) 135 [arXiv:1205.6434 [hep-ph]].
- [33] D. Marzocca, M. Serone and J. Shu, JHEP **1208** (2012) 013 [arXiv:1205.0770 [hep-ph]].
- [34] D. Pappadopulo, A. Thamm and R. Torre, JHEP **1307** (2013) 058 [arXiv:1303.3062 [hep-ph]].

-
- [35] R. Contino, L. Da Rold and A. Pomarol, Phys. Rev. D **75** (2007) 055014 [hep-ph/0612048].
- [36] O. Matsedonskyi, G. Panico and A. Wulzer, JHEP **1604**, 003 (2016) doi:10.1007/JHEP04(2016)003 [arXiv:1512.04356 [hep-ph]].
- [37] O. Matsedonskyi, G. Panico and A. Wulzer, JHEP **1412**, 097 (2014) doi:10.1007/JHEP12(2014)097 [arXiv:1409.0100 [hep-ph]].
- [38] J. Mrazek, A. Pomarol, R. Rattazzi, M. Redi, J. Serra and A. Wulzer, Nucl. Phys. B **853** (2011) 1 [arXiv:1105.5403 [hep-ph]].
- [39] K. Agashe, R. Contino, L. Da Rold and A. Pomarol, Phys. Lett. B **641** (2006) 62 [hep-ph/0605341].
- [40] D. Pappadopulo, A. Thamm, R. Torre and A. Wulzer, arXiv:1402.4431 [hep-ph].
- [41] J. de Blas, J. M. Lizana and M. Perez-Victoria, JHEP **1301** (2013) 166 [arXiv:1211.2229 [hep-ph]].
- [42] O. Matsedonskyi, F. Riva and T. Vantalón, JHEP **1404** (2014) 059 [arXiv:1401.3740 [hep-ph]].
- [43] K. Agashe, H. Davoudiasl, S. Gopalakrishna, T. Han, G. Y. Huang, G. Perez, Z. G. Si and A. Soni, Phys. Rev. D **76** (2007) 115015 [arXiv:0709.0007 [hep-ph]].
- [44] K. Agashe, S. Gopalakrishna, T. Han, G. Y. Huang and A. Soni, Phys. Rev. D **80** (2009) 075007 [arXiv:0810.1497 [hep-ph]].
- [45] K. Agashe, H. Davoudiasl, G. Perez and A. Soni, Phys. Rev. D **76** (2007) 036006 [hep-ph/0701186].
- [46] K. Agashe, A. Belyaev, T. Krupovnickas, G. Perez and J. Virzi, Phys. Rev. D **77** (2008) 015003 [hep-ph/0612015].
- [47] D. Barducci, A. Belyaev, S. De Curtis, S. Moretti and G. M. Pruna, JHEP **1304** (2013) 152 [arXiv:1210.2927 [hep-ph]].
- [48] R. Barbieri, A. E. Carcamo Hernandez, G. Corcella, R. Torre and E. Trincherini, JHEP **1003** (2010) 068 [arXiv:0911.1942 [hep-ph]].
- [49] C. Bini, R. Contino and N. Vignaroli, JHEP **1201** (2012) 157 [arXiv:1110.6058 [hep-ph]].
- [50] R. Contino, C. Grojean, M. Moretti, F. Piccinini and R. Rattazzi, JHEP **1005** (2010) 089 [arXiv:1002.1011 [hep-ph]].
- [51] N. Vignaroli, Phys. Rev. D **89** (2014) 095027 [arXiv:1404.5558 [hep-ph]].

Bibliography

- [52] G. Brooijmans, R. Contino, B. Fuks, F. Moortgat, P. Richardson, S. Sekmen, A. Weiler and A. Alloul *et al.*, arXiv:1405.1617 [hep-ph].
- [53] R. Contino, C. Grojean, D. Pappadopulo, R. Rattazzi and A. Thamm, JHEP **1402** (2014) 006 [arXiv:1309.7038 [hep-ph]].
- [54] A. Thamm, R. Torre and A. Wulzer, JHEP **1507**, 100 (2015) doi:10.1007/JHEP07(2015)100 [arXiv:1502.01701 [hep-ph]].
- [55] M. E. Peskin and T. Takeuchi, Phys. Rev. D **46** (1992) 381.
- [56] R. Barbieri, A. Pomarol, R. Rattazzi and A. Strumia, Nucl. Phys. B **703** (2004) 127 [hep-ph/0405040].
- [57] M. Ciuchini, E. Franco, S. Mishima and L. Silvestrini, JHEP **1308** (2013) 106 [arXiv:1306.4644 [hep-ph]].
- [58] B. Grinstein and M. B. Wise, Phys. Lett. B **265**, 326 (1991). doi:10.1016/0370-2693(91)90061-T
- [59] J. de Blas, M. Ciuchini, E. Franco, S. Mishima, M. Pierini, L. Reina and L. Silvestrini, arXiv:1611.05354 [hep-ph].
- [60] M. Ciuchini, E. Franco, S. Mishima, M. Pierini, L. Reina and L. Silvestrini, Nucl. Part. Phys. Proc. **273-275** (2016) 2219 doi:10.1016/j.nuclphysbps.2015.09.361 [arXiv:1410.6940 [hep-ph]].
- [61] G. Altarelli and R. Barbieri, Phys. Lett. B **253**, 161 (1991). doi:10.1016/0370-2693(91)91378-9
- [62] G. Altarelli, R. Barbieri and S. Jadach, Nucl. Phys. B **369** (1992) 3 Erratum: [Nucl. Phys. B **376** (1992) 444]. doi:10.1016/0550-3213(92)90376-M
- [63] G. Altarelli, R. Barbieri and F. Caravaglios, Nucl. Phys. B **405**, 3 (1993). doi:10.1016/0550-3213(93)90424-N
- [64] A. Alloul, N. D. Christensen, C. Degrande, C. Duhr and B. Fuks, Comput. Phys. Commun. **185** (2014) 2250 [arXiv:1310.1921 [hep-ph]].
- [65] J. Alwall, M. Herquet, F. Maltoni, O. Mattelaer and T. Stelzer, JHEP **1106** (2011) 128 [arXiv:1106.0522 [hep-ph]].
- [66] R. Contino, D. Greco and D. Liu, “Rho resonances in composite Higgs model”, URL: <http://hepmdb.soton.ac.uk/hepmdb:1014.0179>.

-
- [67] V. Khachatryan *et al.* [CMS Collaboration], Phys. Rev. D **93**, no. 11, 112009 (2016) doi:10.1103/PhysRevD.93.112009 [arXiv:1507.07129 [hep-ex]].
- [68] A. M. Sirunyan *et al.* [CMS Collaboration], arXiv:1701.08328 [hep-ex].
- [69] A. M. Sirunyan *et al.* [CMS Collaboration], arXiv:1701.07409 [hep-ex].
- [70] CMS Collaboration [CMS Collaboration], CMS-PAS-B2G-16-011.
- [71] CMS Collaboration [CMS Collaboration], CMS-PAS-B2G-16-006.
- [72] CMS Collaboration [CMS Collaboration], CMS-PAS-B2G-16-001.
- [73] CMS Collaboration [CMS Collaboration], CMS-PAS-BTV-15-002.
- [74] G. Aad *et al.* [ATLAS Collaboration], JHEP **1508**, 105 (2015) doi:10.1007/JHEP08(2015)105 [arXiv:1505.04306 [hep-ex]].
- [75] J. P. Araque [ATLAS Collaboration], arXiv:1611.09056 [hep-ex].
- [76] The ATLAS collaboration [ATLAS Collaboration], ATLAS-CONF-2016-102.
- [77] The ATLAS collaboration [ATLAS Collaboration], ATLAS-CONF-2016-101.
- [78] The ATLAS collaboration [ATLAS Collaboration], ATLAS-CONF-2016-072.
- [79] The ATLAS collaboration, ATLAS-CONF-2016-013.
- [80] G. Aad *et al.* [ATLAS Collaboration], Eur. Phys. J. C **76**, no. 8, 442 (2016) doi:10.1140/epjc/s10052-016-4281-8 [arXiv:1602.05606 [hep-ex]].
- [81] S. Chatrchyan *et al.* [CMS Collaboration], Phys. Rev. Lett. **112** (2014) 171801 [arXiv:1312.2391 [hep-ex]].
- [82] CMS Collaboration [CMS Collaboration], CMS-PAS-EXO-12-061.
- [83] CMS Collaboration [CMS Collaboration], CMS-PAS-EXO-12-021.
- [84] CMS Collaboration [CMS Collaboration], CMS-PAS-B2G-12-005.
- [85] CMS Collaboration [CMS Collaboration], CMS-PAS-EXO-12-024.
- [86] V. Khachatryan *et al.* [CMS Collaboration], arXiv:1405.1994 [hep-ex].
- [87] V. Khachatryan *et al.* [CMS Collaboration], arXiv:1405.3447 [hep-ex].
- [88] [CMS Collaboration], CMS-PAS-B2G-12-010.
- [89] CMS Collaboration [CMS Collaboration], CMS-PAS-EXO-12-025.

Bibliography

- [90] V. Khachatryan *et al.* [CMS Collaboration], arXiv:1408.2745 [hep-ex].
- [91] The ATLAS collaboration, ATLAS-CONF-2013-052.
- [92] G. Aad *et al.* [ATLAS Collaboration], arXiv:1405.4123 [hep-ex].
- [93] The ATLAS collaboration, ATLAS-CONF-2013-066.
- [94] The ATLAS collaboration, ATLAS-CONF-2014-017.
- [95] The ATLAS collaboration, ATLAS-CONF-2013-050.
- [96] The ATLAS collaboration, ATLAS-CONF-2014-015.
- [97] The ATLAS collaboration [ATLAS Collaboration], ATLAS-CONF-2016-101.
- [98] CMS Collaboration [CMS Collaboration], CMS-PAS-B2G-16-011.
- [99] G. Aad *et al.* [ATLAS and CMS Collaborations], JHEP **1608**, 045 (2016) doi:10.1007/JHEP08(2016)045 [arXiv:1606.02266 [hep-ex]].
- [100] C. Patrignani *et al.* [Particle Data Group], Chin. Phys. C **40**, no. 10, 100001 (2016). doi:10.1088/1674-1137/40/10/100001
- [101] T. Golling *et al.*, [arXiv:1606.00947 [hep-ph]].
- [102] R. Barbieri, B. Bellazzini, V. S. Rychkov and A. Varagnolo, Phys. Rev. D **76** (2007) 115008 [arXiv:0706.0432 [hep-ph]].
- [103] D. Buttazzo, F. Sala and A. Tesi, JHEP **1511**, 158 (2015) doi:10.1007/JHEP11(2015)158 [arXiv:1505.05488 [hep-ph]].
- [104] P. Lodone, JHEP **0812** (2008) 029 [arXiv:0806.1472 [hep-ph]].
- [105] M. Gillioz, Phys. Rev. D **80** (2009) 055003 [arXiv:0806.3450 [hep-ph]].
- [106] R. Rattazzi, Nucl. Phys. B **335**, 301 (1990). doi:10.1016/0550-3213(90)90495-Y
- [107] C. Anastasiou, E. Furlan and J. Santiago, Phys. Rev. D **79** (2009) 075003 [arXiv:0901.2117 [hep-ph]].
- [108] C. Grojean, O. Matsedonskyi and G. Panico, JHEP **1310** (2013) 160 [arXiv:1306.4655 [hep-ph]].
- [109] M. Carena, E. Ponton, J. Santiago and C. E. M. Wagner, Phys. Rev. D **76**, 035006 (2007) doi:10.1103/PhysRevD.76.035006 [hep-ph/0701055].
- [110] D. Ghosh, M. Salvarezza and F. Senia, arXiv:1511.08235 [hep-ph].

-
- [111] R. Contino and M. Salvarezza, JHEP **1507** (2015) 065 doi:10.1007/JHEP07(2015)065 [arXiv:1504.02750 [hep-ph]].
- [112] R. Contino and M. Salvarezza, Phys. Rev. D **92** (2015) no.11, 115010 doi:10.1103/PhysRevD.92.115010 [arXiv:1511.00592 [hep-ph]].
- [113] L. Lavoura and J. P. Silva, Phys. Rev. D **47** (1993) 1117.
- [114] L. Lavoura and J. P. Silva, Phys. Rev. D **47** (1993) 2046.
- [115] S. R. Coleman and E. J. Weinberg, Phys. Rev. D **7** (1973) 1888.
- [116] R. Barbieri, M. Beccaria, P. Ciafaloni, G. Curci and A. Vicere, Phys. Lett. B **288** (1992) 95 [Phys. Lett. B **312** (1993) 511] [hep-ph/9205238].
- [117] G. Panico and A. Wulzer, JHEP **1109** (2011) 135 [arXiv:1106.2719 [hep-ph]].
- [118] R. Barbieri, D. Greco, R. Rattazzi and A. Wulzer, JHEP **1508** (2015) 161 doi:10.1007/JHEP08(2015)161 [arXiv:1501.07803 [hep-ph]].
- [119] M. Low, A. Tesi and L. T. Wang, Phys. Rev. D **91** (2015) 095012 [arXiv:1501.07890 [hep-ph]].
- [120] M. Geller and O. Telem, Phys. Rev. Lett. **114**, 191801 (2015) doi:10.1103/PhysRevLett.114.191801 [arXiv:1411.2974 [hep-ph]].
- [121] C. Csaki, M. Geller, O. Telem and A. Weiler, JHEP **1609** (2016) 146 doi:10.1007/JHEP09(2016)146 [arXiv:1512.03427 [hep-ph]].
- [122] D. Greco and K. Mimouni, JHEP **1611**, 108 (2016) doi:10.1007/JHEP11(2016)108 [arXiv:1609.05922 [hep-ph]].
- [123] R. Contino, D. Greco, R. Mahbubani, R. Rattazzi and R. Torre, arXiv:1702.00797 [hep-ph].
- [124] G. Degrandi, S. Di Vita, J. Elias-Miro, J. R. Espinosa, G. F. Giudice, G. Isidori and A. Strumia, JHEP **1208**, 098 (2012) doi:10.1007/JHEP08(2012)098 [arXiv:1205.6497 [hep-ph]].
- [125] Z. Chacko, H. S. Goh and R. Harnik, Phys. Rev. Lett. **96** (2006) 231802 [hep-ph/0506256].
- [126] R. Barbieri, T. Gregoire and L. J. Hall, hep-ph/0509242.
- [127] Z. Chacko, Y. Nomura, M. Papucci and G. Perez, JHEP **0601** (2006) 126 [hep-ph/0510273].
- [128] Z. Chacko, H. S. Goh and R. Harnik, JHEP **0601** (2006) 108 [hep-ph/0512088].
- [129] S. Chang, L. J. Hall and N. Weiner, Phys. Rev. D **75** (2007) 035009 [hep-ph/0604076].

Bibliography

- [130] J. Galloway, M. A. Luty, Y. Tsai and Y. Zhao, Phys. Rev. D **89**, no. 7, 075003 (2014) doi:10.1103/PhysRevD.89.075003 [arXiv:1306.6354 [hep-ph]].
- [131] S. Chang, J. Galloway, M. Luty, E. Salvioni and Y. Tsai, JHEP **1503**, 017 (2015) doi:10.1007/JHEP03(2015)017 [arXiv:1411.6023 [hep-ph]].
- [132] N. Craig and K. Howe, JHEP **1403** (2014) 140 [arXiv:1312.1341 [hep-ph]].
- [133] P. Batra and Z. Chacko, Phys. Rev. D **79** (2009) 095012 [arXiv:0811.0394 [hep-ph]].
- [134] N. Craig, S. Knapen and P. Longhi, arXiv:1410.6808 [hep-ph].
- [135] N. Craig, S. Knapen and P. Longhi, arXiv:1411.7393 [hep-ph].
- [136] G. Burdman, Z. Chacko, R. Harnik, L. de Lima and C. B. Verhaaren, arXiv:1411.3310 [hep-ph].
- [137] N. Craig, A. Katz, M. Strassler and R. Sundrum, JHEP **1507**, 105 (2015) doi:10.1007/JHEP07(2015)105 [arXiv:1501.05310 [hep-ph]].
- [138] N. Craig, S. Knapen, P. Longhi and M. Strassler, JHEP **1607** (2016) 002 doi:10.1007/JHEP07(2016)002 [arXiv:1601.07181 [hep-ph]].
- [139] A. Katz, A. Mariotti, S. Pokorski, D. Redigolo and R. Ziegler, arXiv:1611.08615 [hep-ph].
- [140] Z. Chacko, N. Craig, P. J. Fox and R. Harnik, [arXiv:1611.07975 [hep-ph]].
- [141] R. Harnik, K. Howe and J. Kearney, [arXiv:1603.03772 [hep-ph]].
- [142] R. Barbieri, L. J. Hall and K. Harigaya, JHEP **1611** (2016) 172 doi:10.1007/JHEP11(2016)172 [arXiv:1609.05589 [hep-ph]].
- [143] P. A. R. Ade *et al.* [Planck Collaboration], Astron. Astrophys. **594**, A13 (2016) doi:10.1051/0004-6361/201525830 [arXiv:1502.01589 [astro-ph.CO]].
- [144] H. C. Cheng, E. Salvioni and Y. Tsai, arXiv:1612.03176 [hep-ph].

Davide Greco

Avenue de la Rochelle 10, 1008, Prilly (VD), Switzerland

+41 21 69 30565, +39 338 56 16 268

Skype: davidegreco33

E-mail address: davide.greco45@gmail.com

[LinkedIn](#)



PROFILE

Educated as a Theoretical Physicist, I have strong mathematical, analytical and problem-solving skills. Experienced in mathematical modelling, statistical data analysis, numerical simulations and programming, I am a quick learner with a strong adaptability and team spirit.

EDUCATION

EPFL (École Polytechnique Fédérale de Lausanne)

Ph. D. researcher in Theoretical Particle Physics

Graduation: April 26th 2017.

Lausanne (VD), Switzerland

May 2013 - Present

Università degli Studi di Milano-Bicocca

Laurea Magistrale (Master of Science) in Theoretical Physics

Final grade: 110/110 cum laude.

Grade Point Average: 30/30.

Milano (MI), Italy

Nov. 2011 – Mar. 2013

Università degli Studi di Milano-Bicocca

Laurea Triennale (Bachelor of Science) in Physics

Final grade: 110/110 cum laude.

Grade Point Average: 30/30.

Milano (MI), Italy

Oct. 2008 – Sep. 2011

Liceo Scientifico Ettore-Majorana

Diploma di Maturità Scientifica (Secondary School Diploma)

Final grade: 100/100 cum laude.

Desio (MI), Italy

Sept. 2003 – July 2008

PROJECTS AND EXPERIENCE

Doctoral Thesis (“*Naturalness and Neutral Naturalness in the LHC Era*”):

- **Theoretical mathematical modelling:** developed analytical mathematical models for particle physics phenomenology; implemented them in Mathematica and C++ codes;
- **Algorithm development** for the **modelling** of physical processes using **Monte Carlo numerical simulations**;
- **Data analysis:** analyzed large data sets from the CERN LHC with complex **statistical** and **computational** methods to set confidence levels on theoretical predictions;
- authored several research and conference papers (see here the [complete list](#)).

Master Thesis ("*Supersymmetry on Curved Backgrounds*"):

- developed a **Mathematica code** to solve a system of partial differential equations that are of key importance in String Theory.

Bachelor Thesis ("*Matrix Models: from Nuclear Theory to Quantum Chaos*"):

- developed analytical techniques to compute relevant physical quantities in Nuclear Physics.

TECHNICAL SKILLS

Programming Languages: C, C++, Mathematica, Matlab, SQL, Python.

Operating system: Windows, MacOSX, Unix/Linux.

Software skills: LaTeX, MS Office Package, ROOT (CERN version of R).

SOFT SKILLS

Teaching experience: teaching assistant for a number of physics and mathematics courses at EPFL, both at the Bachelor and Master level.

Talks at international conferences: presented my research at several international conferences (see here an [example](#)).

AWARDS AND DISTINCTIONS

Oct. 2008: Recipient of the Italian Ministry of Education award for the best final score in the Secondary School final examination ([link](#)).

May 2013: Awarded an EPFL scholarship to carry out PhD studies in Theoretical Physics.

LANGUAGES

| | |
|----------------|--|
| English | Full Professional Proficiency (C2) TOEFL certificate, score 105/120 |
| French | Full Professional Proficiency (C2) |
| Italian | Mother Tongue |

EXTRACURRICULAR ACTIVITIES

- Cyclist activity: I toured Switzerland and part of the Alps by bike, both alone and in company of other bikers, for a total of 5000 km ridden in three years.
- Hiking: together with other mountaineers, I hiked the Alps, the Rocky Mountains in Colorado (USA) and spent two weeks hiking in the Lofoten islands (Norway).

PERSONAL INFORMATION

Age: 27

Swiss Work Permit: Type B since 2013

Nationality: Italian

Civil Status: single

